

POLYTECHNIQUE MONTRÉAL

affiliée à l'Université de Montréal

et

l'Université du Québec en Abitibi-Témiscamingue

**Application de la tomographie de résistivité électrique pour la surveillance
de la teneur en eau volumique dans les ouvrages de restauration minière**

ADRIEN DIMECH

Département des génies civil, géologique et des mines

Thèse présentée en vue de l'obtention du diplôme de *Philosophiæ Doctor*
Génie minéral

Avril 2023

POLYTECHNIQUE MONTRÉAL

affiliée à l'Université de Montréal

et

l'Université du Québec en Abitibi-Témiscamingue

Cette thèse intitulée :

**Application de la tomographie de résistivité électrique pour la surveillance
de la teneur en eau volumique dans les ouvrages de restauration minière**

présentée par **Adrien DIMECH**

en vue de l'obtention du diplôme de *Philosophiæ Doctor*
a été dûment acceptée par le jury d'examen constitué de :

Éric ROSA, président

LiZhen CHENG, membre et directrice de recherche

Bruno BUSSIÈRE, membre et codirecteur de recherche

Michel CHOUTEAU, membre et codirecteur de recherche

Vincent BOULANGER-MARTEL, membre

Rémi CLÉMENT, membre externe

DÉDICACE

À ma famille, merci pour votre soutien sans faille

REMERCIEMENTS

Je tiens avant tout à remercier ma directrice Lizhen Cheng et mes co-directeurs Bruno Busière et Michel Chouteau pour leur encadrement, leur soutien et leur confiance constants au cours de ces cinq dernières années. Merci pour votre disponibilité, votre humanité, votre bienveillance et vos bons conseils, qui m'ont souvent été nécessaires pour garder le cap et prendre les bonnes décisions. J'estime avoir eu beaucoup de chance d'évoluer au sein de l'IRME et d'apprendre à vos côtés et je pense que c'est en très grande partie grâce à vous que je garderai de cette expérience qu'est le doctorat un souvenir très positif et formateur à l'avenir.

J'aimerais également remercier les membres du jury, Éric Rosa, Vincent Boulanger-Martel et Rémi Clément pour avoir accepté d'évaluer cette thèse et pour le temps qu'ils y ont consacré.

Les résultats présentés dans cette thèse sont le fruit d'un travail mené avec de nombreuses et de nombreux collaborateurs.ice.s que je tiens à remercier ici. Merci à Jonathan Chambers, Paul Wilkinson et Philip Meldrum pour m'avoir aidé à planifier et à mettre en place le résistivimètre autonome PRIME. Merci également à Adam Fullerton et Harry Harrison pour leur patience. Votre grande expérience et vos conseils ont été d'une grande aide pour régler les mille et un petits problèmes de terrain et pour m'aider dans la préparation et la révision des articles. J'aimerais également remercier Gabriel Fabien-Ouellet, Charles Bérubé, Sebastian Uhlemann et Benjamin Mary pour leur expertise, leur disponibilité et leur contribution à la préparation, à la rédaction et à la révision des articles présentés dans cette thèse.

Je tiens à remercier chaleureusement mes collègues étudiant.e.s en géophysique et en hydrogéologie (et autre) à Polytechnique Montréal et à l'UQAT pour m'avoir accompagné dans ce long processus et pour avoir partagé la passion, la sueur et la joie qui viennent avec une maîtrise ou un doctorat. Merci à Anne Isabelle pour ton soutien, ta bonne humeur et pour ton aide précieuse aux travaux de laboratoire et de terrain, à la mise en place de la base de données électrique, au développement des codes python ainsi qu'à la rédaction et la correction des articles. Merci également à Karine Sylvain pour ta passion, ton enthousiasme et ta bonne humeur constante tout au long de ces cinq années, et pour m'avoir aidé à intégrer un suivi électrique dans un de tes montages de laboratoire. Merci également à Jefferson, Gabriel, Myriam, Julien, François, Chérif, Chong et à tous les étudiant.e.s de l'IRME (UQAT-Polytechnique) auprès de qui j'ai eu la chance de partager ces belles années, malgré une certaine pandémie dont je ne prononcerai pas le nom, et qui a quelque peu modifié notre routine et nos habitudes (c'est un euphémisme!). L'expérience aurait été différente sans vous.

Merci à Sylvette Awoh, Jean-Christophe Turcotte, Guillaume Noirant, Yvan Poirier, Alain Perrault, Pierre-Alain Jacques et tous mes collègues de l'Unité de recherche et de service en technologie minérale (URSTM) pour votre disponibilité, votre expertise sur le terrain et au laboratoire et votre bonne humeur. J'adresse aussi des remerciements à Patrick Charron qui m'a donné de précieux conseils lors de la préparation de la demande de subvention qui a contribué à financer ce projet de recherche.

J'aimerais également remercier les partenaires industriels sans qui ce projet de recherche n'aurait pas été possible. Merci dans un premier temps à Nathalie Chev , Blandine Arseneault et Martin Duclos de la Mine Canadian Malartic pour le soutien technique, l'encadrement sur le site et pour leur disponibilité et leur bienveillance. Merci  galement   Guylaine Letourneau et Fran ois Bergeron pour leur aide sur le terrain et leur support   distance quand le syst me de mesures  lectriques ne voulait pas d marrer. J'aimerais adresser un remerciement tout particulier   Guillaume Paquet pour son adresse sans limite   la manipulation de la pelle m canique, pour sa bienveillance et sa curiosit ; c'est en grande partie gr ce   lui si les  lectrodes ont surv cu   leur installation sous 2 m de mat riaux miniers et que les donn es recueillies sont d'aussi bonne qualit .

Merci  galement aux partenaires de l'IRME qui ont cru au potentiel du projet et qui ont accept  de contribuer   financer le projet de recherche. Merci   Martin Duclos de Mine Canadian Malartic, Martin Th riault et Jean Giroux de Rio Tinto, Mario Gagnon de IAMGOLD (mine Doyon) et Genevi ve P pin et France Tr panier de Newmont (mine  l onore) pour avoir support  la demande de subvention pour le projet. Je remercie  galement le Conseil de recherches en sciences naturelles et en g nie du Canada (CRSNG) qui a financ  le projet par son programme de subvention de recherche et d veloppement coop rative (RDC).

Je souhaite  galement remercier chaleureusement le Fonds de recherche du Qu bec - Nature et technologie (FRQNT), la SEG (*Society of Exploration Geophysicists*), la fondation FUQAT et le Fonds Jean-Descarreaux, le KEGS (*Canadian Exploration Geophysical Society*) ainsi que les entreprises Abitibi G ophysique et ERM (*Environmental Resource Management*) pour leur support financier pendant la r alisation de mon doctorat.

Je tiens   adresser ces derniers remerciements   ma famille pour leur confiance et leur soutien sans faille. Merci tout particuli rement   mes parents, Patricia et Jean-Marc. J'esp re continuer   marcher dans vos traces. Je vous d die cette th se.

RÉSUMÉ

L'activité minière génère d'importantes quantités de rejets durant le processus d'extraction et de concentration des métaux. D'une part, les roches peu ou pas minéralisées qui doivent être déplacées pour atteindre le minerai sont appelées roches stériles, et sont généralement empilées pour constituer des haldes à stériles pouvant mesurer plusieurs centaines de mètres de hauteur. D'autre part, les résidus miniers, issus du broyage du minerai et de l'ajout d'eau de procédé pour concentrer les métaux, sont déposés dans des parcs à résidus pouvant mesurer plusieurs dizaines de mètres de hauteur, et s'étendre sur plusieurs kilomètres carrés. La gestion de ces aires d'entreposage de rejets miniers constitue l'un des enjeux environnementaux les plus importants pour les compagnies minières, notamment à cause des risques d'instabilités géotechnique et géochimique. En effet, les faibles propriétés mécaniques des résidus rendent ces matériaux fins sensibles à la liquéfaction, ce qui peut entraîner des ruptures de digues aux conséquences humaines, environnementales et économiques catastrophiques. Par ailleurs, les sulfures contenus dans les rejets miniers peuvent s'oxyder au contact de l'oxygène atmosphérique et de l'eau, ce qui peut engendrer la génération de drainage minier contaminé, caractérisé par des pH très faibles et des concentrations élevées en métaux.

Plusieurs approches de gestion et de restauration ont été développées et mises en place sur les sites miniers au cours des dernières années pour réduire les risques de ruptures de digues en limitant la quantité d'eau dans les résidus et pour limiter en amont l'oxydation des rejets miniers par la mise en place de recouvrements contrôlant les flux d'eau et ou d'oxygène vers les rejets. Les couvertures à effet de barrière capillaire (CEBC) sont particulièrement prometteuses dans ce contexte puisqu'elles permettent de réduire les flux d'oxygène de l'atmosphère vers les rejets en maintenant une couche de rétention constituée de matériaux fins proche de la saturation. Une autre approche consiste à réduire l'infiltration nette d'eau vers les rejets grâce à une couche de matériaux fins compactés de faible conductivité dans des recouvrements appelés LSHCCs (pour *low saturated hydraulic conductivity cover*). La plupart de ces approches de gestion et de restauration sont basées sur le contrôle des flux d'eau dans les rejets ou dans les recouvrements et il est donc essentiel de déterminer la quantité d'eau et sa dynamique d'écoulement dans ces recouvrements pour estimer et surveiller leur performance en conditions réelles.

Néanmoins, les techniques de mesure conventionnellement utilisées pour mesurer la teneur en eau volumique dans les rejets miniers et les recouvrements sont basées sur des instruments ponctuels, dont le volume d'investigation est généralement limité à moins d'un litre (e.g.,

sondes de teneur en eau volumique ou piézomètres) ou des observations de surface, dont la profondeur d'investigation est limitée à quelques centimètres (e.g., observations visuelles ou télédétection). Par conséquent, les mesures de teneur en eau volumique dans les rejets et les recouvrements sont très limitées dans l'espace et ne permettent de surveiller qu'une infime fraction des recouvrements qui sont mis en place sur des parcs à résidus à l'échelle du terrain. Il existe donc un besoin de développer des techniques de suivi de la teneur en eau volumique dans les rejets miniers et les recouvrements qui soient applicables à l'échelle des aires d'entreposage des rejets miniers, et qui puissent être utilisées en complément des approches traditionnelles pour étendre spatialement les mesures ponctuelles.

Les mesures géophysiques peuvent sembler prometteuses dans ce contexte puisqu'elles permettent d'estimer des paramètres physiques dans le milieu à partir de mesures indirectes, typiquement depuis la surface. Par ailleurs les mesures géophysiques sont non-invasives et applicables à de plus grandes échelles, typiquement le long de profils pouvant mesurer plusieurs kilomètres de longueur avec des profondeurs d'investigation pouvant aller à plusieurs centaines de mètres sous la surface. En particulier, la méthode électrique permet d'imager la distribution de la conductivité électrique dans le milieu, qui est directement affectée par la teneur en eau ainsi que par d'autres paramètres physiques tels que la température, la conductivité électrique du fluide interstitiel ainsi que la granulométrie et la minéralogie du milieu. Cette approche a un fort potentiel puisqu'il existe dans la littérature de nombreux exemples d'application pour lesquels la méthode électrique a permis de suivre l'écoulement de traceurs et d'imager la distribution spatio-temporelle de la teneur en eau. Néanmoins, il n'existe que peu d'applications de cette approche au suivi temporel de la teneur en eau dans des rejets miniers. En particulier aucune étude à ce jour ne permet d'établir la faisabilité et la pertinence de cette approche dans le contexte de la surveillance de la performance des ouvrages de restauration minière ni de quantifier la précision de la teneur en eau qui serait estimée à partir des mesures électriques dans des recouvrements multicouches construits en partie avec des rejets miniers.

Dans ce contexte, cette thèse vise à évaluer le potentiel de la méthode électrique comme approche complémentaire aux techniques conventionnelles pour effectuer un suivi autonome de la teneur en eau dans les ouvrages de restauration minière à l'échelle pilote sur le terrain. En particulier, des recouvrements expérimentaux à l'échelle pilote ont été instrumentés et suivi durant deux ans pour évaluer la précision de l'estimation de la teneur en eau à partir des mesures électriques et servir de "preuve de concept" en conditions réelles sur un site minier.

Dans un premier temps, une revue bibliographique exhaustive a permis de constituer une base de données comprenant 650 études permettant d'identifier les meilleures pratiques de suivi

électrique disponibles dans la littérature pour de nombreux types d'application tel que le suivi des glissements de terrain ou du pergélisol. La revue a notamment permis de mettre en évidence les récents développements qui favoriseront l'application de la méthode électrique pour le suivi des rejets miniers, comme le développement de résistivimètres autonomes permettant d'acquérir les données électriques quotidiennement et de les transférer vers des serveurs à distance. Une base de données de 150 études ayant appliqué la méthode électrique pour la caractérisation des rejets miniers a également été constituée. Cette deuxième base de données a permis d'identifier les applications les plus prometteuses pour le suivi temporel des rejets. La revue a aussi permis de mettre en évidence les défis posés par l'application de la méthode électrique dans les rejets miniers, comme la complexité de prédire avec précision la teneur en eau dans des matériaux où la température et la conductivité électrique du fluide interstitiel peuvent varier significativement dans le temps et dans l'espace. Ces observations ont permis d'établir une méthodologie de recherche pour étudier ces enjeux à l'échelle de l'échantillon, du laboratoire et du terrain afin de maximiser la précision de l'approche électrique.

Plusieurs dispositifs expérimentaux de laboratoire ont été mis en place pour mesurer simultanément la teneur en eau et la conductivité électrique du milieu dans les matériaux utilisés pour la construction des recouvrements expérimentaux à l'échelle pilote. Ainsi, un dispositif basé sur les cellules Tempe a été proposé pour inclure des mesures électriques dans un échantillon de petite taille soumis à une pression croissante conduisant à son drainage. Ces "cellules Tempe électrique" ont ainsi permis d'établir la relation entre succion, teneur en eau et conductivité électrique en conditions contrôlées (température et conductivité électrique du fluide connues) pour calibrer des modèles pétrophysiques simples dans les résidus miniers. Des dispositifs expérimentaux de plus grandes dimensions ont également été mis en place pour mesurer l'évolution spatio-temporelle de la teneur en eau à l'aide de sondes et de la conductivité électrique à l'aide d'électrodes. Ces données ont également permis d'estimer la relation pétrophysique *in situ* des matériaux. La comparaison entre les modèles pétrophysiques calibrés à petite, moyenne échelle en laboratoire et à l'échelle pilote sur le terrain a permis de démontrer que la relation pétrophysique déterminée à l'échelle du laboratoire restait applicable à l'échelle pilote sur le terrain. Cette comparaison multi-échelle a aussi permis de quantifier la précision des estimations de teneur en eau par la méthode électrique qui était de $\pm 0.03 \text{ m}^3/\text{m}^3$, soit une précision similaire à celle des sondes hydrogéologiques conventionnelles. Néanmoins, cette approche a mis en évidence l'importance de prendre en compte l'effet de la température et de la conductivité électrique du fluide interstitiel dans les rejets pour estimer la teneur en eau volumique à partir des données électriques avec précision. En effet, la précision des estimations de teneur en eau volumique était diminuée d'un facteur dix si ces paramètres n'étaient pas pris en compte adéquatement sur le terrain.

La méthode électrique a également été testée en conditions réelles dans des recouvrements expérimentaux mesurant 280 m de long et 18 m de large, construits à la Mine Canadian Malartic entre 2019 et 2020. Des sections mesurant 23 m de long ont été instrumentées de sondes de teneur en eau et d'électrodes pour imager distribution spatio-temporelle de la teneur en eau en continu pendant plus d'un an. Les électrodes géophysiques ont été installées dans la couche de rétention d'eau constituée de résidus de deux sections de CEBC, et dans la couche de faible conductivité hydraulique constituée de mort-terrain compactés pour deux sections de LSHCC. Un résistivimètre autonome PRIME a été installé sur le site et les données quotidiennes ont été inversées pour imager la teneur en eau dans les recouvrements pour différentes conditions hydrogéologiques (avec ou sans pente, en haut ou en bas de pente, avec ou sans végétation). Les données de terrain ont permis de caractériser le comportement hydrogéologique des sections de CEBC et de LSHCC instrumentées, et ont été utilisées pour quantifier la performance des sections de CEBCs en utilisant un degré de saturation de 85% dans la couche de rétention d'eau comme critère de performance. La comparaison entre les données ponctuelles et géophysiques a permis de quantifier la précision des teneurs en eau prédites par la méthode électrique pour les différents recouvrements expérimentaux (entre $\pm 0.02 \text{ m}^3/\text{m}^3$ et $\pm 0.03 \text{ m}^3/\text{m}^3$), ce qui constitue une "preuve de concept" du potentiel que représente l'approche électrique comme méthode complémentaire à la surveillance de performance des ouvrages de restauration minière à l'échelle du terrain.

L'ensemble des travaux, des observations et des résultats présentés dans cette thèse ont été combinés pour mettre en place un guide de conception pour de futurs dispositifs de suivi de performance d'ouvrages de restauration à l'échelle du terrain incluant des mesures électriques. L'objectif de cette discussion est d'aider quiconque serait intéressé.e à ré-appliquer la méthodologie présentée dans cette thèse à identifier les éléments les plus importants qui seront nécessaires à la conception et la mise en place d'un dispositif de suivi adapté ainsi que pour l'acquisition, le traitement et l'interprétation des données électriques dans le contexte de la restauration minière.

ABSTRACT

Mining activity generates significant amounts of wastes during the metal extraction and concentration process. On the one hand, the rocks with little or no mineralization that must be moved to reach the ore are referred to as waste rocks, and are generally stored into waste rock piles, which can be several hundred meters high. On the other hand, the tailings, resulting from the crushing of the ore and the addition of process water to concentrate the metals, are deposited in tailings storage facilities that can be several tens of meters high and extend over several square kilometers. The management of these waste storage facilities is one of the most important environmental challenges for mining companies, particularly because of the risks of geotechnical and geochemical instabilities. Indeed, the poor mechanical properties of tailings make these fine materials sensitive to liquefaction, which can lead to dam failures with catastrophic human, environmental and economic consequences. In addition, the sulfides contained in the mining wastes can oxidize upon contact with atmospheric oxygen and water, which can result in the generation of contaminated mine drainage, characterized by very low pH and high metal concentrations.

Several management and remediation approaches have been developed and implemented at mine sites in recent years to reduce the risk of dam failures by limiting the amount of water in the tailings and to limit oxidation of mine tailings by installing covers that control water and/or oxygen flows to the tailings. Covers with capillary barrier effects (CCBEs) are particularly promising in this context as they reduce oxygen fluxes from the atmosphere to the tailings by maintaining a moisture retaining layer made of fine materials close to saturation. Another approach consists in reducing the net infiltration of water towards the mine wastes by installing low saturated hydraulic conductivity covers (LSHCCs) which limit water percolation thanks to a layer made of a fine compacted materials. Overall, most of these management and remediation approaches are based on controlling water flows into mine wastes or in covers. Therefore, determining the amount and dynamics of water in these overlays is essential to estimate and monitor their performance under real-world conditions.

However, the conventional measurement techniques used to measure water content in mine wastes and in reclamation covers are based on point instruments, which generally have a volume of investigation smaller than one liter (e.g., water content probes or piezometers) or surface observations, which are limited to a few centimeters in depth of investigation (e.g., visual observations or remote sensing). As a result, measurements of water content in wastes and covers are very spatially limited and can only monitor a tiny fraction of the covers that

are placed on full-scale tailings facilities. There is therefore a need to develop techniques for monitoring water content in mine wastes and covers that are applicable at the scale of mine waste storage facilities, and that can be used to complement traditional approaches to spatially expand point measurements.

Geophysical measurements may seem promising in this context since they allow the estimation of physical parameters in the environment from indirect measurements, typically from the surface. Moreover, geophysical measurements are non-invasive and applicable on larger scales, typically along profiles that can measure up to several kilometers in length with depths of investigation that can reach up to several hundred meters below the surface. In particular, the electrical method allows imaging the distribution of electrical conductivity in the medium, which is directly affected by the water content as well as by other physical parameters such as temperature and electrical conductivity of the interstitial fluid. This approach has a strong potential since there are many examples in the literature where the electrical method has been used to track tracer flows and to image the spatio-temporal distribution of the water content. However, there are only a few applications of this approach to the temporal monitoring of water content in mining wastes. In particular, no study to date allows to establish the feasibility and relevance of this approach in the context of monitoring the performance of mine reclamation covers, or to quantify the accuracy of the water content that would be estimated from electrical measurements in covers constructed using mine wastes.

In this context, this thesis aims to evaluate the potential of the electrical method as a complementary approach to conventional techniques for autonomous monitoring of water content in mine reclamation covers at pilot scale on the field. In particular, pilot-scale experimental multilayer covers were instrumented and monitored for two years to evaluate the accuracy of water content estimation from electrical measurements and to serve as a "proof of concept" under real conditions on an active mining site.

In a first step, an exhaustive bibliographical review allowed to build a database including 650 studies, which allowed to identify the best practices of electrical monitoring available in the literature for many types of applications such as landslides or permafrost monitoring. In particular, the review highlighted recent developments that will promote the application of the electrical method for monitoring mining wastes, such as the development of autonomous resistivity meters that can acquire electrical data on a daily basis and transfer them to remote servers. A database of 150 studies that have applied the electrical method to characterize mining wastes has also been compiled. This second database was used to identify the most promising applications for temporal monitoring of mine wastes. The review also highlighted the challenges posed by the application of the electrical method in mine tailings, such as

the complexity of accurately predicting water content in materials where the temperature and electrical conductivity of the pore fluid can vary significantly in time and space. These observations have led to the development of a research methodology to address these issues at the sample, laboratory and field scales.

In a second step, several laboratory experiments were carried out to simultaneously measure water content and bulk electrical conductivity in the materials used for the construction of the pilot-scale experimental covers. A device based on Tempe cells was proposed to include electrical measurements in a small sample submitted to increasing pressures, which in turn caused its drainage. These "electrical Tempe cells" have been used to establish the relationship between suction, water content and electrical conductivity under controlled conditions (known temperature and electrical conductivity of the fluid) to calibrate simple petrophysical models in mine tailings. Larger experimental setups were also carried out to measure the spatio-temporal evolution of water content using sensors and electrical conductivity using electrodes. These data were used to estimate the in-situ petrophysical relationships of the materials. The comparison between the petrophysical models calibrated small, medium scales in the laboratory and at pilot scale on the field demonstrated that the petrophysical relationship determined at the laboratory scale remained applicable at field scale. This multiscale comparison also quantified the accuracy of water content estimates by the electrical method to be $\pm 0.03 \text{ m}^3/\text{m}^3$, similar to the accuracy of conventional hydrogeological probes. Nevertheless, this approach highlighted the importance of considering the effect of temperature and electrical conductivity of the pore fluid in the discharges when estimating water content from electrical data, since the accuracy was decreased by a factor of ten if these parameters were not adequately accounted for in the field.

In a third phase, the electrical method was tested under field conditions in 280 m long and 18 m wide experimental multilayer covers, constructed at the Canadian Malartic Mine between 2019 and 2020. Sections measuring 23 m in length were instrumented with water content probes and electrodes to image the spatio-temporal distribution of water content continuously for over a year. The geophysical electrodes were installed in the moisture retaining layer consisting of tailings from two sections of CCBE, and in the low hydraulic conductivity layer consisting of compacted overburden for two sections of LSHCC. A PRIME stand-alone resistivity meter was installed at the site and daily data were inverted to image the water content distributions in the covers for different hydrogeological conditions (inclined or flat sections, upslope and downslope, vegetated and unvegetated). The field data were used to characterize the hydrogeological behavior of the instrumented CCBE and LSHCC sections, and were used to quantify the performance of the CCBEs sections using a degree of satura-

tion of 85% in the moisture retaining layer as a performance criterion. Comparison between local and geophysical data allowed quantifying the accuracy of the water content predicted by the electrical method for the different experimental covers (between $\pm 0.02 \text{ m}^3/\text{m}^3$ and $\pm 0.03 \text{ m}^3/\text{m}^3$), providing a "proof of concept" of the potential that the electrical approach represents as a complementary method for performance monitoring of full-scale mine reclamation covers.

Finally, the experiments, observations, and results presented in this thesis have been combined to suggest a guide for the design of future reclamation performance monitoring programs that include electrical measurements at field scale. The purpose of this discussion is to help anyone interested in re-applying the methodology presented in this thesis to identify the most important elements that will be required for the design and implementation of a suitable monitoring system as well as for the acquisition, processing and interpretation of electrical data in the context of mine reclamation.

TABLE DES MATIÈRES

DÉDICACE	iv
REMERCIEMENTS	v
RÉSUMÉ	vii
ABSTRACT	xi
TABLE DES MATIÈRES	xv
LISTE DES TABLEAUX	xix
LISTE DES FIGURES	xx
LISTE DES SIGLES ET ABRÉVIATIONS	xxviii
LISTE DES ANNEXES	xxxiii
CHAPITRE 1 INTRODUCTION	1
1.1 Contexte de l'étude	1
1.1.1 Génération de rejets par les activités minières	1
1.1.2 Stabilité géotechnique et géochimique des parcs à résidus	2
1.1.3 Méthodes de gestion et de restauration des parcs à résidus	3
1.1.4 Surveillance de la teneur en eau dans les résidus miniers	6
1.1.5 Potentiel de l'imagerie électrique comme méthode de suivi	8
1.2 Origine et objectifs du projet	9
1.3 Structure de la thèse	10
1.3.1 Présentation des articles	11
1.4 Contributions scientifiques	14
1.5 Description du site à l'étude	15
1.5.1 Présentation de la Mine Canadian Malartic	15
1.5.2 Recouvrements expérimentaux de la Mine Canadian Malartic	17

CHAPITRE 2 REVUE DE LITTÉRATURE :

ARTICLE 1 - A REVIEW ON APPLICATIONS OF TIME-LAPSE ELECTRICAL RESISTIVITY TOMOGRAPHY OVER THE LAST 30 YEARS : PERSPECTIVES FOR MINING WASTE MONITORING	20
2.1 Abstract	21
2.2 Introduction	21
2.3 Monitoring subsurface processes with TL-ERT	27
2.3.1 Objectives of TL-ERT	27
2.3.2 Key parameters of TL-ERT surveys	29
2.3.3 TL-ERT data acquisition, processing and inversion	33
2.4 Review of TL-ERT applications over the past 30 years	38
2.4.1 TL-ERT studies over the last 30 years	38
2.4.2 Description of the different fields of applications for TL-ERT	42
2.5 Emergence, challenges and perspectives of TL-ERT for mining wastes	46
2.5.1 Review of promising applications of TL-ERT for mining wastes	46
2.5.2 Challenges that need to be addressed to improve TL-ERT monitoring in mining wastes	52
2.5.3 Perspectives for future applications of TL-ERT on mining waste monitoring	55
2.6 Conclusion	68

CHAPITRE 3 ARTICLE 2 - A MULTISCALE ACCURACY ASSESSMENT OF MOISTURE CONTENT PREDICTIONS USING TIME-LAPSE ELECTRICAL RESISTIVITY TOMOGRAPHY IN MINE TAILINGS

ARTICLE 2 - A MULTISCALE ACCURACY ASSESSMENT OF MOISTURE CONTENT PREDICTIONS USING TIME-LAPSE ELECTRICAL RESISTIVITY TOMOGRAPHY IN MINE TAILINGS	77
3.1 Abstract	78
3.2 Introduction	78
3.3 Materials and methods	81
3.3.1 Site description and materials	81
3.3.2 Experimental setups	81
3.3.3 Measurements and data processing	85
3.4 Results	90
3.4.1 Scale 1 - Electrical Resistivity Tempe Cell	90
3.4.2 Scale 2 - Laboratory bucket	91
3.4.3 Scale 3 - Laboratory column	92
3.4.4 Scale 4 - Field cover at local scale	95
3.4.5 Scale 5 - Field cover at pilot scale	96

3.4.6	Relative importance of temperature and pore water EC corrections at different scales	98
3.4.7	Multi-scale comparison of petrophysical models and ERT-predicted VWC accuracy	100
3.5	Discussion	100
3.5.1	Overall accuracy of ERT-predicted VWC	100
3.5.2	Importance of temperature and pore water EC corrections for field applications	102
3.5.3	Validity of Archie model for mine tailings	103
3.5.4	Scale influence on petrophysical models	105
3.6	Conclusion	107
CHAPITRE 4	ARTICLE 3 - MONITORING MOISTURE DYNAMICS IN MULTI-LAYER COVER SYSTEMS FOR MINE TAILINGS RECLAMATION USING AUTONOMOUS AND REMOTE TIME-LAPSE ELECTRICAL RESISTIVITY TOMOGRAPHY	108
4.1	Abstract	109
4.2	Introduction	109
4.3	Site description	113
4.4	Materials and methods	115
4.4.1	Physico-chemical, hydrogeological, and electrical characterizations	115
4.4.2	Design, instrumentation, and monitoring of experimental covers	117
4.4.3	Construction of pilot-scale field experimental covers	119
4.4.4	Time-lapse ERT data acquisition and processing	122
4.5	Results	126
4.5.1	Physico-chemical, hydrogeological, and electrical properties	126
4.5.2	Moisture content dynamics from the hydrogeological sensors	129
4.5.3	Time-lapse electrical resistivity tomography results	130
4.6	Discussion	137
4.6.1	Performance assessment of the multi-layer covers from hydrogeophysical monitoring data	137
4.6.2	Advantages of TL-ERT for multi-layer cover performance monitoring	140
4.6.3	Limitations and challenges of TL-ERT for monitoring of multi-layer cover performance	142
4.7	Conclusion	143
CHAPITRE 5	DISCUSSION GÉNÉRALE	145

5.1	Guide méthodologique proposé pour appliquer la surveillance électrique sur des aires de stockage de rejets miniers à pleine échelle	146
5.1.1	Étape 1 : Étude de faisabilité	147
5.1.2	Étape 2 : Planification de l'instrumentation	150
5.1.3	Étape 3 : Instrumentation sur le terrain	156
5.1.4	Étape 4 : Collecte et traitement de données	159
5.1.5	Étape 5 : Surveillance de performance autonome	164
5.1.6	Étape 6 : Retour d'expérience	168
CHAPITRE 6	CONCLUSION ET RECOMMANDATIONS	171
RÉFÉRENCES	176
ANNEXES	231

LISTE DES TABLEAUX

Tableau 2.1	Review of studies using ERT to monitor metal extraction in heap leaching pads (HLP)	69
Tableau 2.2	Review of studies using ERT to estimate the volume of mining wastes for valorization	70
Tableau 2.3	Review of some studies using ERT to characterize mining wastes and storage facilities	71
Tableau 2.4	Review of the most recent studies using ERT to characterize AMD flows from mining wastes	73
Tableau 2.5	Review of studies using ERT to evaluate the geotechnical stability of WRP and TSF	75
Tableau 2.6	Review of studies using ERT to evaluate mining wastes reclamation efficiency	76
Tableau 4.1	Summary of the physico-chemical, hydrogeological, and electrical properties of materials :	128
Tableau 5.1	Synthèse des coûts d'instrumentation électrique sur les recouvrements	156

LISTE DES FIGURES

Figure 1.1	Schéma simplifié d'une mine à ciel ouvert représentatif d'une mine d'or de type haut tonnage, faible teneur (teneur moyenne de 1 g d'or par tonne de minerai).	2
Figure 1.2	Images satellites Google Earth du parc à résidus de Brumadinho au Brésil avant et après rupture. Photographies montrant l'impact du drainage minier acide, adapté de Chen et al. (2021). Photographies tirées initialement de A - Yan et al. (2020), Australie, B - González et al. (2020), Espagne, C - Bortnikova et al. (2020), Russie, D - Sandlin et al. (2020), États-Unis, E - López et al. (2021), Espagne et F - Markovic et al. (2020), Serbie.	4
Figure 1.3	Recouvrement multi-couche de type CEBC et principales composantes du bilan hydrique (inspiré de Demers and Pabst (2021b) et MEND (2004)).	6
Figure 1.4	Localisation de la Mine Canadian Malartic au Québec (carte modifiée de l'institut de la statistique du Québec) et imagerie satellite du site montrant la halde à stériles (bleu et orange) et le parc à résidus (jaune et mauve), tiré de Canadian Malartic (2020).	16
Figure 1.5	Schéma simplifié et coupes transversales des recouvrements à l'échelle pilote ayant été instrumentés dans le cadre de cette thèse, tiré de Canadian Malartic (2020).	18
Figure 1.6	Coupes longitudinales des recouvrements à grande échelle instrumentés dans le cadre de ce projet de recherche, soit la LSHCC avec une épaisseur de mort-terrain de 2 m (en bleu) et la CEBC avec les résidus non amendés (en orange). Les stériles sont indiqués en gris (bermes) et vert. Schémas préparés par Golder, et tirés de Canadian Malartic (2020).	19
Figure 2.1	Diagram of an open-pit mine operation and simplified mass balance of wastes and minerals.	22
Figure 2.2	Distribution and surface of mining waste storage facilities across Canada in 2020. Each mining site in Canada (active, closed or abandoned) has been identified and the areas occupied by TSFs, WRPs and open-pits have been calculated with Google Earth satellite imagery. The database and interactive maps can be accessed and downloaded through the supplementary material webpage	23

Figure 2.3	Example of TL-ERT monitoring of a tracer infiltration with surface and borehole electrodes. (i) Top panel shows the true spatio-temporal distribution of tracer concentration in the medium, (ii) medium panel presents the corresponding distribution of electrical resistivity and (iii) the inverted distribution of resistivity obtained from TL-ERT monitoring. Finally, (iv) bottom panel shows the ERT-predicted tracer concentration using petrophysical relationship (based on Singha et al. (2015)).	30
Figure 2.4	Spatio-temporal parameters of TL-ERT surveys (inspired from Rucker (2014))	31
Figure 2.5	Diagram of ERT inversion routine used to reconstruct distribution of electrical resistivity ρ	34
Figure 2.6	Review of the main applications of TL-ERT for various domains . . .	40
Figure 2.7	General statistics for each field of applications identified in the database of TL-ERT studies : (a) evolution of the number of published studies per year from 1991 to 2020 for each type of application and (b) distribution of the 651 published studies according to the classification proposed in Figure 2.6. Note that the identification of TL-ERT studies has been carried out during Summer 2020, which explains the relatively low number of publications identified for 2020 (shaded).	41
Figure 2.8	Review of the main applications of ERT for mining wastes imaging and monitoring	47
Figure 2.9	Review of the key parameters that can be imaged or monitored in WRPs with TL-ERT as identified from the database of ERT studies in mining wastes (adapted from Aubertin et al. (2005)).	53
Figure 2.10	Review of the key parameters that can be imaged or monitored in TSFs with TL-ERT as identified from the database of ERT studies in mining wastes (adapted from Aubertin et al. (2016)).	53
Figure 2.11	Recent developments and perspectives for geoelectrical monitoring of mining wastes.	56
Figure 2.12	(a) Evolution of the number of electrodes, the monitoring period and the temporal resolution for the 173 semi-permanent TL-ERT studies identified in the database. For each study, the size of the circle is proportional to the monitoring period while the color of the circle corresponds to the temporal resolution. (b) Histogram of semi-permanent TL-ERT studies according to the temporal resolution.	59

Figure 2.13	Flowchart of permanent TL-ERT monitoring system describing autonomous data acquisition, remote data transfer, automated processing and interpretation for long-term monitoring. Figure inspired from Holmes et al. (2020) presenting the workflow of the PRIME system applied to landslide monitoring in British Columbia (Canada).	63
Figure 3.1	Grain size distribution of the materials used in the experiment. In total, 44 different samples of tailings (black), 8 samples of waste rocks (grey) and 47 samples of overburden (brown) have been analyzed. Each individual grain size distribution is shown using shaded lines. The mean, minimum and maximum grain size distributions are shown in solid line and dashed lines.	82
Figure 3.2	Illustration of the five scales investigated in this study to assess petrophysical relationships in mine tailings in the laboratory (S1 - cell scale, S2 - bucket scale and S3 - column scale), and in the field (S4 - local scale and S5 - pilot scale). Detailed schematics and photographs are available in "Supplementary Materials" for each experimental setup.	83
Figure 3.3	Workflow of hydrogeophysical data acquisition and processing used to recover petrophysical relationships from multi-scale experimental setups. The laboratory column (scale 3) is used as an example.	87
Figure 3.4	Results from the monitoring of the Electrical Resistivity Tempe Cells (scale 1). Evolution of (a) measured VWC and (b) inverted bulk EC in the tailings for several pressure steps. (c) Relationship between VWC and bulk EC in the ER-TC.	91
Figure 3.5	Top panel : 2D slices of the 3D inverted bulk EC distribution and sensitivity for the laboratory bucket (scale S2) at selected time steps. The VWC sensor location is indicated by a white dot and the white rectangle corresponds to its volume of investigation, where inverted bulk EC is extracted to be compared with VWC measurements. Bottom panel : evolution of (a) artificial precipitations, (b) VWC and (c) inverted bulk EC in the tailings during the artificial precipitation event and (d) petrophysical relationship between VWC and bulk EC in the bucket.	93

Figure 3.6	<p>Top panel : 2D slices of the 3D inverted bulk EC distribution and sensitivity for the laboratory column (scale S3) at selected time steps. The VWC sensor location is indicated by white dots and the white rectangles correspond to their volumes of investigation. Bottom panel : evolution of (a) VWC and (b) inverted bulk EC in the tailings during the artificial precipitation event and (c) petrophysical relationship between VWC and bulk EC in the bucket.</p>	94
Figure 3.7	<p>Top panel : inversion mesh, 2D inverted bulk EC distribution and sensitivity in the experimental field cover at local scale (scale S4) for a representative time step. The VWC sensors are indicated by white dots and electrodes correspond to red dots. Bottom panel : evolution of (a) precipitations, (b) VWC and (c) inverted bulk EC in the tailings from May to November 2021 and (d) relationship between VWC and bulk EC in the experimental CCBE cover at local scale.</p>	96
Figure 3.8	<p>Top panel : inversion mesh, 2D inverted bulk EC distribution and sensitivity in the experimental field cover at pilot scale (scale S5) for a representative time step. The VWC sensors are indicated by white dots and electrodes correspond to red dots. Bottom panel : evolution of (a) precipitations, (b) VWC and (c) inverted bulk EC in the tailings from May to November 2021 and (d) relationship between VWC and bulk EC in the experimental CCBE cover at pilot scale.</p>	97
Figure 3.9	<p>Influence of temperature and pore water EC corrections on the accuracy of ERT-predicted VWC for (a) Scale S1 - ER Tempe Cell, (b) Scale S2 - laboratory bucket, (c) Scale S3 - Laboratory column and (d) Scale S4 - Field cover at local scale.</p>	99
Figure 3.10	<p>Assessment of the scale influence on petrophysical models and on the accuracy of ERT-predicted VWC. Top left - Comparison of the petrophysical models calibrated using hydrogeophysical datasets from scales S1 to S5. Top right - Histograms of the error between measured and ERT-predicted VWC using data and petrophysical models from different scales. Bottom panel - RMSE, bias and standard deviation of VWC prediction errors using ERT data and petrophysical models from different scales.</p>	101

Figure 4.1	(a) Satellite view of Canadian Malartic gold mine located in Quebec, Canada (48.11°N, 78.12°W). Identification of the open-pit, WRP and TSF that are planned to be reclaimed. (b) Aerial photography of the four pilot-scale experimental multi-layer covers and simplified composition of the CCBE and LSHCC multi-layer covers investigated in this study.	114
Figure 4.2	Grain size distribution (GSD) for the materials used in the experimental covers. Each sample is shown in light brown, black and grey for the overburden, tailings and waste rocks, respectively.	115
Figure 4.3	(a) Schematic view of the modified Tempe Cell used to characterize electrical properties of samples. (b) Photographs showing the modified Tempe Cell, the porous ceramic plate, the six stainless steel electrodes and the ABEM Terrameter LS resistivity meter.	117
Figure 4.4	Geometry of the experimental CCBE (a) and the LSHCC (b) built on the TSF of MCM. The location of hydrogeophysical instruments is presented on the vertical sections (longitudinal profiles of electrodes in red and Teros 12 sensors along a vertical profile in the center of the 23 m-long cover sections).	118
Figure 4.5	(a) Photographs showing the different steps of pilot-scale experimental CCBE and LSHCC construction at the TSF of Canadian Malartic Mine. (b) Photographs showing the main components of the geoelectrical monitoring station, including the PRIME resistivity meter, the electrode cables, the batteries, the router, and the antenna.	121
Figure 4.6	(a) Wenner measurement protocol used in the experimental covers with electrode spacing ranging from 1 m to 5 m. (b) Raw conductance time-series measured with the PRIME system for an electrode spacing of 2 m and 5 m with the top electrodes of each cover (mean of all measurements).	123
Figure 4.7	Precipitation data, spatio-temporal variation of temperature measured by the Teros 12 sensors, and spatio-temporal variation of pore water electrical conductivity derived from the Teros 12 measurements at the center of the CCBE experimental cover section on the plateau.	125
Figure 4.8	Daily precipitation and unfrozen volumetric water content measured by the Teros 12 sensors for the four cover sections. The vertical dashed lines correspond to the wet and dry dates referred to in Fig. 4.9	131

Figure 4.9	VWC distribution derived from inverted resistivity models using the Archie-based resistivity-to-VWC relationship in the CCBEs (first and second panels) and in the LSHCCs (third and fourth panels) for the two dates identified on Fig. 4.8 corresponding to wet and dry conditions (the 0.1 m-thick layer of topsoil at the top of the covers is not shown in these plots).	132
Figure 4.10	Spatio-temporal dynamics of VWC in the field experimental CCBEs (two vertical panels on the left) and in the LSHCCs (two vertical panels on the right) at selected dates. As shown in Fig. 4.8, the last week of June 2021 was particularly wet while drier conditions were recorded during August 2021.	133
Figure 4.11	Accuracy of ERT-predicted VWC using the VWC measured by the hydrogeological sensors at the center of the covers as a reference for the four experimental multi-layer covers. (a) Temporal evolution and (b) comparison of measured (dashed lines) and ERT-predicted (solid line) VWC.	135
Figure 4.12	(a) Distribution of the degree of saturation predicted from ERT measurements for the four experimental cover sections. (b) Surface percentage of the fine-grained layers at different intervals of degrees of saturation for a given period of time and summary for the one-year monitoring period.	137
Figure 5.1	Guide de conception de dispositif de suivi électrique dans les recouvrements.	146
Figure 5.2	Approche méthodologique proposée dans cette thèse pour effectuer la surveillance de la performance de CEBC à l'échelle pilote par la méthode électrique.	148
Figure 5.3	Méthodologie proposée par Robinson et al. (2019) pour effectuer une étude de faisabilité pour le suivi temporel par la méthode électrique à partir de modélisations.	149
Figure 5.4	Exemples de quatre systèmes de suivi électrique à grande échelle ayant différentes fonctions, résolutions spatio-temporelle et profondeurs d'investigation, avec des électrodes installées en surface, en forage ou enterrées dans le recouvrement lors de sa construction.	151

Figure 5.5	Approche méthodologique suivie au début de la thèse pour identifier la configuration d'électrodes maximisant la résolution spatiale de l'imagerie de teneur en eau dans la couche de rétention de la CEBC construite à la mine Canadian Malartic.	153
Figure 5.6	Optimisation simultanée de protocoles de mesures et de la localisation / du nombre d'électrodes tel que proposé par Uhlemann et al. (2018b).	154
Figure 5.7	Vue par drone des recouvrements expérimentaux à grande échelle construits à la mine Canadian Malartic. Les principales composantes du dispositif de suivi électrique à l'échelle pilote dont les coûts sont résumés au Tableau 5.1 sont identifiées.	155
Figure 5.8	Influence de la forme, de la taille de l'électrode et de sa mise en place dans le milieu sur la résistance de contact. Photographies tirées de Tomaškovičová et al. (2016) (en haut), (Arosio et al., 2017) (en bas à gauche) et Ogilvy et al. (2009) (en bas à droite).	158
Figure 5.9	Dispositifs de laboratoire normés pour caractériser la relation entre l'indice des vides et la conductivité électrique (tiré de Bryson and Bathe (2009) et Comina et al. (2008)).	161
Figure 5.10	Schéma simplifié d'un pénétromètre conique (CPT) équipé d'électrodes, tiré de Morey et al. (1999). Résultats typiques d'une investigation à 50 m de profondeur avec un CPT équipé d'électrodes, soit la résistance à la pénétration, la pression interstitielle, l'indice de la qualité des sols I_c et la résistivité électrique, tiré du site web de ConeTec, accès le 26/02/2023.	162
Figure 5.11	Choix du protocole de type Wenner dans les recouvrements expérimentaux de la mine Canadian Malartic pour maximiser la sensibilité et le rapport signal sur bruit.	163
Figure 5.12	Effet de la régularisation sur la précision des résultats d'inversion (CEBC).	165
Figure 5.13	Maillage 2D utilisé pour effectuer les inversions avec pygimli dans la CEBC.	166
Figure 5.14	Évaluation de la performance de la CEBC à l'échelle pilote dans la section dite "plateau" à partir des mesures électriques (adapté de Dimech et al. (2023a), chapitre 4).	167
Figure 5.15	Principales composantes d'un système d'alerte précoce (EWS pour <i>Early Warning System</i> en anglais) tiré de Budler (2017), adapté de Intrieri et al. (2013).	168

Figure 5.16	Exemple de surveillance automatisée d'un talus de voie ferrée à l'aide de la méthode électrique autonome (tiré de Chambers et al. (2014a) et Gunn et al. (2015)). Les imageries de teneur en eau réalisées à l'aide de la méthode électrique sont comparées à des valeurs seuils pour alerter les opérateurs en cas de dépassement et localiser les anomalies.	169
Figure A.1	Detailed schematics for the experimental laboratory setups. (a) S1 - electrical resistivity Tempe cell scale (ER-TC), (b) S2 - bucket scale and (c) S3 - column scale.	231
Figure B.1	Detailed schematics and photographs for the experimental field cover with capillary barrier effect. (a) S4 - field CCBE at local scale, (b) S5 - field CCBE at pilot scale.	232
Figure C.1	Illustration of the configurations used to carry out TL-ERT monitoring in the tailings at different scales. Red and blue electrodes represent respectively current and potential electrodes.	233

LISTE DES SIGLES ET ABRÉVIATIONS

Abbreviations

1D	Une dimension
2D	Deux dimensions
3D	Trois dimensions
AEV	<i>Air Entry Value</i> (Pression d'entrée d'air)
ALERT	<i>Automated Time-Lapse Electrical Resistivity Tomography</i> (Resistivimètre autonome développé par le BGS)
AMD	<i>Acid Mine Drainage</i> (Drainage minier acide)
ASTM	<i>American Society for Testing and Materials</i>
AWG	<i>American Wire Gauge</i> (Unité de mesure américaine de diamètre de câble)
BGL	<i>Below ground level</i> (Profondeur sous la surface)
BGS	<i>British Geological Survey</i> (Commission géologique de Grande-Bretagne)
CCBE	<i>Cover with Capillary Barrier Effects</i> (CEBC)
CEBC	Couverture avec Effet de Barrière Capillaire
CPT	<i>Cone Penetration Testing</i> (Investigation par pénétromètre conique)
CRSNG	Conseil de Recherches en Sciences Naturelles et en Génie du Canada
DC	<i>Direct Current</i> (Courant continu)
DMA	Drainage Minier Acide
DOI	<i>Depth of Investigation</i> (Profondeur d'investigation d'un protocole)
DTS	<i>Distributed Temperature Sensing</i> (Mesure de température distribuée)
EC	<i>Electrical Conductivity</i> (Conductivité électrique)
ER	<i>Electrical Resistivity</i> (Résistivité électrique)
ERT	<i>Electrical Resistivity Tomography</i> (Tomo. de résistivité électrique)
ER-TC	<i>Electrical Resistivity Tempe Cell</i> (Cellules Tempe avec résistivité électrique)

EWS	<i>Early Warning System</i> (Système d'alerte précoce)
GMC	<i>Gravimetric Moisture Content</i> (Teneur en eau massique)
GRETA	<i>GeoResistivimeter for Time lapse Analysis</i> (Résistivimètre autonome développé par LSI-Lastem)
GSD	<i>Grain Size Distribution</i> (Distribution granulométrique)
GTP	<i>Global Tailings Portal</i> (Portail effectuant l'inventaire mondial des parcs à résidus miniers)
HLP	<i>Heap Leaching Pad</i> (Remblai de lixiviation en tas)
ICOLD	<i>International Commission on Large Dams</i> (Commission internationale des barrages de grandes dimensions)
INRP	Institut National des Rejets Polluants
InSAR	<i>Interferometric Synthetic Aperture Radar</i> (Radar à synthèse d'ouverture interférométrique)
IRME	Institut de Recherche en Mines et Environnement
LBNL	Lawrence Berkeley National Laboratory
LIDAR	<i>Light Detection and Ranging</i> (Détection et télémétrie par la lumière)
LSHCC	<i>Low Saturated Hydraulic Conductivity Cover</i> (Couverture de faible conductivité hydraulique saturée)
LTA	Les Terrains Aurifères
MCM	Mine Canadian Malartic
MDDELCC	Ministère du Développement durable, de l'Environnement et de la Lutte contre les Changements Climatiques
MDDEP	Ministère du Développement Durable, de l'Environnement et des Parcs
MELCC	Ministère de l'Environnement et de la Lutte contre les Changements Climatiques
MEND	<i>Mine Environment Neutral Drainage</i> (Programme de neutralisation des eaux de drainage dans l'environnement minier - NEDEM)
MERN	Ministère de l'Énergie et des Ressources Naturelles
MKC	<i>Modified Kozeny-Carman model</i> (modèle Kozeny-Carman modifié)
MRL	<i>Moisture Retaining Layer</i> (Couche de rétention d'eau)
NPRI	<i>Canadian National Pollutant Release Inventory</i> (INRP)

OS	Objectif Spécifique
PCA	<i>Principal Component Analysis</i> (Analyse par composante principale)
PRIME	<i>PRoactive Infrastructure Monitoring and Evaluation system</i> (Résistivimètre autonome développé par le BGS)
PVC	Polychlorure de vinyle
QC	Québec
RIME	<i>Research Institute of Mines and Environment</i> (IRME)
RMSE	<i>Root Mean Square Error</i> (Erreur moyenne quadratique)
TDS	<i>Total Dissolved Solids</i> (Total de solides dissous)
TL-ERT	<i>Time-Lapse Electrical Resistivity Tomography</i> (ERT en suivi temporel)
TSF	<i>Tailings Storage Facility</i> (Parc à résidus miniers)
UQAT	Université du Québec en Abitibi-Témiscamingue
USGS	<i>United States Geological Survey</i> (Commission géologique des États-Unis)
VES	<i>Vertical Electrical Sounding</i> (Sondages électriques verticaux)
VWC	<i>Volumetric Water Content</i> (Teneur en eau volumique)
WEV	<i>Water Entry Value</i> (Pression résiduelle)
WMTF	<i>World Mine Tailings Failure</i> (Inventaire des ruptures de parcs à résidus miniers)
WRC	<i>Water Retention Curve</i> (Courbe de rétention d'eau)
WRP	<i>Waste Rock Pile</i> (Halde à stériles)

Symboles mathématiques et physiques

$\%C$	Pourcentage de carbone dans un échantillon (en %)
$\%S_{\text{tot}}$	Pourcentage de soufre total dans un échantillon (en %)
c	Facteur de dépendance de la conductivité électrique à la température (en $^{\circ}C^{-1}$), noté tc dans le Chapitre 3 et δT dans le Chapitre 4
CO_2	Dioxyde de carbone
C_u	Coefficient d'uniformité (-)
D_{10}	Diamètre passant - 10 % (μm)

D_{30}	Diamètre passant - 30 % (μm)
D_{60}	Diamètre passant - 60 % (μm)
\mathbf{d}_{calc}	Jeu de données de résistances synthétiques (en Ω)
\mathbf{d}_{meas}	Jeu de données de résistances mesurées (en Ω)
δ	Fonction de Dirac
G	Opérateur de modélisation directe
G_s	Densité relative des grains solides (g/cm^3)
J	Matrice Jacobienne
k_{sat}	Conductivité hydraulique en milieu saturé (en cm/s)
m	Coefficient de cimentation ou premier exposant d'Archie (sans unité) - noté m_a dans le Chapitre 4
n	Second exposant d'Archie (sans unité) - noté n_a dans le Chapitre 4
n	Porosité du milieu (sans unité) - notée ϕ dans les Chapitres 2 et 3
$\Phi_d(\mathbf{m})$	Erreur entre les données mesurées et simulées pour une distribution de résistivité m
ϕ	Porosité du milieu (sans unité) - notée n dans le Chapitre 4
ψ	Succion dans le milieu (en kPa)
ψ_a	Pression d'entrée d'air (en kPa) (AEV en anglais)
ψ_r	Pression résiduelle (en kPa) (WEV en anglais)
R	Résistance électrique (en Ω)
ρ_b	Résistivité électrique du milieu (en $\Omega.m$)
ρ_w	Résistivité électrique de l'eau (en $\Omega.m$)
σ_b	Conductivité électrique du milieu (en S/m)
σ_{el}	Conduction électrolytique (en S/m)
σ_s	Conductivité électrique de surface (en S/m)
σ_w	Conductivité électrique du fluide interstitiel (en S/m)
$\sigma_{w,\text{std}}$	Conductivité électrique du fluide interstitiel de référence (en S/m)
S_w	Degré de saturation du milieu (sans unité)
T_{std}	Température de référence (généralement $25^\circ C$)

θ	Teneur en eau volumique du milieu (m^3/m^3)
θ_r	Teneur en eau volumique résiduelle (m^3/m^3)
θ_{sat}	Teneur en eau volumique à saturation (m^3/m^3)
W_d	Matrice de poids appliqués aux données pour prendre en compte l'erreur
W_m	Matrice de poids appliqués aux paramètres du modèles (régularisation)
W_t	Matrice de poids (régularisation temporelle des modèles)

LISTE DES ANNEXES

Annexe A	Détails des dispositifs de laboratoire	231
Annexe B	Détails de l'instrumentation de terrain	232
Annexe C	Protocole de mesures électriques	233

CHAPITRE 1 INTRODUCTION

1.1 Contexte de l'étude

1.1.1 Génération de rejets par les activités minières

L'industrie minière produit d'importantes quantités de rejets durant les processus d'extraction et de concentration des métaux. D'une part, les roches stériles sont générées par le sautage de la roche encaissante, peu ou pas minéralisée, qui entoure le minerai et qui doit être déplacée pour l'atteindre. Comme illustré par la Figure 1.1, les roches stériles sont stockées dans des haldes à stériles pouvant atteindre plusieurs centaines de mètres de hauteur (Aubertin et al., 2016). D'autre part, les résidus miniers sont générés lors du processus de concentration du métal exploité. En effet, le minerai est broyé, concassé et mélangé à de l'eau de procédé pour faciliter la concentration du métal par flottation (Bussière, 2007). Le mélange de roches finement broyées et d'eau d'où les métaux ont été extraits est ainsi déposé dans des parcs à résidus, mesurant généralement plusieurs dizaines de mètres de hauteur, dont les digues sont construites à partir de matériaux plus grossiers, comme les roches stériles ou les fractions les plus grossières des résidus (Kossoff et al., 2014).

Les teneurs en métaux sont généralement faibles pour la plupart des mines à ciel ouvert, soit de l'ordre de quelques pourcents pour les métaux communs comme le cuivre et de l'ordre de quelques grammes par tonne de minerai pour les métaux précieux comme l'or (Nassar et al., 2022). Par conséquent, plus de 99% de la roche extraite est considérée comme un rejet minier après séparation des métaux pour la plupart des opérations à ciel ouvert. Ceci explique les dimensions considérables de ces aires de stockage, s'étendant souvent sur plusieurs kilomètres carrés, qui ont même été décrites comme "les plus grandes structures construites par l'Homme sur Terre" (Bowker and Chambers, 2015). Par ailleurs, la production de rejets miniers va considérablement augmenter dans les prochaines années en raison de l'effet combiné de (i) la hausse de la demande, à la fois pour les métaux de base, les métaux précieux et les minéraux critiques et stratégiques (ex. terres rares, lithium, nickel et autres), (ii) la diminution des teneurs des gisements facilement exploitables et (iii) les développements technologiques qui rendent de plus en plus économique l'exploitation de gisements à faible teneur et haut tonnage (Calvo et al., 2016; Chambers, 2016; Rötzer and Schmidt, 2018). À titre d'exemple, une étude récente (WMTF, 2019) estimait à 50 milliards de tonnes la quantité de résidus qui seront produits sur la période 2020-2025 à l'échelle mondiale, soit une augmentation de près de 25% de la masse totale de résidus estimée sur la planète.

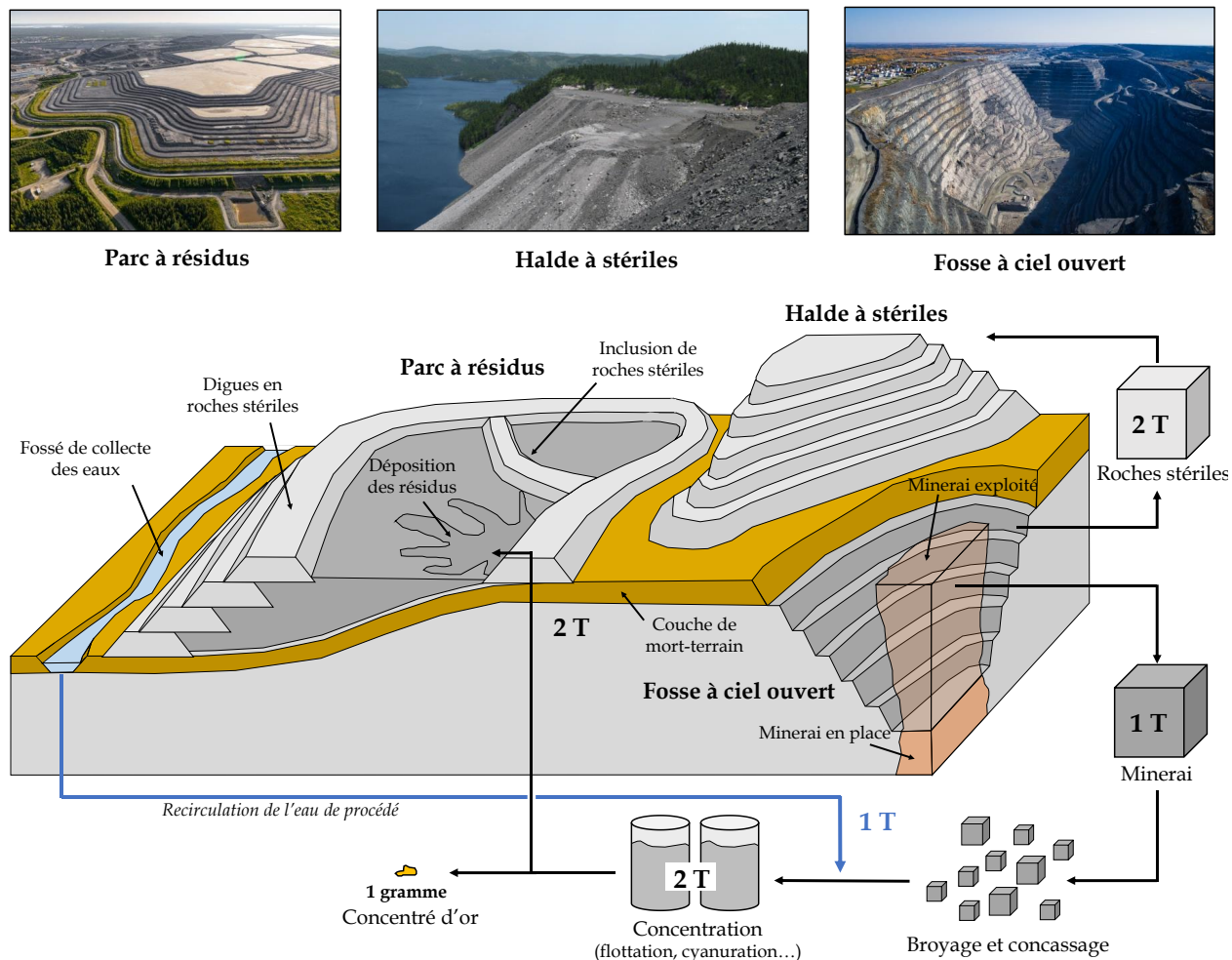


FIGURE 1.1 Schéma simplifié d'une mine à ciel ouvert représentatif d'une mine d'or de type haut tonnage, faible teneur (teneur moyenne de 1 g d'or par tonne de minerai).

1.1.2 Stabilité géotechnique et géochimique des parcs à résidus

La gestion des rejets miniers est un des principaux enjeux environnementaux auxquels l'industrie minière doit faire face, notamment à cause des problématiques de stabilité géotechnique et géochimique des aires de stockage de rejets (Bussière, 2007). En effet, la granulométrie fine des résidus miniers (sable fin à silt) ainsi que la teneur en eau généralement élevée dans les parcs à résidus en font des structures à risque de rupture, et qui doivent être adéquatement conçues et opérées pour résister à des événements extrêmes comme des tremblements de terre ou de fortes pluies (Azam and Li, 2010). Ces dernières années, des ruptures de digues catastrophiques se sont produites et ont causé des dégâts humains et environnementaux considérables comme illustré sur la Figure 1.2, notamment au Canada (Mount Polley, 2016), en Australie (Cadia, 2018), au Brésil (Fundão, 2015 et Brumadinho, 2019) et en Afrique du Sud

(Jagersfontein, 2022) (Rotta et al., 2020; Clarkson et al., 2021). Comme Lyu et al. (2019b) l'ont noté, la majorité des 300 ruptures de digues rapportées de 1910 à 2018 ont été attribuées à des problématiques dans la gestion de l'eau dans les parcs (soit par infiltration, soit par débordement), et par des problèmes liés à la stabilité des fondations et à la liquéfaction des résidus, cette dernière étant aussi impactée par la quantité d'eau dans les résidus.

La stabilité géochimique des rejets miniers peut également constituer une problématique environnementale majeure si les rejets contiennent des sulfures, comme la pyrite ou la pyrrhotite, qui peuvent s'oxyder au contact de l'eau et de l'oxygène (Plante et al., 2021b). En l'absence d'espèces minérales neutralisantes comme la calcite, l'oxydation des sulfures peut générer du drainage minier acide (DMA), qui est généralement caractérisé par un faible pH (< 6), des concentrations en métaux dissous élevées et une couleur orange ou rouge due aux précipités d'hydroxyde de fer, comme illustré sur la figure 1.2b (Blowes et al., 2003; Nordstrom, 2011). Lorsqu'elle n'est pas contrôlée adéquatement, la génération de DMA peut avoir des conséquences sur l'environnement à court et long terme, par exemple si le DMA se décharge dans des cours d'eau par exemple, entraînant des conséquences graves sur les organismes vivants (Rezaei et al., 2019; Rotta et al., 2020). De nombreux sites miniers au Québec sont concernés par des enjeux associés à la génération de DMA, ce qui est particulièrement problématique pour les anciennes aires de stockage de résidus et de roches stériles de sites miniers abandonnés (Dagenais et al., 2005; Ethier et al., 2018). De même que pour la stabilité physique des parcs à résidus, la teneur en eau joue un rôle crucial dans la génération de DMA, à la fois puisqu'elle est un réactif nécessaire à l'oxydation des sulfures, mais aussi parce que la distribution d'eau dans les résidus affecte significativement les flux d'oxygène de l'atmosphère vers les résidus (Aachib et al., 2004; Mbonimpa et al., 2021). Ainsi, les objectifs en termes de stabilité géotechnique et géochimique sont souvent opposés puisqu'une saturation complète des résidus permettra de réduire les flux d'oxygène et limitera donc la réaction d'oxydation, mais augmentera en revanche le risque de liquéfaction des résidus et de rupture du parc (Williams, 2021). L'étude sur la distribution de l'eau dans un ouvrage minier est donc importante dans toutes les situations.

1.1.3 Méthodes de gestion et de restauration des parcs à résidus

Plusieurs approches de gestion et de restauration des aires de stockage ont été proposées dans les dernières années pour mieux contrôler le risque d'instabilité géotechnique et géochimique des rejets miniers (Bussière and Guittonny, 2021a; Wilson, 2021). Du point de vue de la géotechnique, il est recommandé de réduire autant que possible la quantité d'eau dans les parcs à résidus sur le long terme en séchant les résidus avant leur déposition dans les parcs (résidus



FIGURE 1.2 Images satellites Google Earth du parc à résidus de Brumadinho au Brésil avant et après rupture. Photographies montrant l'impact du drainage minier acide, adapté de Chen et al. (2021). Photographies tirées initialement de A - Yan et al. (2020), Australie, B - González et al. (2020), Espagne, C - Bortnikova et al. (2020), Russie, D - Sandlin et al. (2020), États-Unis, E - López et al. (2021), Espagne et F - Markovic et al. (2020), Serbie.

séchés empilés), en évacuant les eaux de surface, en favorisant des conditions drainantes dans les parcs (digues perméables ou co-disposition de roches stériles) et en élargissant les digues à la base (Bussière, 2007). Du point de vue géochimique, la construction de recouvrements est une option qui a fait ses preuves sur le terrain pour contrôler les flux d'eau et d'oxygène de l'atmosphère vers les rejets potentiellement générateurs de DMA (Bussière et al., 2003; Bussière et al., 2006; Dagenais et al., 2012). Parmi les différents types de recouvrements décrits par Bussière and Guittonny (2021a), les couvertures avec effets de barrières capillaires (CEBC) comme celle schématisée sur la Figure 1.3, sont particulièrement adaptées au climat humide du Québec (Demers and Pabst, 2021b). En effet, ces recouvrements multi-couches comprennent une couche de faible perméabilité constituée de matériaux fins qui est intercalée entre deux couches de matériaux plus grossier (couche de support et couche drainante), ce qui a pour fonction de préserver la quasi-saturation en tout temps afin de réduire les flux d'oxygène vers les rejets (couche de rétention d'eau). La valeur du degré de saturation de 85% dans la couche de rétention d'eau est souvent considérée comme critère de performance pour les CEBCs pour réduire les flux d'oxygène (Aubertin et al., 1998; Bussière, 2007). Une couche de protection et une couche superficielle jouent également un rôle dans la CEBC pour réduire le risque d'intrusions humaines, animales ou végétales dans le recouvrement et pour favoriser la colonisation végétale, composante principale de la restauration des parcs à résidus (Demers and Pabst, 2021b).

Bien que les coûts de construction associés à la mise en place de CEBC soient souvent plus élevés que pour d'autres recouvrements moins complexes (e.g., recouvrements monocouche (Pabst, 2021), recouvrements de type stockage-relargage (Bussière and Wilson, 2021) ou recouvrements avec des couches de faible conductivité hydraulique saturée - notés LSHCC (Maqsooud et al., 2021)), les CEBCs ont l'avantage d'être une technique robuste et mature, dont l'efficacité a été démontrée sur plusieurs sites restaurés à l'échelle du terrain (e.g., Bussière et al. (2006)). L'utilisation de matériaux peu sensibles aux cycles de gel-dégel constitue également un atout, par opposition aux recouvrements de faible conductivité nécessitant des matériaux plus fins. La durabilité des matériaux constituant la couche de rétention d'eau est également plus élevée que celle de membranes géotextiles parfois utilisées dans les recouvrements de faible conductivité (Maqsooud et al., 2021). De plus, la possibilité de valoriser des rejets miniers dans la construction des CEBCs, notamment en utilisant des roches stériles pour les couches de support et de drainage et des résidus pour la couche de rétention d'eau, permet de réduire les coûts de construction et l'empreinte de la restauration sur le milieu (Larochelle et al., 2019; Kalonji-Kabambi et al., 2020). Enfin, ce type de recouvrement permet l'implantation de la végétation à long terme (Proteau et al., 2020b), ce qui n'est pas possible avec certains recouvrements comme les recouvrements en eau (Awoh et al., 2021).

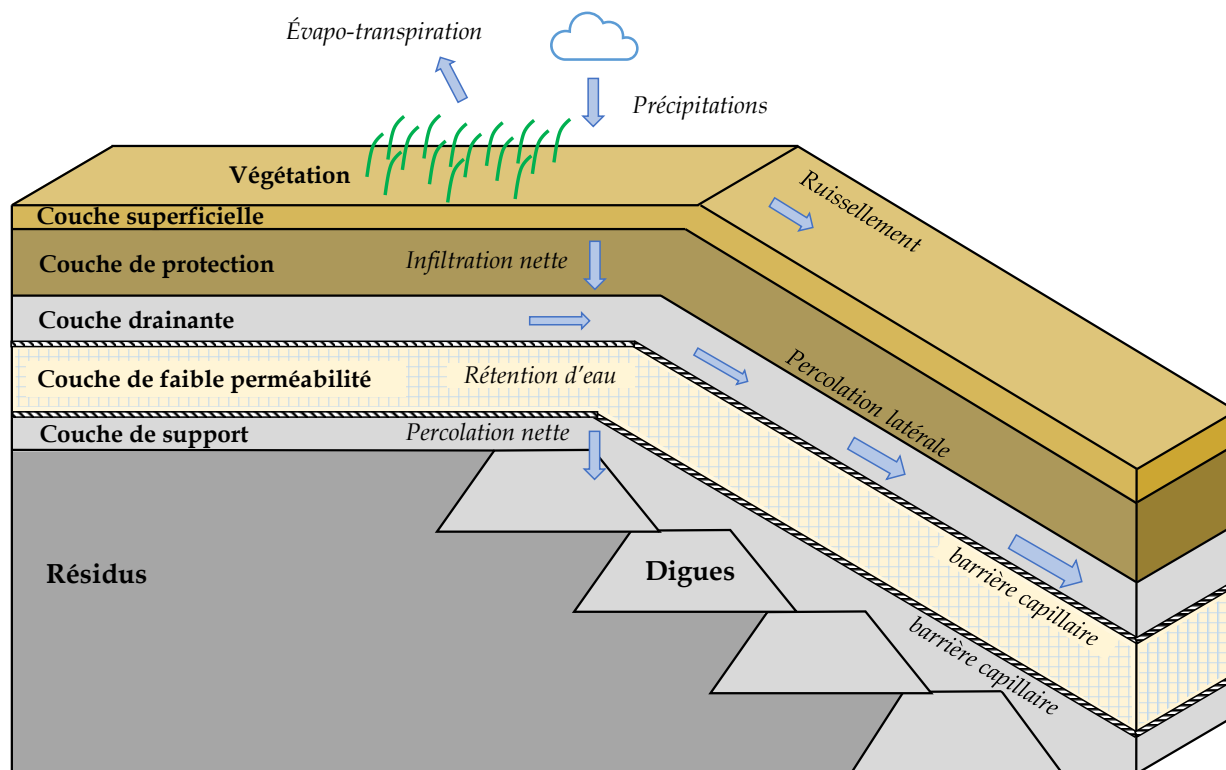


FIGURE 1.3 Recouvrement multi-couche de type CEBC et principales composantes du bilan hydrique (inspiré de Demers and Pabst (2021b) et MEND (2004)).

1.1.4 Surveillance de la teneur en eau dans les résidus miniers

Une bonne conception des aires de stockage de rejets miniers, suivie par une opération adéquate et une surveillance adaptée pourra réduire les risques d'instabilité géotechnique et géochimique (Hui et al., 2018). En particulier, Clarkson and Williams (2020) indiquent que la surveillance des paramètres physiques (notamment la teneur en eau) dans les rejets, les digues et les recouvrements devrait être continue, peu coûteuse et, dans la mesure du possible, effectuée en temps réel. Une telle surveillance permettrait ainsi aux opérateurs de détecter rapidement des situations à risques pour pouvoir prendre les mesures adéquates (e.g., accumulation anormale d'eau dans la surface des résidus, infiltration à travers les digues ou désaturation excessive des couches de rétention d'eau dans une CEBC). De plus, les données de terrain permettent d'étudier le comportement hydrogéologique du système, souvent davantage connu à plus petite échelle (laboratoire ou cellules de terrain) et de calibrer des modèles numériques permettant de prédire le comportement à plus long terme, ou en réponse à des événements extrêmes (e.g., tremblement de terre, pluie abondante ou sécheresse prolongée) (Bussière et al., 2021).

De manière générale, les techniques de mesure dans les rejets et les recouvrements miniers peuvent être classées en deux catégories. D'une part, les mesures locales permettent d'estimer relativement précisément un paramètre physique à un endroit donné dans le milieu (Hui et al., 2018). Les sondes hydrogéologiques mesurant généralement la teneur en eau, la température, la conductivité électrique ou la succion dans un volume limité (typiquement <1 L) rentrent dans cette catégorie, ainsi que les piézomètres mesurant localement le niveau piézométrique et la pression interstitielle dans un parc (Clarkson et al., 2021) et le suivi de la performance des recouvrements en restauration (MEND, 2004; Bussière et al., 2021). D'autre part, les observations de surface comme (i) les inspections visuelles, (ii) la photogrammétrie aérienne par drone ou avion ou (iii) la télédétection permettent de couvrir des étendues plus importantes mais ont des profondeurs d'investigation généralement limitées (en surface uniquement ou quelques centimètres dans le milieu) (Hui et al., 2018; Li et al., 2020; Rotta et al., 2020; Grebby et al., 2021; Lumbroso et al., 2021).

Bien que complémentaires, ces deux approches ont des limites en ce qui concerne le suivi des aires d'entreposage de rejets miniers, qui s'étendent parfois sur des centaines d'hectares et pour lesquelles les paramètres physiques d'intérêt doivent généralement être déterminés dans le milieu et non dans les premiers centimètres sous la surface (MEND, 2004; Bussière et al., 2021). À titre d'exemple, les programmes de surveillance de performance des CEBCs construites sur les sites miniers Lorraine et Les Terrains Aurifères (LTA) illustrent bien ces enjeux puisque le degré de saturation dans les couches de rétention d'eau doit être estimé pour des profondeurs allant de 30 cm à 1 m sous la surface, ce qui reste relativement superficiel, mais qui est au-delà de la zone investiguée par les techniques de surface (Bussière et al., 2006, 2009; Dagenais et al., 2012). Par ailleurs, de nombreux instruments ponctuels ont été installés pour ces deux sites de relativement petite taille (20 piézomètres et 160 sondes (20 stations) à Lorraine pour une surface de 11 ha et 120 sondes (40 stations) à LTA pour une surface 60 ha, respectivement). Par conséquent, une telle approche de suivi pourrait difficilement être mise en place pour la restauration de parcs à résidus de plus grandes dimensions comme celui de la Mine Canadian Malartic, qui s'étend sur plus de 600 ha. En effet, l'installation des milliers de sondes ponctuelles qui seraient nécessaires pour investiguer un volume représentatif des aires de stockage correspondrait à des coûts importants et à des défis en termes d'installation, de calibration, de collecte, de stockage et d'interprétation de données (Rykaart et al., 2006; Le Borgne et al., 2022). Finalement, l'unique recours à des outils de mesures ponctuels, aussi nombreux soient-ils, pourrait être inadéquat à détecter des anomalies locales de baisse de performance ou d'instabilité physique (accumulation d'eau, désaturation ou infiltration) si aucun instrument ponctuel n'est positionné spécifiquement où cette anomalie se produit.

1.1.5 Potentiel de l'imagerie électrique comme méthode de suivi

Dans ce contexte, les mesures géophysiques sont souvent décrites comme des outils adaptés pour combler les lacunes des mesures ponctuelles et de surface en termes de résolution spatiale et de volume d'investigation, notamment pour l'estimation de la teneur en eau dans le sol (Robinson et al., 2008b). En effet, les mesures géophysiques permettent d'estimer de façon indirecte la distribution de paramètres physiques d'intérêt dans le sol à partir de mesures de surface, de manière non invasive et non destructrice (Parsekian et al., 2015). De plus, les méthodes géophysiques peuvent être appliquées à différentes échelles, du centimètre en laboratoire à l'échelle du kilomètre sur le terrain (Auken et al., 2014; Binley et al., 2015a; Ulusoy et al., 2015). En particulier, la méthode de tomographie de résistivité électrique (ERT pour *electrical resistivity tomography* en anglais) permet d'imager la distribution de la résistivité électrique du milieu, qui peut être corrélée avec la distribution de teneur en eau volumique notamment en utilisant des relations pétrophysiques (Chambers et al., 2014a; Uhlemann et al., 2017a). Cette méthode géophysique est particulièrement intéressante puisqu'elle est relativement peu dispendieuse, robuste et directement utilisable sur le terrain pour effectuer un suivi temporel (TL-ERT pour *time-lapse ERT* en anglais). En particulier, de récents progrès ont été réalisés en ce qui concerne le développement de résistivimètres autonomes, capables d'effectuer plusieurs mesures ERT quotidiennement et de transférer les données automatiquement à des serveurs à distance (Holmes et al., 2020; Chambers et al., 2022). De tels développements ont rendu possible l'application de la méthode électrique pour le suivi temporel et à l'échelle du terrain pour de nombreuses applications comme les glissements de terrain, le pergélisol ou l'intrusion saline (Whiteley et al., 2019; Slater and Binley, 2021).

Il est par conséquent surprenant de constater que relativement peu d'applications de la méthode électrique ont été encore publiées dans le contexte de la surveillance temporelle de la stabilité géotechnique des parcs à résidus et de la performance des recouvrements en restauration. En effet, Martinez-Pagan et al. (2021) mentionnent que la plupart des usages de la méthode ERT rapportés dans la littérature pour les rejets miniers sont ponctuels dans le temps ou sur des périodes de temps courtes comme pour la caractérisation des rejets miniers (Anterrieu et al., 2010; Power et al., 2018b), la détection de DMA (Tycholiz et al., 2016; Bortnikova et al., 2018; Jodeiri Shokri et al., 2022) ou l'imagerie de la nappe phréatique dans les parcs (Booterbaugh et al., 2015; Epov et al., 2017) par exemple. Néanmoins, de récentes publications semblent indiquer un engouement dans les dernières années pour l'application de la méthode électrique comme technique de suivi de la teneur en eau dans les digues de parcs à résidus (e.g., da Rocha et al. (2019); Tresoldi et al. (2020a,c,b, 2021); Oliveira et al. (2023)). De même, quelques publications ont démontré l'intérêt de la méthode électrique pour étudier

le comportement hydrogéologique des recouvrements miniers pendant des courtes périodes de temps (e.g., Maqsoud et al. (2011); Dimech et al. (2018, 2019); Sylvain et al. (2019); Rey et al. (2020b)). On peut donc penser que de telles applications de la méthode électrique en suivi temporel dans les rejets miniers vont probablement devenir de plus en plus fréquentes à l’avenir pour les raisons mentionnées précédemment.

1.2 Origine et objectifs du projet

Plusieurs sites miniers majeurs au Québec sont en train, à l’écriture de ces lignes, de planifier la restauration de leurs aires de stockage de rejets miniers qui se déroulera au cours des dix prochaines années. À titre d’exemple, la Mine Canadian Malartic prévoyait dans son plan de restauration (2020) de cesser la déposition de matériel dans ses parcs à résidus en 2023 et de passer à la phase de restauration à pleine échelle par la suite (parc à résidus de 620 hectares environ) (Canadian Malartic, 2020). De même, la mise en place de recouvrements sur les parcs à résidus de la mine Éléonore ($\simeq 40$ ha), de la mine Raglan ($\simeq 60$ ha), du site Doyon-Westwood ($\simeq 280$ ha) et de la mine LaRonde ($\simeq 320$ ha) a commencé ou est prévue de débuter dans les prochaines années (SNC Lavalin, 2018, 2021a,b, 2020; Agnico Eagle Mine Laronde, 2021). Il existe donc un besoin de développement de techniques de suivi à l’échelle du terrain de la performance *in situ* des recouvrements qui vont être construits dans les prochaines années au Québec, et ce afin de respecter les exigences en matières de surveillance post-restauration énoncées dans la Directive 019 sur l’industrie minière (MDDEP, 2012).

Les travaux de l’Institut de Recherche en Mines et Environnement UQAT-Polytechnique (IRME) ont permis de développer, tester et valider la plupart des méthodes de restauration appliquées par l’industrie minière au Québec et ailleurs depuis une vingtaine d’années (Aznar-Sánchez et al., 2018; Bussière and Guittonny, 2021a). Depuis une dizaine d’années, l’IRME effectue des travaux de recherche pour tester des méthodes de suivi de la teneur en eau qui pourraient être utilisées en complément des instruments traditionnels ponctuels dans les recouvrements à plus grande échelle (e.g., mesure distribuée de la température (DTS pour *distributed temperature sensing* en anglais par Martin et al. (2017); Wu et al. (2020, 2021)). En particulier, la méthode électrique a été employée dans le contexte de la caractérisation des rejets miniers dès les années 2000-2010 (e.g., Campos et al. (2003); Poisson et al. (2009); Anterrieu et al. (2010); Maqsoud et al. (2011)). Plus récemment, une halde à stériles expérimentale à l’échelle pilote a été instrumentée avec des électrodes pour permettre un suivi temporel de l’écoulement de traceurs (Martin et al., 2017; Dimech et al., 2017). Ces données ont été utilisées pour caractériser le comportement hydrogéologique d’un recouvrement

visant à réduire l'infiltration d'eau (Dimech, 2018; Dimech et al., 2018, 2019; Martin et al., 2019). Les résultats encourageants, la robustesse et le faible coût des électrodes ainsi que l'applicabilité de la méthode à grande échelle dans d'autres recouvrements miniers ont ainsi motivé la mise en place du projet de recherche présenté dans le cadre de cette thèse.

Cette thèse de doctorat vise à développer et tester à l'échelle pilote une approche de surveillance de la teneur en eau dans des recouvrements miniers par tomographie de résistivité électrique de manière continue, autonome et à distance. Plus spécifiquement, le projet de recherche s'articule autour de la réalisation des trois objectifs spécifiques (OS) suivants.

- **OS1** - Mettre en place une méthodologie pour caractériser la relation entre la conductivité électrique, la teneur en eau et la succion dans les matériaux miniers
- **OS2** - Évaluer la précision de l'estimation de teneur en eau par la méthode électrique à diverses échelles et établir une méthodologie maximisant cette précision
- **OS3** - Proposer une méthodologie pour réaliser la surveillance de la performance d'ouvrages de restauration minière et appliquer cette approche sur un site pilote

1.3 Structure de la thèse

La thèse est divisée en six chapitres distincts et structurée autour de trois articles publiés ou soumis pour publication à des revues avec comité de lecture. Après l'introduction (Chap. 1), le chapitre 2 présente une revue de littérature servant à établir les bases techniques et pratiques de cette thèse, qui a été publiée dans la revue **Surveys in Geophysics**. Les chapitres 3 et 4 constituent le corps de la thèse et présentent deux articles soumis respectivement à **Scientific Reports** et à **Canadian Geotechnical Journal**. Les chapitres présentant les trois articles de la thèse sont présentés en anglais et sont détaillés dans la section qui suit. La combinaison des approches méthodologiques et des résultats exposés dans les articles permet de répondre à l'objectif général qui consiste à développer et tester à l'échelle pilote une approche de surveillance de la teneur en eau basée sur des mesures électriques. Le chapitre 5 propose une discussion générale des travaux réalisés dans la thèse focalisée sur les applications pratiques futures de l'approche proposée. Finalement, le chapitre 6 résume les principales conclusions de la thèse et propose plusieurs recommandations pour quiconque serait intéressé.e par la poursuite de ces travaux ou leur application pratique sur un site minier.

1.3.1 Présentation des articles

Article 1 - Revue de littérature - *Surveys in Geophysics*

Le premier article, présenté au chapitre 2, s'intitule *A Review on applications of time-lapse electrical resistivity tomography over the last 30 years : perspectives for mining waste monitoring* de Dimech, Cheng, Chouteau, Chambers, Uhlemann, Wilkinson, Meldrum, Mary, Fabien-Ouellet et Isabelle (2022) et a été publié dans la revue **Surveys in Geophysics**.

Cet article a pour objectif de placer les bases théoriques du projet de recherche, notamment en ce qui concerne l'imagerie spatio-temporelle par tomographie de résistivité électrique, et d'effectuer un survol des meilleures pratiques disponibles dans la littérature concernant sa mise en application dans plusieurs domaines. Une revue des articles publiés dans des revues avec comité de lecture et qui utilisent la méthode électrique en suivi temporel a permis de mettre en place une base de données contenant environ 650 articles. Cette base de données a été utilisée pour identifier les principaux types d'application pour lesquels l'approche était la plus employée (e.g., suivi de contaminant, imagerie de la teneur en eau dans les glissements de terrain ou le pergélisol) ainsi que d'identifier les meilleures approches de suivi spatio-temporel développées au cours des dernières années, notamment en ce qui concerne l'instrumentation, l'acquisition et le traitement de données ainsi que pour l'interprétation des résultats. En particulier, la revue a permis d'identifier environ 150 articles qui ont utilisé la méthode électrique avec des instruments et appareils de mesures installés sur les sites de manière permanente, et effectuant des mesures quotidiennes pour certains sites depuis un vingtaine d'années (e.g., pour les glissements de terrain et le pergélisol). Cette revue a donc permis d'orienter les choix et les approches suivies dans le cadre de cette thèse, puisque les récents développements de la méthode sont susceptibles d'être appliqués avec succès au domaine des rejets miniers, représentant moins de 3% des articles de la base de données.

L'article propose également une revue des applications de la méthode électrique au contexte de l'environnement et de la géotechnique des résidus miniers. Une base de données contenant une centaine d'articles a été mise en place pour analyser les principales approches de caractérisation et de suivi appliquées au cours des trente dernières années. Cette revue bibliographique a permis d'identifier les principaux défis existants dans le contexte des rejets miniers et les approches les plus prometteuses pour résoudre ces problématiques. En particulier, l'article propose une synthèse des applications possibles de la méthode de suivi électrique appliquée à la surveillance de la stabilité géotechnique et géochimique des rejets miniers (e.g., suivi de la teneur en eau, détection et cartographie du DMA, détection d'infiltrations dans les digues). Enfin, une base de données Google Earth des sites miniers a été développée, ce

qui a permis d'estimer la surface et la répartition des aires de stockage de rejets miniers au Canada. La combinaison de tous ces éléments a permis (i) de justifier l'importance et la pertinence de développer la méthode électrique pour le suivi des rejets miniers et (ii) d'identifier la meilleure méthodologie à mettre en place pour effectuer le suivi de la teneur en eau à grande échelle et en continu par la méthode électrique à partir des meilleures pratiques disponibles dans la littérature. Le premier article répond donc à l'objectif général de la thèse.

Article 2 - Analyse de précision multi-échelle - Scientific Reports

Le second article, présenté au chapitre 3, intitulé *A multiscale accuracy assessment of moisture content predictions using time-lapse electrical resistivity tomography in mine tailings* de Dimech, Isabelle, Sylvain, Liu, Cheng, Bussière, Chouteau, Fabien-Ouellet, Bérubé, Wilkinson, Meldrum et Chambers a été soumis à la revue **Scientific Reports**.

D'une part, cet article vise à proposer une méthodologie permettant de caractériser simultanément les propriétés hydrogéologiques et électriques des matériaux utilisés pour la construction des recouvrements miniers expérimentaux, et ce, afin de répondre à l'**OS1** décrit à la section 1.2. Un dispositif de laboratoire innovant a ainsi été développé pour adapter des cellules Tempe, couramment utilisées en hydrogéologie non-saturée pour déterminer la courbe de rétention d'eau, qui permet d'établir une relation directe entre la succion et la teneur en eau dans le matériau. Une légère modification des cellules Tempe utilisées à l'IRME a permis de mesurer la conductivité électrique de l'échantillon au fur et à mesure qu'il se désature sous l'effet d'une pression appliquée par le haut. Ce dispositif peu coûteux, pratique et reproductible dans la plupart des laboratoires a ainsi permis de calibrer des modèles pétrophysiques d'Archie reliant la conductivité électrique et la teneur en eau pour différents échantillons de résidus miniers et de mort-terrain. Les mesures ont été effectuées en laboratoire sur des échantillons de petite dimension, ce qui a permis de contrôler toutes les conditions de l'essai (porosité, homogénéité des matériaux, conductivité électrique de l'eau interstitielle et température). Ces relations pétrophysiques ont ainsi pu être appliquées pour la suite du projet afin d'imager la teneur en eau dans les matériaux à partir des données électrique.

D'autre part, l'article propose une méthodologie permettant d'évaluer la précision de la teneur en eau prédite dans les matériaux à partir des données électriques et des relations pétrophysiques établies en laboratoire, ce qui permet de répondre à l'**OS2**. En effet, le principal frein à l'utilisation de la méthode électrique dans le contexte du suivi de la performance des recouvrements est la précision des mesures. La méthodologie de suivi proposée doit permettre d'estimer la teneur en eau dans les couches d'intérêt (e.g. la couche de rétention d'eau d'une

CEBC) avec une précision permettant de détecter une baisse de performance (e.g. désaturation en dessous de 85 % de saturation pendant une certaine période). Une stratégie a été proposée à l'aide d'expériences à plusieurs échelles pour comparer la teneur en eau prédite par la méthode électrique avec la teneur en eau mesurée par les sondes hydrogéologiques. Différentes conditions hydrogéologiques ont été appliquées aux matériaux miniers (drainage, infiltration, précipitations réelles) pour des expériences dont la taille varie à quelques dizaines de centimètres en laboratoire (chaudière et colonne) à plusieurs dizaines de mètres sur le terrain dans des recouvrements expérimentaux à la Mine Canadian Malartic. Ces expériences ont permis d'estimer et d'améliorer la précision de la conversion de la conductivité électrique du milieu en teneur en eau, en particulier par la prise en compte de la variation spatio-temporelle de la température et de la conductivité du fluide interstitiel. De plus, les expériences à différentes échelles ont été utilisées pour valider que la relation pétrophysique déterminée à l'échelle de l'échantillon en laboratoire demeure valide à plus grande échelle, ce qui constitue un élément crucial pour l'application de la méthode sur le terrain.

Article 3 - Cas d'application à l'échelle pilote - Canadian Geotechnical Journal

Le troisième article (Chap. 4) qui s'intitule *Monitoring moisture dynamics in multi-layer cover systems for mine tailings reclamation using autonomous and remote time-lapse electrical resistivity tomography* de Dimech, Bussière, Cheng, Chouteau, Fabien-Ouellet, Chev , Isabelle, Wilkinson, Meldrum et Chambers a  t  soumis   **Canadian Geotechnical Journal**.

Cet article vise   mettre en application et   tester la m thode  lectrique   l' chelle pilote dans des recouvrements exp rimentaux de grande dimension et en conditions r elles, ce qui permet de r pondre   l'**OS3**. Les recouvrements exp rimentaux ont  t  construits en 2019-2020 par la Mine Canadian Malartic dans le cadre de la planification de la restauration du parc   r siduals   pleine  chelle. Au total, quatre sc narios de recouvrements sont test s et instrument s, mesurant chacun 280 m de long et 18 m de large. Les travaux de cette partie de la th se ont port  sur le suivi hydrog ophysique de deux recouvrements parmi ces quatre sc narios de restauration, soit une CEBC dont la couche de r tention d'eau est constitu e de r siduals miniers de 1 m d' paisseur, et une couverture avec couche de faible conductivit  hydraulique satur e (LSHCC pour *low saturated hydraulic conductivity cover* en anglais), dont la couche de faible conductivit  hydraulique est constitu e de mort-terrain compact  de 1 m d' paisseur. Quatre sections de 23 m de long et 6 m de large sont  quip es de nombreuses  lectrodes enterr es et de sondes hydrog ologiques mesurant localement la teneur en eau, la temp rature et la conductivit   lectrique. La m thodologie d velopp e dans l'**OS1** et l'**OS2** pour convertir les imageries  lectriques en imageries de teneur en eau est mise

en place pour effectuer un suivi de teneur en eau le long de quatre profils de 23 m de long, et ce quotidiennement. Le résistivimètre autonome PRIME (pour *PRoactive Infrastructure Monitoring and Evaluation system*) développé par le BGS (*British Geological Survey*) a été installé dans un conteneur à proximité des recouvrements, ce qui a permis d'acquérir plusieurs images électrique par jour dans chacune des quatre sections expérimentales et de transférer les données à distance. Les mesures hydrogéophysiques, automatisées à partir de mai 2021 ont été utilisées pour prédire la distribution de teneur en eau dans les recouvrements. Finalement, une approche a été développée pour relier ces données au comportement hydrogéologique et à la performance des recouvrements testés. Les résultats de ces travaux jouent le rôle de "preuve de concept" à l'échelle pilote, à la fois pour démontrer la précision et la faisabilité de l'approche géophysique proposée pour estimer la teneur en eau dans les recouvrements.

1.4 Contributions scientifiques

Cette thèse permet d'apporter plusieurs contributions scientifiques au domaine de la géophysique appliquée et de l'environnement minier. De manière globale, il s'agit, à la connaissance de l'auteur, de la première application du genre de la méthode de tomographie de résistivité électrique pour le suivi en continu et à l'échelle pilote de la teneur en eau dans des résidus miniers et dans des recouvrements en restauration. Bien que la revue de littérature présentée au chapitre 2 ait mis en évidence quelques applications de la méthode électrique au contexte du suivi temporel des rejets miniers, il a aussi été démontré que ce type d'application est sous-représenté par rapport à la démocratisation de cet outil pour l'étude des glissements de terrain, du pergélisol ou en géothermie par exemple. Cette thèse peut donc contribuer à favoriser l'application future de la géophysique dans ce domaine pour lequel l'apport de cette approche non-invasive de suivi à grande échelle pourra être prometteur.

De manière plus spécifique, le développement de la méthode de caractérisation simultanée des propriétés hydrogéologiques et électriques en conditions non-saturées présenté au chapitre 3 est innovant puisque c'est, à la connaissance de l'auteur, la première fois ou un tel dispositif de laboratoire a été proposé et testé pour des rejets miniers. Cette contribution est d'autant plus pertinente qu'elle repose principalement sur des dispositifs de laboratoire peu coûteux, disponibles dans la plupart des laboratoires d'hydrogéologie non-saturée et que la démarche peut être facilement reproduite avec d'autres résidus miniers et matériaux fins. Par conséquent, cette contribution pourrait amener vers une standardisation de la calibration des relations pétrophysiques dans les matériaux miniers, ce qui pourrait amener à une meilleure compréhension de la relation entre teneur en eau, succion et conductivité électrique et améliorer la précision de l'estimation de la teneur en eau à partir des mesures électriques.

Par ailleurs, la démarche présentée dans le chapitre 3 n'avait encore jamais été appliquée, à la connaissance de l'auteur, pour vérifier que la relation pétrophysique établie en laboratoire demeure valide à plus grande échelle en laboratoire et sur le terrain dans les résidus miniers, ce qui constitue pourtant un important postulat pour l'application de la géophysique sur le terrain. L'approche proposée reposant sur des mesures simultanées et co-localisées de teneur en eau par la méthode électrique et des sondes hydrogéologiques pourra également être appliquée dans d'autres études pour lesquelles l'hétérogénéité des matériaux et leur granulométrie pourrait compliquer l'utilisation de relations déterminées à petite échelle en laboratoire. Enfin, cette thèse a confirmé l'importance de la correction de température et de conductivité électrique du fluide interstitiel pour l'estimation de la teneur en eau par la méthode ERT.

Finalement, l'application de la méthode à l'échelle pilote présentée dans le chapitre 4 constitue, à la connaissance de l'auteur, la première preuve de concept de la faisabilité de l'approche électrique pour effectuer un suivi de la teneur en eau dans des recouvrements en restauration minière. Cette contribution pourrait jouer un rôle non négligeable dans la démocratisation de la surveillance géophysique pour les rejets miniers. En effet, ces travaux pourraient encourager les acteur.rice.s du domaine à développer des approches similaires pour surveiller la teneur en eau en temps réel et à grande échelle, paramètre crucial à la fois pour la stabilité géotechnique des aires de stockage et pour le suivi de performance des ouvrages en restauration minière. Dans ce sens, l'approche de conception généralisée de dispositifs de surveillance incluant la méthode électrique qui est proposée en discussion (Chap. 5) permettra de fournir des outils méthodologiques utiles à la communauté scientifique et à l'industrie.

1.5 Description du site à l'étude

1.5.1 Présentation de la Mine Canadian Malartic

La Mine Canadian Malartic est une mine d'or à ciel ouvert située en Abitibi-Témiscamingue, au Nord-Ouest du Québec comme le montre la Figure 1.4). Elle est exploitée par un partenariat entre Yamana Gold et Agnico Eagle depuis 2014. Le gisement d'or disséminé de Canadian Malartic est associé à des altérations hydrothermales dues à des intrusions magmatiques dans les roches sédimentaires et a une teneur moyenne en or d'environ 1.1 gramme par tonne de minerai (Lafrenière-Bérubé, 2018). Il s'agit de l'une des plus grandes mines d'or à ciel ouvert au Canada, avec des réserves estimées à 3.5 millions d'onces d'or, et une production moyenne de 57 000 tonnes de minerai par jour à son usine de concentrateur, ce qui correspond à environ 60 kg d'or extrait quotidiennement. Il est estimé dans le plan de restauration de la mine (2020) qu'environ 620 millions de tonnes de roches stériles et 300 millions de tonnes

de résidus auront été générées à la fin des opérations prévue en 2029 (Canadian Malartic, 2020), stockés respectivement dans des haldes à stériles (≈ 370 ha) et des parcs à résidus (≈ 620 ha) visibles sur la vue satellite de la Figure 1.4.

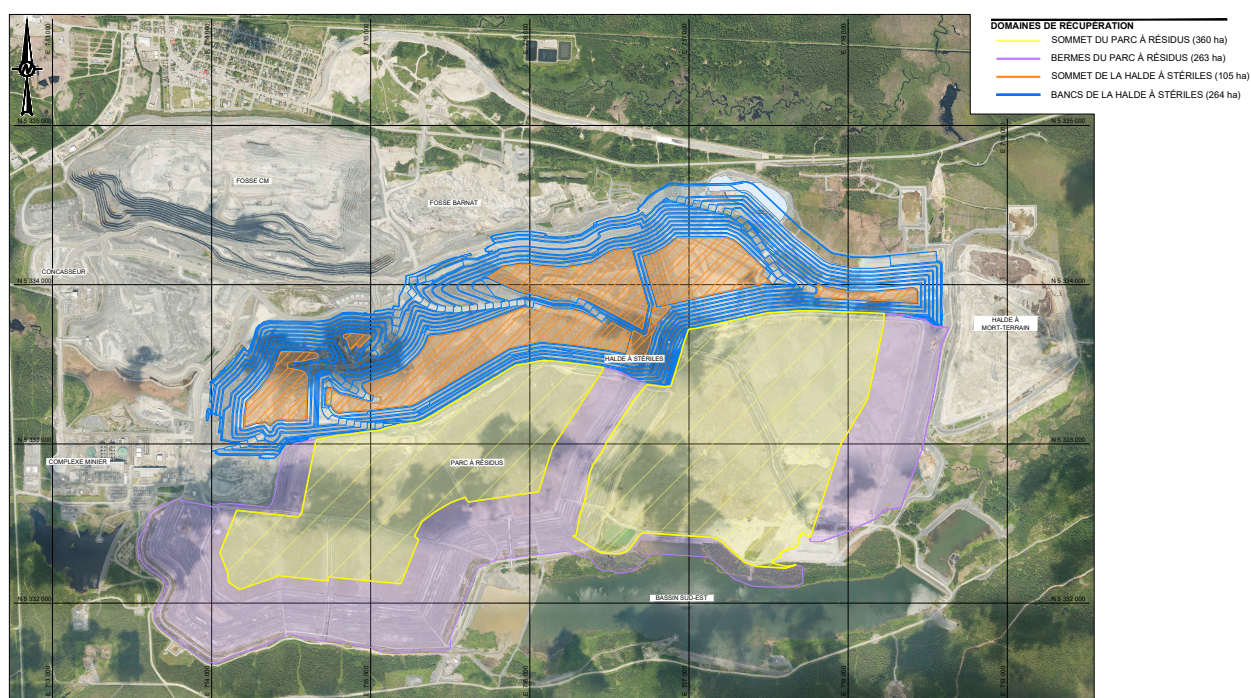
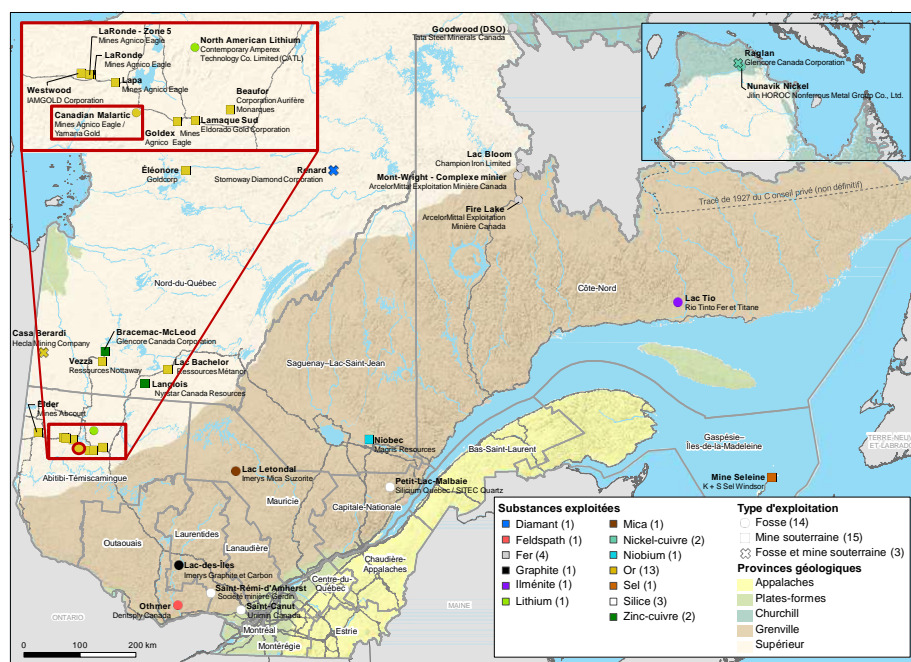


FIGURE 1.4 Localisation de la Mine Canadian Malartic au Québec (carte modifiée de l'institut de la statistique du Québec) et imagerie satellite du site montrant la halde à stériles (bleu et orange) et le parc à résidus (jaune et mauve), tiré de Canadian Malartic (2020).

1.5.2 Recouvrements expérimentaux de la Mine Canadian Malartic

Les résidus de la Mine Canadian Malartic sont considérés comme étant potentiellement acidogènes selon la Directive 019 (MDDEP, 2012) et le nouveau guide de caractérisation des rejets du MELCC (MELCC, 2020). En moyenne, les résidus du parc ont une teneur en soufre proche de 1.2 % et une teneur en carbone d'environ 0.6 % (Canadian Malartic, 2020). Cependant, le comportement géochimique des résidus à long terme est encore incertain et reste à l'étude. En effet, si la réactivité des résidus à court et moyen terme est jugée faible suite à des essais cinétiques, des essais en cellule humide ont toutefois relevé des taux d'oxydation de sulfures élevés (Canadian Malartic, 2020). Par conséquent, "le moment du début de la génération d'acide, dans le cas où il y aura génération d'acide, la durée de la génération ainsi que son intensité demeurent à l'étude" (Canadian Malartic, 2020).

Par conséquent, le plan de restauration des parcs à résidus de la mine, mis à jour en 2020, inclut la mise en place d'un recouvrement avec un élément de faible perméabilité permettant de limiter les infiltrations d'eau et la diffusion d'oxygène atteignant les résidus (Canadian Malartic, 2020). Suite à une analyse des modes de défaillance et de leurs effets, la Mine Canadian Malartic a décidé de construire quatre recouvrements expérimentaux à l'échelle pilote de 2019 à 2020, et qui permettent de comparer la performance de quatre scénarios de recouvrements en conditions réelles. Il est attendu que la construction et le suivi de ces recouvrements expérimentaux apporteront des informations qui permettront d'orienter les décisions concernant la restauration à plein échelle du parc (Canadian Malartic, 2020), notamment en ce qui concerne la performance, la constructibilité et les coûts de construction et d'instrumentation. La mise en place de ces recouvrements expérimentaux de grande dimension a constitué une opportunité unique pour le projet de recherche présenté dans cette thèse puisque la Mine Canadian Malartic a accepté de mettre à notre disposition certaines sections des recouvrements. Ainsi, nous avons pu être impliqués lors de la planification et la construction des recouvrements afin d'installer les équipements hydrogéophysiques nécessaires à la mise en application des **OS2** et **OS3**. Les échantillons de matériaux utilisés pour l'**OS1** ont également été prélevés lors de la construction des recouvrements.

La Figure 1.5 présente une vue d'ensemble ainsi que les coupes transversales des quatre recouvrements qui ont été construits par la Mine Canadian Malartic, tandis que la Figure 1.6 en présente les coupes longitudinales. Les recouvrements mesurent environ 280 m de long et 18 m de large et sont isolés les uns des autres par une séparation imperméable. Une partie des recouvrements présente une très faible pente (section dite "plateau") tandis que l'autre partie présente une pente de 10H : 1V (section dite "pente"). Deux recouvrements différents ont été construits, soit (i) une LSHCC composée de mort-terrain jouant le rôle de couche de

faible conductivité hydraulique de 1 à 2 m d'épaisseur et de terre végétale et (ii) une CEBC composée de roches stériles, de résidus miniers constituant la couche de rétention d'eau de 1 m d'épaisseur, de mort-terrain et de terre végétale. Les recouvrements et leurs fonctions sont décrits dans le chapitre 4. Pour finir, environ 1000 instruments hydrogéologiques (e.g., sondes de teneur en eau et de succion, capteurs d'oxygène) ont été installés dans les recouvrements pour suivre leur performance en conditions réelles (Canadian Malartic, 2020).

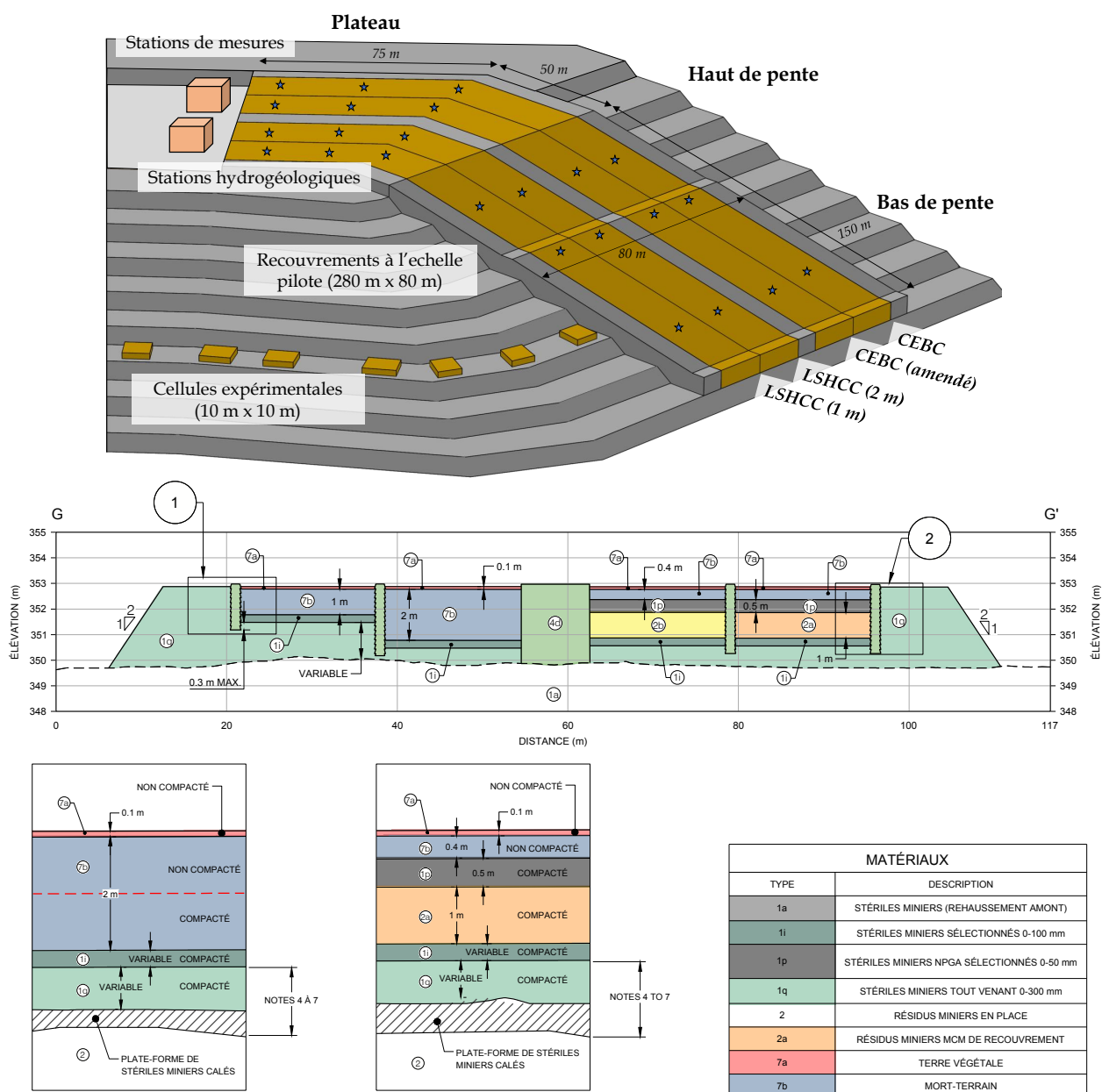


FIGURE 1.5 Schéma simplifié et coupes transversales des recouvrements à l'échelle pilote ayant été instrumentés dans le cadre de cette thèse, tiré de Canadian Malartic (2020).

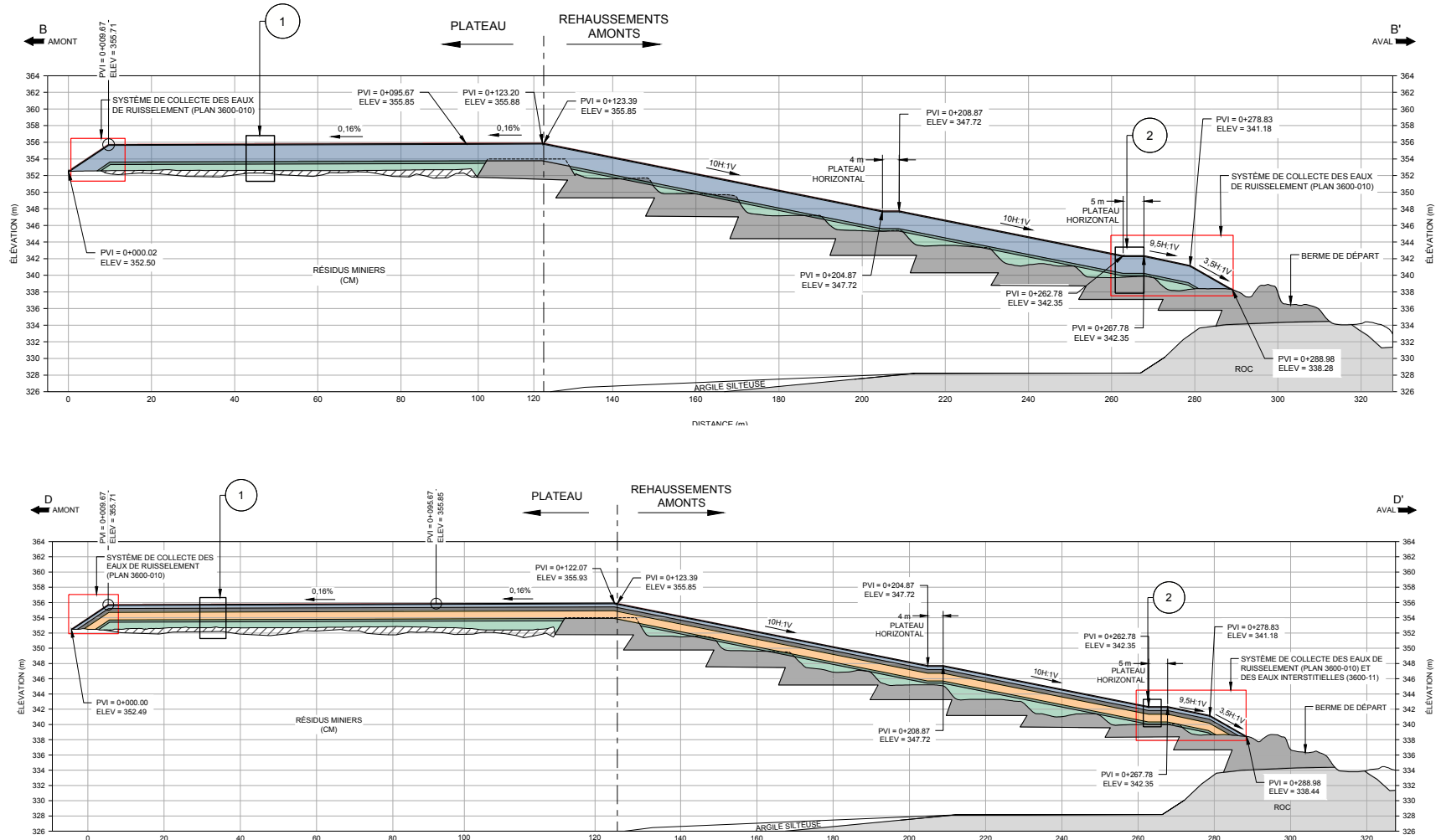


FIGURE 1.6 Coupes longitudinales des recouvrements à grande échelle instrumentés dans le cadre de ce projet de recherche, soit la LSHCC avec une épaisseur de mort-terrain de 2 m (en bleu) et la CEBC avec les résidus non amendés (en orange). Les stériles sont indiqués en gris (bermes) et vert. Schémas préparés par Golder, et tirés de Canadian Malartic (2020).

CHAPITRE 2 REVUE DE LITTÉRATURE :
ARTICLE 1 - A REVIEW ON APPLICATIONS OF TIME-LAPSE
ELECTRICAL RESISTIVITY TOMOGRAPHY OVER THE LAST 30
YEARS : PERSPECTIVES FOR MINING WASTE MONITORING

Adrien Dimech ^{1,3,*}, LiZhen Cheng ^{1,3}, Michel Chouteau ^{2,3}, Jonathan Chambers ⁴,
Sebastian Uhlemann ⁵, Paul Wilkinson ⁴, Philip Meldrum ⁴, Benjamin Mary ⁶,
Gabriel Fabien-Ouellet ² and Anne Isabelle ^{2,3}

Surveys in Geophysics, Volume 43, 1699–1759 (August 12, 2022).

doi : <https://doi.org/10.1007/s10712-022-09731-2>

¹ Université du Québec en Abitibi-Témiscamingue (UQAT), Rouyn-Noranda, QC, Canada

² Polytechnique Montréal, Montréal, Québec, H3T 1J4, Canada

³ Research Institute of Mines and Environment (RIME), Québec, Canada

⁴ British Geological Survey (BGS), Nottingham, NG12 5GG, United Kingdom

⁵ Lawrence Berkeley National Laboratory (LBNL), California, 94720, United States

⁶ Department of Geosciences, University of Padua, Padua, 35122, Italy

Ce chapitre vise à effectuer une revue de littérature portant sur l'application de la méthode de tomographie de résistivité électrique au contexte des rejets miniers. Deux bases de données d'articles publiés entre 1990 et 2020 ont été constituées par cette étude, la première portant sur l'application de la méthode électrique au suivi temporel pour différents types d'application, la deuxième portant sur l'application de la méthode électrique (suivi temporel ou non) exclusivement dans le contexte des rejets miniers. Cette revue est importante pour (i) poser les bases théoriques nécessaires et identifier les meilleures approches méthodologiques, (ii) dresser un historique de la méthode électrique et établir les plus récents développements qui seront pertinents pour la réalisation des travaux et (iii) identifier les principaux avantages et défis de l'approche électrique appliquée au contexte du suivi des rejets miniers.

2.1 Abstract

Mining operations generate large amounts of wastes which are usually stored into large-scale storage facilities which pose major environmental concerns and must be properly monitored to manage the risk of catastrophic failures and also to control the generation of contaminated mine drainage. In this context, non-invasive monitoring techniques such as time-lapse electrical resistivity tomography (TL-ERT) are promising since they provide large-scale subsurface information that complements surface observations (walkover, aerial photogrammetry or remote sensing) and traditional monitoring tools, which often sample a tiny proportion of the mining waste storage facilities. The purposes of this review are : (i) to understand the current state of research on TL-ERT for various applications ; (ii) to create a reference library for future research on TL-ERT and geoelectrical monitoring mining waste ; and (iii) to identify promising areas of development and future research needs on this issue according to our experience. This review describes the theoretical basis of geoelectrical monitoring and provides an overview of TL-ERT applications and developments over the last 30 years from a database of over 650 case studies, not limited to mining operations (e.g., landslide, permafrost). In particular, the review focuses on the applications of ERT for mining waste characterization and monitoring and a database of 150 case studies is used to identify promising applications for long-term autonomous geoelectrical monitoring of the geotechnical and geochemical stability of mining wastes. Potential challenges that could emerge from a broader adoption of TL-ERT monitoring for mining wastes are discussed. The review also considers recent advances in instrumentation, data acquisition, processing and interpretation for long-term monitoring and draws future research perspectives and promising avenues which could help improve the design and accuracy of future geoelectric monitoring programs in mining wastes.

2.2 Introduction

Large volumes of wastes are produced as a result of mining and overburden removal, and during the processing of ore (Nassar et al., 2022). Figure 2.1 presents a simplified mass balance of mining wastes for a gold open-pit operation with an average grade of 1 g/ton. In this example, two tons of waste rocks are extracted from the open pit and stored into waste rock piles (WRP) in order to reach and extract one ton of ore. The ore is then crushed into fine particles, mixed with one ton of water to concentrate and extract one gram of gold. The remaining two tons of crushed rocks and water are called tailings and are generally pumped into tailing storage facilities (TSF) (Bussière and Guittonny, 2021a). Although other types of mining operations generate less mining wastes (e.g., underground mining), this example

illustrates that for most mineral deposits, more than 99 % of the rocks extracted from large-scale and low-grade open-pit operations would be stored either in WRPs or TSFs (Vriens et al., 2020a).

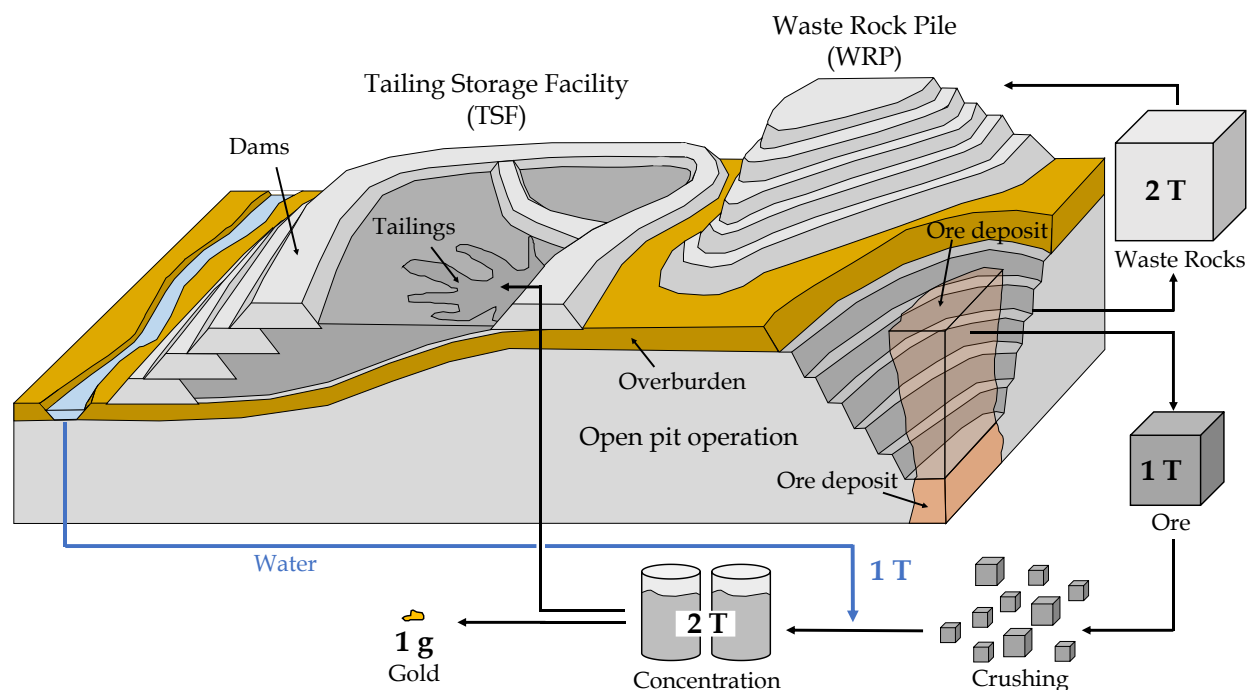


FIGURE 2.1 Diagram of an open-pit mine operation and simplified mass balance of wastes and minerals.

From a global point of view, it is estimated that between 29 000 and 35 000 active and inactive TSFs contain over 200 billion tons of tailings worldwide (World Mine Tailings Failures database, **WMTF**). In Canada alone, the **Global Tailings Portal (GTP)** program initiated in 2019 reports more than 200 TSFs which contain approximately 4.5 billion tons of tailings (data accessed on October 2021). Although these programs provide for the first time free access to searchable databases of mining wastes worldwide, they might not include all mining sites (e.g., orphaned mines or unregistered active mines) and do not provide information concerning the surface area occupied by mining wastes, which is a key aspect for the assessment of mining operations environmental legacy (Bussière et al., 2021).

We have compiled a specific database to address these limitations and estimate the surface of mining wastes in Canada with Google Earth satellite imagery. Figure 2.2 shows the distribution of most Canadian mining operations (both active and inactive), and the estimated surface of TSFs, WRPs and open-pits. The mining sites have been identified from the **GTP** and several other sources including Canadian National Pollutant Release Inventory (**NPRI**), United States Geological Survey (**USGS**) and International Commission on Large

Dams (ICOLD) databases. In total, the 200 TSFs, 185 WRPs and 200 open-pits identified across Canada cover approximately 1 500 km², 600 km² and 500 km² respectively. These mining waste storage facilities can reach large dimensions (70 TSFs exceed 100 m in height worldwide) (Kossoff et al., 2014), cover large surfaces (20 TSFs and 15 WRPs exceed 10 km² in Canada) (Bussière and Guittonny, 2021a) and have even been described as "the largest man-made structures on earth" by some authors (Bowker and Chambers, 2015; Lyu et al., 2019b; Owen et al., 2020).

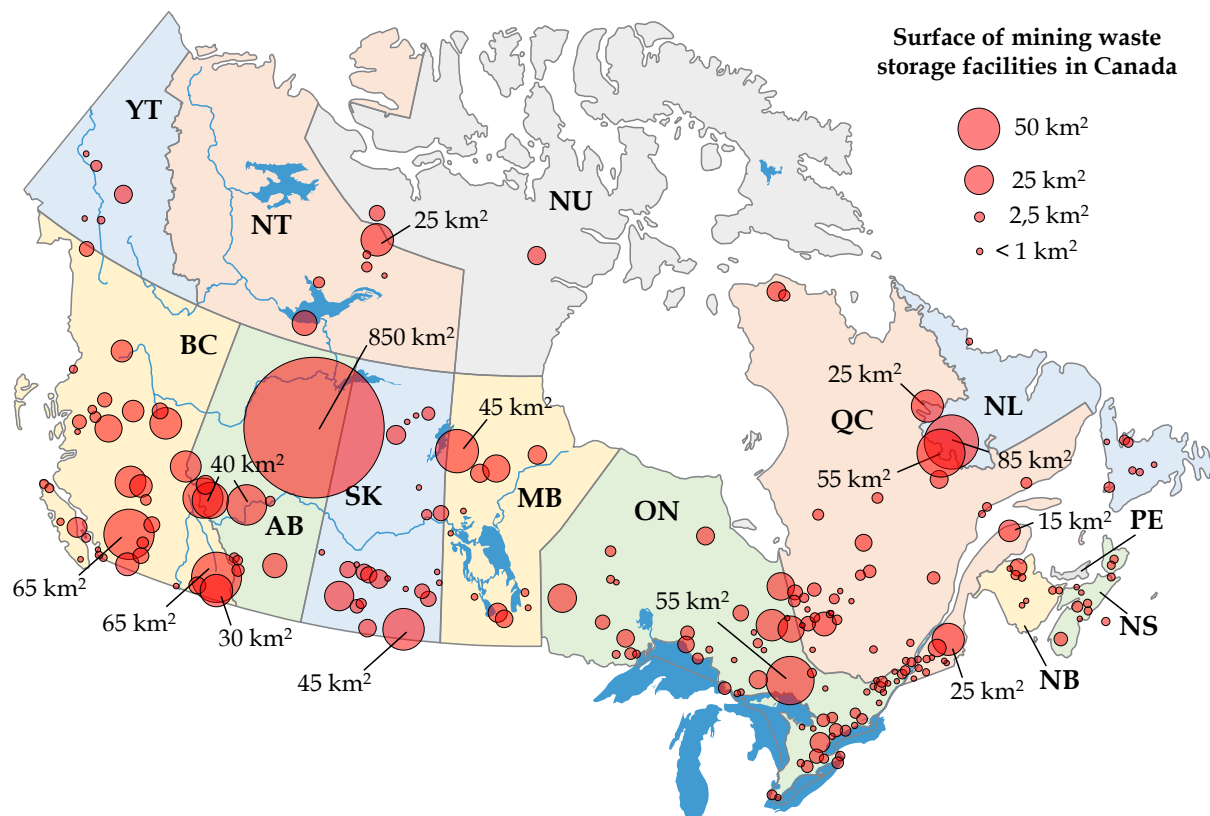


FIGURE 2.2 Distribution and surface of mining waste storage facilities across Canada in 2020. Each mining site in Canada (active, closed or abandoned) has been identified and the areas occupied by TSFs, WRPs and open-pits have been calculated with Google Earth satellite imagery. The database and interactive maps can be accessed and downloaded through the **supplementary material webpage**.

Although increasing efforts are being made toward the recycling of non-renewable mineral resources, the growing need for base and precious metals from both developed and developing countries as well as the energy transition requires the development of existing mining operations and the exploitation of new deposits (Vriens et al., 2020a; Bussière and Guittonny, 2021a). However, a global depletion of ore grades has been observed worldwide for various

metals over the last ten years since most high-grade deposits have already been mined out (Mudd, 2007; Calvo et al., 2016). In the meantime, recent technological advances in milling and concentration processes have decreased the cost of large-scale mining operations (Rötzer and Schmidt, 2018; Bussière and Guittonny, 2021a). As a result, the global trend is toward larger-scale and lower-grade deposit exploitation, which increases the generation of mining wastes (Kossoff et al., 2014; Chambers, 2016). In practice, 40 to 50 billion tons of tailings are expected to be generated over the next five years, which would represent an increase of nearly 25 % of the current TSFs capacity worldwide by 2025 (**WMTF**) and a similar increase could be expected for WRPs.

As reported by Bussière (2007), "the safe disposal of [mining wastes] is certainly one of the most important environmental challenges for the mining industry". This can be explained by two major aspects; the physical and the geochemical stability of both tailings and waste rocks. From the geotechnical perspective, the poor mechanical properties of tailings (fine particles initially saturated) increase the risk of TSF failures if the containment dams are poorly designed and/or exposed to extreme conditions (earthquakes, landslides or heavy rains) (Azam and Li, 2010; Bowker and Chambers, 2015). In recent years, several catastrophic TSF failures have been reported worldwide, claiming hundreds of lives, displacing thousands of families and releasing hundreds of million tons of tailings into the environment, with an average estimated cost of over \$500 million USD per failure (Rotta et al., 2020; Clarkson et al., 2021). From the geochemical perspective, the generation of contaminated drainage from mining wastes has been recognized as a potential threat to the environment since Georgius Agricola's book in 1556 entitled *De re metallica* (Agricola and Hoover, 1556/1912), and has been intensively studied worldwide since the 1970s (e.g., Blowes et al. (2003); Nordstrom et al. (2015)), especially in recent years (Aznar-Sánchez et al., 2018; Tomiyama and Igarashi, 2022). Acid mine drainage (AMD) is generally caused by the oxidation of sulfides (e.g., pyrite or pyrrhotite) present in the waste rocks or tailings when the mining wastes are exposed to water and oxygen flows from the atmosphere (Plante et al., 2021b). Sulfide oxidation generates acidity, and thus decreases pH below 7 to extremely low values (even negative), which in turn increases the solubility of most metal species (e.g., Nordstrom et al. (2000)). When the oxidation process is poorly controlled, AMD can have a significant impact on groundwater quality in nearby ecosystems and may extend to distances if acidic waters discharge into water streams (Blowes et al., 2003; Rezaie and Anderson, 2020). AMD can be responsible for making both surface and groundwater unsuitable for the use of plants, animals and humans, causing diseases and disorders (e.g., Rotta et al. (2020)).

As discussed by Wilson (2021), the recent TSF failures have generated an unprecedented

response in the global mining community, from shareholders, stakeholders to governmental legislation including public opinion. As a result, more efforts have been directed toward innovative construction designs that would increase TSF geotechnical stability such as the inclusion of waste rocks within TSFs (James et al., 2013) or the use of dry tailings to favor unsaturated conditions and reduce the risk of liquefaction (Bussière, 2007; Wilson, 2021). In the meantime, different reclamation approaches have been proposed to reduce the economic and environmental burden that AMD-generating TSFs and WRPs represent for communities, governments and taxpayers (Bussière and Guittonny, 2021a; Madejón et al., 2021). Among other techniques, the construction of multi-layer covers on WRPs or TSFs to reduce water and/or oxygen flows towards the reactive mining wastes is particularly promising. Indeed, such reclamation approaches allow controlling at the source the long-term generation of contaminated drainage and to reuse mining wastes (Park et al., 2019; Vriens et al., 2020a).

Although "conservative design and diligent operation" of TSFs and WRPs are critical for ensuring both geotechnical and geochemical long-term stability, Hui et al. (2018) stressed the need for "continuous, efficient and cost-effective monitoring" of these large-scale structures, before and after mine closure. As discussed by Clarkson and Williams (2020), real-time monitoring of TSF geotechnical stability allows for a better characterization of potential internal deformations, water table elevation in the tailings as well as abnormal seepage. Such monitoring enables TSFs operators to take the possible measures to mitigate the consequence or even interrupt the deterioration before failure occurs (Hui et al., 2018; Clarkson et al., 2021). From the geochemical stability perspective, three types of processes can diminish the long-term performance of multi-layer covers according to the **MEND** report 2.21.4d (2004). The report identified physical processes (e.g., erosion, extreme precipitations or droughts or freeze/thaw cycles), chemical processes (e.g., mineralogical dissolution or consolidation) and biological processes (e.g., root penetration, root water uptake, burrowing animals or human intervention) (MEND, 2004), all of which can occur both locally or globally, progressively or suddenly (Rykaart et al., 2006). Here again, Bussière et al. (2021) highlighted the need for long-term monitoring of covers for TSFs and WRPs reclamation since a decrease in performance could be detected by a drop or an increase in water content, suction or temperature for instance, which would allow to take actions in the early stages of the tailings oxidation process (Dagenais et al., 2001). As noted by the **MEND** report, there is no clear consensus or legislation regarding the duration of such monitoring programs. However, some mining companies have developed closure standards which specify that the geotechnical and geochemical stability of mining waste storage must be ensured for a 200 to 500 year time frame (MEND, 2004; Bussière and Guittonny, 2021b).

As reported by Hui et al. (2018), the conventional monitoring techniques used to assess the stability of WRPs and TSFs can be classified into two categories; surface observations and point sensing (Hui et al., 2018). Surface observations provide detailed information over large-scales, but only skin deep (e.g., visual inspections, satellite imagery for moisture content and aerial photogrammetry, interferometric synthetic aperture radar - InSAR or light detection and ranging - LIDAR for surface deformations) (Smethurst et al., 2017; Clarkson and Williams, 2020). On the contrary, point sensing instruments are generally installed within TSFs and WRPs to monitor a physical property, but only with a limited volume of investigation, typically of a few centimeters around each sensor (e.g., geodetic systems for ground displacement, piezometers for pore-water pressure, hydrogeological sensors for moisture content, suction or temperature) (Hui et al., 2018; Bussière et al., 2021). Generally, several monitoring stations (e.g., using vertical profiles of point sensors) are placed at critical locations to monitor the stability of WRPs or TSFs under various conditions (MEND, 2004; Bussière et al., 2021). Although there is no single rule for the number of instruments needed, it is generally established that a dense network of instruments is needed to cover a representative area of mining waste storage facilities (MEND, 2004). As discussed by Bussière et al. (2021) and Rykaart et al. (2006) such a monitoring approach can represent significant costs given the spatial extent of TSFs and WRPs.

The recent reviews from Loke et al. (2013), Binley et al. (2015b) and Slater and Binley (2021) have highlighted the emergence of time-lapse electrical resistivity tomography (TL-ERT) as a promising technique for monitoring of various subsurface processes across multiple scales. This non-destructive imaging approach has been combined with surface observations and point sensors measurements for long-term monitoring of landslides (Whiteley et al., 2019), permafrost (Mollaret et al., 2019), infrastructure (Chambers et al., 2014b) and many other fields (Falzone et al., 2019). Although several other geophysical methods such as self-potential (Jougnot et al., 2015; Soupios and Kokinou, 2016), induced polarization (Abdulsamad et al., 2019; Saneiyani et al., 2019), active and passive seismic (Grandjean et al., 2009; Olivier et al., 2017) or ground-penetrating radar (Steelman et al., 2017; Giertzuch et al., 2021) have been applied in similar contexts, the focus of this review is on TL-ERT since this technique is cost-efficient, robust and readily deployable for large-scale monitoring. Furthermore, TL-ERT is one of the most well understood near surface geophysical techniques, and is particularly sensitive to moisture driven processes, which play a key role in mining waste stability.

In the context of mining wastes monitoring, TL-ERT could be applied as a complementary method to extend traditional measurements, thus reducing the number of conventional sensors needed for large-scale TSFs and WRPs while increasing the volume of investigation for

long-term stability monitoring programs (Bussière et al., 2021). Although several examples have been reported in the literature (e.g., Dimech et al. (2019); Tresoldi et al. (2020a)), the relative scarcity of studies using TL-ERT for mining wastes monitoring is surprising given (i) the critical need for efficient long-term and large-scale monitoring techniques in WRPs and TSFs, (ii) the numerous applications of static ERT imaging in this domain reported by the review from Martinez-Pagan et al. (2021), and (iii) the recent developments which have improved TL-ERT for long-term remote monitoring of various subsurface processes (Binley and Slater, 2020; Slater and Binley, 2021).

In this regard, the present review summarizes the state of the art and the development of time-lapse ERT over the last 30 years. A database of TL-ERT studies since 1990 is used to identify and describe the different types of application, and review the recent developments that made TL-ERT a recognized and complementary tool for long-term remote monitoring. In the meantime, a database of studies using ERT for mining waste characterization and monitoring allows to identify promising avenues for long-term monitoring of TSFs and WRPs. The article reviews some lessons learned from three decades of TL-ERT development in other domains. Finally, suggestions are proposed to overcome the challenges that could arise from a more widespread application of TL-ERT for long-term mining waste monitoring. In particular, several research perspectives are suggested to improve the accuracy of future ERT monitoring programs and upscale stability assessment in mining waste storage facilities.

2.3 Monitoring subsurface processes with TL-ERT

2.3.1 Objectives of TL-ERT

Electrical conductivity (EC in S/m) (or its inverse electrical resistivity ER in Ωm) describes the ability of a medium to conduct electrical current under a given electrical field (Samouëlian et al., 2005). Three electrical conduction modes can contribute to the porous medium EC (Revil et al., 2012; Corwin and Scudiero, 2019) :

- **Electrolytic conduction** is caused by the displacement of ions present in the interstitial fluid (Revil et al., 2014) and is a major contribution for ionized fluids (e.g., saline water). It can be negligible for low-porosity media, low ion content fluids (e.g., pure water) or frozen fluids.
- **Surface conduction** occurs at the surface of solid grains due to the accumulation of ions in the electrical double layer surrounding each grain. Surface conduction can be a major contribution to the total conduction when the medium contains clay particles (Revil et al., 2012).

- **Solid matrix conduction** is caused by the displacement of mobile electrons within solid grains and is negligible for most rocks and soils which do not contain metallic particles (Rhoades et al., 1989).

Since the electrical conductivity of a medium depends on many parameters (e.g., water content, temperature and ionic content of the interstitial fluid), it can be used as a proxy to image various subsurface processes (Falzone et al., 2019). Several reviews present the physical parameters affecting porous medium EC such as Friedman (2005) and Samouëlian et al. (2005). Corwin and Scudiero (2019) also reviewed many published studies using EC to image (a) water content, (b) pore fluid composition (salinity, ion content and pH), (c) solid matrix properties (grain size, mineralogy and compaction), (d) temperature and (e) organic materials. Moreover, they provided a review of the relationships found in the literature to link EC with these key parameters (referred to as petrophysical relationships).

Arguably, the semi-empirical Archie’s law (Archie et al., 1942) is the most commonly used petrophysical relationship to link electrolytic conduction σ_{el} , pore fluid EC σ_{w} , saturation S_{w} and porosity ϕ :

$$\sigma_{\text{el}} = \sigma_{\text{w}} \cdot \phi^m \cdot S_{\text{w}}^n \quad (2.1)$$

where m and n are respectively the cementation and the saturation exponents, related to the pore structure, tortuosity, connectivity and fluid properties (Glover, 2009). Other popular models based on Archie’s law also incorporate surface conduction and solid matrix conduction such as Waxman-Smits relationship (1968) (Waxman and Smits, 1968) or the Generalized Archie’s Law (Glover, 2010). Notably, the latter has been applied to estimate moisture content in mine tailings from bulk EC (Mollehuara-Canales et al., 2020).

ERT allows imaging of the ER distribution of the subsurface with electrodes inserted in the ground. Two electrodes are used to transmit current and two potential electrodes measure the resultant voltage, which depends on the subsurface resistivity distribution (Lesmes and Friedman, 2005). Many measurements are made using different combinations of current and potential bipoles. The resulting data set is then inverted to recover a distribution of electrical resistivity (see Section 2.3.3 for details on ERT inversion). At the end of the inversion procedure, the resistivity distribution obtained is consistent with the measured data. This distribution is assumed to be representative of the true subsurface resistivity distribution, subject to limitations of a priori assumptions, data and modeling errors, model resolution and non-uniqueness (Whiteley et al., 2019).

As reported by Binley and Slater (2020), the first application of resistivity measurements for

subsurface investigation dates back to Conrad Schlumberger’s work in the 1910s (Schlumberger, 1920). Since then, resistivity measurements have been used to recover (i) one-dimensional (1D) vertical electrical soundings with four electrodes using different spacing in the 1920s, (ii) two-dimensional (2D) profiles of resistivity using linear arrays of electrodes installed at the surface in the 1960s and (iii) three-dimensional (3D) images using several parallel linear arrays of surface or borehole electrodes in the 1970s (Binley and Slater, 2020) and more complex 3D arrays since the 2000s (e.g., Star array (Clément et al., 2010; Rucker, 2015) and L-array (Tejero-Andrade et al., 2015)). Since the 1990s, subsurface monitoring has been conducted by time-repetitive ERT imaging at the same location (Singha et al., 2015). This approach, referred to as TL-ERT, is used to recover spatio-temporal changes in medium ER, and to monitor various dynamic processes such as tracer migration (Perri et al., 2012), water infiltration (Hübner et al., 2017), root water uptake (Mary et al., 2020), permafrost dynamic (Uhlemann et al., 2021) or geothermal operations (Robert et al., 2019).

Figure 2.3 illustrates a TL-ERT survey used to monitor tracer flow in a medium (based on Singha et al. (2015)). The first panel represents the initial tracer distribution. Assuming that the tracer resistivity is different from the initial pore fluid resistivity, the evolution of tracer concentration causes changes in the medium resistivity as shown on the second panel. Several ERT snapshots can then be obtained with surface and/or borehole electrodes remaining at the same position during a period of time. The third panel illustrates the time-lapse inversion results : the medium resistivity distribution is reconstructed for a discretized medium at the measured time steps. Finally, the tracer concentration can be estimated from the inverted resistivity distribution using a petrophysical relationship such as Archie’s law (Equation 2.1) assuming that pore fluid resistivity is the only parameter changing over time and that there is no matrix or mineral surface conductance (fourth panel).

2.3.2 Key parameters of TL-ERT surveys

Each TL-ERT monitoring survey can be described by several key parameters which are divided into two categories : the spatial and the temporal parameters illustrated in Figure 2.4. As discussed by several authors (e.g., Rucker (2014); Tildy et al. (2017)), such parameters should be appropriately determined for each specific field site objectives as well as for each subsurface process that is to be monitored. The spatial parameters on the left part of Fig. 2.4 include (i) the spatial extent, (ii) the depth of investigation and (iii) the spatial resolution. The temporal parameters on the right part of Fig. 2.4 are (i) the monitoring period and (ii) the temporal resolution (Friedel, 2003). Following the example of Rucker (2014), a brief description of each of these spatio-temporal parameters is proposed below.

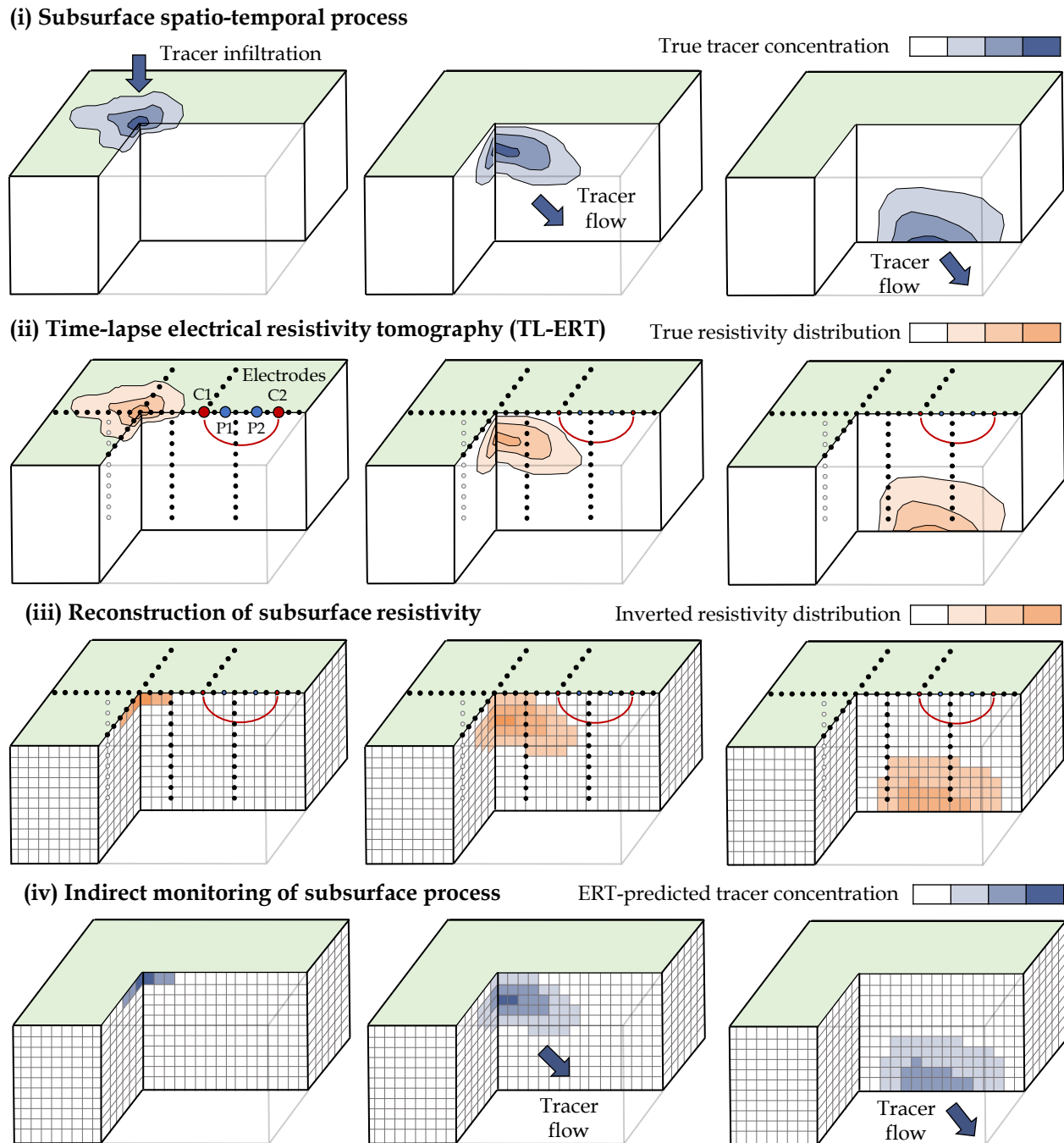


FIGURE 2.3 Example of TL-ERT monitoring of a tracer infiltration with surface and borehole electrodes. (i) Top panel shows the true spatio-temporal distribution of tracer concentration in the medium, (ii) medium panel presents the corresponding distribution of electrical resistivity and (iii) the inverted distribution of resistivity obtained from TL-ERT monitoring. Finally, (iv) bottom panel shows the ERT-predicted tracer concentration using petrophysical relationship (based on Singha et al. (2015)).

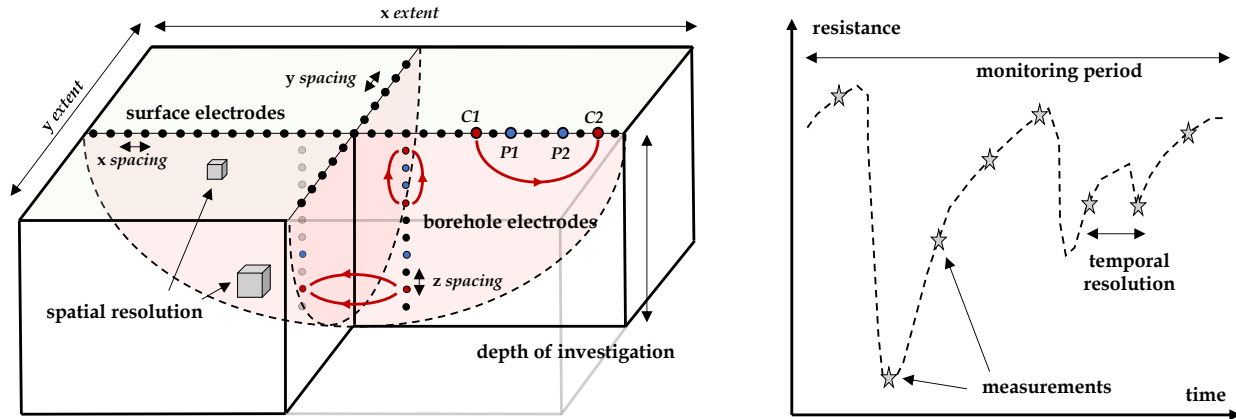


FIGURE 2.4 Spatio-temporal parameters of TL-ERT surveys (inspired from Rucker (2014))

- **Spatial extent** describes the dimension of the investigated area (x and y extent) and is determined by electrode positions (i.e. geometry of the electrode layout, number of electrodes and x , y spacing). The spatial extent of a TL-survey can range from a few centimeters for laboratory experiments (Corona-Lopez et al., 2019) to hundreds of meters for large-scale surveys (Uhlemann et al., 2017b).
- **Spatial resolution** refers to the dimension of the smallest resistivity anomaly that can be imaged by ERT. Although explicitly calculated by some studies (e.g., Friedel (2003)), spatial resolution is generally assessed with sensitivity distribution and depends on electrode spacing, electrode positioning (e.g., surface or borehole electrodes (Singha et al., 2015)) and measurement protocols (Stummer et al., 2004).
- **Depth of investigation (DOI)** corresponds to the depth below which changes of resistivity in the medium would not affect the measurements (Oldenburg and Li, 1999) (i.e. z extent of the survey). DOI is determined by spatial extension and measurement protocols (Samouëlian et al., 2005) and can be either explicitly calculated (Oldenburg and Li, 1999), assessed from sensitivity distribution (Carey et al., 2017) or from basic rules of thumbs (Henderson et al., 2010; Greggio et al., 2018).
- **Monitoring period** represents the duration of the time-lapse survey (i.e. time difference between the first and the last ERT snapshot). Monitoring periods found in the literature vary from a few hours for short surveys (Kuras et al., 2009), a few months for seasonal dynamics (Mojica et al., 2013; Jodry et al., 2019) to several years for long-term studies (Caterina et al., 2017; Palis et al., 2017) (e.g., more than 20 years for permafrost monitoring (Mollaret et al., 2019)).

- **Temporal resolution** refers to the fastest dynamic event that can be reconstructed by ERT (i.e. temporal counterpart of spatial resolution). Temporal resolution depends on the ERT measurement rate (e.g., one snapshot per day (Palis et al., 2017)) and the time needed to perform each ERT snapshot. Temporal resolution should be defined appropriately for each TL-ERT survey to avoid motion blur if the process is occurring at a significantly faster rate than the ERT measurement frequency (e.g., quick tracer infiltration (Kuras et al., 2009)).
- **Measurement protocol** corresponds to the ensemble of four electrode measurements used to measure each ERT snapshot. Given the large number of possible configurations (Loke et al., 2013), the measurement should be designed to provide the best trade-off between how many measurements are made for an ERT snapshot (i.e. spatial resolution) and how much time it takes (i.e. temporal resolution) (Wilkinson et al., 2012a).

As discussed by Whiteley et al. (2019), the monitoring strategy is another important parameter describing each TL-ERT survey. Three categories of strategies can be identified in the literature depending on the duration of TL-ERT as well as the type of measurements carried out :

- **Transient measurements** typically involve static ERT measurements repeated after a certain period of time (e.g., one month to one year) to characterize seasonal variations. The measuring devices (cables, electrodes, resistivity meters) are usually installed during a few hours for each snapshot and removed from the field after each acquisition (e.g., Beff et al. (2013); Binley et al. (2015b)).
- **Controlled tests** are usually short monitoring campaigns with high temporal resolution (e.g., one image every hour) which aim to image the medium in response to artificial perturbations (e.g., irrigation (Hardie et al., 2018; Dimech et al., 2019), water depletion due to pumping (Kuras et al., 2009), injection of tracer (Monego et al., 2010)) or natural perturbations (e.g., rain events (Scaini et al., 2017)) .
- **"Semi"-permanent installations** typically use a dedicated measurement system permanently installed on the site during long periods of time (e.g., 1 year or more) with high temporal resolution (e.g., one ERT snapshot per day) (see for instance Chambers et al. (2014b); Mollaret et al. (2019)). This type of installation is usually preferred to monitor long-term and/or slow-changing subsurface processes (Slater and Binley, 2021).

2.3.3 TL-ERT data acquisition, processing and inversion

Figure 2.5 synthesizes graphically ERT field measurements, data filtering and inversion, which are the three main steps used to reconstruct the subsurface distribution of ER at a specific time (i.e. static imaging). Each of these steps is discussed below :

- (i) In the field, each measurement is made using a pair of electrodes transmitting current in the medium and a pair of receiver electrodes measuring the resultant voltage. A dataset \mathbf{d}_{meas} of M resistances is formed by repeating measurements according to strategies outlined above.
- (ii) Once data acquisition is over, the data filtering step is critical to (i) remove measurements from dysfunctional electrodes, (ii) identify and remove outliers in data and (iii) properly assess the error of each measurement, which will be needed during the inversion process.
- (iii) The objective of the inversion is to optimize the distribution of resistivity \mathbf{m} of a discretized medium with N cells by reducing the data misfit $\Phi_d(\mathbf{m})$ between the measured dataset \mathbf{d}_{meas} and a calculated dataset \mathbf{d}_{calc} , obtained by simulating measurements for a ER model.
- (iv) Once the data misfit $\Phi_d(\mathbf{m})$ between measured and calculated voltages reaches the level of noise of the measured data determined at the pre-processing step, the distribution of resistivity of the model \mathbf{m} can be considered as a representative image of the true resistivity distribution.

As reported by Tso et al. (2017), the assessment of measurement errors is a critical step to remove outliers, ensure good results for the inversion process and to carry out uncertainty estimation . Several strategies have been developed for error estimations. (i) Contact resistance tests allow the identification of dysfunctional electrodes and the removal of corresponding measurements (Deceuster et al., 2013). (ii) Stacking errors are obtained by calculating the standard deviation of repeated measurements (within a few seconds), which can be done with most commercial resistivity meters (Day-Lewis et al., 2008). (iii) Repeatability errors can be assessed from several measurements typically separated by a few hours. However, repeatability cannot always be assessed in TL-ERT measurements, especially in the case of imaging rapid processes. Finally, (iv) reciprocal errors are calculated by comparing forward measurements with their reciprocal measurements, which are done by exchanging current and potential electrodes (Tso et al., 2017). Although more time is required for completing forward and reciprocal measurements, this option is generally recommended to identify outliers (i.e. configurations that exhibit more than 5 % of difference between forward and reciprocal

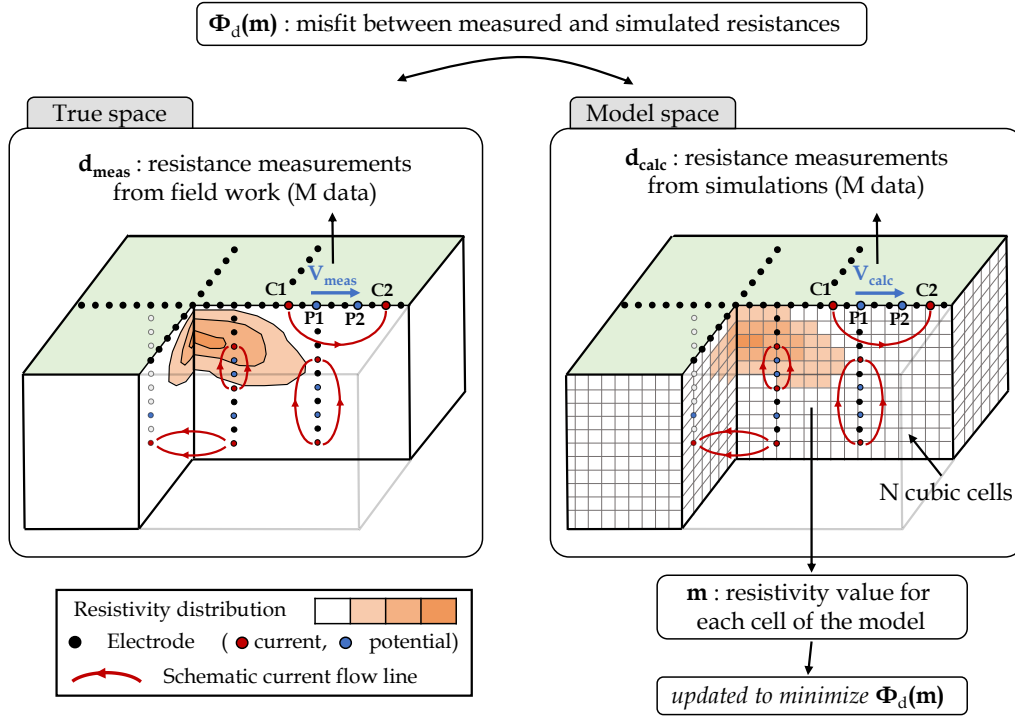


FIGURE 2.5 Diagram of ERT inversion routine used to reconstruct distribution of electrical resistivity ρ

measurements for instance (Chambers et al., 2014b; Tso et al., 2017)) and certain sources of systematic errors. Moreover, this approach provides better estimations of measurement errors, which can be used to define a linear data error model of the form $\epsilon = a + b \cdot \mathbf{d}_{\text{meas}}$, where a and b are two constants (Lesparre et al., 2017; Wagner and Wiese, 2018) (see. Tso et al. (2017) for a review of a and b values found in the literature for data error models).

From a theoretical point of view, \mathbf{d}_{calc} can be calculated by solving Poisson's equation (Dey and Morrison, 1979) in the medium of heterogeneous ER distribution ρ to compute the voltage distribution V caused by a transmitted current I at (x_I, y_I, z_I) for each four-electrodes configuration (Rucker, 2010) :

$$\frac{\partial}{\partial x} \left(\frac{1}{\rho} \frac{\partial V}{\partial x} \right) + \frac{\partial}{\partial y} \left(\frac{1}{\rho} \frac{\partial V}{\partial y} \right) + \frac{\partial}{\partial z} \left(\frac{1}{\rho} \frac{\partial V}{\partial z} \right) = I \delta(x_I) \delta(y_I) \delta(z_I) \quad (2.2)$$

In practice, the forward problem is usually solved with finite element or finite difference methods (Rücker et al., 2006). The forward modeling operation can then be expressed as $\mathbf{d}_{\text{calc}} = \mathbf{G}(\mathbf{m})$, given that \mathbf{m} is the resistivity distribution of the discretized model and \mathbf{G} is the forward operator (Johnson et al., 2012b).

The calculated dataset \mathbf{d}_{calc} is then used to compute the data cost-function Φ_{d} which will be minimized by the inversion procedure. $\Phi_{\text{d}}(\mathbf{m})$ represents the error between \mathbf{d}_{meas} and \mathbf{d}_{calc} for the resistivity distribution \mathbf{m} and is usually expressed by a **L2** norm as :

$$\Phi(\mathbf{m}) = \|\mathbf{W}_{\text{d}} \cdot (\mathbf{d}_{\text{calc}} - \mathbf{d}_{\text{meas}})\|^2 \quad (2.3)$$

where \mathbf{W}_{d} is a data weighting matrix calculated from the measurement errors (Singha et al., 2015; Lesparre et al., 2017). It is worth mentioning that other types of regularization terms can be applied such as the **L1** norm (also referred to as "robust" inversion), which makes the inversion process less sensitive to data outliers (Auken et al., 2006; Day-Lewis et al., 2006).

Generally, the Gauss-Newton scheme is used to update iteratively the resistivity distribution \mathbf{m} to reduce $\Phi_{\text{d}}(\mathbf{m})$. The Gauss-Newton procedure can be divided into three steps as follows (Günther et al., 2006) :

- (i) The model resistivity distribution is initialized to \mathbf{m}_0 , which could be a mean resistivity value or a reference model based on a priori information about the medium (e.g., geological model).
- (ii) The resistivity distribution \mathbf{m}_0 is updated into \mathbf{m}_1 according to $\mathbf{m}_1 = \mathbf{m}_0 + \Delta\mathbf{m}$ where the incremental change of resistivity $\Delta\mathbf{m}$ verifies the normal equation (Günther et al., 2006) :

$$\mathbf{J}^T \mathbf{W}_{\text{d}} \mathbf{J} \cdot \Delta\mathbf{m} = \mathbf{J}^T \mathbf{W}_{\text{d}} \cdot (\mathbf{d}_{\text{calc}} - \mathbf{d}_{\text{meas}}) \quad (2.4)$$

where \mathbf{J} is the Jacobian matrix of size $M \times N$ (also called sensitivity matrix) containing the first-order derivative of the calculated data with respect to model parameters.

- (iii) The same procedure is repeated from the iteration k to the next one by updating resistivity distribution \mathbf{m}_k according to $\mathbf{m}_{k+1} = \mathbf{m}_k + \Delta\mathbf{m}$ until (a) the cost function reduction stagnates (Rucker, 2010) or (b) the cost function $\Phi(\mathbf{m}_{k+1})$ reaches a target value, which typically corresponds to the level of noise of the measured data (Johnson et al., 2012b). As a result, many studies use the target value of $\chi^2 = 1$ as a stopping criterion for the inversion to prevent data overfitting and underfitting (given ϵ the error of the M measured data \mathbf{d}_{meas}) with χ^2 expressed by : (Johnson et al., 2012b)

$$\chi^2 = \frac{1}{M} \sum_{i=1}^M \left(\frac{d_{\text{calc},i} - d_{\text{meas},i}}{\epsilon_i} \right)^2 \quad (2.5)$$

At the end of the inversion procedure, the resistivity distribution obtained is assumed to be the most representative. However, the inverse problem presented above is non-unique and has an infinite number of solutions. Moreover, the resistivity distribution can be unrealistic, especially when a priori information about the medium is known. This issue is solved by adding to the data cost function $\Phi_d(\mathbf{m})$ a model constraint $\Phi_m(\mathbf{m})$ which penalizes unsuitable ER distributions (Günther et al., 2006). The corresponding cost function can be expressed by the following **L2** norm (using Equation 2.3) :

$$\Phi(\mathbf{m}) = \|\mathbf{W}_d \cdot (\mathbf{d}_{\text{calc}} - \mathbf{d}_{\text{meas}})\|^2 + \lambda \|\mathbf{W}_m \cdot (\mathbf{m} - \mathbf{m}_0)\|^2 \quad (2.6)$$

where \mathbf{m}_0 is the reference resistivity distribution, \mathbf{W}_m is the regularization matrix (eg. $\mathbf{W}_m = \mathbf{I}$ if the model \mathbf{m} must be close to \mathbf{m}_0) and λ is a regularization coefficient (Günther et al., 2006). Similarly to Eq. 2.3, while the **L2** norm corresponds to a smoothness regularization, other norms could be applied such as the **L1** norm which favors sharp boundaries to mimic geometrical structures (Loke et al., 2003; Auken et al., 2006) (referred to as "blocky" constraint). As detailed by Johnson et al. (2012), other formulations can be used to ensure maximum, minimum or known resistivities at given locations for example (Johnson et al., 2012b). Although these model constraints are necessary to regularize the inversion results and respect a-priori information, several authors noted the risk of (i) overfitting (i.e. fitting data too well subject to model simplifications (Johnson et al., 2012b; Wagner and Wiese, 2018)) and (ii) underfitting (i.e. poor fit between measured and synthetic data due to model constraints that prevent the inversion process from converging towards a suitable resistivity distribution (Tso et al., 2017; Watlet et al., 2018)).

The diagram presented in Figure 2.5 can be extended to image subsurface evolution over time if ERT measurements are repeated several times as shown in Figure 2.3. A set of T datasets $(\mathbf{d}_{\text{meas}}^{t_1}, \dots, \mathbf{d}_{\text{meas}}^{t_T})$ are obtained for measurement times (t_1, \dots, t_T) and inverted to recover the resistivity distributions $(\mathbf{m}^{t_1}, \dots, \mathbf{m}^{t_T})$. As discussed by Hayley et al. (2011), several inversion strategies can be used to image resistivity distribution changes over time.

Independent inversions. Each dataset can be inverted separately using the methodology presented above; the inverted resistivity distributions would then be compared in absolute values, difference values or relative variations from the starting image. Alternatively, the ratio (or the difference) between consecutive datasets can be considered as input data for the inversion; deviation from 1 (respectively 0) in the inverted images would then be interpreted as an increase or decrease of resistivity (LaBrecque and Yang, 2001; Hayley et al., 2011). These approaches are usually referred to as independent inversions (or single snapshot inversions

(Karaoulis et al., 2014)) since the result of one time step is independent from the others.

Time-constrained inversions. More recent time-lapse inversion strategies impose a similarity between consecutive distributions of resistivity to mimic smooth evolution in time of the medium and discard non-realistic changes of resistivity (Hayley et al., 2011). By analogy with the model constraint presented in Eq. 2.6, the time constraint $\Phi_t(\mathbf{m}^t)$ can be added to the cost function $\Phi(\mathbf{m}^t)$ to penalize resistivity distributions \mathbf{m}^t that differ from the previous one \mathbf{m}^{t-1} . The general expression of $\Phi_t(\mathbf{m}^t)$ is (Loke et al., 2014a; Singha et al., 2015) :

$$\Phi_t(\mathbf{m}^t) = \beta \left\| \mathbf{W}_t \cdot (\mathbf{m}^t - \mathbf{m}^{t-1}) \right\|^2 \quad (2.7)$$

where \mathbf{W}_t is the temporal regularization matrix (Hayley et al., 2011). Such a time constraint can be applied (i) to invert individual snapshots by using previous inversion results as reference (referred to as "cascade inversion" (Hayley et al., 2011; Singha et al., 2015)) or (ii) to invert simultaneously all datasets which is referred to as "simultaneous" or "4D" inversion (Kim et al., 2009; Karaoulis et al., 2014) (see Kim et al. (2009), Hayley et al. (2011), Karaoulis et al. (2014) and Loke et al. (2014a) for the explicit formulation of 4D inversion).

As discussed by several authors, the resistivity models obtained from time-lapse inversions often need to be corrected to a standard temperature, typically laboratory temperature or mean annual air temperature (e.g., Brunet et al. (2010); Uhlemann et al. (2016b)). This temperature correction is generally expressed by (Hayley et al., 2010) :

$$\rho_{T_{\text{std}}} = \rho_T \cdot [1 + c \cdot (T - T_{\text{std}})] \quad (2.8)$$

where ρ_T and $\rho_{T_{\text{std}}}$ are respectively the electrical resistivities at temperature T and at T_{std} and c is the fractional change in ρ per degree Celsius. Typically, c values range between $0.018 \text{ } ^\circ\text{C}^{-1}$ and $0.025 \text{ } ^\circ\text{C}^{-1}$ (Hayashi, 2004; Hayley et al., 2007), which means that electrical resistivity decreases by a factor close to 2 % for a temperature increase of $1 \text{ } ^\circ\text{C}$ in the medium (Besson et al., 2008; Chambers et al., 2014b). As noted by Uhlemann et al. (2016b), the temperature correction is critical for long-term TL-ERT surveys to correct inversion results for seasonal and diurnal variations of temperature, and avoid misinterpretation of resistivity data.

2.4 Review of TL-ERT applications over the past 30 years

2.4.1 TL-ERT studies over the last 30 years

Several insightful reviews have been dedicated to TL-ERT monitoring over the past 30 years. Samouëlian et al. (2005) established the first review of TL-ERT applications for soil sciences, stressing its strong potential as a non-destructive and large-scale monitoring technique. Slater (2007) described the relationships between electrical and hydrogeological properties of the medium and presented a review of TL-ERT studies to characterize aquifers. Kneisel et al. (2008) reviewed different geophysical methods for permafrost investigations and highlighted the emergence of autonomous TL-ERT as a promising tool for long-term monitoring. Finally, Robinson et al. (2008b) also described the development of TL-ERT applications to bridge the gap between point measurements and large-scale moisture content monitoring from surface techniques (walkover, aerial photogrammetry or remote sensing).

From 2012 to 2015, five well-known reviews have been published to present the developments and perspectives of TL-ERT for subsurface monitoring. Loke et al. (2013) presented a comprehensive overview of measurement system developments, optimized field acquisition methods (2D, 3D and 4D) and data processing techniques. The emergence of hydrogeophysics as a powerful monitoring tool across multiple scales was also discussed by Revil et al. (2012), Binley et al. (2015b) and Parsekian et al. (2015). Finally, Singha et al. (2015) published a review describing the geoelectrical monitoring method, from field measurements to data interpretation with various examples of applications .

Since 2014, more than 20 reviews have been published for TL-ERT applications to specific fields such as landslides monitoring (Whiteley et al., 2019; Perrone, 2020), ecological applications (e.g., root propagation or water uptake) (Zhao et al., 2019; Cimpoiășu et al., 2020), geothermal applications (Hermans et al., 2014), salinity issues (e.g., saline intrusion) (Costall et al., 2018; Corwin and Scudiero, 2019), infrastructure, buildings or landfill monitoring (Romero-Ruiz et al., 2018; Dezert et al., 2019), groundwater-surface water interactions (McLachlan et al., 2017; Fan et al., 2020) or bioremediation monitoring (Johnson et al., 2015). Falzone et al. (2019) provided a comprehensive review of TL-ERT studies for multiple domains of geosciences involving fluid dynamics monitoring (e.g., hydrogeology, gas flows and contaminant migrations). Wagner and Uhlemann (2021) recently published a review on multi-method geophysical imaging, highlighting promising approaches for the combination of multiple geophysical datasets (including TL-ERT) and numerical models to obtain quantitative estimates of hydrological parameters. Finally, Slater and Binley (2021) recently published a review focusing specifically on advances and perspectives for long-term monitoring of hy-

drological processes at different scales using TL-ERT.

The present study aims to widen the sphere of these reviews by discussing the strong potential of TL-ERT for mining waste monitoring in the future. A systematic review of TL-ERT applications across various domains from 1991 to 2020 is proposed following the methodology of Aznar-Sánchez et al. (2018) and Zhao et al. (2019). Published studies using TL-ERT (i.e. with at least two ERT snapshots at the same position) have been identified with article searching platforms (Google Scholar, Scopus, Web of Science and Compendex) and the full-texts have been examined to select only the relevant articles. Each relevant article has been classified into the database and its characteristics have been recorded (i.e. year of publication, number of citations, journal, type of application, country, type of TL-ERT measurements, number of electrodes). Finally, the database has been used to classify the different studies and describe the TL-ERT evolution over the past 30 years. A large number of examples of TL-ERT applications in various contexts are used to identify the criteria for success of such TL-ERT surveys. The database is also used to identify the recent developments that could be transferred to future applications of TL-ERT for long-term monitoring of mining wastes. Finally, the present review can serve as a database of TL-ERT studies for various types of application, which can be accessed on the **supplementary material webpage** following the example of the **catalog of agrogeophysical studies** (Blanchy et al., 2020b; Garré et al., 2021; Mary and Blanchy, 2021).

The diagrams presented in Figure 2.6 and 2.7 review the various fields of applications of the TL-ERT studies identified in the database and present the development of TL-ERT for each of these fields. Each article is classified into four types of monitoring (hydro-geothermal, environmental, geotechnical and ecological) which are themselves divided into three types of applications. Two observations can be made from Figure 2.7. On the one hand, the number of publications involving TL-ERT has significantly increased over the past 30 years as reported by the review of Binley et al. (2015b) for hydrogeophysics-related applications. Notably, almost 75 % of TL-ERT studies have been published during the last decade, which denotes TL-ERT development over the past years. On the other hand, TL-ERT has been used for an increasing number of fields of applications. While TL-ERT was mostly applied to hydrogeological studies and contaminant monitoring from 1990 to 2010, new types of applications such as ecological applications, permafrost and landslide monitoring have emerged since then. Finally, the pie chart of Figure 2.7 presents the distribution of the published studies of the database according to the classification of Figure 2.6, highlighting the prominence of hydrogeological and contaminant monitoring applications.

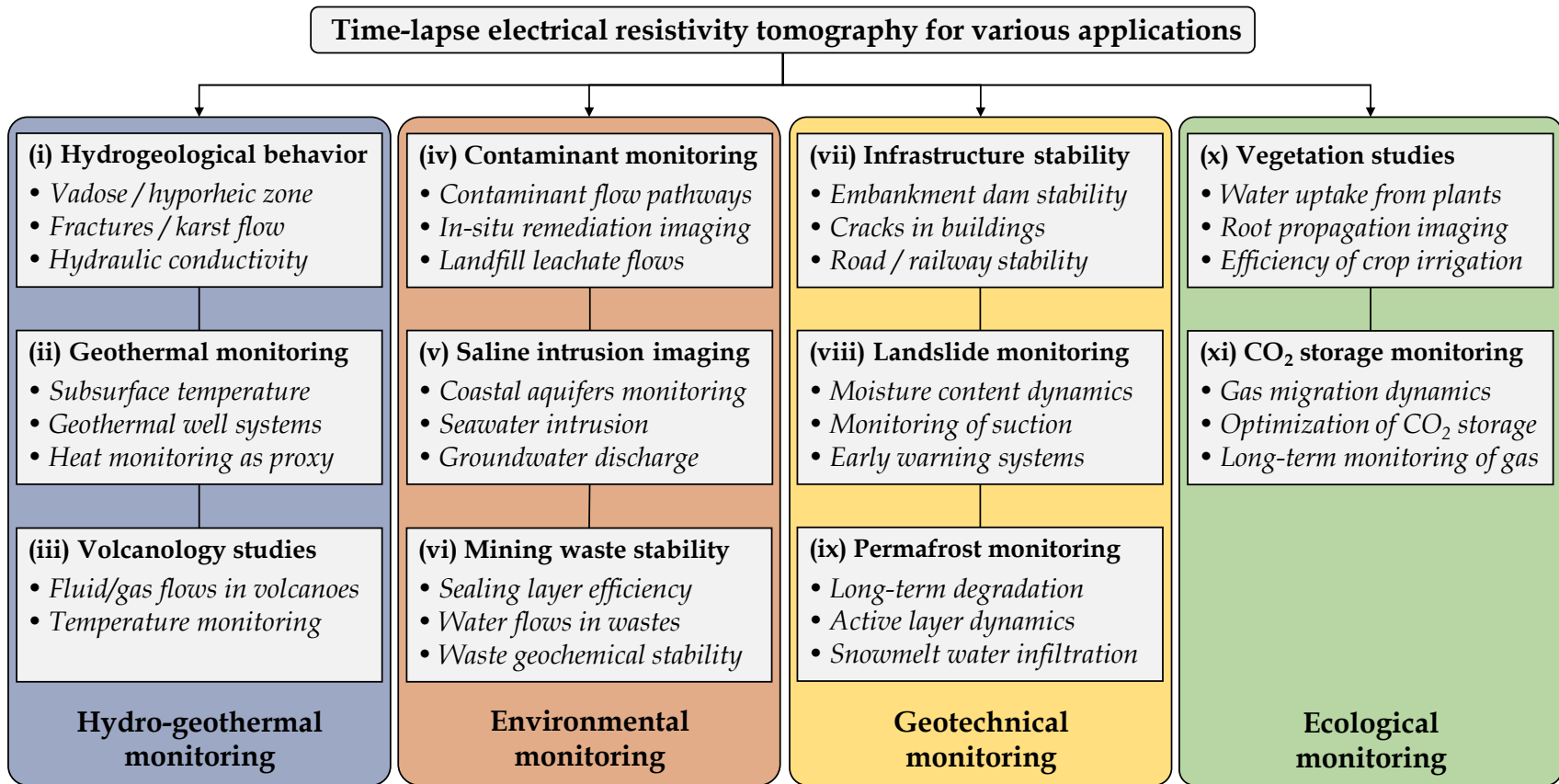


FIGURE 2.6 Review of the main applications of TL-ERT for various domains

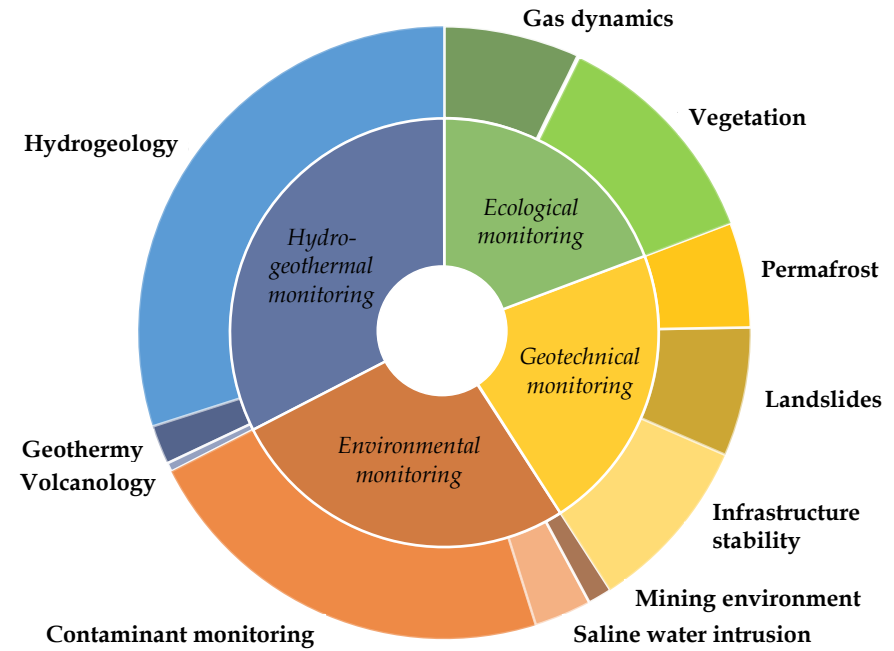
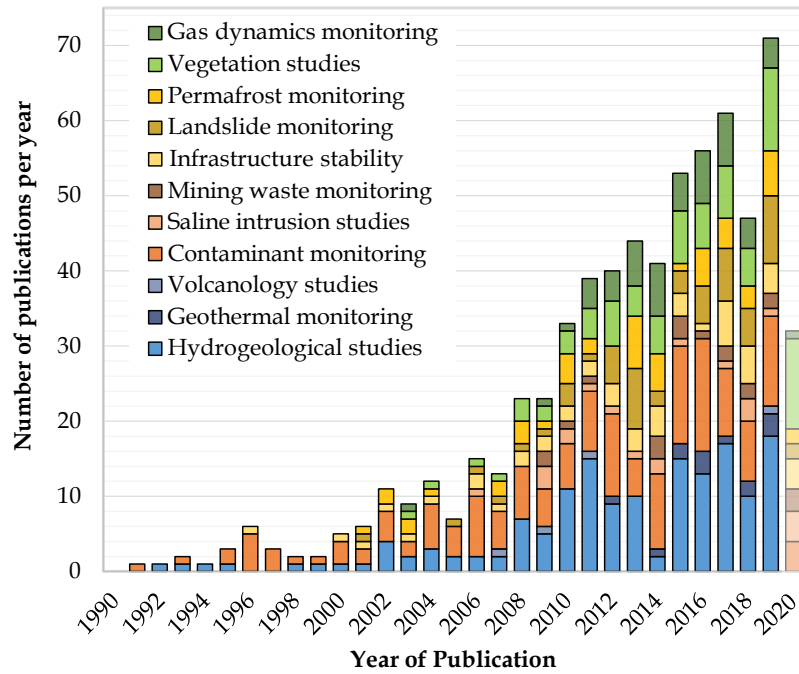


FIGURE 2.7 General statistics for each field of applications identified in the database of TL-ERT studies : (a) evolution of the number of published studies per year from 1991 to 2020 for each type of application and (b) distribution of the 651 published studies according to the classification proposed in Figure 2.6. Note that the identification of TL-ERT studies has been carried out during Summer 2020, which explains the relatively low number of publications identified for 2020 (shaded).

2.4.2 Description of the different fields of applications for TL-ERT

- (i) **Hydrogeological monitoring** corresponds to all applications of TL-ERT used to characterize and monitor the hydrogeological behavior of the subsurface. This field of application accounts for one quarter of the total number of TL-ERT studies in the database and has been a primary application of geoelectrical monitoring from 1990 to 2002 (cf. Figure 2.7). Since 1990, TL-ERT has been used to image water flow in saturated media (e.g., Miller et al. (2008); Busato et al. (2019)), in the vadose zone (e.g., Parsekian et al. (2015); Uhlemann et al. (2016a); Petit et al. (2021)) or in fractured media (e.g., Carriere et al. (2015); Watlet et al. (2018)). While most studies use the relationship between saturation and electrical resistivity to describe qualitatively the medium behavior (see Eq. 2.1) (Hübner et al., 2015; Scaini et al., 2017), TL-ERT is sometimes used to characterize quantitatively the medium parameter distribution over large scales such as hydraulic conductivity for instance (Slater, 2007; Singha et al., 2015).
- (ii) **Geothermal monitoring** is a relatively recent application of TL-ERT, the first occurrence in the literature being studies from Hermans et al. (2012, 2014) on the monitoring of shallow geothermal experiments with TL-ERT. Geothermal monitoring studies aim to recover the spatio-temporal evolution of the subsurface temperature based on its influence on electrical resistivity (see Eq 4.2.) (Hayley et al., 2007; Ma et al., 2011). This application of TL-ERT is experiencing strong growth since 2015 to describe qualitatively the geothermal behavior of a medium (e.g., Giordano et al. (2016); Robert et al. (2019)) as well as to recover quantitative distribution of temperature in various contexts (e.g., Lesparre et al. (2019); Comina et al. (2019)). Recently, Robert et al. (2019) described the potential of temperature monitoring with TL-ERT as a proxy to study other processes (i.e. use of temperature as a tracer).
- (iii) Only a few **volcanology studies** using TL-ERT for volcanoes monitoring have been reported in the literature since 2007. As described by these studies, volcanic activity affects electrical conductivity of the subsurface because of temperature changes, water and gas flows (Turner et al., 2011; Di Giuseppe and Troiano, 2019). Although quantitative integration of geophysical, geochemical and geological monitoring datasets is still a challenge, TL-ERT is considered by these authors as a promising monitoring tool to characterize these complex media and processes (Di Giuseppe and Troiano, 2019).
- (iv) **Contaminant monitoring** refers to all studies using TL-ERT to image the flow of contaminants or tracers which exhibit contrasts of electrical resistivity in comparison

with the in-situ pore fluids (see Eq. 2.1). This type of application accounts for one quarter of the number of TL-ERT studies identified in the database and has been intensively used since the beginning of the 1990s (Bevc and Morrison, 1991; Ramirez et al., 1993). While in most studies, the fluids monitored are more conductive than the surrounding pore fluid (e.g., saline fluids (Singha and Gorelick, 2005; Cassiani et al., 2006), nitrate plumes (Johnson et al., 2012b; Wallin et al., 2013) and leachates from (i) landfills (Audebert et al., 2016; Inauen et al., 2019; Morita et al., 2020), (ii) waste storage ponds (Binley and Daily, 2003; Revil et al., 2013) or (iii) olive-oil industry (Simyrdanis et al., 2018)), some contaminants are known to be more resistive (e.g., fresh hydrocarbon plumes (Deng et al., 2017; Trento et al., 2021)). From 1990 to 2010, a vast majority of studies used TL-ERT monitoring either to detect environmental contaminants plumes (Power et al., 2015; Kuras et al., 2016; Almpanis et al., 2021) or to track tracers injected in the subsurface to study its behavior (Koestel et al., 2009). Moreover, TL-ERT has become increasingly popular since the beginning of the 2010s to (i) assess the efficiency of in-situ remediation in contaminated media (Tildy et al., 2017; Nivorlis et al., 2019) or (ii) track leachate recirculation to enhance waste degradation in landfills (Grellier et al., 2008; Clément et al., 2010).

- (v) **Saline intrusion monitoring** with TL-ERT aims to characterize and monitor the migration of saline seawater to fresh groundwater or vice versa (Costall et al., 2018). This type of application has been reported since the beginning of the 2010s in Spain (Nguyen et al., 2009; Ogilvy et al., 2009), Italy (De Franco et al., 2009) and USA (Henderson et al., 2010). Most of the studies report electrical resistivity contrasts between groundwater and seawater ranging from one to two orders of magnitude (Costall et al., 2018, 2020). Such high contrasts make TL-ERT a suitable tool (i) to monitor seawater intrusion which could lead to groundwater salinization (Chen et al., 2018a; Palacios et al., 2020) and (ii) to characterize submarine groundwater discharge when contaminants flow from land to sea (Henderson et al., 2010; Paepen et al., 2020).
- (vi) **Mining waste monitoring** is a relatively uncommon application for TL-ERT since only 20 studies have been identified in the database (less than 3 %). Use of TL-ERT in this context started to be reported in the literature since the beginning of the 2010s (Anterrieu et al., 2010; Maqsoud et al., 2011). Since then, TL-ERT has been used (i) to monitor leachate flows into heap leaching pads in order to maximize mineral recovery (mostly through the work of Rucker (2015) and Rucker et al. (2014)) and

(ii) to monitor the geotechnical stability of mining waste storage facilities or mining operations (Mainali et al., 2015; Tresoldi et al., 2020c). Although less common, a few studies have used TL-ERT as a tool (i) to characterize the hydrogeological behavior of mining wastes or storage facilities (Greer et al., 2017; Hester et al., 2019) and (ii) to assess the efficiency of reclamation covers designed to reduce the environmental footprint of mining wastes (Maqsoud et al., 2011; Dimech et al., 2019). As discussed in Section 2.5.1, the scarcity of studies using TL-ERT for mining waste monitoring contrasts with the numerous examples of applications of static ERT imaging in this domain (Martinez-Pagan et al., 2021).

- (vii) The potential of TL-ERT for **infrastructure stability** assessment is known since the end of the 1990s with the early study of Johansson et al. (1996) using repeated ERT measurements to monitor the internal erosion and abnormal seepage in dams. Since then, other studies have monitored the increase of electrical resistivity over time in dams or levees as a proxy for voids development due to internal erosion, both at laboratory scale (Shin et al., 2019; Masi et al., 2020) or at field scale (Sjödahl et al., 2008, 2009). Tang et al. (2018) and others applied TL-ERT to evaluate the development of cracks and sinkholes by monitoring the temporal variations of resistivity (Samouëlian et al., 2004; Fabregat et al., 2017). As discussed in the review of Smethurst et al. (2017), TL-ERT is also becoming increasingly popular to monitor abnormal water accumulation, infiltration or seepage in structures since these processes usually correspond to a decrease in ER. Such resistivity anomalies can then be used as a proxy for deterioration of geotechnical stability (i) in earth embankments and levees (Arosio et al., 2017; Tresoldi et al., 2019) (ii) in railway embankments and road structures (Chambers et al., 2014b; Rasul et al., 2018) or (iii) in buildings (De Donno et al., 2017; Voss et al., 2019).
- (viii) **Landslide monitoring** programs have recognized TL-ERT as an efficient, economical and complementary tool since the beginning of the 2000s (Lebourg et al., 2005; Supper et al., 2008). Recently, this type of application has experienced strong growth. Indeed, more than half of the studies identified in the database have been published during the past five years. Nowadays, TL-ERT is considered as one of the most popular geophysical techniques for long-term landslide monitoring and several recent reviews are available in the literature (Whiteley et al., 2019; Perrone, 2020). From a qualitative point of view, TL-ERT has been used as early as 2006 to characterize the internal structure of landslides (e.g., Crawford and Bryson (2018); Huntley et al. (2019)) and to assess their hydrogeological behavior (e.g., Chen et al. (2018a); Peng

et al. (2019)). In addition, many studies have used TL-ERT in a quantitative way since 2015 to recover (i) landslide displacements (Uhlemann et al., 2015; Wilkinson et al., 2016; Boyle et al., 2018), (ii) moisture content distribution (Gunn et al., 2015; Gance et al., 2016; Uhlemann et al., 2017b) and (iii) suction stress distribution (Hen-Jones et al., 2017b; Crawford et al., 2019). As discussed by Whiteley et al. (2019), such applications have a great potential in the future for the understanding of processes that trigger landslide activation (e.g., Uhlemann et al. (2017b); Merritt et al. (2018)), making TL-ERT a promising tool for landslide long-term monitoring and early warning (e.g., Supper et al. (2014); Holmes et al. (2020)).

- (ix) **Permafrost monitoring** with TL-ERT has been reported in the literature since the early 2000s, mostly with the studies of Hauck (2001) and Hauck et al. (2003). The authors identified TL-ERT as a promising and robust method to monitor permafrost dynamics since unfrozen water, ice and air have strong electrical resistivity contrasts that can be well resolved by ERT (Hauck, 2001). Since then, TL-ERT has been used (i) to image the internal structure of permafrost (Fortier et al., 2008; Dafflon et al., 2017), (ii) to track snowmelt infiltration (French and Binley, 2004; Thayer et al., 2018), (iii) to monitor unstable permafrost rock walls (Krautblatter et al., 2010; Keuschnig et al., 2017), (iv) to study the dynamics of freeze-thaw processes in the active layer (Murton et al., 2016; Farzamian et al., 2019) and (v) to monitor long-term permafrost degradation (Mewes et al., 2017; Mollaret et al., 2019). Today, TL-ERT is recognized as a mature, efficient and robust tool for long-term permafrost studies. For instance, some sites in the Alps have been monitored with autonomous remote TL-ERT for more than 20 years (Mollaret et al., 2019; Etzelmüller et al., 2020). Notably, recent developments have focused on quantitative monitoring of ice, water, air and rock content from TL-ERT and seismic monitoring (Wagner et al., 2019; Mollaret et al., 2020) as well as improvement of semi-empirical relationships (Toran et al., 2013; Herring et al., 2019).
- (x) **Vegetation studies** use TL-ERT to monitor the soil-plant-atmosphere interactions from repeated resistivity measurements (Garré et al., 2021). This type of application is known since the beginning of the 2000s with the studies of Michot et al. (2003) and al Hagrey et al. (2004); Al Hagrey (2006). Since then, TL-ERT has become a popular tool in this context. More than 60 % of the 80 studies referenced in the database have been published during the past five years. As described by Garré et al. (2021), many studies have used TL-ERT to monitor the water dynamics around and in the plants at different scales using petrophysical relationships described above (Eq. 2.1) (Mi-

chot et al., 2003). Such applications range from (i) the characterization of root-water uptake (Garré et al., 2013; Dick et al., 2018; Mary et al., 2020), (ii) the circulation of water within trunks and stems (Al Hagrey, 2006; Luo et al., 2019) to (iii) the assessment of water budget for the soil/plant/atmosphere system (Brillante et al., 2015; Cassiani et al., 2016; Vanella et al., 2019). Moreover, TL-ERT has been used for agriculture purposes (i) to monitor water availability for crops (Beff et al., 2013; Brillante et al., 2016a), (ii) to assess the plant response to drought or unconventional irrigation (De Carlo et al., 2019; Carrière et al., 2020) or (iii) to monitor the performance of crop irrigation (Hardie et al., 2018; Vanella et al., 2021). Finally, several studies have used TL-ERT to monitor root propagation, both at the laboratory scale (e.g., Corona-Lopez et al. (2019); Weigand and Kemna (2019)) and in the field (e.g., Mary et al. (2016); Whalley et al. (2017)).

- (xi) **Gas dynamics monitoring** with TL-ERT has been reported since the early 2000s with the study of Ramirez et al. (1993) where the infinite electrical resistivity of gas was used to track carbon dioxide flow inside experimental tanks. Since then, this approach has been popular for various applications as 50 TL-ERT studies have been published since 2010. TL-ERT has been used (i) to monitor induced carbon dioxide flooding during oil extraction (Ramirez et al., 1993; White et al., 2011), (ii) to track gas flows in landfills (Rosqvist et al., 2011), and (iii) to study carbon dioxide or methane migration in the subsurface (e.g., Kremer et al. (2018); Klazinga et al. (2019)). As reported by the review of Bergmann et al. (2016), TL-ERT has also been used as a long-term surveillance tool for carbon dioxide sequestration, for example at the Ketzin CO₂ storage pilot site in Germany (Bergmann et al., 2012; Schmidt-Hattenberger et al., 2016). TL-ERT is promising in this regard since abnormal resistivity increases can be interpreted as CO₂ leaks (Dafflon et al., 2013; Yang et al., 2019).

2.5 Emergence, challenges and perspectives of TL-ERT for mining wastes

2.5.1 Review of promising applications of TL-ERT for mining wastes

Although TL-ERT has been recognized as a valuable tool to provide additional information about subsurface processes in many domains, there are few examples of applications for mining wastes monitoring, either for short or long periods of time. This observation is all the more striking considering (i) the need for efficient mining waste monitoring techniques and (ii) the numerous applications of single-time ERT in mining wastes, as reported by Martinez-

Pagan et al. (2021), the first review of ERT applications in this context. Therefore, the review below aims to identify promising avenues for TL-ERT monitoring of mining wastes.

The methodology presented in Section 2.4.1 has been followed to build a database of published studies using ERT for mining wastes since 1990, with most studies published over the last decade. Figure 2.8 presents the different types of applications of ERT in mining wastes identified from the database. Each study has been classified into six types of applications, themselves classified into three broader domains : waste valorization, waste characterization and waste monitoring. A brief overview of each type of application is proposed below (i) to present the objective of ERT measurements in mining wastes, (ii) to discuss about the advantages and limitations of ERT in each context, and finally (iii) to identify promising applications for TL-ERT monitoring on mining wastes.

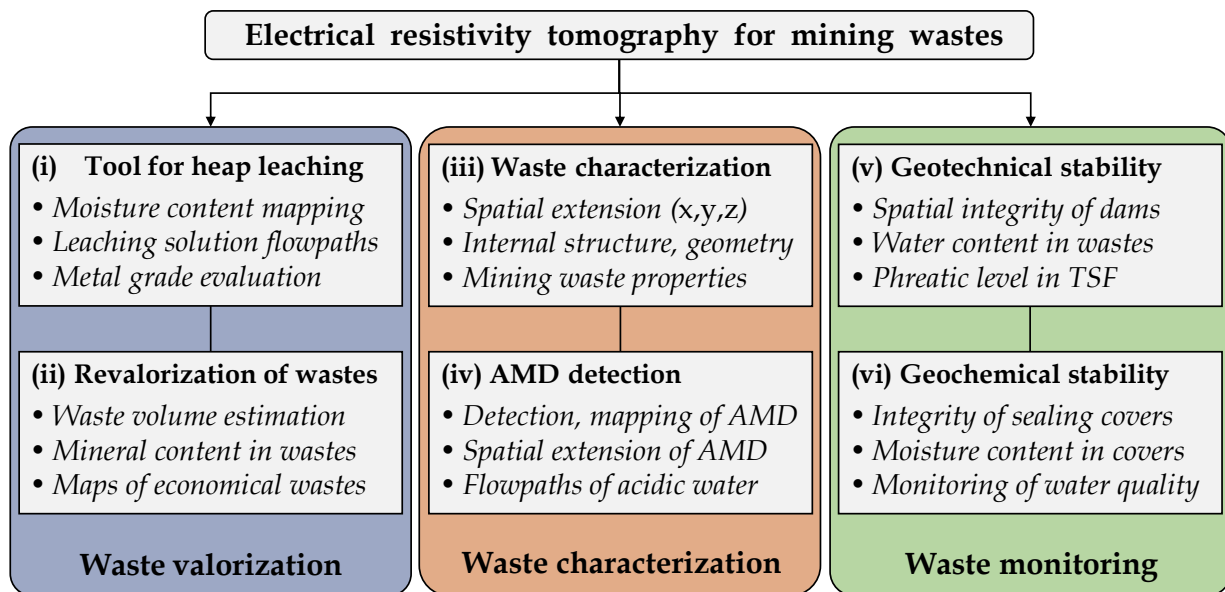


FIGURE 2.8 Review of the main applications of ERT for mining wastes imaging and monitoring

- (i) ERT has been used as a **support tool for mineral extraction** in heap leaching pads (HLP) since the beginning of the 2010s, mostly through the work of Rucker et al. (Rucker et al., 2009a, 2017) (c.f. Table 2.1). As described by Maghsoudy et al. (2019), heap leaching is a common mineral extraction process. Leaching solutions are injected into ore piles to mobilize metals which are then collected through drainage pipe networks (Rucker, 2010). ERT has been applied to track leaching solutions flowpath since these solutions are usually highly conductive (Rucker et al., 2009a; Maghsoudy et al., 2019). As a result, ERT has been used to improve heap leaching

efficiency by (i) imaging heterogeneous water distribution in HLPs (Rucker, 2010), (ii) estimating remaining fractions of metals (Rucker et al., 2009c, 2017) and (iii) evidencing HLP heterogeneity effects on macropore flows, leachate solution accumulation or dry areas (Maghsoudy et al., 2019). These studies provide valuable insights for (i) advanced ERT instrumentation strategies in mining wastes (large-scale imaging (Cubbage et al., 2016; Rucker et al., 2017), borehole-surface layouts (Rucker, 2014)) as well as for (ii) data-processing and interpretation developments for mining waste monitoring (real-time monitoring (Rucker et al., 2014), quantitative interpretation (Rucker, 2010), and complex 3D visualization (Rucker et al., 2017)). Such strategies can be transferable to future studies on WRPs to provide large-scale and non-destructive information that could help (i) to assess their hydrogeological behavior (e.g., Dimech et al. (2019)), (ii) to track meteoritic water flows or tracers within WRP (e.g., Hester et al. (2019)) or (iii) to delineate and monitor acidic water flows within mining wastes (e.g., Bortnikova et al. (2018)).

- (ii) Applications of ERT for **revalorization of mining wastes** have been reported since 2016 with the study from Günther and Martin (2016). The authors used ERT and spectral induced polarization to map mineralized areas in a mining slag heap for potential future mineral reuse (Günther and Martin, 2016). Since then, ERT has been applied to reconstruct the spatial distribution of mining wastes over large scales and estimate the remaining mineralization, both for WRPs (Qi et al., 2018; Martin et al., 2020) and TSFs (Saladich et al., 2016; Martínez-Segura et al., 2020) (c.f. Table 2.2). In most cases, a threshold in electrical resistivity has been defined to delineate the mineralized wastes, which are generally more conductive (Saladich et al., 2016; Martin et al., 2020). Moreover, ERT has been combined with aerial photogrammetry or LIDAR surface topography to recover the volume of mineralized mining wastes (Markovaara-Koivisto et al., 2018; Martín-Crespo et al., 2018). These results are of great interest for the development of circular economy in mining. Indeed, the knowledge about spatial distribution and mineralization is identified as a limiting factor for mining waste reuse as discussed by Kinnunen and Kaksonen (2019). It is worth noting that the methodology followed by these studies could be applied in the future (i) to provide complementary data for systematic geochemical sampling of mining wastes (e.g., Elghali et al. (2019); Gabarrón et al. (2020)) or (ii) to identify areas that could be prone to contaminated drainage generation due to high mineralization (e.g., Epov et al. (2017); Power et al. (2018b)).
- (iii) **TSF and WRP characterization** using ERT has been increasingly popular since

the early studies of (i) Martínez-Pagán et al. (2009) for TSF characterization and (ii) Poisson et al. (2009) and Anterrieu et al. (2010) for WRP internal structure investigations (c.f. Table 2.3). Since then, ERT has been used (i) to determine the spatial extension of old/abandoned WRPs (Martin et al., 2020) and TSFs (Martín-Crespo et al., 2018, 2020) and (ii) to image the internal structure and heterogeneity of WRPs and TSFs (Martinez-Pagan et al., 2021; Mollehuara-Canales et al., 2021a). In particular for WRPs, the coarse waste rocks have been reported to be more resistive than the compacted layers of fine particles (Poisson et al., 2009; Anterrieu et al., 2010), which has led to a better understanding of WRP hydrogeochemical behavior (e.g., Martin et al. (2017); Raymond et al. (2021)). Similarly, the tailings are usually more conductive than the surrounding media, which allows mapping properly the bedrock interface and the dams used to contain tailings (e.g., Booterbaugh et al. (2015); Gabarrón et al. (2020)). Notably, Gabarrón et al. (2020) used ERT to differentiate coarse and fine tailings in a TSF from their contrast of resistivity. Many authors have also used ERT along with geochemical analysis to map potentially reactive wastes (e.g., Dimech et al. (2017); Power et al. (2018b) in WRPs and (Martínez et al., 2012, 2016) in TSFs) and even quantitatively predict (i) total dissolved solids (TDS) (Rucker et al., 2009a; Epov et al., 2017), (ii) pH (Yurkevich et al., 2017), or (iii) the concentration of various contaminants in tailings (e.g., Vásconez-Maza et al. (2019); Mollehuara-Canales et al. (2020)). Finally, a few studies have used ERT to characterize the hydrogeological behavior of mining wastes (i) by assessing relationships between electrical resistivity and the hydrogeological properties of tailings (Banerjee et al., 2011; Mollehuara-Canales et al., 2020) and (ii) by tracking water flows in WRPs under natural or artificial precipitation events (Greer et al., 2017; Dimech et al., 2019). Although less common, these types of applications have great potential for mining waste characterization since TL-ERT provides large-scale data that allows taking into account WRP and TSF heterogeneous composition in a non-destructive manner (Poisson et al., 2009; Hester et al., 2019) and recover information where no other hydrogeological data is available, such as in the core of WRPs (Greer et al., 2017; Dimech et al., 2019).

- (iv) Studies of **acid mine drainage (AMD)** with ERT have been reported in the literature since the 1990s, both for AMD detection (Ebraheem et al., 1990; Benson and Addams, 1998) and AMD monitoring (King and McNeill, 1994; Buselli and Lu, 2001) (c.f. Table 2.4). AMD is generally associated with high concentrations of metallic ions in the pore water (Cravotta III, 2008; Blowes et al., 2014), which increases the electrical conductivity of pore water (up to several orders of magnitude (Mon-

terroso and Macías, 1998)). As a result, AMD is a suitable target for ERT imaging and TL-ERT monitoring (Buselli and Lu, 2001; Johnston et al., 2017), which enables the detection and delineation of areas within TSFs or WRPs where contaminated drainage is generated (e.g., Bortnikova et al. (2013); Tycholiz et al. (2016); Shokri et al. (2022)). Such information have been used (i) to extend spatially geochemical sampling (Martínez-Pagán et al., 2009; Pierwoła et al., 2020) and (ii) to help design future reclamation covers which would reduce the environmental impacts of mining wastes (Martínez-Pagán et al., 2009; Hudson et al., 2018). Similarly, ERT has been used (i) to track AMD migration within TSFs (Bortnikova et al., 2018; Hudson et al., 2018) and WRPs (Shokri et al., 2016a; Casagrande et al., 2020) and (ii) to identify the mechanisms of contaminants transport from the storage facilities to the surrounding medium (e.g., preferential flow of contaminated water (Bethune et al., 2015; Casagrande et al., 2018; do Nascimento et al., 2022), fractures flow inside the bedrock (Olenchenko et al., 2016; Benyassine et al., 2017), eolian transport (Lachhab et al., 2020) or leaks from sealing layers (Cortada et al., 2017; Rey et al., 2020a)). As illustrated by the recent study from Puttiwongrak et al. (2019), semi-permanent TL-ERT installations have a strong potential for the long-term monitoring of AMD. Permanent electrode arrays could be installed near or within the mining wastes to track electrical resistivity changes over large scales, hence increasing the capacity of traditional monitoring techniques. Electrical resistivity could then be used as a proxy indicating possible AMD generation or migration from the wastes, as it has already been done in the past for other types of contaminants (e.g., Heenan et al. (2015); Denham et al. (2020)).

- (v) Application of ERT for **geotechnical stability** assessment of TSFs has been reported since 2005 with the early study from Sjö Dahl et al. (2005) in TSF dams (c.f. Table 2.5). Since then, ERT has been used in TSFs (i) to detect anomalous seepage and internal erosion within the dams (Sjö Dahl et al., 2005; Li et al., 2015; Mainali et al., 2015; Coulibaly et al., 2017; Paria et al., 2020) and (ii) to image water table elevation in the TSFs, which can help to manage the risk of water overtopping (Mainali, 2006; Booterbaugh et al., 2015; Mainali et al., 2015). Such applications have a great potential for geotechnical stability monitoring of TSFs since seepage, dam erosion and overtopping have been the cause of almost 60 % of TSF failures worldwide since 1910, as detailed by the comprehensive review of Lyu et al. (2019b). Moreover, several studies have combined ERT and geotechnical modeling to study the stability of WRPs (Li et al., 2015) and TSFs (Coulibaly et al., 2017; Paria et al., 2020) as it has already been done for landslide monitoring (Lehmann et al., 2013; Zieher et al., 2017)

or levee monitoring (Weller et al., 2014; Dezert et al., 2019). As discussed by Sjö Dahl et al. (2005), TL-ERT monitoring has great potential in this context since repeated ERT images allow tracking changes in resistivity across large scales, which can reduce ambiguities in ERT data interpretation. Following the recent developments of TL-ERT for real-time monitoring of landslides, permanent arrays could be installed within TSFs to monitor remotely their geotechnical stability as part of early warning systems (Kłosowski et al., 2018; Whiteley et al., 2019). As discussed by Tresoldi et al. (2020a), such applications of TL-ERT are expected to become increasingly popular given raising awareness toward the environmental and human risks that TSFs and WRPs can represent.

- (vi) ERT has been used for **geochemical stability** assessment of mining wastes since the beginning of the 2000s (Bergström, 1998; Binley and Daily, 2003) (c.f. Table 2.6). As discussed by Bussière and Guittony (2021a), most reclamation approaches aim to control oxygen or water flows toward the mining wastes with engineered covers installed on TSFs or WRPs since AMD generation is mostly controlled by the oxidation of the sulfide contained in wastes (Mbonimpa et al., 2021; Plante et al., 2021b). ERT has been mostly used in this context (i) to assess the efficiency of mining reclamation by detecting AMD generation on reclaimed TSFs (Rucker et al., 2009a; Power et al., 2018b), (ii) to detect leaks from sealing layers (such as geotextiles) used to encapsulate reactive tailings (Binley and Daily, 2003; Villain et al., 2015), and lastly (iii) to provide insights about how reclamation designs could be improved (Acosta et al., 2014; Sylvain et al., 2019; Rey et al., 2020a). Although less common, several studies also used TL-ERT to monitor the efficiency of multilayer covers made of granular materials which offer better durability than geotextiles (e.g., store and release covers (Bussière and Wilson, 2021), covers with capillary barrier effects (Demers and Pabst, 2021b) or flow control layers (Demers and Pabst, 2021a)). For instance, Maqsoud et al. (2011) used TL-ERT to ensure that a retention layer made of fine materials remained near saturation over time, which would allow reducing oxygen migration from the atmosphere toward the tailing storage facility, hence decreasing the risk of AMD generation. More recently, TL-ERT has been used to track water flows in an experimental WRP to assess the performance of a flow control layer designed to divert water from the reactive core of the WRP (Dimech et al., 2019; Martin et al., 2019). Semi-permanent TL-ERT monitoring systems could be used along with traditional monitoring techniques to provide early warnings if reclamation does not meet the initial design objectives or if its performance decreases over time (e.g., Bussière et al. (2021); Dimech et al. (2021)).

In summary, Figure 2.9 and 2.10 review graphically the different parameters that have been imaged with ERT in WRPs and TSFs respectively. These figures highlight the types of application for which TL-ERT is the most promising for both short-term and long-term monitoring of mining wastes as discussed above. The diagrams of the internal structures of WRPs and TSFs on Figure 2.9 and Figure 2.10 are inspired by the work of Aubertin et al. (2005) and Aubertin et al. (2016).

2.5.2 Challenges that need to be addressed to improve TL-ERT monitoring in mining wastes

Although TL-ERT has been identified as a promising non-destructive imaging approach for monitoring of various dynamic processes in WRPs and TSFs, several challenges are likely to emerge from a wider adoption in mining wastes. The following section discusses three categories of challenges that have been identified for future TL-ERT applications on WRPs and TSFs. (i) Mining sites are generally complex and often remote sites, in constant evolution with harsh field conditions. (ii) Both high spatial and temporal resolutions are needed while maintaining reliable and consistent monitoring over large scales for long periods of time. (iii) Many physical parameters can change simultaneously in mining wastes, although high accuracy of measurements is generally needed for mining waste monitoring. For a broader discussion on advantages and limitations of TL-ERT, the reader is referred to the comprehensive studies of Samouëlian et al. (2005), Binley et al. (2015b), Parsekian et al. (2015), Soupios and Kokinou (2016), McLachlan et al. (2017) and Whiteley et al. (2019).

(i) Complex sites and harsh field conditions

Firstly, mining sites present generally harsh field conditions for long-term monitoring programs since some mines are in remote locations, with few road access and limited power supply, especially after the end of mining operations. In addition, when mining operations are over, monitoring instruments could be damaged by wildlife, vandalized, or stolen, which would undermine the success of long-term monitoring and could represent high maintenance costs. Even active mines can represent challenging conditions because of security limitations, circulation of heavy machinery and rapid evolution of the site that may affect measurements (e.g., change of electrodes, cables and resistivity meters location or update of topography models). In addition, the instrumentation of WRPs and TSFs is highly challenging in itself. Indeed, WRPs are built by high benches (typically between 10 m and 30 m in height) with strong slopes, contain large blocks (typically over one meter in size), are highly heterogeneous and can exhibit electrical resistivity over 10 k Ω m (Dimech et al., 2017; Vriens et al.,

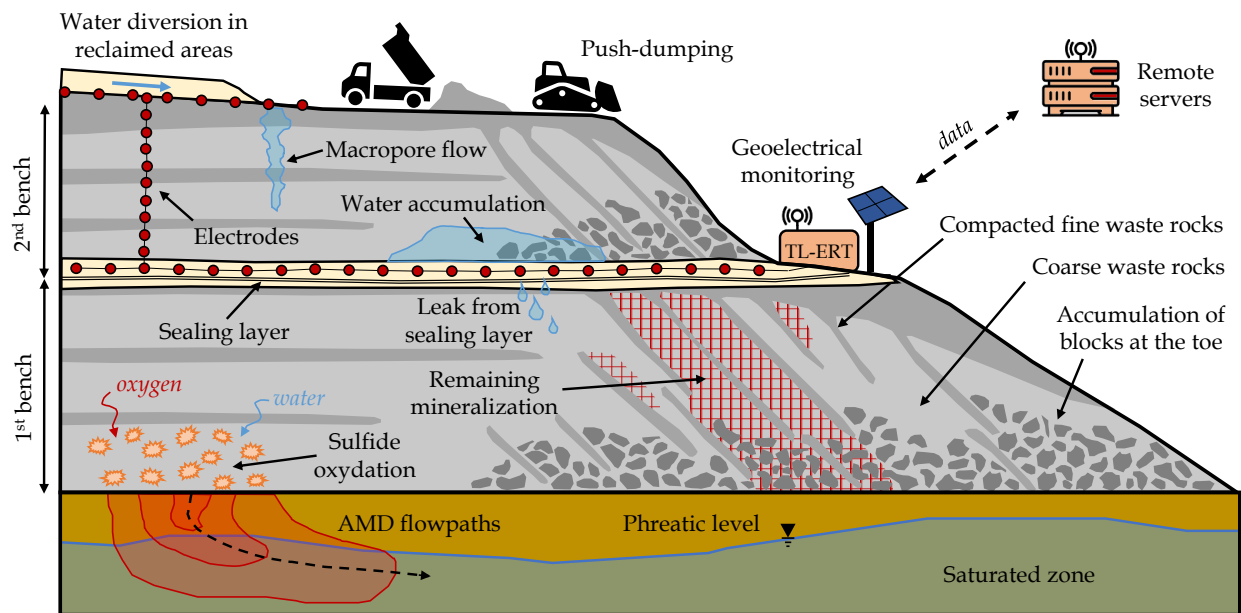


FIGURE 2.9 Review of the key parameters that can be imaged or monitored in WRPs with TL-ERT as identified from the database of ERT studies in mining wastes (adapted from Aubertin et al. (2005)).

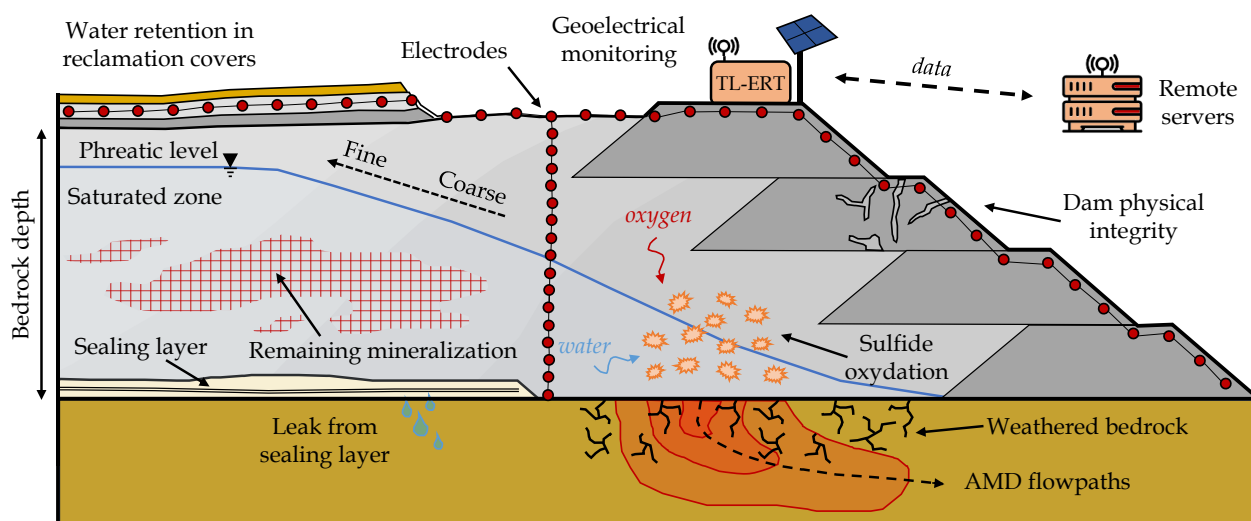


FIGURE 2.10 Review of the key parameters that can be imaged or monitored in TSFs with TL-ERT as identified from the database of ERT studies in mining wastes (adapted from Aubertin et al. (2016)).

2020a). As reported by several authors, such internal structure makes it extremely challenging to install any sensor or electrode within the core of WRPs, and may cause long-term data quality issues due to poor electrode grounding or cable deterioration (Deceuster et al.,

2013; Greer et al., 2017). Although TSFs are generally more homogeneous structures with better electrode contact conditions (fine and conductive material, typically less than 100 Ωm (Martinez-Pagan et al., 2021)), the installation of ERT monitoring systems might be challenging as well if the tailings are too wet to allow operators to walk on them (e.g., MEND (2000)). Finally, the long-term durability of electrodes and cables in mining wastes has still not been studied, but it is likely that such pieces of equipment could suffer from corrosion issues in media with low pH and high EC (Peter-Borie et al., 2011; Palacios et al., 2020).

(ii) High spatio-temporal resolution for long time periods at large scales

Secondly, the spatio-temporal characteristics needed for monitoring programs on mining wastes are also especially challenging since high spatial and temporal resolution are generally required over large distances and during long periods of times (MEND, 2004; Bussière et al., 2021). From the temporal perspective, suitable resolution (i.e. sampling rate) depends on the process studied as discussed in Section 2.3.2. For instance, high resolution is needed to properly recover water infiltration into mining wastes (e.g., one snapshot every 30 minutes, typically during a few days (Dimech et al., 2019; Hester et al., 2019)), while a lower resolution might be sufficient to recover long-term desaturation of a moisture-retaining layer or an abnormal accumulation of water within a TSF (e.g., one snapshot every day, typically during several years (Tresoldi et al., 2020a; Dimech et al., 2021)). Although there is no consensus about how long TSFs and WRPs monitoring programs should last, the geotechnical and geochemical stability of these mining waste storage facilities must be ensured for hundreds of years (MEND, 2004). Since TL-ERT is a relatively new monitoring technique, the longest monitoring period recorded in the literature is approximately 20 years (Mollaret et al., 2019; Etzelmüller et al., 2020). As a result, it is challenging to predict the lifetime of a monitoring system (electrode, cables, battery, resistivity meter), and future work might be necessary to improve the robustness of TL-ERT systems in the context of mining wastes to prevent electrode loss, long-term drifts and noise issues (Peter-Borie et al., 2011; Watlet et al., 2018). From the spatial perspective, monitoring large areas such as TSFs and WRPs generally requires to find a compromise between spatial extension, electrode number and spatial resolution (see Section 2.3.2). Moreover, since most processes summarized in Figures 2.9 and 2.10 occur in the shallow subsurface (typically in the first ten meters), small electrode spacing (such as 1 m or 2 m) might be needed to monitor them accurately. As a result, for a single TL-ERT profile of 1 km across a TSF or a WRP, between 500 and 1000 electrodes might be needed, which is challenging both in terms of data acquisition system capacity, monitoring costs, time needed for each snapshot, power supply needed for measurements and volume of data (Parsekian et al., 2015; Falzone et al., 2019). Given that in Canada alone, almost 200

mining operations have TSFs or WRPs that exceed 1 km², upscaling TL-ERT monitoring systems while ensuring a decent spatial resolution at shallow depths is expected to be one of the main challenges for a broader application of this technique to mining wastes. In the meantime, new strategies must be developed to define optimized location for the TL-ERT monitoring systems, which would allow monitoring the stability of TSFs and WRPs where it is crucial.

(iii) Simultaneous evolution of many physical parameters affecting electrical resistivity

Lastly, as reported by the review of Vriens et al. (2020a), many physical processes can occur simultaneously at different scales in mining waste storage facilities (e.g., various geochemical reactions, water and air advection, dispersion and diffusion). As a result, several physical parameters that affect electrical resistivity can vary simultaneously and have confounding effects (e.g., temperature, moisture content, ice content, pore water EC, pH, porosity), which could make the conversion of electrical resistivity imaged by TL-ERT into a physical parameter useful for geotechnical or geochemical stability monitoring challenging (Parsekian et al., 2015; Dimech et al., 2019). On the opposite, some hydrogeological or geotechnical properties of the mining wastes might not have a direct influence on electrical resistivity (such as the interstitial pressure or the hydraulic conductivity, for instance). Moreover, the relative scarcity of petrophysical models developed for mining wastes reported by Mollehuara-Canales et al. (2020) increases the uncertainty and variability of petrophysical approaches discussed by Tso et al. (2019) and others. Such limitations could have consequences on the accuracy of quantitative interpretations derived from TL-ERT, especially since they are combined with the well-known limitations of ERT data inversion (e.g., non-uniqueness of inversion (Samouëlian et al., 2005), inversion artifacts (Carey et al., 2017; Greer et al., 2017), non-uniform sensitivity distribution and spatial resolution (Clément et al., 2010; Rucker, 2014)). This issue is all the more challenging given the need for high accuracy for monitoring techniques in mining wastes, since slight changes of moisture content (for instance) could correspond to significant deterioration of WRPs and TSFs geotechnical and geochemical stability (MEND, 2004; Bussière et al., 2021; Demers and Pabst, 2021b).

2.5.3 Perspectives for future applications of TL-ERT on mining waste monitoring

The lessons learned from the numerous TL-ERT studies can provide valuable insights to address, at least in part, the challenges mentioned above for long-term monitoring of mining waste stability. For instance, several studies using TL-ERT for long-term monitoring of per-

mafrost noted the complexity of ensuring good data quality in frozen soils and in remote areas (e.g., Tomaškovičová et al. (2016)). The strategies that have been developed to address such issues in permafrost might be suitable as well for waste rocks, for instance. More generally, the "tremendous progress made by the geoelectrical method over the past 25 years" described by Loke et al. (2013) and by other reviews since then (e.g., Binley et al. (2015b); Singha et al. (2015)) can help to identify promising avenues for the application of TL-ERT in WRPs and TSFs. The following section summarizes these technological advances in regard to the TL-ERT studies that carried out long-term monitoring with semi-permanent installations. In particular, several perspectives are proposed for instrumentation, data acquisition and data interpretation as illustrated by Figure 2.11.

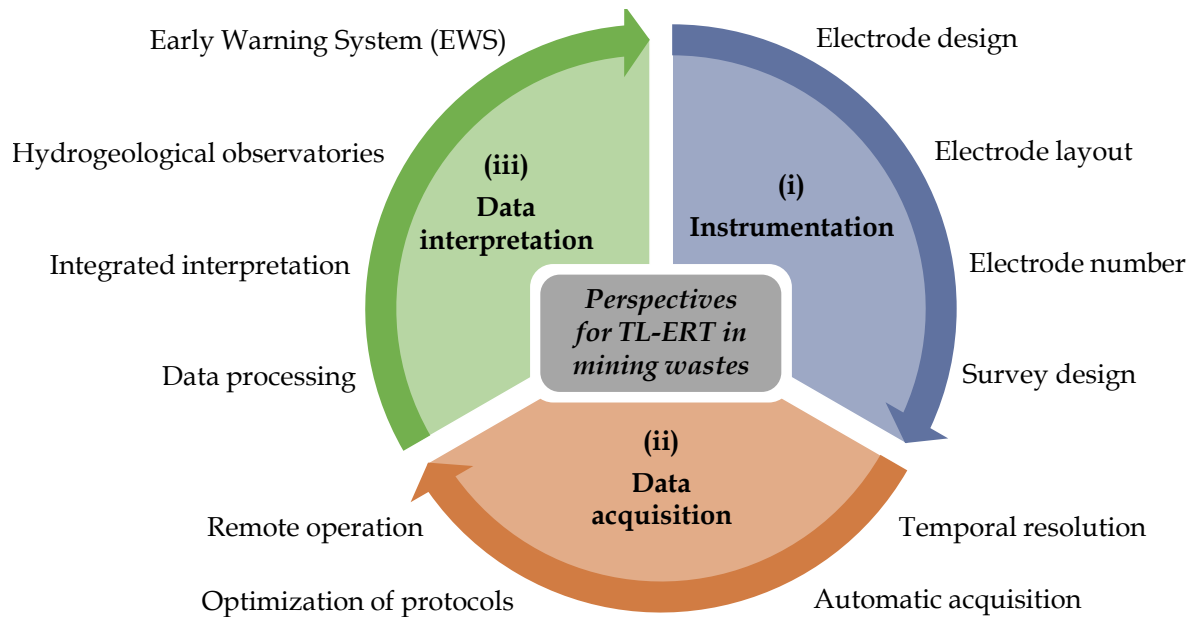


FIGURE 2.11 Recent developments and perspectives for geoelectrical monitoring of mining wastes.

- **Electrode design** (i.e. shape, size and material) is recognized by many authors as a possible source of erroneous measurements if the contact resistance between the electrodes and the medium is too high (e.g., in the presence of rocks, dry medium, macropores or ice) (Dick et al., 2018; Oldenborger and LeBlanc, 2018). This issue could be particularly challenging for long-term ERT monitoring in mining wastes because the deterioration of the electrode-ground contact over time can lead to misinterpretation of the data and increase the cumulative error of the measurement (Deceuster et al., 2013). Recently, Tomaškovičová et al. (2016) carried out a long-term TL-ERT study

in arctic conditions to compare several designs of electrodes. Their results evidenced (i) that plate electrodes ensure better grounding than vertical rods and (ii) that mesh electrodes further improve coupling with the medium thanks to a larger effective surface area. As a result, buried plate electrodes (or disks) are becoming increasingly common for long-term studies to increase electrical grounding and protect electrodes from animals, human or vegetation disturbance (Arosio et al., 2017; Tresoldi et al., 2019). Large mesh plates and robust cables should be favored for future long-term monitoring of WRPs since the contact resistance in waste rocks is expected to be high and to minimize the risk of cable damage due to large rocks (e.g., Tresoldi et al. (2020a)). Moreover, the electrodes should be buried during the construction of TSFs and WRPs or inside small trenches to further improve the grounding following the example of Tresoldi et al. for long-term mining wastes monitoring (Tresoldi et al., 2020c,a). Notably, the vast majority of TL-ERT studies referenced in the database have used stainless-steel electrodes to reduce long-term corrosion (LaBrecque and Daily, 2008). However, few studies have focused on the long-term corrosion effects on electrodes in acidic conditions that could be found in some TSFs or WRPs. We suggest that future studies could focus on identifying strategies to improve the durability of electrodes and cables in mining wastes, following the methodology developed by Tomaškovičová et al. (2016).

- **Electrode layout** in the field is also an important aspect of TL-ERT, since it determines the spatial extension, the depth of investigation and the spatial resolution (Loke et al., 2013). While most semi-permanent TL-ERT studies have used standard 2D lines of electrodes (buried or not) (De Franco et al., 2009; Brunet et al., 2010), it is worth noting that about a third of the semi-permanent monitoring studies have used more complex electrode layouts to improve spatial resolution where needed (Loke et al., 2013). On the one hand, several TL-ERT surveys have used (i) 3D grids of electrodes (Chambers et al., 2011; Uhlemann et al., 2016a), (ii) borehole electrodes in 2D or 3D (Kiessling et al., 2010; Carrigan et al., 2013) or (iii) combination of surface and borehole electrodes (Clément et al., 2010; Kiflu, 2016). Future studies could take advantage of the high modularity of TL-ERT layouts in order to maximize the sensitivity of geoelectrical monitoring where needed within WRPs and TSFs (Rucker et al., 2009c; Rucker, 2014). On the other hand, half of long-term TL-ERT surveys of the database have favored permanent electrodes buried in the medium rather than standard surface arrays to (i) improve electrode grounding (Busato et al., 2019; Tresoldi et al., 2019), (ii) reduce errors associated with electrode mislocation (Peter-Borie et al., 2011; Wilkinson et al., 2015a), (iii) protect electrodes and cables from animal or human deterioration (Auken et al., 2014; Perrone et al., 2014), (iv) minimize disturbance of the medium

during measurements (Jayawickreme et al., 2010) and (v) reduce time and labor costs needed to install electrodes for each snapshot (French et al., 2002; Peter-Borie et al., 2011). The latter could be done for long-term monitoring of mining wastes given the risk of human and animal deterioration in remote locations, especially after the end of mining operations. Finally, most authors agree on the importance of electrode surveying to accurately include electrode positions and topography within inversion models (e.g., Wilkinson et al. (2015a); Uhlemann et al. (2016a)).

- The **number of electrodes** used for ERT surveys has increased significantly over the last 30 years, which in turn has improved spatial resolution and/or spatial extension (Loke et al., 2013). Following the example of Whiteley et al. (2019), Figure 2.12 presents for each semi-permanent TL-ERT study (i) the year of publication (x-axis), (ii) the number of electrodes used (y-axis), (iii) the duration of the monitoring period (size of the circle) and (iv) the temporal resolution (color of the circle). This plot illustrates that long-term monitoring studies using more than 100 electrodes for daily measurements have become common practice since the end of the 2000s (e.g., Nguyen et al. (2009); Ogilvy et al. (2009)). Since 2010, several TL-ERT studies with more than 250 electrodes are reported in the literature. Such studies benefit from increased electrode capacity to carry out (i) high spatial resolution monitoring surveys (with electrode spacing as low as 50 cm (Dahlin et al., 2014; Palacios et al., 2020)) or (ii) large scale monitoring surveys covering up to 1.5 km in length (Auken et al., 2014; Ulusoy et al., 2015). Such improvements are of great interest for future applications on large-scale monitoring of mining waste storage facilities since they allow to increase the monitored area while maintaining a decent spatial resolution. In particular, TL-ERT surveys with improved spatial resolution and spatial extension represent a strong potential for a better characterization of material heterogeneity within mining wastes (Dick et al., 2018; Slater and Binley, 2021). For instance, the spatio-temporal dynamics of electrical resistivity across WRPs and TSFs could be used to identify distinct regions that exhibit different behaviors, following the unsupervised classification approach of Whiteley et al. (2021), Watlet et al. (2018), McLachlan et al. (2020) and Delforge et al. (2021).
- **Survey design** has been recognized by some authors as a critical step for the successful application of long-term TL-ERT (Robinson et al., 2019; Slater and Binley, 2021). For instance, Slater and Binley (2021) stressed the need to know "what to measure and when" for long-term resistivity monitoring systems to ensure that the spatio-temporal resolution is suitable for the dynamic process monitored. In practice, the latter can be done with feasibility studies that evaluate the potential effectiveness of TL-ERT surveys

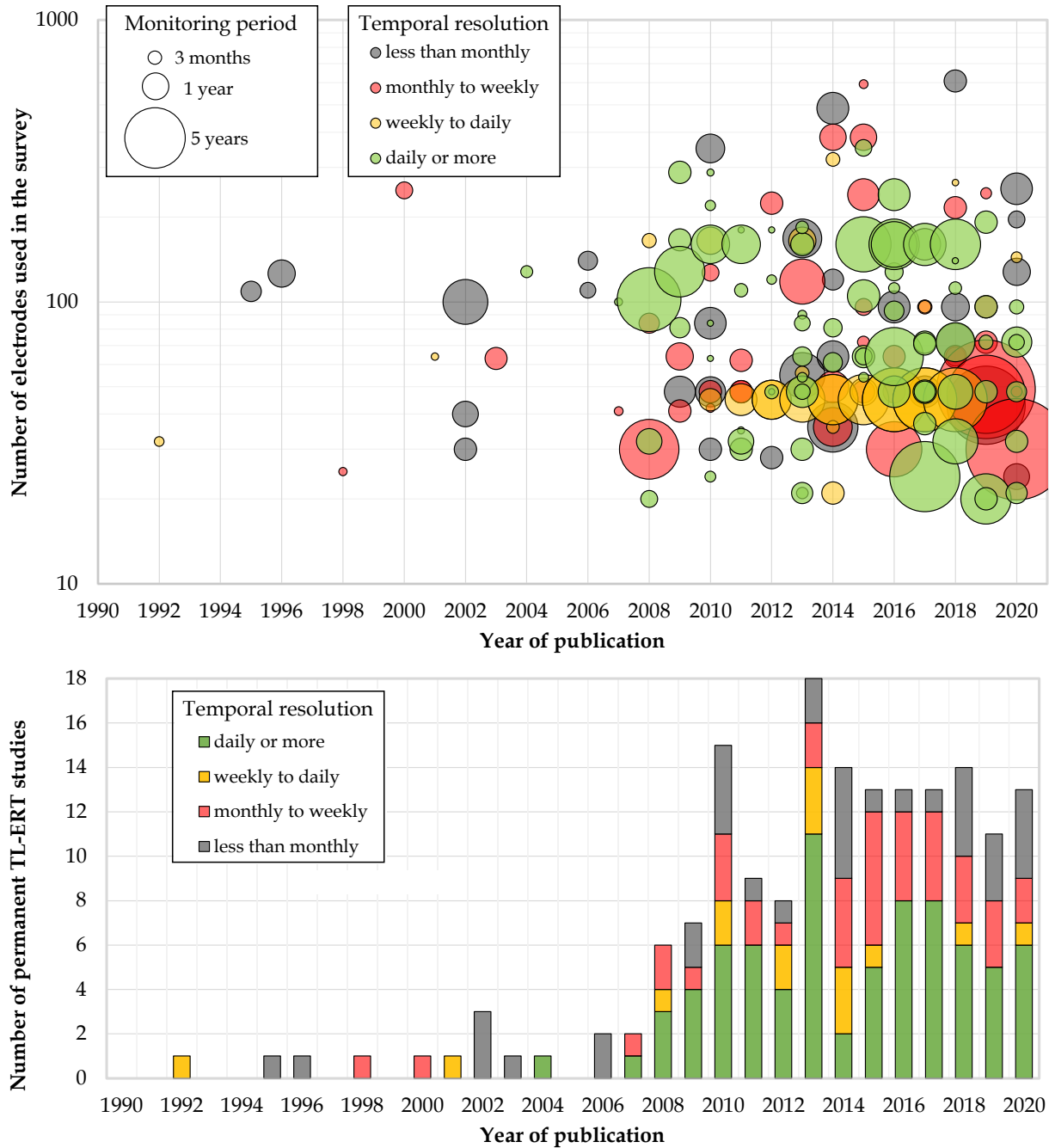


FIGURE 2.12 (a) Evolution of the number of electrodes, the monitoring period and the temporal resolution for the 173 semi-permanent TL-ERT studies identified in the database. For each study, the size of the circle is proportional to the monitoring period while the color of the circle corresponds to the temporal resolution. (b) Histogram of semi-permanent TL-ERT studies according to the temporal resolution.

prior to actual field measurements. Following the example of Robinson et al. (2019), modeling tools could be used to simulate the spatio-temporal dynamics of a specific

subsurface process (e.g., migration of contaminants). Synthetic TL-ERT datasets can then be compared to identify the electrode spacing, electrode location, electrode layout, measurement protocol or temporal sampling that are the most appropriate to image properly the dynamic process of interest (cf Section 2.3.2). Such feasibility studies have been carried out either (i) numerically (e.g., Mewes et al. (2017); Klazinga et al. (2019)), (ii) with laboratory experiments in columns or in tanks (e.g., Kremer et al. (2018); Hojat et al. (2020)) or even (iii) with simplified field surveys (e.g., Tresoldi et al. (2020a)). We suggest that similar approaches should be developed to improve the design of future TL-ERT surveys in mining wastes, given the complexity of these sites, both in terms of geometry and material properties. Moreover, prior hydro-geothermal modeling and reactive transport modeling in mining wastes could (i) help to identify the physical parameters that are likely to change in the wastes over time and (ii) estimate the corresponding spatio-temporal changes in electrical resistivity. These modeling results could allow identifying TL-ERT survey designs that are the most likely to provide satisfying monitoring results in TSFs or WRPs. As discussed by Henderson et al. (2010), such preliminary studies could help reduce the risk of installing poorly designed ERT monitoring systems on the field, which would represent missed opportunities and significant costs. Last but not least, the location of TL-ERT surveys within TSFs and WRPs must be determined appropriately, since these structures usually cover several hundreds of hectares and could not be entirely monitored. It might be relevant to develop methodologies to identify critical areas of TSFs and WRPs where long-term ERT monitoring would be most needed depending on the slope, vegetation cover, material property, heterogeneity and water table elevation for instance (Bussi ere et al., 2021).

- In recent years, the **temporal resolution** of semi-permanent TL-ERT monitoring has improved, both for (i) the duration of TL-ERT monitoring studies (denoted as "monitoring period" on Fig. 2.12) as well as (ii) for the interval between each ERT snapshot (i.e. temporal resolution). As illustrated in Figure 2.12, the monitoring period of semi-permanent TL-ERT studies has significantly increased since the first applications in the 1990s (size of the circles). Indeed, 20 studies with continuous TL-ERT data covering 5 years or more have been published since 2010 (e.g., Uhlemann et al. (2016a); Schmidt-Hattenberger et al. (2017)). For instance, Mollaret et al. (2019) and Etzelm uller et al. (2020) reported the longest acquisition period (20 years) for permafrost monitoring. In the meantime, the temporal resolution has also increased (color of the circles in Fig. 2.12), which has been allowed by low-power resistivity meter developments that allow carrying out several measurements per day while being powered by off-grid power systems (Holmes et al., 2020). As shown by Figure 2.12, more than half of the

semi-permanent studies published in the last decade have acquired at least one ERT snapshot per day (e.g., Chambers et al. (2008); Nguyen et al. (2009)). While in most cases, a trade-off needs to be found between the spatial extension/resolution (i.e. electrode number), the temporal resolution and the monitoring period, some studies have demonstrated that TL-ERT monitoring systems can handle hundreds of electrodes while acquiring ERT snapshots daily during several years (e.g., Johnson et al. (2015); Kuras et al. (2016)). Such improvements are particularly promising for long-term monitoring of large-scale TSFs and WRPs, given the need for both high spatio-temporal resolution and large monitored areas discussed above. For instance, horizontal profiles containing several hundred of electrodes could be used to monitor WRPs an TSFs for decades with a temporal resolution greater than one image per day.

- **Automatic resistivity meters** have been greatly improved since the start of their commercialization in the 1990s (Loke et al., 2013; Binley and Slater, 2020). As discussed by many authors, resistivity meter recent developments include an increased number of electrodes and data-storage capacity, the development of multi-channel measurement, an improved data quality with reduced power consumption and a better robustness for harsh field conditions (McLachlan et al., 2017; Binley and Slater, 2020). The resistivity meters used in the 173 semi-permanent surveys presented in Fig. 2.12 can be classified into two categories. On the one hand, several resistivity meters, well-known for single-time acquisition, have been adapted to carry out long-term monitoring (e.g., Syscal (Arosio et al., 2017; Palis et al., 2017) or ABEM instruments (Caterina et al., 2017; Bièvre et al., 2018)). On the other hand, several resistivity meters have been designed for long-term, autonomous and remote monitoring since the end of the 2000s (e.g., ALERT (Ogilvy et al., 2009; Kuras et al., 2009)), GEOMON-4D (Supper et al., 2008, 2014)), PRIME (Holmes et al., 2020; McLachlan et al., 2020) and GRETA systems (Arosio et al., 2017; Tresoldi et al., 2019)). Such resistivity meters are particularly well suited for long-term monitoring in remote areas such as mining sites since they are self-powered (with solar panels or wind turbines), they need less power for measurements and they can transfer data remotely (Slater and Binley, 2021). Finally, Binley and Slater (2020) noted the growing interest in low-cost and open-source resistivity meters (Sherrod et al., 2012), such as the OhmPi instrument (Clement et al., 2020).
- **Optimized data acquisition protocols** for ERT surveys have been studied since the beginning of the 2000s with the work of Stummer et al. (2004), Furman et al. (2007) and Wilkinson et al. (2006). By definition, optimized protocols are measurement protocols which maximize the spatial resolution of each ERT survey with the minimal number

of four-electrode measurements, thus reducing the time needed to perform each ERT snapshot (e.g., Wilkinson et al. (2006); Palacios et al. (2020); Qiang et al. (2022)). Since then, several studies have been published to improve optimized protocols design by (i) taking into account multi-channel capacity (Wilkinson et al., 2012a), (ii) minimizing electrode polarization effects (Wilkinson et al., 2012a) and (iii) managing complex electrode layouts such as borehole electrodes (Loke et al., 2014b), 3D ERT surveys (Loke et al., 2014c), combined surface and buried arrays (Loke et al., 2015a) and large numbers of electrodes (Loke et al., 2015b). Optimized protocols are particularly promising for TL-ERT monitoring of dynamic processes (such as in mining wastes) since they allow to increase both spatial and temporal resolution, especially for surveys with large numbers of electrodes and/or unconventional layouts (Wilkinson et al., 2015b; Binley and Slater, 2020). Finally, recent studies have demonstrated the potential of simultaneous optimization of measurement protocols and electrode location, which ensures maximal TL-ERT spatio-temporal resolution while reducing the number of electrodes needed, and the instrumentation costs (Wagner et al., 2015b; Uhlemann et al., 2018b). Moreover, Wilkinson et al. (2015b) have developed a methodology to further improve spatio-temporal resolution by updating the measurement protocols over time in order to maximize ERT resolution where temporal changes are observed. Such approaches could be useful in the context of TSFs and WRPs monitoring to design optimized electrode layouts and help improve temporal and spatial resolution where and when it is the most needed (e.g., after heavy rains or in unstable areas).

- **Remote operation** of resistivity meters has become increasingly popular since the beginning of the 2010s (Versteeg and Johnson, 2013; Binley and Slater, 2020). Autonomous resistivity meters can be connected to electrode arrays and left on-site during several years (Holmes et al., 2020). They are usually installed in protective housing and powered by solar panels or wind turbines, which allows carrying out autonomous measurements throughout the year in remote areas (e.g., Merritt et al. (2018); Holmes et al. (2020)). A wireless internet connection can be used to remotely upload command files, schedule measurements and download data files from the resistivity meters to remote servers (Holmes et al., 2020). It is worth noting that external sensors such as rain gauge or moisture sensors can be connected to resistivity meters to detect specific meteorological conditions and trigger higher temporal resolution TL-ERT acquisition (Binley and Slater, 2020). Figure 2.13 presents one of these autonomous resistivity meters; the PRIME system (see Holmes et al. (2020) for details). These developments have a great potential for long-term monitoring of mining wastes since they reduce the frequency of installation, maintenance and data acquisition field campaigns, which can be ex-

pensive, time-consuming or even not possible at all for extreme conditions or remote mining sites (French et al., 2002; Uhlemann et al., 2021). Moreover, this type of autonomous monitoring system allows for near real-time data transfer, processing and can send alerts (Web, email or SMS) if predefined thresholds of moisture content (or other parameters) are exceeded, which could be highly valuable to detect any deterioration of the geochemical or geotechnical stability of mining wastes.

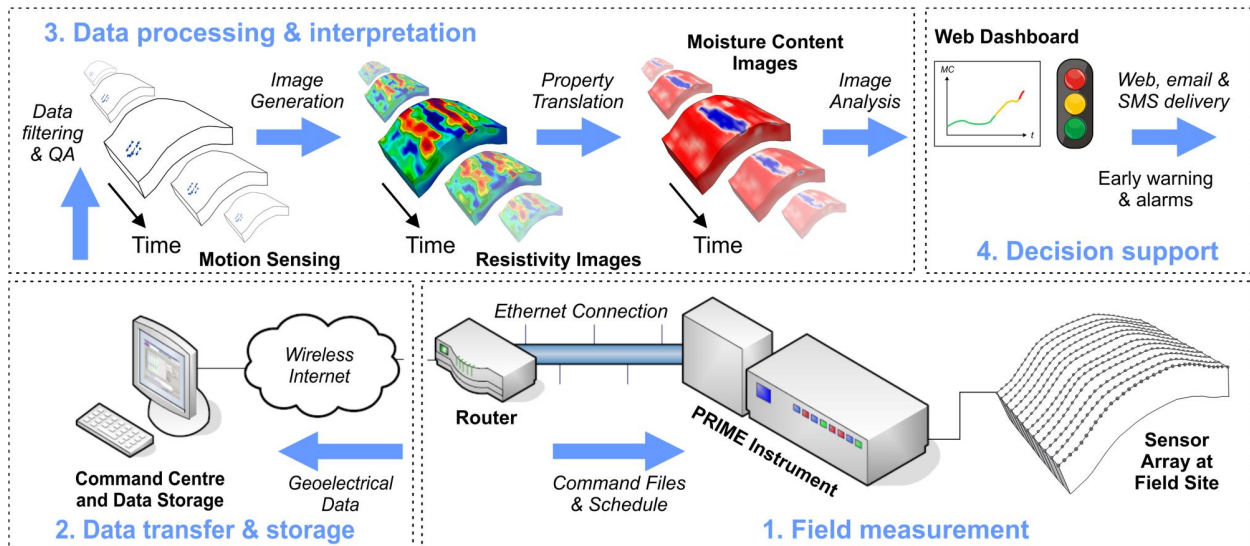


FIGURE 2.13 Flowchart of permanent TL-ERT monitoring system describing autonomous data acquisition, remote data transfer, automated processing and interpretation for long-term monitoring. Figure inspired from Holmes et al. (2020) presenting the workflow of the PRIME system applied to landslide monitoring in British Columbia (Canada).

- **Data processing** tools and frameworks for TL-ERT have experienced strong growth over the last years, which in turn increased the reliability of geoelectrical monitoring (Binley and Slater, 2020). On the one hand, several modeling and inversion algorithms have been developed to allow TL-ERT data processing with large 2D or 3D models, using complex boundaries and advanced spatio-temporal constraints (e.g., R2/R3t (Binley and Slater, 2020), pyGIMLi (Günther et al., 2006; Rücker et al., 2017), ResIPy (Boyd et al., 2019; Blanchy et al., 2020a) and E4D (Johnson et al., 2010, 2012b)). These features are necessary to increase the accuracy of inversion results, especially in complex media such as in TSFs or WRPs. It is worth mentioning that most of these recent software are open-source, free for academic use, and are usually based on well-known numerical computing platforms such as MATLAB® or python (e.g., Eidors (Adler and Lionheart, 2006; De Donno and Cardarelli, 2017), pyGIMLi or SimPEG (Cockett

et al., 2015; Heagy et al., 2017)). Moreover, some of these recent modeling and inversion tools have been adapted to link TL-ERT to (i) hydrogeological, thermal and reactive transport modeling (e.g., PFLOTRAN-E4D (Johnson et al., 2017; Tso et al., 2020)), or (ii) other geophysical methods (e.g., pyGIMLi and SimPEG). In particular, TL-ERT datasets could be combined to modeling tools widely used for mining wastes such as MIN3P-HCP (e.g., (Raymond et al., 2020; Vriens et al., 2020b)), which would allow comparing the spatio-temporal dynamics of electrical resistivity with the predicted thermal, hydrogeological and chemical behavior of TSFs and WRPs. Such approaches have a strong potential for mining waste monitoring since TL-ERT datasets would extend spatially the area covered by conventional sensors and help to validate the predicted behavior of TSFs and WRPs across larger scales. On the other hand, automated processing workflows have been developed, which help to reduce the time needed for traditional data filtering, data processing and inversion (Versteeg and Johnson, 2013; Watlet et al., 2018). These autonomous data processing techniques are all the more promising given the increasing size of long-term LT-ERT datasets. Finally, the review from Khan and Ling (2019) noted that alternative approaches such as machine learning techniques are emerging for TL-ERT data processing (e.g., artificial neural networks (Kłosowski et al., 2018; Rymarczyk et al., 2019) or random forest algorithms (Brillante et al., 2016b)). Moreover, data assimilation techniques such as ensemble Kalman filters are especially promising for the integration of TL-ERT into conventional monitoring programs for various applications (including mining waste monitoring) and to estimate model uncertainties (e.g., Vereecken et al. (2008); Camporese et al. (2015); Bouzaglou et al. (2018); Kang et al. (2018); Tso et al. (2020)). In the context of mining wastes, data assimilation techniques would then allow combining TL-ERT datasets and conventional hydrogeological sensors with multi-physical modeling tools to predict more accurately the behavior of these complex media.

- **Integrated interpretations** of TL-ERT datasets are increasingly popular for the monitoring of key physical parameters such as water, gas or ice content (Michot et al., 2003; Rucker, 2010), temperature (Hermans et al., 2018; Herring et al., 2019), suction (Lehmann et al., 2013; Crawford et al., 2019) or contaminant concentration (Doetsch et al., 2012; Deng et al., 2017) in the subsurface. As discussed in Section 2.3.1, the empirical petrophysical approach introduced by Archie in the 1940s (Archie et al., 1942) for oil reservoirs remains widely used by TL-ERT studies and recent work has been done to refine and improve our physical comprehension of these relationships (e.g., Glover (2015); Cai et al. (2017)). Quantitative approaches are of great interest for mining waste monitoring in particular given that all the physical parameters mentioned above

could play a role in mining waste geotechnical and geochemical stability (MEND, 2004; Bussi re et al., 2021). As discussed in the review of Friedman (2005), it is generally recommended to determine site-specific petrophysical relationships for each TL-ERT survey to improve the precision of key physical parameter estimation. These calibrations are usually done with simultaneous and co-located measurements of the physical property to be recovered and electrical resistivity in the laboratory (i) in core samples (< 10 L) (Hen-Jones et al., 2017b; Corona-Lopez et al., 2019), (ii) in columns (< 100 L) (Priegnitz et al., 2013; Dimech et al., 2018) and (iii) with tank experiments (> 100 L) (Bechtold et al., 2012a; Lyu et al., 2019a; Roodposhti et al., 2019). We suggest that future studies could focus on improving petrophysical models for mining wastes, following the recent examples of Mollehuara-Canales et al. (2020), Wayal et al. (2021) and others. In particular, the development of predictive petrophysical relationships from basic geotechnical properties (e.g., grain size distribution, porosity) and geochemical properties (e.g., mineralogy) seems promising given that such information is widely available in the literature and for most mining sites (Aubertin et al., 2003; Mbonimpa et al., 2003). Moreover, the development of standardized and replicable procedures to calibrate petrophysical relationships in the laboratory seems highly promising since it would allow comparing different datasets and different mining wastes from various sites (e.g., Ling and Zhang (2017); Chen et al. (2018a)). Finally, direct in-situ characterization with hydrogeological sensors and TL-ERT has also been increasingly popular and we suggest that similar approaches could be used more frequently under field conditions in mining wastes (e.g., Crawford and Bryson (2018); Watlet et al. (2018)).

Although the calibration of site-specific relationships improves the accuracy of moisture content estimations from TL-ERT, most authors warn against solely relying on TL-ERT to predict moisture content (Dimech et al., 2019; Tso et al., 2019). A recent study from Tso et al. (2019) highlighted the importance of validating TL-ERT results with other monitoring techniques (such as moisture content sensors) or with hydrogeological modeling. In this regard, coupling between hydrogeological, thermal and geophysical modeling has been used to (i) explicitly integrate the dependency of electrical resistivity on temperature and moisture content and (ii) take into account the hydrogeo-thermal behavior of the materials (e.g., Kuhl et al. (2018); Wagner and Wiese (2018)). In practice, this type of approach is promising in mining wastes since it would allow the quantification of the uncertainty of petrophysical relationships on moisture content values for instance (e.g., Tso et al. (2019)), and would help to carry out sensitivity analysis on TL-ERT results (Brunet et al., 2010). Finally, the recent review from Wagner and Uhlmann (2021) discussed the development of multi-method geophysical imaging which

allows the uncertainty of inversion to be reduced. For instance, TL-ERT could be combined with seismic imaging in TSFs or WRPs to improve the estimation of water content, ice and porosity, following the recent examples of Wagner et al. (2019) and Mollaret et al. (2020) for permafrost monitoring. Among other geophysical methods that could be combined with TL-ERT monitoring of mining wastes, passive seismic methods are particularly promising since they provide complementary information with a low power consumption for long-term monitoring (e.g., Planès et al. (2016); Olivier et al. (2017); Whiteley et al. (2019)). Distributed acoustic sensing cables could be installed along with TL-ERT electrode cables across large-scale profiles in TSFs and WRPs, which would allow the simultaneous monitoring of electrical resistivity and seismic velocities in mining wastes (e.g., Bakulin et al. (2020); Verdon et al. (2020); Mollehuara-Canales et al. (2021a)). Finally, it is worth mentioning that other electrical methods such as self-polarization, induced polarization or spectral-induced polarization are promising for mining wastes monitoring since they are affected by different physical parameters of interest (e.g., Mainali et al. (2015); Saneiyani et al. (2019)).

- The integration of TL-ERT into **hydrogeological observatories** has been identified by Slater and Binley (2021) and other authors as a key to success for the future development of long-term electrical monitoring studies (Parsekian et al., 2015). Indeed, hydrogeological observatories are well-known sites that are generally heavily instrumented using multiple monitoring techniques across different spatio-temporal scales (Robinson et al., 2008b; Jensen and Refsgaard, 2018). For instance, such observatories have played a critical role in the recent development of long-term TL-ERT monitoring of landslides processes (e.g., Hollin Hill site in the UK (Uhlemann et al., 2017b; Boyd et al., 2021)), for CO₂ storage monitoring (e.g., Ketzin site in Germany (Bergmann et al., 2016; Schmidt-Hattenberger et al., 2017)), contaminant monitoring (e.g., Hanford site in the USA (Johnson et al., 2015; Robinson et al., 2019)) and for permafrost studies (e.g., Murtel site in the Alps (Supper et al., 2014; Mollaret et al., 2019)). We suggest that a similar approach could be followed for the monitoring of geotechnical and geochemical stability of mining wastes with experimental WRPs and TSFs observatories in the future. For instance, critical sections of TSFs and WRPs could be instrumented with a dense network of conventional monitoring instruments, TL-ERT profiles and other geophysical methods (e.g., Dimech et al. (2019); Martin et al. (2019)). These multi-physical datasets could be used to (i) validate and improve TL-ERT monitoring results under field conditions, (ii) to test new integrated data processing approaches, (iii) to assess the advantages of TL-ERT as a complementary monitoring technique over large scales and lastly (iv) to support long-term research programs and train future hydro-

geophysicists in the context of mining waste geochemical and geotechnical monitoring. Moreover, such large-scale field tests would be "proofs of concept" to demonstrate the feasibility and the value of TL-ERT for mining waste monitoring. As discussed by Parsekian et al. (2015), such effort could be helpful to address what can be identified as a primary challenge; "the resistance to adoption of geophysical measurements" from operators that "have relied on traditional measurements of the subsurface", who can be "hesitant to adopt new technologies that may be viewed as untested".

- **Early Warning Systems (EWS)** are "monitoring devices designed to avoid or to mitigate the impact posed by a threat" (Medina-Cetina and Nadim, 2008). The potential of semi-permanent TL-ERT monitoring to provide additional information for existing EWS has been identified since the end of the 2000s with the studies from Kuras et al. (2006) and Ogilvy et al. (2009) in the context of saline intrusion monitoring. Since then TL-ERT has been part of EWS for many geo-hazards surveillance programs, although none has been reported for mining wastes. The main examples of applications are (i) landslide prediction and surveillance (Supper et al., 2014; Budler; Smethurst et al., 2017), (ii) dam and levee geotechnical stability monitoring (Arosio et al., 2017; Tresoldi et al., 2020c), (iii) railway embankment stability monitoring (Chambers et al., 2014b; Gunn et al., 2018), (iv) unstable permafrost rock wall surveillance (Keuschnig et al., 2017; Weber et al., 2019), (v) monitoring of saline water intrusion into groundwater aquifers (Ogilvy et al., 2009; Chen et al., 2018a), (vi) surveillance of flash flooding from both natural causes or human activities (Liu et al., 2017; El-Saadawy et al., 2020) and (vii) monitoring of contaminant leaks from industrial and mining sites (Puttiwongrak et al., 2019; Denham et al., 2020). Such an approach is promising for mining wastes since TL-ERT monitoring could be used for the early detection of any condition associated with the deterioration of geotechnical or geochemical stability of WRPs and TSFs (e.g., sudden change of water table elevation, abnormal seepage in TSF dams, abnormal increase or decrease in moisture content or sudden increase of pore water electrical conductivity). In this regard, some on-going projects are currently testing long-term TL-ERT monitoring for the assessment of mining waste geotechnical and geochemical stability at pilot scale (e.g., Kłosowski et al. (2018); Tresoldi et al. (2020a)). We suggest that future monitoring studies could define critical threshold values (either for moisture content or electrical resistivity). Alerts could then be transferred to the operators if these values are exceeded, which would help to prevent catastrophic failures or environmental contamination (e.g., Arosio et al. (2017); Gunn et al. (2018)). Following the example of Gunn et al. (2015), detailed daily reports assessing the level of risk for specific areas of TSFs and WRPs could be generated from TL-ERT measurements to

support the operators in charge of stability monitoring. As discussed by Robinson et al. (2008b), TL-ERT could be used to "fill the gap" between point sensor measurements and remote sensing imagery, that are currently the two main strategies developed in EWS monitoring programs for mining wastes (e.g., Li et al. (2020); Lumbroso et al. (2021)).

2.6 Conclusion

Tailing storage facilities (TSF) and waste rock piles (WRP) represent one of the main environmental concerns related to the mining activities. These large scale structures must be properly monitored in order to manage the risk of geotechnical and geochemical instabilities, which can have dramatic consequences. This review discusses the strong potential of long-term time-lapse electrical resistivity tomography (TL-ERT) for the monitoring of key physical properties within mining wastes. Indeed, TL-ERT could fill the gap between conventional point sensors and surface observations, both in terms of spatial and temporal resolution. A systematic review of TL-ERT studies over the last 30 years has been carried out to appraise a state of the art of geoelectrical monitoring and review recent developments, both in terms of types of application and technical advances. The present systematic review of ERT studies applied to mining wastes helps to identify future promising applications of TL-ERT for (i) mining waste valorization, (ii) mining waste characterization, (iii) early detection of contaminated drainage generation, and lastly for (iv) long-term geotechnical and geochemical stability monitoring of TSFs and WRPs. Finally, the most promising perspectives for the future development of TL-ERT monitoring in mining wastes are discussed. In particular, several recommendations concerning field instrumentation, data acquisition and data interpretation are proposed to overcome the challenges that are likely to emerge from a broader use of TL-ERT monitoring in mining wastes.

TABLEAU 2.1 Review of studies using ERT to monitor metal extraction in heap leaching pads (HLP)

Reference	Country	TSF / WRP	ERT setup	Remarks
Rucker et al. (2009c)	United States <i>Nevada</i>	WRP <i>HLP</i>	pseudo-3D ERT <i>160m x 420m</i>	3D imaging of HLP Conversion of ρ into gold with drill-core sampling
Rucker et al. (2009b)	United States <i>Nevada</i>	WRP <i>HLP</i>	2D ERT lines (x2) <i>150m to 240m</i> STAR array (x2)	Monitoring of moisture content changes over time Leachate solution pathways
Rucker (2010)	United States <i>Nevada</i>	WRP <i>HLP</i>	pseudo-3D ERT <i>160m x 420m</i>	3D estimation of moisture content in HLP from ERT data with cokriging
Rucker et al. (2014)	United States <i>Colorado</i>	WRP <i>HLP</i>	3D STAR array Boreholes (x6)	Real-time monitoring of reagent pathways in HLP
Cubbage et al. (2016)	United States <i>Arizona</i>	WRP <i>HLP</i>	2D ERT lines (x50) Boreholes (x20)	Operational use of TL-ERT to optimize metal extraction
Rucker et al. (2017)	United States <i>Arizona</i>	WRP <i>HLP</i>	2D ERT Lines (x4) <i>400m to 850m</i> Boreholes (x24)	3D TL-monitoring of reagent Estimation of total and extracted copper in HLP
Maghsoudy et al. (2019)	Iran <i>Kerman</i>	WRP <i>HLP</i>	2D ERT Lines (x5) <i>200m to 400m</i>	Identification of macropore flow, dry areas and water accumulation in the HLP

TABLEAU 2.2 Review of studies using ERT to estimate the volume of mining wastes for valorization

Reference	Country / State	TSF / WRP	ERT setup	Remarks
Florsch et al. (2012)	France <i>Occitanie</i>	WRP <i>Slag heap</i>	pseudo-3D ERT <i>25m x 18m</i>	3D imaging of a slag heap for estimation of archaeological metal production (130 tons)
Günther and Martin (2016)	Germany <i>Lower-Saxony</i>	WRP <i>Slag heap</i>	2D ERT line <i>42m</i>	Use of ERT and SIP to map mineralized areas for reuse
Saladich et al. (2016)	Spain <i>Catalonia</i>	TSF	2D ERT lines (x10) <i>50m to 100m</i>	Threshold in ρ to discriminate bedrock, cover and tailings
Markovaara-Koivisto et al. (2018)	Finland <i>Western Finland</i>	TSF	pseudo-3D ERT <i>200m x 300m</i>	Threshold in ρ to identify high-grade copper wastes LIDAR data for volume
Nikonow et al. (2019)	Chile <i>Santiago</i>	TSF	2D ERT lines (x13) <i>120m to 1300m</i>	3D distribution of fine/coarse grained tailings Correlation with copper
Martin et al. (2020)	Germany <i>Lower-Saxony</i>	WRP	2D ERT lines (x27) <i>25m to 99m</i>	Sampling data to estimate threshold in ρ for wastes with economic potential
Martínez-Segura et al. (2020)	Spain <i>Murcia</i>	TSF	2D ERT lines (x16) <i>85m to 215m</i>	Thresholds in ρ to estimate depth of wastes and volume estimation with LIDAR data

TABLEAU 2.3 Review of some studies using ERT to characterize mining wastes and storage facilities

Reference	Country	TSF / WRP	ERT setup	Remarks
Poisson et al. (2009)	Canada <i>Quebec</i>	WRP	pseudo-3D ERT <i>36m x 30m</i>	Identification of fine-grained and coarse-grained layers Validation with two trenches
Anterrieu et al. (2010)	Canada <i>Quebec</i>	WRP	2D ERT lines (x12) <i>26m to 160m</i>	Large-scale internal structure of WRP from ERT inversions History of WRP construction
Martinez et al. (2014)	Spain <i>Andalucia</i>	TSF	2D ERT lines (x2) <i>400m to 480m</i>	Large-scale internal structure of TSF and assessment of environmental risk
Booterbaugh et al. (2015)	Canada <i>Alberta</i>	TSF	2D ERT lines (x3) <i>600m to 800m</i>	Comparison of TL-ERT with direct measurements of water content and EC Identification of water table
Martínez et al. (2016)	Spain <i>Andalucia</i>	TSF	2D ERT line <i>290m</i>	Combined ERT and hydrogeochemical internal characterization of TSF
Epov et al. (2017)	Russia <i>Kemerovo</i>	TSF	2D ERT lines (x3) <i>235m</i>	Mapping of reactive tailings Relationship between $\rho - \theta$, sulfide content and TDS
Greer et al. (2017)	United States <i>Virginia</i>	WRP <i>Valley fill</i>	2D TL-ERT lines <i>90m to 315m</i>	TL-monitoring of water infiltration (artificial event) Hydrogeological behavior

TABLEAU 2.3 (SUITE) Review of some studies using ERT to characterize mining wastes and storage facilities

Reference	Country	TSF / WRP	ERT setup	Remarks
Yurkevich et al. (2017)	Russia <i>Kemerovo</i>	TSF	2D ERT lines (x6) <i>14m to 33m</i>	Delineation of oxidized tailings with ERT ρ - pH relationship
Martín-Crespo et al. (2018)	Spain <i>Murcia</i>	TSF	2D ERT lines (x6) <i>165m to 260m</i>	TSF history and tailing volumes estimated from ERT and aerial photogrammetry
Power et al. (2018b)	Canada <i>Nova-Scotia</i>	WRP	2D ERT lines (x7) <i>140m to 365m</i> pseudo-3D ERT <i>140m x 80m</i>	Internal composition of WRP Validation with logging Delineation of AMD and future sources of AMD
Hester et al. (2019)	United States <i>Virginia</i>	WRP <i>Valley fill</i>	2D TL-ERT lines <i>45m to 422m</i>	TL-monitoring of water infiltration (artificial event) Hydrogeological behavior
Martín-Crespo et al. (2019)	Spain	TSF	Multiple 2D ERT <i>45m to 500m</i>	Review of ERT imaging for 7 abandoned TSF in Spain
Vásconez-Maza et al. (2019)	Spain <i>Murcia</i>	WRP/ TSF	2D ERT lines (x4) <i>90m to 215m</i>	Prediction of Chromium content from ρ values with ρ - Cr in-situ relationship
Gabarrón et al. (2020)	Spain <i>Murcia</i>	TSF	2D ERT lines (x7) <i>10m to 180m</i>	Systematic sampling and high-resolution ERT to assess various relationships
Mollehuara-Canales et al. (2020)	Australia <i>South Australia</i>	TSF	2D ERT line <i>410m</i>	Sampling of tailings to assess petrophysical relationship with fluid EC and saturation
Vásconez-Maza et al. (2020)	Spain <i>Murcia</i>	WRP/ TSF	2D ERT lines (x8) <i>90m to 215m</i>	Classification of wastes with PCA (Principal Component Analysis) of ERT results

TABLEAU 2.4 Review of the most recent studies using ERT to characterize AMD flows from mining wastes

Reference	Country	TSF / WRP	ERT setup	Remarks
Pierwoła (2015)	Poland <i>Małopolska</i>	TSF	2D ERT lines (x2) <i>27m to 90m</i>	Delimitation of Zn-Pb tailings prone to AMD Gradation in sulfide content
Shafaei et al. (2016)	Iran <i>Semnan</i>	WRP	2D ERT lines (x4) <i>90m to 170m</i>	TL-ERT to track AMD plume Identification of AMD source
Shokri et al. (2016b)	Iran <i>Semnan</i>	WRP	pseudo-3D ERT <i>65m x 75m</i>	Modeling of O_2 diffusion to validate correlation between low ρ and FeS_2 oxidation
Tycholiz et al. (2016)	Canada <i>Manitoba</i>	TSF	VES (x2)	VES / electromagnetic used to map pH and Cu^{2+} Comparison with systematic sampling of tailings (2D)
Benyassine et al. (2017)	Morocco <i>Drâa-Tafilalet</i>	TSF	2D ERT lines (x5) <i>300m to 1200m</i>	Imaging of potential AMD flowpaths in abandoned TSF Identification of fractures
Johnston et al. (2017)	United States <i>Colorado</i>	TSF	2D ERT line <i>500m</i>	ERT mapping of potential diffuse sources of AMD Comparison with local geochemical and water EC
Casagrande et al. (2018)	Brazil <i>Minas Gerais</i>	WRP	pseudo-3D ERT <i>600m x 900m</i>	Large-scale 3D mapping of AMD affected water Design of future reclamation
Bortnikova et al. (2018)	Russia <i>Kemerovo</i>	TSF	pseudo-3D ERT <i>350m x 500m</i>	AMD flowpaths imaged with large-scale 3D-ERT Tailing volume calculation

TABLEAU 2.4 (SUITE) Review of the most recent studies using ERT to characterize AMD flows from mining wastes

Reference	Country	TSF / WRP	ERT setup	Remarks
Hudson et al. (2018)	United Kingdom <i>Wales</i>	TSF	2D ERT lines (x8) <i>100m to 120m</i>	Mapping of contaminated streams, calculation of heavy metal efflux, identification of remediation strategies
Targa et al. (2019)	Brazil <i>Minas Gerais</i>	WRP	2D ERT lines (x4) <i>400m</i>	Identification of flowpaths for AMD through fractures Mapping of sulfides in WRP
Casagrande et al. (2020)	Brazil <i>Minas Gerais</i>	WRP	pseudo-3D ERT <i>600m x 900m</i>	Large-scale 3D mapping of AMD affected water Design of future reclamation
Lachhab et al. (2020)	Morocco <i>Drâa-Tafilalet</i>	TSF	2D ERT lines (x3) <i>630m to 790m</i>	ERT combined with seismic to identify AMD pathways from TSF through fractures
Martín-Crespo et al. (2020)	Spain <i>Murcia</i>	WRP/ TSF	2D ERT lines (x2) <i>120m</i>	Combination of aerial photogrammetry and ERT to map AMD occurrence
Moreira et al. (2020)	Brazil <i>Minas Gerais</i>	WRP	pseudo-3D ERT <i>300m x 350m</i>	Mapping of AMD affected water and preferential flow through fractured bedrock
Pierwoła et al. (2020)	Poland <i>Małopolska</i>	TSF	2D ERT lines (x2) <i>50m to 500m</i>	Delineation of contaminated areas from AMD products and eolian transport

TABLEAU 2.5 Review of studies using ERT to evaluate the geotechnical stability of WRP and TSF

Reference	Country / State	TSF / WRP	ERT setup	Remarks
Sjödahl et al. (2005)	Sweden <i>Närke</i>	TSF	2D ERT lines (x4) <i>150m to 825m</i>	Imaging of TSF internal structure (tailings, dam core) Low ρ values for the area with known stability issues
Li et al. (2015)	China <i>Jilin</i>	TSF/ WRP	2D ERT lines (x4) <i>50m to 240m</i>	Identification of loose waste rocks and saturated tailings from ρ for stability analysis
Coulibaly et al. (2017)	Canada <i>Quebec</i>	TSF	2D ERT lines (x2) <i>260m to 340m</i>	Heterogeneity observed in the dam, relationship with geotechnical stability
Paria et al. (2020)	Peru	TSF	2D ERT lines (x4) <i>330m to 560m</i>	Mapping of TSF geometry and underlying material
Tresoldi et al. (2020a)	Chile <i>Santiago</i>	TSF	2D ERT lines (x3) <i>150m</i>	TL autonomous monitoring Field trial to test a system prior to TSF installation

TABLEAU 2.6 Review of studies using ERT to evaluate mining wastes reclamation efficiency

Reference	Country / State	TSF / WRP	ERT setup	Remarks
Rucker et al. (2009a)	United States <i>Montana</i>	WRP/ TSF	pseudo-3D ERT <i>600m x 500m</i>	3D delineation of AMD in a reclaimed TSF validation with sampling
Martín-Crespo et al. (2010)	Spain <i>Andalucia</i>	TSF	2D ERT lines (x6) <i>50m to 190m</i>	Identification of acidic water flows in the TSF ($\rho < 1 \Omega m$) Good performance of sealing
Maqsoud et al. (2011)	Canada <i>Quebec</i>	TSF	2D ERT line <i>30m</i>	Accumulation of water in the retention layer of a cover with capillary barrier effects
Acosta et al. (2014)	Spain <i>Murcia</i>	TSF	2D ERT lines (x9) <i>175m to 355m</i>	Evidence of erosion of the cover layers (wind or water) Good quality of bedrock
Villain et al. (2015)	Sweden <i>Norrbotten</i>	WRP Pit	2D ERT lines (x4) <i>200m to 280m</i>	Existence of seepage within a dry cover, risk of erosion
Cortada et al. (2017)	Spain <i>Andalucia</i>	TSF	2D ERT lines (x4) <i>190m to 315m</i>	High-moisture zones interpreted as faults in the insulation of the tailings
Dimech et al. (2018)	Canada <i>Quebec</i>	WRP	3D TL-ERT <i>60m x 10m x 7m</i>	Moisture content monitoring in a reclamation cover Laboratory calibration
Dimech et al. (2019)	Canada <i>Quebec</i>	WRP	3D TL-ERT <i>60m x 10m x 7m</i>	Monitoring of water flows in an experimental WRP Validation with point sensors
Rey et al. (2020a)	Spain <i>Andalucia</i>	TSF	2D ERT lines (x2) <i>180m to 390m</i>	Detection of acidic leaks from the reclaimed TSF

CHAPITRE 3 ARTICLE 2 - A MULTISCALE ACCURACY ASSESSMENT OF MOISTURE CONTENT PREDICTIONS USING TIME-LAPSE ELECTRICAL RESISTIVITY TOMOGRAPHY IN MINE TAILINGS

Adrien Dimech ^{1,3,*}, Anne Isabelle ^{2,3}, Karine Sylvain ^{2,3}, Chong Liu ¹, LiZhen Cheng ^{1,3},
Bruno Bussière ^{1,3}, Michel Chouteau ^{2,3}, Gabriel Fabien-Ouellet ², Charles Bérubé ²,
Paul Wilkinson ⁴, Philip Meldrum ⁴ and Jonathan Chambers ⁴

Submitted to Scientific Reports (October 13, 2022).

¹ Université du Québec en Abitibi-Témiscamingue (UQAT), Rouyn-Noranda, QC, Canada

² Polytechnique Montréal, Montréal, Québec, H3T 1J4, Canada

³ Research Institute of Mines and Environment (RIME), Québec, Canada

⁴ British Geological Survey (BGS), Nottingham, NG12 5GG, United Kingdom

Ce chapitre présente le développement d'une méthodologie de laboratoire qui permet de caractériser simultanément les propriétés hydrogéologiques et électriques dans des matériaux miniers pour répondre à l'**OS1**. Ce chapitre présente également l'approche suivie pour effectuer l'estimation de la précision de la teneur en eau volumique estimée à l'aide de la méthode électrique, et ce à différentes échelles pour répondre à l'**OS2**. Ces deux aspects sont cruciaux pour la réalisation du projet de doctorat puisque la revue de littérature présentée au chapitre 2 a permis de mettre en évidence certaines lacunes concernant la détermination des relations pétrophysiques sur les matériaux miniers. Par ailleurs, la précision de l'estimation de la teneur en eau volumique par la méthode électrique a aussi été identifiée comme un élément crucial dans le contexte du suivi de performance en restauration minière, notamment en raison des variations simultanées de teneur en eau volumique, de température et de conductivité électrique du fluide interstitiel, qui peuvent avoir un effet confondant sur la conductivité électrique du milieu. Cet article vise donc à répondre à ces problématiques à l'aide de plusieurs expériences réalisées avec les matériaux miniers utilisés dans les recouvrements à l'échelle du terrain, et pour des conditions hydrogéologiques diverses.

3.1 Abstract

Accurate and large-scale assessment of volumetric water content (VWC) plays a critical role in mining waste monitoring to mitigate potential geotechnical and environmental risks. In recent years, time-lapse electrical resistivity tomography (TL-ERT) has emerged as a promising monitoring approach that can be used in combination with invasive and point-measurements techniques to predict VWC in mine tailings. Generally, the bulk electrical conductivity (EC) imaged using TL-ERT is converted into VWC in the field using petrophysical relationships calibrated in the laboratory. This study is the first to assess the scale effect on the accuracy of ERT-predicted VWC in tailings. Simultaneous and co-located monitoring of bulk EC and VWC are carried out in tailings at five different scales, in the laboratory and in the field. The hydrogeophysical datasets are used to calibrate a petrophysical model used to predict VWC from TL-ERT data. Overall, the accuracy of ERT-predicted VWC is $\pm 0.03 \text{ m}^3/\text{m}^3$, and the petrophysical models determined at sample-scale in the laboratory remain valid at larger scales. Notably, the impact of temperature and pore water EC evolution plays a major role in VWC predictions at the field scale (tenfold reduction of accuracy) and, therefore, must be properly taken into account during the TL-ERT data processing using complementary hydrogeological sensors. Based on these results, we suggest that future studies using TL-ERT to predict VWC in mine tailings could use sample-scale laboratory apparatus similar to the electrical resistivity Tempe cell presented here to calibrate petrophysical models and carefully upscale them to field applications.

3.2 Introduction

Accurate estimation of the spatial distribution of volumetric water content (VWC) is important for understanding most hydrogeological processes in the vadose zone (Robinson et al., 2008a; Beff et al., 2013). Among others fields of application, the spatio-temporal dynamics of VWC are key parameters for (i) weather and climate predictions (Vereecken et al., 2008; Brocca et al., 2011; Dorigo et al., 2017), (ii) moisture-induced landslides, floods and droughts prevention (Macleod et al., 2013; Massari et al., 2014; Thober et al., 2015; Uhlemann et al., 2017b; Belabid et al., 2019; Whiteley et al., 2019), (iii) agricultural and irrigation scheduling (Beff et al., 2013; Acharya et al., 2017; Mary et al., 2019; Blanchy et al., 2020b; Garré et al., 2021), (iv) infrastructure stability assessment (Chambers et al., 2014b; Romero-Ruiz et al., 2018) and (v) water resource management (Binley et al., 2015b; McLachlan et al., 2017; Costall et al., 2020). As discussed by Bussière et al. (2021) and Dimech et al. (2022), VWC monitoring is also a key component for monitoring programs of tailings storage facilities

(TSF) and waste rock piles (WRP), which typically extend across several km² and can be highly heterogeneous (Bowker and Chambers, 2015; Lyu et al., 2019b). Indeed, most of the geotechnical and geochemical stability issues in WRP and TSF are closely connected to (i) moisture content distribution (e.g., Power et al. (2018a); Mbonimpa et al. (2021); Maqsoud et al. (2021)) and/or (ii) water infiltration, seepage and evapo-transpiration (e.g., Mainali et al. (2015); Martin et al. (2017); Dimech et al. (2019); Demers and Pabst (2021a)). Several mining waste reclamation approaches such as covers with capillary barrier effects (CCBE) rely on VWC in moisture-retaining layers to control the oxygen migration from the atmosphere, which limits the risk of acid mine drainage (AMD) generation (Kalonji-Kabambi et al., 2017; Demers and Pabst, 2021b).

Classical methods for measuring VWC in the field are divided into two categories with different spatial extent (i.e., overall coverage of measurements) and spatial support (i.e., integration volume or area of measurements) (Western et al., 1999; Robinson et al., 2008b; Vereecken et al., 2008). On the one hand, point sensing instrument networks such as time-domain reflectometry or capacitance sensors are known to measure VWC accurately but locally (typically a few centimeters around the sensors) with limited perturbation of the subsurface, as opposed to destructive sampling (Beff et al., 2013). On the other hand, remote sensing approaches (passive and active, using aerial measurements or satellite) allow estimating VWC across large-scale areas without subsurface perturbation. Reported spatio-temporal resolutions range from 10 to 500 m (Robinson et al., 2008b; Amazirh et al., 2018) with a revisit time as low as a few days (Gascoïn et al., 2019). However, these methods have a shallow penetration depth (generally less than ten centimeters) (Robinson et al., 2008b; Vereecken et al., 2008). Geophysical approaches have been identified as promising monitoring tools to fill the gap between local and surface VWC observations since they aim to recover the distribution of physical properties in the subsurface, from centimetric to kilometeric scales (Martínez-Pagán et al., 2009; Binley et al., 2015b; Parsekian et al., 2015; Thompson et al., 2017; Cultrera et al., 2019; Troiano et al., 2019; Hasan et al., 2021).

Time-lapse electrical resistivity tomography (TL-ERT) is one of the most effective geophysical methods for the characterization of VWC dynamics (Falzone et al., 2019; Martínez-Pagán et al., 2021; Slater and Binley, 2021). TL-ERT can be used to image the distribution of subsurface bulk electrical conductivity (referred to as EC), whose spatio-temporal changes have been extensively used as a proxy for VWC changes in various contexts over the past 30 years (e.g., hydrogeothermal, environmental, geotechnical and ecological monitoring, following the classification of TL-ERT studies proposed by Dimech et al. (2022)). Recently, particular attention has been given to the quantitative interpretation of TL-ERT results (i.e., conversion

of bulk EC into VWC). The latter can be challenging due to the many physical parameters also affecting subsurface bulk EC (such as temperature, pore water EC, porosity, grain size distribution and mineralogy (Friedman, 2005; Revil et al., 2018)). In this context, some studies have assessed the accuracy of the ERT-predicted VWC, for example, by comparing them with conventional gravimetric methods (Laloy et al., 2011; Hen-Jones et al., 2017b; Acosta et al., 2022) or hydrogeological sensors data (Brunet et al., 2010; Jayawickreme et al., 2010; Beff et al., 2013; Fan et al., 2015; Steiner et al., 2022).

Most studies aiming to predict VWC using TL-ERT at the field scale rely on petrophysical relationships connecting bulk EC and VWC, which are generally determined from small-scale disturbed samples in the laboratory (e.g., Calamita et al. (2012); Mollehuara-Canales et al. (2020)). However, several studies mention that a sample-size laboratory characterization may not be representative of field conditions (Merritt et al., 2016). For example, (i) the presence of macropores, desiccation cracks or bedding planes in the sample, (ii) small-scale heterogeneity or (iii) multiphase composition of the material could have greater influence at sample scale, as opposed to field scale measurements, which capture the bulk electrical properties averaged across larger volumes (Karkkainen et al., 2000; Brovelli and Cassiani, 2010; Glover, 2010; Wehrer et al., 2014; Merritt et al., 2016).

Few studies have focused on the accuracy of VWC estimation in mine tailings using TL-ERT. Moreover, few studies have investigated the validity of laboratory-determined petrophysical relationships up-scaling from sample-scale to laboratory and/or field scale applications, especially in mining wastes. However, these two aspects are crucial to successful applications of TL-ERT for VWC monitoring in mining wastes. Indeed, high accuracy of predicted VWC and better understanding of uncertainties are usually needed for geotechnical and geochemical stability monitoring of mining wastes at field scale (Hui et al., 2018; Clarkson and Williams, 2020; Bussière et al., 2021; Dimech et al., 2022). This study aims to (i) develop a methodology for calibrating petrophysical relationships between bulk EC and VWC in mine tailings, both at sample-scale and at larger scales and (ii) assess the accuracy of the VWC predicted by ERT using the petrophysical relationships specific to each experiment, and using the relationships determined at different scales to study the scaling impact on petrophysical models. Quantifying the accuracy of ERT-predicted VWC in mine tailings will aid in supporting future monitoring studies using TL-ERT as a complementary tool to measure VWC, along with conventional hydrogeological methods. Moreover, developing strategies to up-scale petrophysical relationships accurately will allow the recovery of complex spatio-temporal dynamics of VWC in mine tailings across large scales, which may not be possible when solely relying on point data.

3.3 Materials and methods

3.3.1 Site description and materials

The study site is located at Canadian Malartic mine, a world-class, large tonnage and low-grade intrusion-related gold deposit located in Québec, Canada (Bérubé et al., 2018). Gold mineralization is hosted mainly in meta sedimentary rocks (metaturbidite) and porphyritic intrusions (quartz-monzodiorite) (Bérubé et al., 2019), with a mean grade of 1.07 g/t Au (Darijani and Farquharson, 2021) and an estimated total gold resource exceeding 10 million ounces (Gervais et al., 2014). Four large-scale experimental multi-layer covers were built in 2019 and 2020 to identify the future reclamation of the TSF covering nearly 6 km². The 300 m-long, 10 m-large and 2.3 m-high covers are expected to provide valuable information at the pilot scale and under real meteorological conditions to guide the design of TSF reclamation (Dimech et al., 2021). This study focuses on the experimental CCBE made of waste rocks, tailings and overburden, whose role is to reduce the downward oxygen flux from the atmosphere to the tailings, thanks to the high VWC of a 1 m-thick moisture-retaining layer made of compacted tailings (Maqsoud et al., 2011; Demers and Pabst, 2021b).

The materials used for this study were sampled from 2017 to 2020 at Canadian Malartic mine. As shown in Figure 3.1, the tailings consist of finely milled rocks with nearly 80 % of particles ranging from 2 µm to 80 µm (i.e., mostly silt), 1.22 ± 0.08 % sulfide content, 0.55 ± 0.03 % carbon content ($n = 44$ samples), and some trace metals (see Guittonny-Larchevêque et al. (2016a,b); Lavoie-Deraspe (2019) for more details). The 44 tailings samples collected for grain-size, sulfide and carbon content analysis have similar properties, which suggests a overall homogeneity of tailings. The grain size distribution of overburden (47 samples) and waste rocks (8 samples) are also presented in Fig. 3.1 in brown and grey, respectively. The overburden material is finer than the tailings (mostly clay and silt) and a greater variability is observed between each sample (e.g., $D_{60} = 20.9 \pm 7.8$ µm for overburden and $D_{60} = 40.6 \pm 3.2$ µm for tailings). Finally, the waste rocks used in this study mostly consist of gravel and sand, with nearly 5 % of particles smaller than 100 µm.

3.3.2 Experimental setups

The relationship between VWC measured by hydrogeological sensors and the bulk EC imaged using TL-ERT measurements is investigated at five different scales, summarized in Figure 3.2 (detailed diagrams "Supplementary Materials"). The size of these setups ranges from a few centimeters in the laboratory (**S1**, **S2** and **S3**) to several meters in the field (**S4** and **S5**). The same procedure was followed for the preparation and installation of the tailings for each

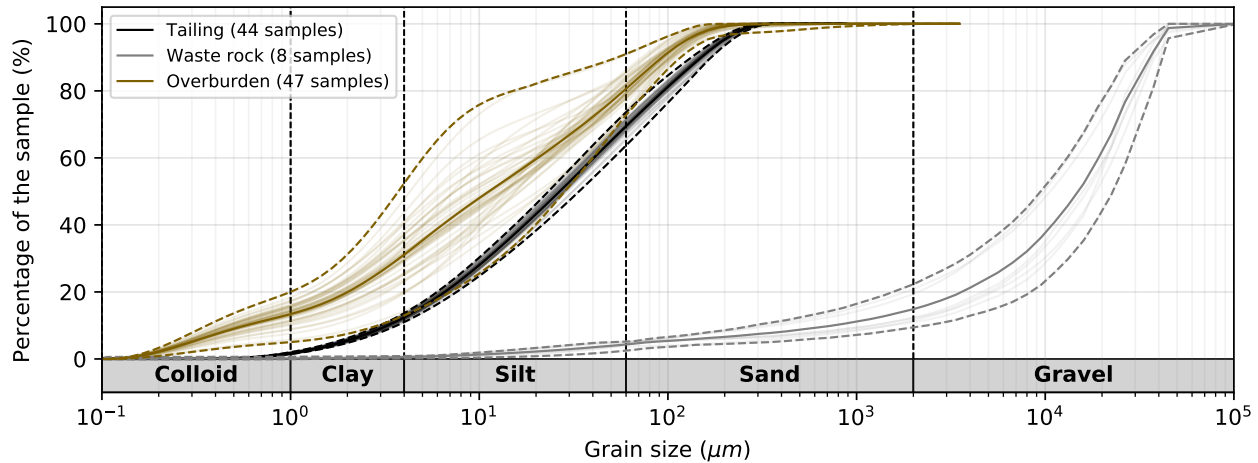


FIGURE 3.1 Grain size distribution of the materials used in the experiment. In total, 44 different samples of tailings (black), 8 samples of waste rocks (grey) and 47 samples of overburden (brown) have been analyzed. Each individual grain size distribution is shown using shaded lines. The mean, minimum and maximum grain size distributions are shown in solid line and dashed lines.

experimental setup to ensure maximum comparability between the different scales. In the laboratory, the tailings material is dried using an oven at 60 °C. The dry material is then deagglomerated into a fine powder (without changing the grain size distribution) and homogenized. A predetermined volume of deionized water is then added to the dry samples to reach an initial VWC of $0.40 \text{ m}^3/\text{m}^3$, which corresponds to the full saturation of the sample, knowing the dry density of the tailings ($2.68 \pm 0.01 \text{ g}/\text{cm}^3$, $n = 44$ samples) and a target porosity of $\phi = 0.4$. Successive 5 cm-high layers of wet tailings samples are compacted inside the laboratory cells at the needed porosity to ensure homogeneity of the material compaction. In the field, the wet tailings were compacted using a power shovel and the porosity of successive 25 cm-high layers was measured in-situ using a nucleodensimeter ($\phi = 0.40 \pm 0.02$, $n = 73$ measurements), which is consistent with previous experimental cells built at Canadian Malartic mine (e.g., Lavoie-Deraspe (2019)).

Scale 1 - Electrical Resistivity Tempe Cell

Figure 3.2.S1 presents a new laboratory apparatus inspired from Tempe cells (ASTM, 2016) designed to simultaneously recover VWC and bulk EC within a soil sample under different pressure conditions, hence referred to as electrical resistivity Tempe cell (ER-TC). A Tempe cell (model 1405 - SoilMoisture Equipment) is modified by including six stainless steel electrodes to carry out ERT measurements during drying of the tailings sample. The dimension

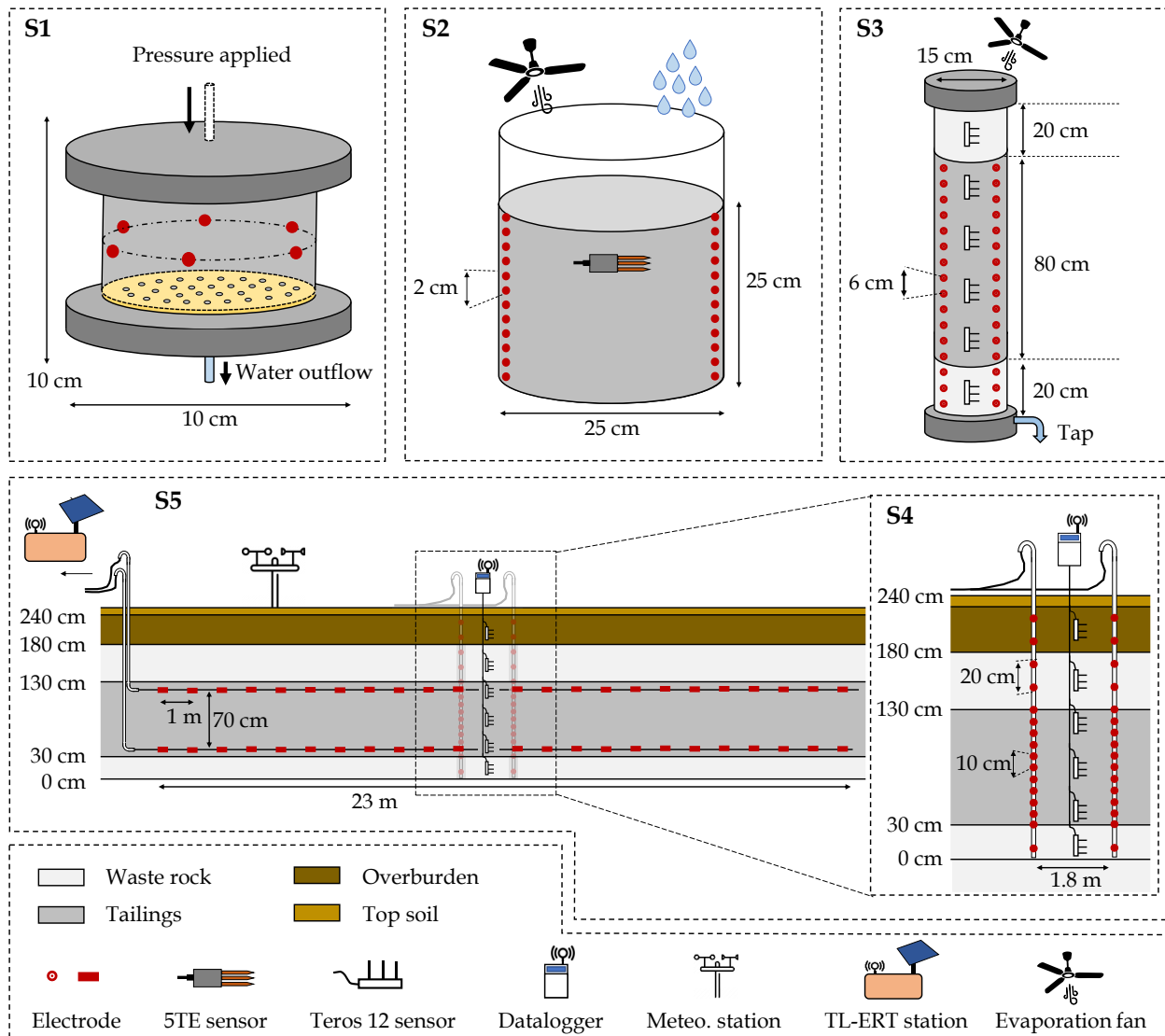


FIGURE 3.2 Illustration of the five scales investigated in this study to assess petrophysical relationships in mine tailings in the laboratory (**S1** - cell scale, **S2** - bucket scale and **S3** - column scale), and in the field (**S4** - local scale and **S5** - pilot scale). Detailed schematics and photographs are available in "Supplementary Materials" for each experimental setup.

of the electrodes (width and length) and their location in the cylindrical cell are determined following the practical guidelines discussed by Lee and Santamarina (2010) and Clement and Moreau (2016). The conventional brass cylinder is replaced by a PVC pipe that can withstand pressures of up to 350 kPa. 15 different steps of pressure are then applied to the top of the cell using air pressure controllers and nitrogen high-pressure bottles to drive changes in VWC (ASTM, 2016, 2000). The positive pressure applied on the top of the cell allows mimicking a corresponding suction which would be applied at the bottom of the cell in the

vadose zone (Sakaki and Illangasekare, 2007). The ER-TCs are weighed after two days at each pressure increment to calculate VWC in the sample. Pore water EC is also monitored by sampling the water coming out of the cell. In the meantime, ERT monitoring is carried out to recover bulk EC variations in the ER-TC using a Terrameter LS (ABEM).

Scale 2 - Laboratory bucket

Figure 3.2.S2 presents the laboratory bucket used to monitor the temporal variations of VWC and bulk EC in tailings under controlled cycles of wetting and drainage (Sylvain et al., 2019). A 30 cm-high, 25 cm-diameter bucket is filled with compacted tailings and instrumented with a 5TE sensor (measuring VWC, bulk EC and temperature every 15 minutes) and two vertical profiles of 12 stainless-steel electrodes each. Each electrode is made of a 1 cm-diameter flat washer fixed by a 5 mm-diameter rivet, with a vertical spacing of 2 cm. As presented by Sylvain et al. (2019), several simulated precipitation events were carried out using deionized water to mimic precipitations (50 mm per simulated precipitation event) and three fans were installed to accelerate evaporation in the tailings. Each wetting and drainage cycle lasted approximately one week and the hydrogeophysical monitoring was performed during two weeks in November 2018. TL-ERT monitoring was carried out using a Terrameter LS and approximately 150 ERT datasets were recorded, with a greater temporal resolution during simulated precipitation events (highest measurement rate of 12 images per hour).

Scale 3 - Laboratory column

Figure 3.2.S3 presents the laboratory column used to reproduce the field-scale experimental CCBE under controlled conditions in the laboratory, as discussed by Isabelle (2022). A 120 cm-high, 15 cm-diameter Plexiglas column is assembled and instrumented to simultaneously monitor VWC and bulk EC. Two layers of waste rocks (20 cm-high each) are installed at the bottom and the top of the column and a 80 cm-high compacted tailings layer, which mimic the geometry of the CCBE built on the field. Initially, the column was fully saturated with deionized water. After a few days, the bottom tap was opened and the materials drained during five months, with an additional evaporation fan installed after 40 days to accelerate the decrease of moisture content in the column (Isabelle, 2022). Six Teros 12 hydrogeological sensors are installed along the flanks of the columns to measure VWC, bulk EC and temperature every 5 min. In addition, two vertical profiles of 16 stainless-steel circular electrodes are installed in the column and connected to a Terrameter LS to carry out ERT monitoring during the free drainage (50 datasets). Each electrode is made of a 1 cm-diameter flat washer fixed by a 5 mm-diameter rivet and the vertical electrode spacing is 6 cm.

Scales 4 and 5 - Field experimental cover

Figures 3.2.S4 and 3.2.S5 present the internal composition of the 2.3 m-high experimental CCBE. The 1 m-thick layer of compacted tailings is expected to behave as a moisture-retaining layer since capillary barrier effects are likely to develop at the boundary between the tailings and the waste rock layers, at the bottom (30 cm-thick) and at the top (50 cm-thick). The capillary barrier effects would then reduce both the downward water percolation and the upward water evaporation from the tailings, hence maintaining a high degree of saturation within the tailings layer. Finally, a 50 cm-thick layer made of overburden and topsoil is placed on the top of the waste rocks to promote vegetation development. Six Teros 12 sensors are installed along a vertical profile at the center of the CCBE and a ZL6 datalogger allows to remotely transfer VWC, bulk EC and temperature measurements for each layer (regular measurement rate of 30 min). At local scale (**S4**), two vertical profiles of 16 electrodes each, separated by 1.8 m, are installed around the profile of Teros 12. Each electrode is made of a 4 cm-diameter and 2.5 cm-long stainless steel cylinder fixed on a PVC pipe using a stainless-steel rivet. The centers of the electrodes are separated by a distance of 10 cm in the tailings and 20 cm elsewhere. In addition, at the pilot scale (**S5**), two 23 m-long horizontal profiles are installed inside the tailings layer 15 cm away from the interfaces with waste rocks. Each parallel profile contains 24 rectangular stainless steel electrodes measuring 6 cm x 2.5 cm and separated by 1 m, which allows monitoring bulk EC in the tailings layer along the 23 m-long profiles. All the electrodes are connected to a PRIME system instrument (Holmes et al., 2020, 2022b), which carries out ERT images four times a day (since the beginning of May 2021, still ongoing in 2022). The PRIME system itself is installed in a cabin powered by an electric line and equipped with an antenna and a router to allow autonomous transfer of TL-ERT data to remote servers. A meteorological station is installed at the surface of the cover to monitor air temperature and precipitations.

3.3.3 Measurements and data processing

Meteorological and hydrogeological data

Figure 3.3 summarizes graphically the main steps proposed in this study to determine petrophysical relationships from the simultaneous and co-located monitoring of VWC and bulk EC at different scales. For all experiments, air temperature and precipitation are monitored using a meteorological station in the field or temperature probes for laboratory experiments (identified as step **(i)** in Fig. 3.3). 5TE or Teros 12 hydrogeological sensors are connected to dataloggers to monitor VWC, bulk EC and temperature (step **(ii)** in Fig. 3.3), which allows

estimating interstitial pore water EC (see Hilhorst (2000); Dimech et al. (2019)). These capacitance sensors measure the dielectric permittivity of the medium using a high-frequency oscillating electrical voltage (i.e., 70 MHz), which is then converted into VWC using Topp's equation and material-specific calibrations (Topp et al., 1980; Noborio, 2001). For these sensors, typical resolution and accuracy of VWC measurements are respectively $0.001 \text{ m}^3/\text{m}^3$ and $\pm 0.02 \text{ m}^3/\text{m}^3$ when the proper calibrations are applied. As mentioned by Hen-Jones et al. (2017b), the hydrogeological sensors use a two-points measurement to monitor bulk EC, which makes them more sensitive to changes in contact resistance than the four-points measurements done by ERT (especially at low moisture content).

Geophysical data acquisition

The electrodes installed along vertical or horizontal profiles are connected to two different resistivity meters (step (iii) in Fig. 3.3). The **Terrameter LS** commercialized by ABEM is used for laboratory-scale experiments. The **PRIME** instrument (*PRoactive Infrastructure Monitoring and Evaluation system*) designed by the British Geological Survey (Holmes et al., 2020, 2022b) is used for continuous monitoring of the field-scale experiment. Both resistivity meters allow to carry out several potential measurements simultaneously according to specific four-electrodes measurement sequences, referred to as protocols (see Figure in "Supplementary Material" for an example of some protocols used). All quadrupoles are used for the ER-TC (scale **S1**), which corresponds to 45 direct measurements and 45 reciprocal measurements (i.e., configurations where current and potential electrodes are exchanged). For the experimental setups which contained more electrodes (scales **S2** to **S5**), dipole-dipole and Wenner-alpha configurations are used with a and n values between 1 and 3 (see Lesmes and Friedman (2005); Samouëlian et al. (2005); Binley and Slater (2020) for details). Reciprocal measurements are integrated into all TL-ERT data acquisition protocols following the guidelines of Tso et al. (2017), since the combination of direct and reciprocal measurements allows data error to be better estimated. Finally, special attention is given to the electrode polarisation issues by ensuring that the same electrode is not used for potential measurements just after being used to inject current (Wilkinson et al., 2012a). The temporal resolution of TL-ERT data acquisition is adapted for each experimental setup. For example, more ERT datasets were recorded for laboratory experiments when the fastest changes of VWC were expected. For the field experiments, ERT datasets are collected with a regular sampling of four images per day.

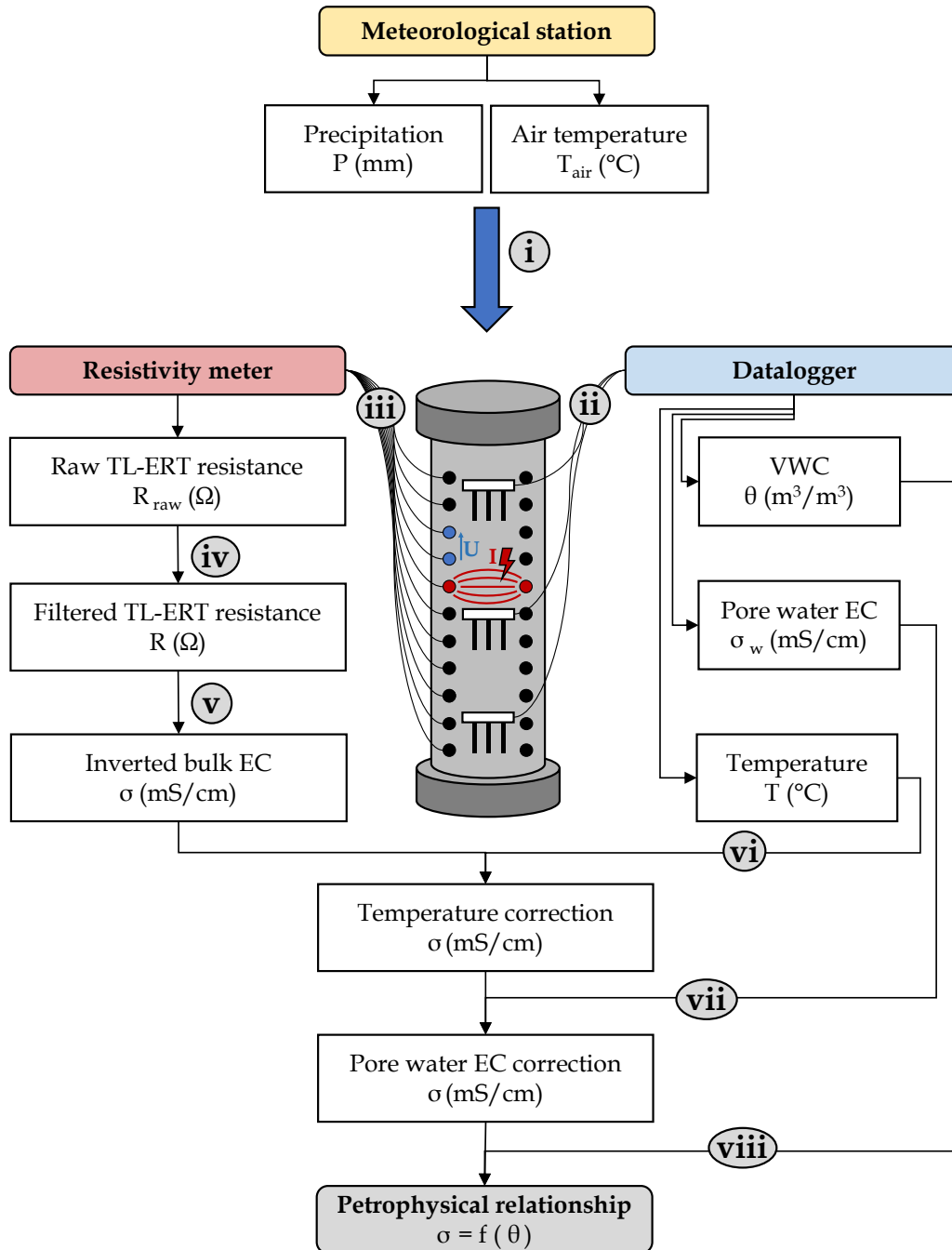


FIGURE 3.3 Workflow of hydrogeophysical data acquisition and processing used to recover petrophysical relationships from multi-scale experimental setups. The laboratory column (scale 3) is used as an example.

Geophysical data processing

For each experimental setup, the apparent resistivity time-series are analyzed in order to identify and remove erroneous measurements, outliers, or unstable noisy data following the methodology described by Tso et al. (2017) and others (Deceuster et al., 2013; Chambers et al., 2014b) (step **(iv)** in Fig. 3.3). Reciprocal errors are estimated for each four-electrodes measurement by calculating the difference between direct and reciprocal configurations and data with a reciprocal error greater than 10 % are removed (Tso et al., 2019). Moreover, filtering is applied on the stacking error ($\epsilon < 10$ %), the injected current intensity ($0.001 \text{ mA} < I < 600 \text{ mA}$) and the contact resistance between current electrodes ($R < 10000 \text{ } \Omega$). A similar data processing approach is applied to the field data collected with the PRIME instrument, which yields to 400 000 valid measurements in total from May to November 2021. Nearly 85 % of the resulting filtered field dataset exhibits a reciprocal error lower than 1 %, which denotes satisfying data quality for the geoelectrical monitoring of tailings. Following the methodology proposed by Koestel et al. (2008), Lesparre et al. (2017) and Tso et al. (2017), an envelope fit error model of the form $\epsilon_R = a \cdot R + b$ is determined for each experiment, where ϵ_R is the difference between direct and reciprocal resistance measurements, a ranges from 0.01 to 0.05 depending on the ERT data quality of each experiment and b equals to $0.001 \text{ } \Omega$.

Geophysical data inversion

For each experimental setup, the filtered resistance data (\mathbf{d}) is inverted using **pyGIMLi** (Günther et al., 2006; Rücker et al., 2006; Rücker et al., 2017) to recover the distribution of bulk EC (\mathbf{m}) (step **(v)** in Fig. 3.3). 3D models are used for laboratory setups given the cylindrical shape of the ER-TC, column or bucket whereas 2D vertical planes are defined for field experiments, given the lateral extension of the experimental cover. The inverted bulk EC distribution \mathbf{m} is assumed to be the best trade-off between two cost functions ; the data misfit constraint and the model regularization constraint. The resulting cost-function (denoted as $\Phi(\mathbf{m})$) is then expressed by (Johnson et al., 2012b) :

$$\Phi(\mathbf{m}) = \|\mathbf{W}_d \cdot (d - F(\mathbf{m}))\| + \lambda \|\mathbf{W}_m \cdot (\mathbf{m} - \mathbf{m}_0)\| \quad (3.1)$$

In this equation, $F(\mathbf{m})$ corresponds to the forward modeling operator, which outputs a set of synthetic resistance data for a given distribution of bulk EC (Rücker et al., 2006). \mathbf{W}_d and \mathbf{W}_m are respectively the data weighting and the model constraint matrices and λ is a regularization coefficient (Johnson et al., 2012b). Finally, \mathbf{m}_0 is a prior model that can be used to constraint the inversion.

For all experimental setups, an anisotropic spatial smoothing is applied to the distribution of bulk EC to reproduce the horizontal layering in VWC observed for unsaturated conditions (sharper changes of VWC in z than in x and y). Moreover, the geometry of the experimental cover is taken into account for the inversion of field data and horizontal layers are included in the 2D model, hence allowing sharp variations at the boundaries between different materials (e.g., Johnson et al. (2012b); Dimech et al. (2017, 2019)). The resulting meshes contain between 4000 and 17000 tetrahedron elements for 3D meshes and between 4000 and 12000 triangular cells for 2D meshes, which allows to perform each inversion in less than one minute. A temporal regularization is also applied for all experiments by using the previous inverted distribution of bulk EC as a starting model for each time step. This approach, referred to as the "cascade inversion", helps limiting the unrealistic and erratic evolution of inverted bulk EC, which could be observed in some areas poorly constrained by the inversion process (Hayley et al., 2011; Singha et al., 2015).

Temperature and pore water EC corrections

After the inversion process, the inverted bulk EC values are extracted from the 3D or 2D models at the location of the hydrogeological sensors, knowing their volume of investigation (approximately 5 cm around each sensor). As illustrated by step **(vi)** in Fig. 3.3, a temperature correction is applied to the extracted inverted bulk EC. This allows to compare the laboratory experiments ($\simeq 23$ °C) and the field experiment (between 0 °C in Winter and 25 °C in Summer), and to account for temperature variations. For all experiments, a standard temperature of $T_{\text{std}} = 25$ °C is used, and the temperature-corrected bulk EC σ_{corr} is calculated by (Ma et al., 2011) :

$$\sigma_{\text{corr}} = \sigma \cdot \left[\frac{1}{1 + tc \cdot (T - T_{\text{std}})} \right] \quad (3.2)$$

where σ is the bulk EC at the temperature T , measured by the hydrogeological sensors and tc is the temperature correction factor, which corresponds to the fractional change in σ per degree Celsius. A value of $tc = 0.02$ °C⁻¹ is used in this study, which means that bulk EC increases by 2% for a temperature increase of 1 °C (Hayashi, 2004; Hayley et al., 2007, 2010).

Similarly, a pore water EC correction is applied (step **(vii)** on Fig. 3.3) to allow the comparison of the laboratory experiments (where water EC ranged between 3 and 6 mS/cm) with the experimental field cover (where water EC ranged between 2 and 3 mS/cm for the time period studied). The corrected bulk EC σ_{corr} is obtained using (e.g., Waxman and Thomas (1972); Mollehuara-Canales et al. (2020)) :

$$\sigma_{\text{corr}} = \sigma \cdot \left[\frac{\sigma_{\text{w std}}}{\sigma_{\text{w}}} \right] \quad (3.3)$$

where σ_{w} is the pore water EC normalized at 25 °C estimated from the hydrogeological sensor measurements. For all experiments, a reference value of $\sigma_{\text{w std}} = 4 \text{ mS/cm}$ is chosen.

Petrophysical relationships

The corrected bulk EC values obtained from the inversion are then compared with VWC measurements at the same location. Arguably, the Archie petrophysical model is the most common model connecting bulk EC σ and saturation S_{w} in unsaturated porous media, neglecting the surface conduction additional term, which is assumed to be small compared to electrolytic conduction (Archie et al., 1942; Cai et al., 2017) :

$$\sigma = a \cdot \phi^m \cdot S_{\text{w}}^n \cdot \sigma_{\text{w}} \quad (3.4)$$

In this model, σ_{w} is the pore fluid EC expressed in mS/cm, ϕ is the porosity (-) such as $\text{VWC} = \phi \cdot S_{\text{w}}$, and a , m and n are three unitless parameters, commonly referred to as the "a parameter" (Glover, 2016), the cementation exponent (Glover, 2009) and the saturation exponent, respectively.

An optimized petrophysical model is obtained for each experiment by fitting the Archie parameters m and n (-) to minimize the root mean square error (RMSE) between the inverted bulk EC and the bulk EC predicted by the petrophysical model for a given measurement of VWC (Holmes et al., 2022b), assuming $a = 1$. Moreover, the RMSE, the bias and the precision of ERT-predicted VWC are calculated to assess the accuracy of VWC estimations at the different scales studied (Ritter and Munoz-Carpena, 2013).

3.4 Results

3.4.1 Scale 1 - Electrical Resistivity Tempe Cell

Figure 3.4 presents the results obtained from the hydrogeophysical measurements in two identical ER-TCs during the drainage of the tailings. The temperature in the cells remained nearly constant at the laboratory temperature ($\simeq 25 \text{ °C}$) and water outlet sampling allowed to monitor pore water EC over time (between 3.5 mS/cm and 4.5 mS/cm). 14 different pressure steps were applied to the top of the cells, ranging from 1 kPa to 250 kPa. The increase in pressure caused a decrease in VWC from $0.4 \text{ m}^3/\text{m}^3$ to $0.15 \text{ m}^3/\text{m}^3$. The increase in pressure is also associated with a decrease in inverted bulk EC, from 1.3 mS/cm at full

saturation to a minimum of 0.1 mS/cm at maximum pressure. Although bulk EC is slightly noisier than VWC, especially at higher pressures, the two parameters seem to be strongly correlated. The evolution of VWC and bulk EC seems consistent with the air entry value of these tailings around 30 kPa (Bussi re, 2007; Lavoie-Deraspe, 2019). As expected, bulk EC in the tailings was maximal at high VWC and decreased progressively for lower VWC. The m and n parameters of an Archie model were optimized to fit the distribution of inverted bulk EC and measured VWC for $a = 1$, $\phi = 0.4$ and using a reference temperature $T = 25 \text{ }^\circ\text{C}$ and a reference pore water EC $\sigma_w = 4 \text{ mS/cm}$. The values $m = 1.22$ and $n = 3.45$ performed the best with a RMSE value of 0.12 mS/cm.

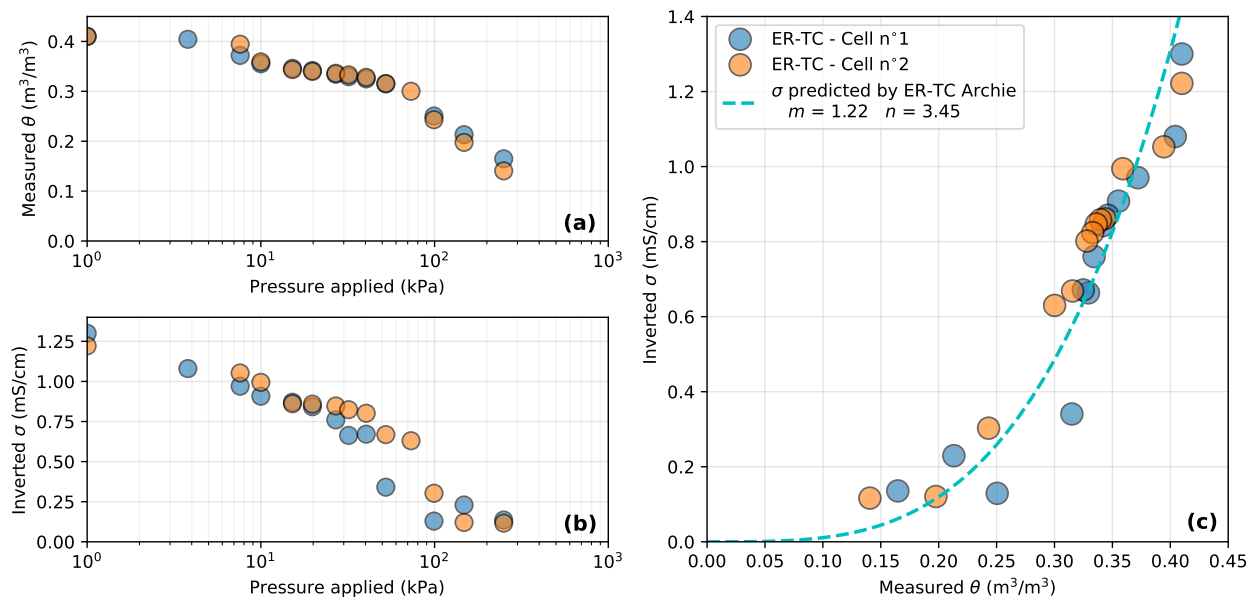


FIGURE 3.4 Results from the monitoring of the Electrical Resistivity Tomography Cells (scale 1). Evolution of (a) measured VWC and (b) inverted bulk EC in the tailings for several pressure steps. (c) Relationship between VWC and bulk EC in the ER-TC.

3.4.2 Scale 2 - Laboratory bucket

The top panel of Figure 3.5 presents the inverted bulk EC distribution in the laboratory bucket at selected time steps, before, during and after an artificial precipitation event of 50 mm. As expected, water infiltration increased bulk EC in the tailings from below 0.1 mS/cm to above 0.6 mS/cm soon after the infiltration event. Bulk EC increased in the bottom of the bucket a few minutes after the start of the experiment, which suggests that preferential flow occurred from the sides of the bucket. Bulk EC slowly decreased after a few days to come back to initial values after 3 days. Finally, the sensitivity distribution indicates that sensi-

vity is maximal near electrodes on the sides of the bucket as expected, and decreases toward the center of the bucket, where the 5TE sensor is installed. As shown on the bottom panel of Figure 3.5 for one precipitation event, VWC and inverted bulk EC show similar patterns in the tailings, apart from the sensor at 50 cm (orange). A sharp increase in VWC and bulk EC was observed following each 50 mm simulated precipitation event and a slower decrease was reported then, which lasted approximately one week after the precipitation event. The temperature in the tailings ranged from 19 to 24 °C throughout the experiment, whereas the pore water EC remained constant at 3.5 mS/cm. The petrophysical model obtained for this experiment (black dashed line on Fig. 3.5d)) with the parameters $m = 0.73$ and $n = 4.96$ fits the hydrogeophysical datasets with a RMSE value of 0.15 mS/cm, and is similar to the ER-TC Archie model (blue dashed line), especially for VWC values lower than $0.35 \text{ m}^3/\text{m}^3$.

3.4.3 Scale 3 - Laboratory column

The top panel of Figure 3.6 presents 2D slices of the inverted bulk EC in the laboratory column at different time steps. Bulk EC was high in the saturated tailings at the beginning of the experiment ($> 0.6 \text{ mS/cm}$) and dropped to below 0.1 mS/cm after 50 days of drainage and evaporation, especially at the top of the tailings layer where the lowest values of bulk EC were observed. Globally, the waste rocks layers at the bottom and the top of the column remained highly resistive throughout the experiment ($< 0.02 \text{ mS/cm}$). The sensitivity was maximal in the tailings layer and around electrodes, while lower sensitivities were observed in the waste rocks. As shown by the bottom panel of Figure 3.6, VWC ranged between 0.38 and $0.40 \text{ m}^3/\text{m}^3$ when the materials were initially saturated. Two sensors on the top of the tailings (in red and green on Fig. 3.6a) evidenced a sharp drop in VWC down to $0.33 \text{ m}^3/\text{m}^3$, approximately five days after the beginning of the experiment, whereas the two sensors in the bottom of the tailings layer (in orange and blue) remained near saturation during approximately 40 days. These sensors evidenced a strong decrease in VWC after 40 days, which corresponds to the installation of an evaporation fan. The same trends were observed from inverted bulk EC variations, especially at the bottom of the tailings, where inverted bulk EC remained near its initial value (0.8 mS/cm) until day 40 and then dropped to 0.1 mS/cm . The temporal variations of VWC and inverted bulk EC values are mostly consistent, except at $z = 50 \text{ cm}$ (orange sensor), where the bulk EC seems to decrease more rapidly than the measured VWC. Finally, the temperature and the pore water EC within the tailings ranged between 21 and 27 °C and between 3.5 and 5.5 mS/cm, respectively. The optimized Archie model (black dashed line on Fig. 3.6c)) with the parameters $m = 1.27$ and $n = 4.20$ fits the data with a RMSE of 0.24 mS/cm .

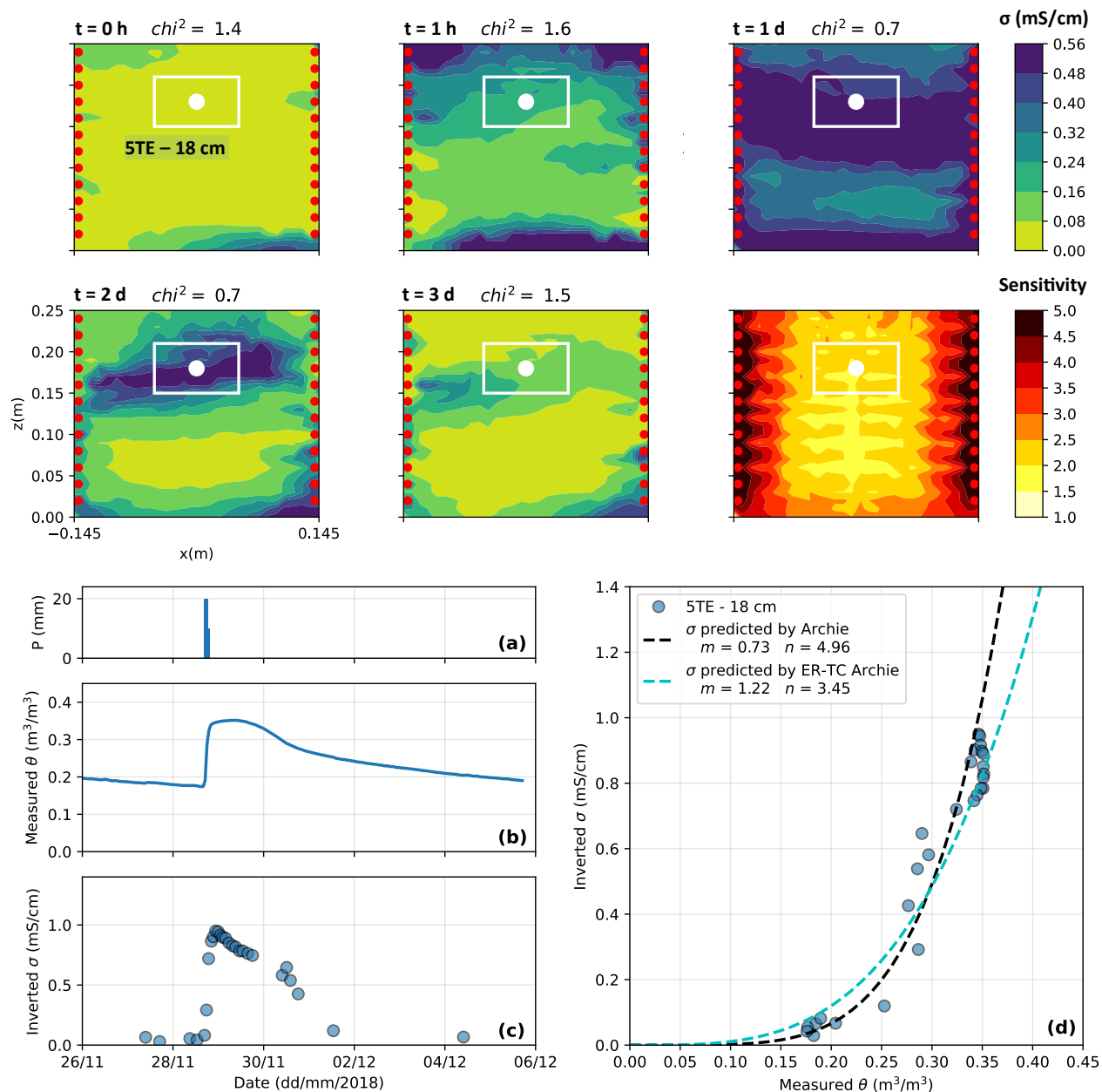


FIGURE 3.5 Top panel : 2D slices of the 3D inverted bulk EC distribution and sensitivity for the laboratory bucket (scale **S2**) at selected time steps. The VWC sensor location is indicated by a white dot and the white rectangle corresponds to its volume of investigation, where inverted bulk EC is extracted to be compared with VWC measurements. Bottom panel : evolution of (a) artificial precipitations, (b) VWC and (c) inverted bulk EC in the tailings during the artificial precipitation event and (d) petrophysical relationship between VWC and bulk EC in the bucket.

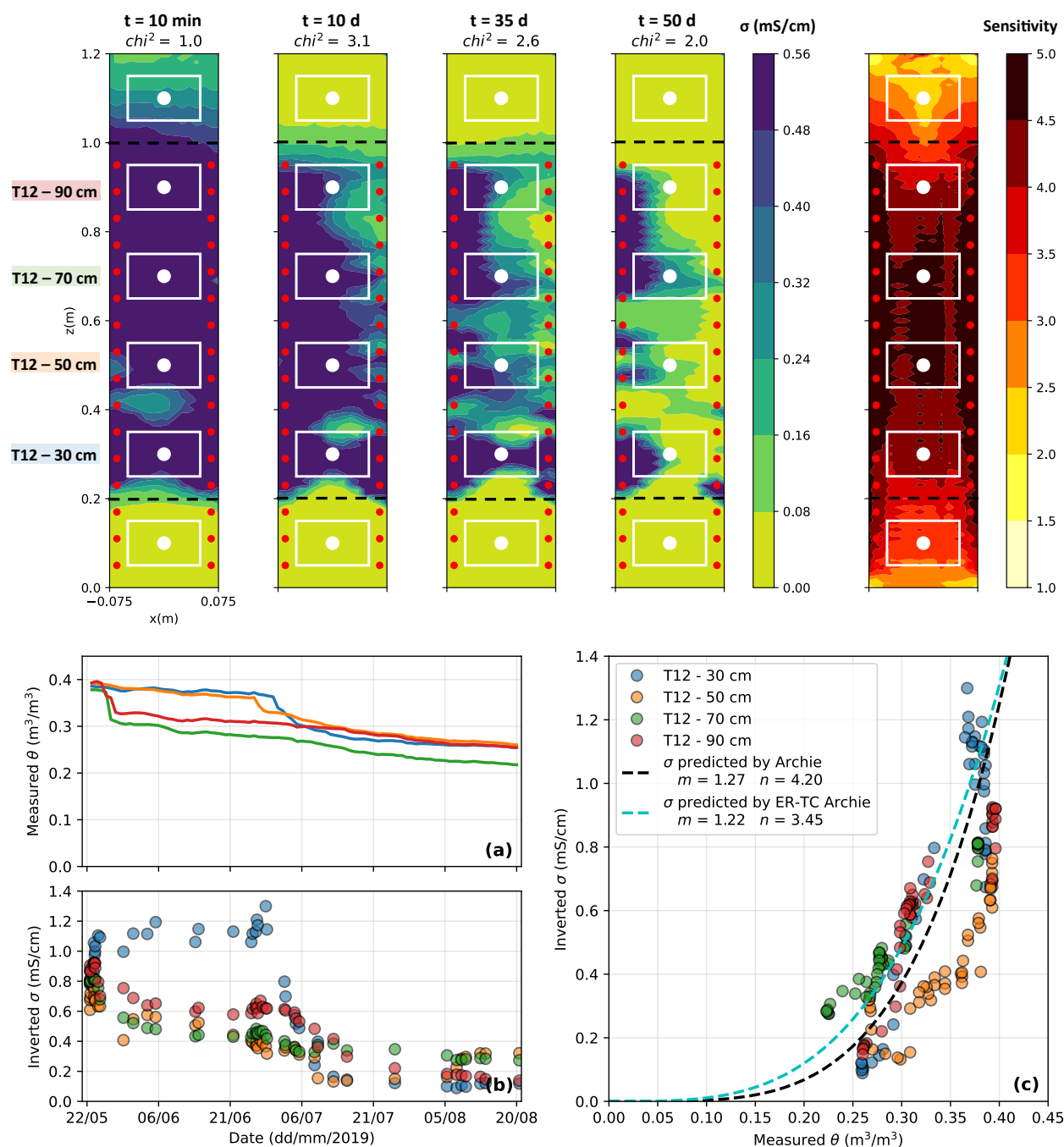


FIGURE 3.6 Top panel : 2D slices of the 3D inverted bulk EC distribution and sensitivity for the laboratory column (scale **S3**) at selected time steps. The VWC sensor location is indicated by white dots and the white rectangles correspond to their volumes of investigation. Bottom panel : evolution of (a) VWC and (b) inverted bulk EC in the tailings during the artificial precipitation event and (c) petrophysical relationship between VWC and bulk EC in the bucket.

3.4.4 Scale 4 - Field cover at local scale

The top panel of Figure 3.7 presents the 2D inversion mesh defined with pyGIMLi/BERT and the distribution of inverted bulk EC and sensitivity in the CCBE at local scale. The addition of refinement nodes, sensors and horizontal layers allowed to refine the mesh where needed. The inversion of field ERT data shows that the waste rocks are highly resistive ($\sigma < 0.02$ mS/cm), whereas the tailings and the overburden materials are more conductive, with bulk EC ranging from 0.3 to 0.6 mS/cm (before temperature and pore water EC corrections). A slight increase in bulk EC with depth is also observed in the tailings layer. As expected, the sensitivity is highest near the electrodes and decreases sharply in the rest of the imaging domain. Higher sensitivities are observed in the tailings layer, which is consistent with the smaller electrode spacing and the higher bulk EC reported in the tailings.

The bottom panel of Figure 3.7 shows the evolution of VWC and bulk EC in the CCBE at local scale from May to November 2021 at local and pilot scale. VWC remained above $0.3 \text{ m}^3/\text{m}^3$ in the tailings (blue, orange and green lines), which suggests that the capillary barrier effects at the bottom and at the top of the moisture-retaining layer are effective. Every significant precipitation event (> 20 mm/day) is followed by an increase in VWC, particularly marked at the top of the tailings layer (green line), where the VWC is always lower than in the rest of the moisture-retaining layer, and in the overburden layer at $z = 200$ cm (red line). Similar trends can be observed from the variations of inverted bulk EC at both scales, which is generally lower at the top of the tailings layer. A slow but steady decrease of both VWC and inverted bulk EC is observed at the bottom of the tailings layer, as well as a lower response to precipitations event. Similarly, both water content and bulk EC are lower at the top of the cover (green and red sensors) than in the rest of the moisture-retaining layer and exhibit greater temporal variations. Teros 12 sensors also monitored the temperature and pore water EC in the CCBE over time. In contrast to laboratory experiments, strong variations of temperature from $5 \text{ }^\circ\text{C}$ to $\simeq 24 \text{ }^\circ\text{C}$ were observed from May to November 2021. The pore water EC remained fairly constant in the tailings layer, with values ranging from 2 to 3 mS/cm throughout the monitoring period. The lower pore water EC values observed in the field (when compared to the laboratory experiments) are likely due to the mixing of initial interstitial pore water ($\sigma_w \simeq 5.0$ mS/cm) and precipitations ($\sigma_w < 0.1$ mS/cm), which has been occurring since the construction of the covers in Fall 2019. Figure 3.7d) demonstrates that the evolution of VWC and bulk EC are consistent in the CCBE at local scale, since the optimized Archie model ($m = 1.22$ and $n = 3.02$) fits the hydrogeophysical data with a RMSE of 0.08 mS/cm.

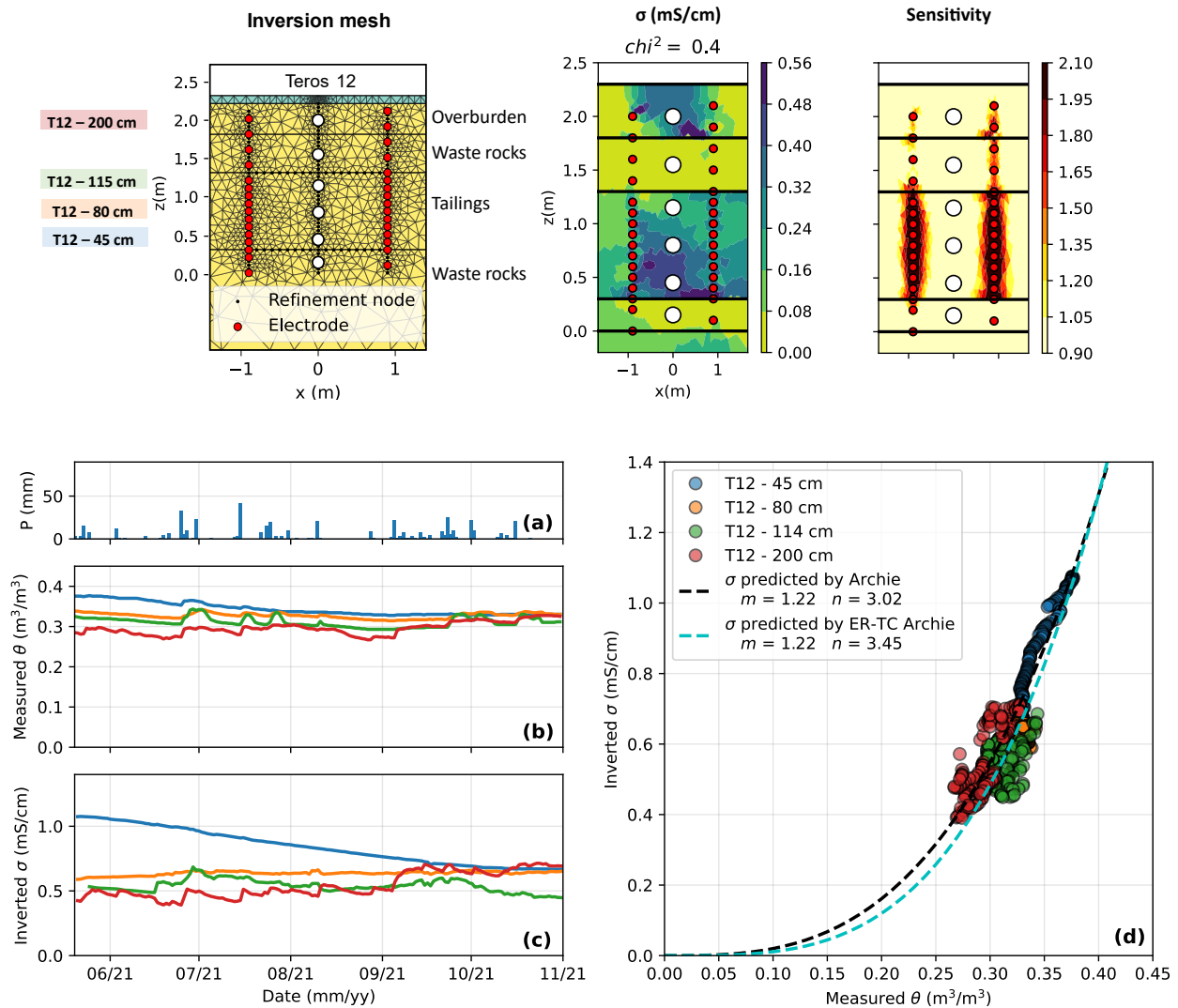


FIGURE 3.7 Top panel : inversion mesh, 2D inverted bulk EC distribution and sensitivity in the experimental field cover at local scale (scale **S4**) for a representative time step. The VWC sensors are indicated by white dots and electrodes correspond to red dots. Bottom panel : evolution of (a) precipitations, (b) VWC and (c) inverted bulk EC in the tailings from May to November 2021 and (d) relationship between VWC and bulk EC in the experimental CCBE cover at local scale.

3.4.5 Scale 5 - Field cover at pilot scale

The top panel of Figure 3.8 shows the inversion mesh used for TL-ERT inversion of field data and the distribution of inverted bulk EC and sensitivity for the 23 m-long CCBE (scale **S5**). The inverted bulk EC values obtained at pilot scale are consistent with the results presented above at local scale. While inversion sensitivity is high near the electrodes in the tailings

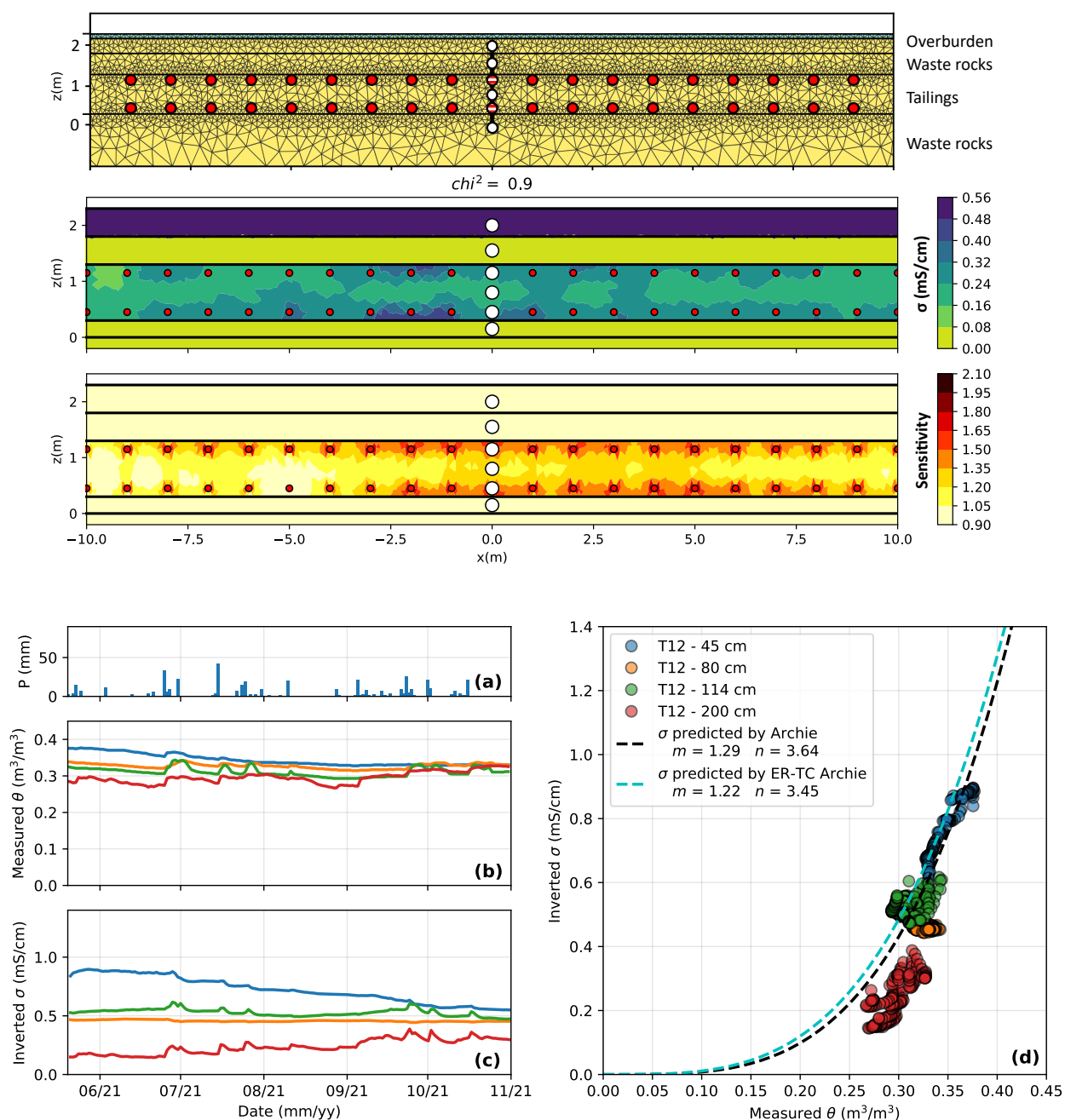


FIGURE 3.8 Top panel : inversion mesh, 2D inverted bulk EC distribution and sensitivity in the experimental field cover at pilot scale (scale **S5**) for a representative time step. The VWC sensors are indicated by white dots and electrodes correspond to red dots. Bottom panel : evolution of (a) precipitations, (b) VWC and (c) inverted bulk EC in the tailings from May to November 2021 and (d) relationship between VWC and bulk EC in the experimental CCBE cover at pilot scale.

layer, poor sensitivity is observed in the overburden and waste rocks layers, as well as in the middle of the tailings layer ($z = 80$ cm) and near dysfunctional electrodes. As shown by

the bottom panel of Figure 3.8, the temporal evolution of VWC and inverted bulk EC are consistent, and bulk EC is particularly well reconstructed by inversion in the tailings layer at the green and blue sensor locations (top and bottom of the tailings). On the contrary, bulk EC does not match well VWC measurements in the middle of the tailings layer (orange sensor on Fig. 3.8b)) and in the overburden (red sensor), which is likely to be due to the lack of sensitivity at these locations. Globally, the optimized petrophysical Archie model ($m = 1.29$ and $n = 3.64$) fits the hydrogeophysical dataset with a RMSE value of 0.13 mS/cm at pilot scale as shown in Fig. 3.8d).

3.4.6 Relative importance of temperature and pore water EC corrections at different scales

Figure 3.9 compares the influence of the temperature correction (left panel) and the pore water EC correction (right panel) applied to the inverted bulk EC to predict VWC. Measured and ERT-predicted VWC are compared (i) when no corrections are applied, (ii) when the temperature correction is not applied, (iii) when the temperature correction is applied using noisy temperature datasets (random noise of ± 5 °C) and (iv) when the temperature correction is applied using exact temperature. The same approach is followed for the pore water EC correction using a random noise of ± 20 % of the measured pore water EC.

For all experiments, most of the ERT-predicted VWC values lie between the two black dashed lines when the two corrections are properly applied, which indicates that the overall accuracy of ERT-predicted VWC is near $0.03 \text{ m}^3/\text{m}^3$. The accuracy of VWC predictions decreases when the temperature or/and the pore water EC corrections are not applied, particularly for the field experiment (Scale **S4**). At this scale in particular, the RMSE between ERT-predicted and measured VWC is $0.077 \text{ m}^3/\text{m}^3$ when no corrections are applied, (ii) $0.038 \text{ m}^3/\text{m}^3$ when the temperature correction is not applied, (iii) $0.053 \text{ m}^3/\text{m}^3$ when the pore water EC correction is not applied, and (iv) $0.013 \text{ m}^3/\text{m}^3$ when the two corrections are properly applied. Similarly, the precision of ERT-predicted VWC decreases when noisy temperature and pore water EC are used, particularly for the field experiment (Scale **S4**). Indeed, the precision of ERT-predicted VWC in the field CCBE is two times lower when a ± 5 °C noise is randomly applied to the temperature dataset (as opposed to an exact temperature). The same observation is made when a ± 20 % noise is randomly applied to the pore water EC dataset. The accuracy of ERT-predicted VWC is less affected by the temperature and pore-water EC corrections for laboratory experiments, which can be explained by smaller variations of temperature and pore water EC.

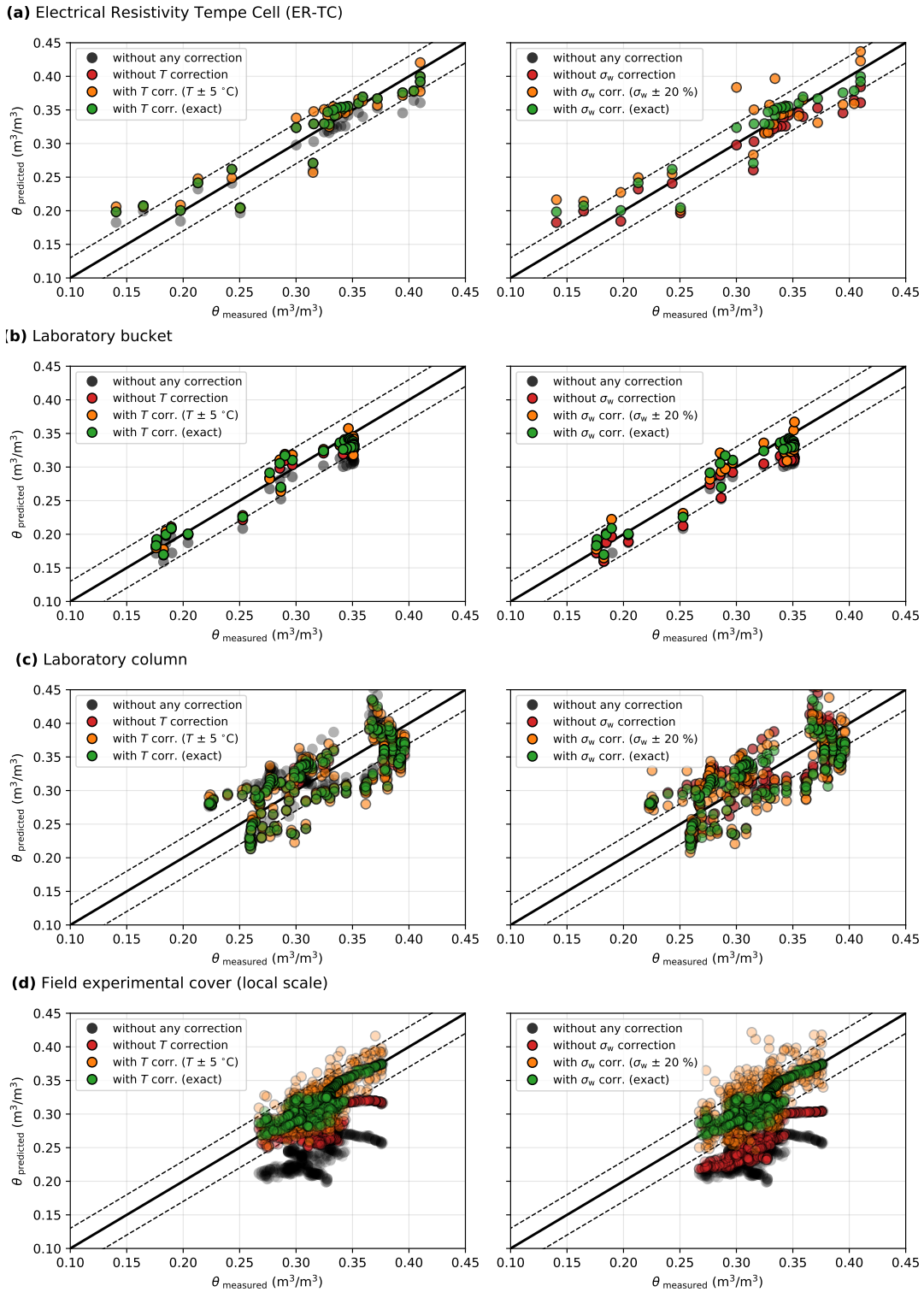


FIGURE 3.9 Influence of temperature and pore water EC corrections on the accuracy of ERT-predicted VWC for (a) Scale S1 - ER Tempe Cell, (b) Scale S2 - laboratory bucket, (c) Scale S3 - Laboratory column and (d) Scale S4 - Field cover at local scale.

3.4.7 Multi-scale comparison of petrophysical models and ERT-predicted VWC accuracy

The top left panel of Figure 3.10 compares the petrophysical models calibrated using hydrogeophysical datasets at various scales. All petrophysical models are similar to each other since the models from scales **S2** to **S5** are encompassed within the area defined around the ER-TC model in shaded blue (scale **S1**), considering an uncertainty of $\pm 0.03 \text{ m}^3/\text{m}^3$. The histograms of errors between measured and ERT-predicted VWC shown in the top right panel of Fig. 3.10 assess the accuracy of ERT-predicted VWC. As expected, the lowest RMSE and bias values are observed for the diagonal elements, i.e., when the same hydrogeophysical datasets are used for the calibration of petrophysical models and the prediction of VWC using ERT for each scale. However, it can be observed that RMSE and bias values remain below $0.03 \text{ m}^3/\text{m}^3$ and $\pm 0.01 \text{ m}^3/\text{m}^3$, respectively, when a petrophysical model defined at a specific scale is used to predict VWC at a different scale (i.e., non-diagonal elements). For instance, the left column of the matrix indicates that RMSE and bias of ERT-predicted VWC using the ER-TC petrophysical model are below $0.04 \text{ m}^3/\text{m}^3$ and $\pm 0.02 \text{ m}^3/\text{m}^3$, respectively, for the different scales.

3.5 Discussion

3.5.1 Overall accuracy of ERT-predicted VWC

This study compares VWC measured using hydrogeological sensors and ERT-predicted VWC using Archie petrophysical models at different scales and for different hydrogeological conditions (drainage, wetting and natural precipitations). Overall, the reliability of ERT-predicted VWC is similar to the accuracy of moisture content sensors at the different scales studied. Indeed, both low bias and high precision are achieved (below $0.01 \text{ m}^3/\text{m}^3$ in absolute value and below $0.03 \text{ m}^3/\text{m}^3$, respectively). In addition, RMSE values do not exceed $0.035 \text{ m}^3/\text{m}^3$ at the different scales investigated in this study. As a result, VWC dynamics are well imaged using TL-ERT at the different scales, both during mine tailings drying, wetting and drying cycles and for field meteorological conditions. The latter highlights the strong potential that TL-ERT could represent as a monitoring approach used in combination with point moisture sensors to increase the investigation volume of future monitoring programs in reclamation covers (e.g., Dimech et al. (2021); Martinez-Pagan et al. (2021)), as this is the case for monitoring landslide, permafrost, geotechnics or CO_2 storage, for example (Whiteley et al., 2019; Falcon-Suarez et al., 2020; Dimech et al., 2022).

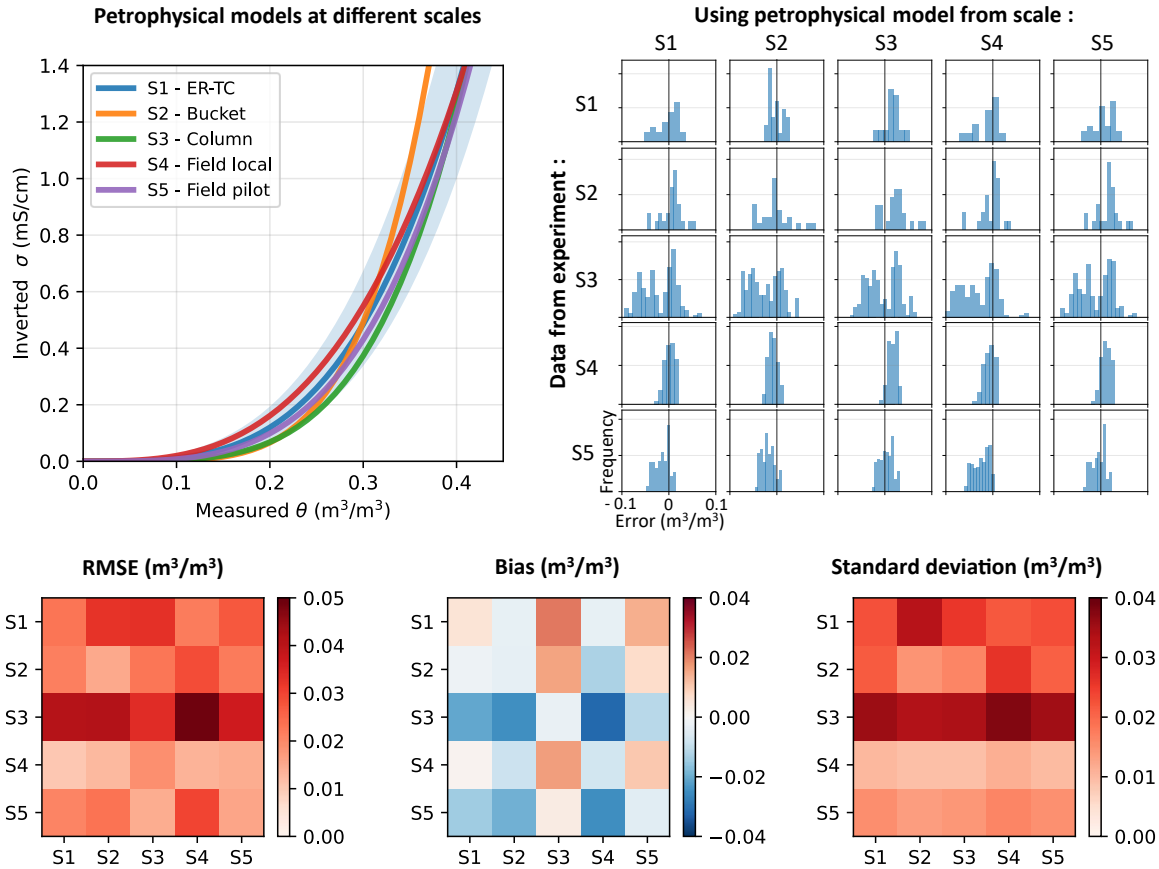


FIGURE 3.10 Assessment of the scale influence on petrophysical models and on the accuracy of ERT-predicted VWC. Top left - Comparison of the petrophysical models calibrated using hydrogeophysical datasets from scales **S1** to **S5**. Top right - Histograms of the error between measured and ERT-predicted VWC using data and petrophysical models from different scales. Bottom panel - RMSE, bias and standard deviation of VWC prediction errors using ERT data and petrophysical models from different scales.

The accuracy of ERT-derived VWC reported in this study is consistent with previous studies for other fields of applications, including hydrogeological studies (Laloy et al., 2011; Dietrich et al., 2014), waste landfills imaging (Neyamadpour, 2019), root zone dynamics monitoring (Garré et al., 2011; Fan et al., 2015) and irrigation studies (Jayawickreme et al., 2010; Beff et al., 2013). Indeed, most of these studies reported RMSE values ranging between 0.01 and 0.04 m^3/m^3 (e.g., Michot et al. (2003); Calamita et al. (2012); Brillante et al. (2014)). Generally, local moisture sensors (e.g., TDR sensors or capacitance probes), neutron probes, numerical modelling or direct oven-weighting methods are used to measure VWC and evaluate the accuracy of ERT-predicted VWC (e.g., Jayawickreme et al. (2010); Laloy et al. (2011); Dietrich et al. (2014); Fan et al. (2015); Hen-Jones et al. (2017b); Sun et al. (2020)). Bias and precision of ERT-predicted VWC reported in some studies are also consistent with the

results of this study (e.g., Zhou et al. (2001); Schwartz et al. (2008); Rucker (2010)).

Some authors report higher accuracy for ERT-predicted VWC in wet conditions (in comparison with dryer conditions) (Laloy et al., 2011; Fan et al., 2015; Merritt et al., 2016). This observation is consistent with the results obtained at the sample scale (scale **S1** - electrical resistivity Tempe cell, see Section 3.4.1). The latter could be explained in part by a better electrical contact between the electrodes and the surrounding medium at higher saturation, which in turn improves the signal-to-noise and reduces measurement errors although in general, more conductive conditions reduce the transfer resistance and reduce signal-to-noise (Merritt et al., 2016).

3.5.2 Importance of temperature and pore water EC corrections for field applications

This study highlights the importance of temperature and pore water EC corrections for accurate predictions of VWC in tailings using ERT, particularly for field applications. Indeed, the ERT-predicted VWC is systematically underestimated when no corrections are applied for field experiments (scales **S4** and **S5**), with a corresponding tenfold reduction in accuracy. Such underestimation is consistent with the lower temperature and the lower pore water EC reported in the field in comparison with laboratory experiments. A decrease of 10 °C in temperature causes a 20% decrease in bulk EC (e.g., Ma et al. (2011); Luo et al. (2019)). As noted by Uhlemann et al. (2016a), the temperature correction is all the more important for geoelectrical monitoring surveys with large temporal changes in temperature (e.g., for field experiments with daily or seasonal variations of subsurface temperature) (Hayley et al., 2010; Jayawickreme et al., 2010). The latter is especially true at Canadian Malartic mine, since extreme air temperature changes are frequently observed between Winter (−30 °C) and Summer (30 °C) (Labonté-Raymond et al., 2020) or in similar contexts (e.g., permafrost monitoring surveys (Herring et al., 2021)). Similarly, this study highlights that pore water EC must be taken into account to accurately predict VWC from ERT datasets since bulk EC and pore water EC are proportional in the Archie petrophysical model. For instance, the lower pore water EC reported for the field cover must be considered in order to avoid underestimation of VWC in the field. Here again, the pore water EC correction is particularly important in the context of mining wastes, given (i) the strong pore water EC contrasts that are generally observed between clean water and water in contact with tailings and waste rocks, whether or not affected by contaminated drainage and (ii) the strong temporal variations of pore water EC in mining wastes (e.g., Nai et al. (2019); Vriens et al. (2020a); Martinez-Pagan et al. (2021)).

For the laboratory experiments, the temperature and pore water EC corrections have a smaller influence on the RMSE between the measured and ERT-predicted VWC. The latter can be explained by smaller temporal variations of temperature throughout the experiment under controlled conditions and by a smaller difference between the actual temperature and the reference value used for the temperature correction (the same observation can be done for the influence of pore water EC correction in the laboratory) (Brunet et al., 2010). As a result, this study shows that considering the temperature and the pore water EC is necessary to up-scale laboratory petrophysical relationships at the field scale in order to accurately predict VWC from TL-ERT monitoring. This further highlights the importance of using complementary hydrogeological sensors for field surveys to locally monitor temperature, pore water EC and VWC, which would be used both as input and validation data for processing TL-ERT datasets (Robinson et al., 2008a; Binley et al., 2015b). As noted by Wagner and Uhlemann (2021), the key question for future hydrogeophysical monitoring programs would then be how to select the critical number of sensors and how to optimally deploy them in the field (Uhlemann et al., 2018b). In particular, strategies should be investigated to tackle the impact of pore water EC at large scales, especially in media where strong spatial variability of pore water EC is expected.

3.5.3 Validity of Archie model for mine tailings

In this study, the Archie petrophysical model seems appropriate given the small RMSE obtained between the inverted and predicted bulk EC ($\epsilon_\sigma < 0.25$ mS/cm) and between measured and ERT-predicted VWC ($\epsilon_\theta < 0.04$ m³/m³). The cementation exponent m and the saturation exponent n obtained for this study range from 0.7 to 1.3 and from 3.0 to 5.0 respectively. It is interesting to note that different couples of m and n parameters yield similar petrophysical models, which highlights the non-uniqueness of such optimization approaches, as discussed recently by Holmes et al. (2022b). As reported by Martinez-Pagan et al. (2021) and Dimech et al. (2022), few studies have investigated the applicability of petrophysical relationships between bulk EC and VWC for mine tailings specifically, although this has been done for other fields of applications (e.g., Revil et al. (2012); Binley and Slater (2020); Slater and Binley (2021)). Nonetheless, the Archie parameters obtained in this study are consistent with the values reported in the literature for tailings. For example, Booterbaugh et al. (2015) obtain a r^2 value of 0.90 between saturation and bulk EC in tailings with a cementation exponent $m = 1.3$ and a saturation exponent $n = 3.8$. Similarly, Mollehuara-Canales et al. (2020) obtain ($m = 2.7, n = 3.0$) in mine tailings.

The values of the cementation exponent m correspond well to the typical values reported in the literature for unconsolidated media, generally between 1.1 and 1.3, whereas m values between 1.7 and 2.1 are generally used for consolidated media (Friedman, 2005; Booterbaugh et al., 2015; Revil et al., 2018). Interestingly, the values of saturation exponent n obtained in this study (between 3.0 and 5.0), and in other ERT studies for tailings do not correspond to the generally assumed value of $n \simeq 2$ for media where the interstitial fluid is water (Glover, 2015, 2017). As discussed by Booterbaugh et al. (2015) and Rucker (2010), such discrepancies are also pointed out by several other studies which consider a larger range for the saturation exponent n (between 1.5 and > 10) (Sen, 1997; Grellier et al., 2008).

Petrophysical models other than the Archie relationship could have been considered in this study to connect bulk EC and VWC in mine tailings. For example, Mollehuara-Canales et al. (2020) successfully applied Waxman-Smits (Waxman and Smits, 1968) and generalized mixing Archie models (Glover, 2010) to predict VWC in mine tailings from geoelectrical monitoring. An advantage of these models is that they allow to include the contribution of surface conduction, which could play a role in the bulk EC of tailings (e.g., Acosta et al. (2014); Pierwoła (2015)). In this study, however, the high pore water EC observed in the tailings is assumed to make the pore fluid conductivity the predominant contribution of bulk EC, thus rendering both solid matrix conduction and surface conduction negligible (Revil et al., 2012; Fu et al., 2021). Nonetheless, further work could be done at the laboratory scale under controlled conditions using tailings with a lower pore water EC to increase the relative contribution of solid matrix and surface conduction (e.g., Dimech et al. (2018)).

Selecting an optimal petrophysical model for tailings is still open to future investigation. Some aspects of the relationship between various physical properties in mine wastes, bulk EC and VWC are still poorly understood, despite recent developments (e.g., Váscónez-Maza et al. (2019); Gabarrón et al. (2020); Mollehuara-Canales et al. (2020, 2021b)). Future efforts could be devoted to the development of predictive models to assess the relationships between bulk EC and VWC for specific tailings, given their grain size distributions, clay content, mineralogy, ionic content and pH of the interstitial fluid, for example, following the work of recent studies (e.g., Shokri et al. (2016b); Tycholiz et al. (2016); Yurkevich et al. (2017); Zhang et al. (2018); Gabarrón et al. (2020); Váscónez-Maza et al. (2020)). The latter is already commonly done for the prediction of hydrogeological properties from basic geotechnical properties of mining wastes (e.g., prediction of water retention curves Mbonimpa et al. (2002); Aubertin et al. (2003)).

3.5.4 Scale influence on petrophysical models

This study also demonstrates that the Archie petrophysical model calibrated at sample scale using the electrical resistivity Tempe cell (ER-TC - scale **S1**) turns out to be valid at larger scales as shown by the maximal RMSE obtained using the ER-TC Archie model remaining below $0.040 \text{ m}^3/\text{m}^3$ for scales **S2** to **S5**. As a result, it seems appropriate for mine tailings to carry out experiments in the laboratory on small samples to calibrate a petrophysical model and to apply this model on a larger scale, given that the suitable corrections are properly applied. This observation is all the more relevant as most studies using TL-ERT to predict VWC rely on laboratory-based petrophysical relationships to quantify VWC at the field scale, assuming that the petrophysical model obtained at sample scale can be scaled up (e.g., Chambers et al. (2014b); Merritt et al. (2016); Hen-Jones et al. (2017b); Uhlemann et al. (2017b)).

For example, Calamita et al. (2012) and Derfouf et al. (2019) review different laboratory apparatus that have been used to characterize the relationship between bulk EC and VWC at sample scale (e.g., Long et al. (2012); De Vita et al. (2012); López-Sánchez et al. (2017); Chen et al. (2018b)). Among the different types of laboratory apparatus developed recently, the most promising are modified from well-documented geotechnical or hydrogeological laboratory apparatus (e.g., permeameter, oedometer, Tempe Cell, pressure plate or triaxial cell) to allow a simultaneous determination of VWC (or other relevant physical parameter) and bulk EC of the sample under controlled conditions (e.g., McCarter et al. (2005); Comina et al. (2008); Cosentini et al. (2012); Kibria et al. (2018); Wayal et al. (2021); Holmes et al. (2022b)). Another popular approach consists in determining the petrophysical relationships from co-located and simultaneous measurements of bulk EC and VWC directly sampled in the field, under natural conditions (Garré et al., 2011; Tso et al., 2019). To our knowledge, this study constitutes the first attempt to compare the petrophysical relationships derived from sample, laboratory and field scale experiments to assess accuracy of moisture content predictions.

In particular, the electrical resistivity Tempe cell (ER-TC) proposed and tested in this study has considerable potential for ensuring rapid, flexible, reproducible and accurate determination of petrophysical relationships for fine-grained materials, such as mine tailings. Indeed, Tempe Cells or equivalent pressure extractor cells (ASTM, 2016, 2000) are widespread and commonly used in most hydrogeological laboratories for the assessment of water retention curves (WRC) (e.g., Aubertin et al. (1998); Maqsoud et al. (2012)). The slight modification of the Tempe Cell needed to add several lateral electrodes allows determining simultaneously the WRC and the relationship between bulk EC and VWC under controlled conditions. For

instance, the experiments can be conducted for controlled temperature, known pore water EC, known porosity and homogeneous compaction, as well as with a lower risk of lateral and preferential flow. Moreover, the number of different pressure steps allows controlling the number of points used to define the petrophysical relationship, and allows defining the range of pressure studied (i.e., the range of VWC of interest), which might not be the case in the field when only small variations of moisture content could be observed. For example, the small variations of VWC in the tailings layer of the field experimental cover only allows to constraint the in-situ petrophysical relationship for the $0.27 - 0.38 \text{ m}^3/\text{m}^3$ VWC interval. In such cases, it might be difficult to extrapolate the petrophysical relationships outside of the range of in-situ observed VWC, as discussed by Tso et al. (2019).

Another advantage of the small-scale ER-TC apparatus is the high certainty of bulk EC values reconstructed by the inversion process, as opposed to the inversion results obtained from experiments at larger scales, in the field or at the laboratory. The inversion results from small-scale laboratory apparatus are less subject to resolution issues (i.e., area of the medium poorly constrained inversion (Luo et al., 2020)), non-uniqueness and artifacts of the inversion (Singha et al., 2015; McLachlan et al., 2017; Whiteley et al., 2019), unsuitable inversion regularization (Johnson et al., 2012b) or uncertainty in electrode location (Clement and Moreau, 2016; Wilkinson et al., 2016; Boyd et al., 2021). Also, data quality issues are more likely to occur for field applications since lower signal over noise ratios or high contact resistance between the medium and the electrode may be encountered (Samouëlian et al., 2005; Deceuster et al., 2013; Tomaškovičová et al., 2016; Greer et al., 2017). Finally, some differences in the investigation volume between ERT and point moisture sensors installed on the field could make it difficult to compare hydrogeological and geophysical results (Robinson et al., 2008a; Jayawickreme et al., 2010; Dimech et al., 2019). Future studies using similar small-scale laboratory apparatus could focus on determining the optimal electrode shape, material and spacing to maximize electrical coupling with the tailings, even for dry conditions, while ensuring the electrodes remain small enough to ensure they can be considered as points in the numerical models (see Rucker and Günther (2011); Clement and Moreau (2016)).

Finally, the use of small-scale, well-constrained and reproducible laboratory apparatus such as the ER-TC presented in this study should be preferred for the assessment of petrophysical relationships and the future investigation of the following challenging issues for VWC prediction in mine tailings using TL-ERT :

- the influence of porosity spatio-temporal evolution on ERT-predicted VWC (e.g., Brunet et al. (2010); Roodposhti et al. (2019); de Melo et al. (2021)),

- the prediction of petrophysical relationships from basic material properties and mineralogy (e.g., Vásconez-Maza et al. (2019); Gabarrón et al. (2020)),
- the hysteresis and other non-stationary aspects of petrophysical relationships (e.g., Michot et al. (2016); Hen-Jones et al. (2017b); Chung et al. (2019)),
- the contribution of the surface conductivity and anisotropy in mining tailings with various mineralogical contents (e.g., Merritt et al. (2016); Mollehuara-Canales et al. (2020)).
- the impact of corrosion or soil clogging around electrodes over the long term (e.g., Peter-Borie et al. (2011)).

3.6 Conclusion

In this study, we assess the scale effect on the accuracy of ERT-predicted VWC in mine tailings. In total, five different experimental setups are used to carry out simultaneous and co-located monitoring of bulk EC using TL-ERT and VWC using hydrogeological sensors. These datasets allow to calibrate Archie petrophysical models at various scales, and assess the accuracy of VWC predictions in mine tailings. The accuracy of ERT-predicted VWC is $\pm 0.03 \text{ m}^3/\text{m}^3$, and the petrophysical models determined at sample-scale in the laboratory remain valid at larger scales. Indeed, a similar accuracy is achieved when the petrophysical model determined from the sample-scale electrical resistivity Tempe cell (ER-TC) is applied to field data.

This study also highlights the strong impact that temperature and pore water EC variations can represent for the accuracy of VWC predictions using TL-ERT, especially for field applications. Indeed, a tenfold reduction of VWC accuracy is observed in the absence of suitable corrections in the experimental field cover. Based on these results, we recommend that future TL-ERT monitoring campaigns should be combined with networks of hydrogeological sensors, providing local validation and calibration measurements of VWC, temperature, bulk and pore water EC in tailings.

Finally, this study discusses the advantages of using small-scale, well-controlled and reproducible laboratory apparatus such as the ER-TC for the determination of petrophysical models in mine tailings, given that the samples used are representative of field conditions. In particular, a widespread use of similar sample-scale apparatus is likely to help refine petrophysical models applied to mine tailings, hence improving the accuracy and applicability of TL-ERT for mining waste monitoring across large scales.

**CHAPITRE 4 ARTICLE 3 - MONITORING MOISTURE DYNAMICS IN
MULTI-LAYER COVER SYSTEMS FOR MINE TAILINGS RECLAMATION
USING AUTONOMOUS AND REMOTE TIME-LAPSE ELECTRICAL
RESISTIVITY TOMOGRAPHY**

Adrien Dimech ^{1,3,*}, Bruno Bussière ^{1,3}, LiZhen Cheng ^{1,3}, Michel Chouteau ^{2,3},
Gabriel Fabien-Ouellet ², Nathalie Chevé ⁴, Anne Isabelle ^{2,3}, Paul Wilkinson ⁴,
Philip Meldrum ⁴ and Jonathan Chambers ⁴

Submitted to Canadian Geotechnical Journal (March 09, 2023).

¹ Université du Québec en Abitibi-Témiscamingue (UQAT), Rouyn-Noranda, QC, Canada

² Polytechnique Montréal, Montréal, Québec, H3T 1J4, Canada

³ Research Institute of Mines and Environment (RIME), Québec, Canada

⁴ Canadian Malartic Mine (CMM), Malartic, Québec, Canada

⁵ British Geological Survey (BGS), Nottingham, NG12 5GG, United Kingdom

Ce chapitre vise à répondre à l'**OS3** qui porte sur l'application de la méthodologie développée pour les **OS1** et **OS2** à l'échelle de terrain sur un site pilote. Plusieurs sections de recouvrements expérimentaux à grande échelle construits par la mine Canadian Malartic ont été instrumentées avec des électrodes géophysiques et des sondes de teneur en eau pour effectuer un suivi temporel de la teneur en eau en continu depuis mai 2021. Les données électriques sont utilisées pour prédire la distribution quotidienne de la teneur en eau le long de profils 2D mesurant 23 m x 2.3 m à l'aide des relations pétrophysiques calibrées en laboratoire pour chaque matériau (**OS1**) et en prenant en compte les variations spatio-temporelles de température et de conductivité électrique de l'eau interstitielle dans le milieu (**OS2**). Ces données sont ensuite combinées aux mesures conventionnelles pour décrire le comportement hydrogéologique d'une CEBC composée de roches stériles et de résidus miniers et d'une LSHCC composée de mort-terrain. La performance des sections instrumentée des CEBCs est également quantifiée en considérant une valeur cible de saturation de 85%, et en prenant en compte l'incertitude de l'estimation de teneur en eau déterminée à l'**OS2**. Dans l'ensemble, l'article permet de valider la pertinence et la faisabilité de la méthode de suivi proposée par mesures électriques à l'aide d'un site en conditions réelles, ce qui constitue une "preuve de concept" permettant de répondre à l'objectif global de la thèse.

4.1 Abstract

The dynamics of moisture content in engineered multi-layer covers constructed on mining wastes were monitored at the pilot scale using 2D autonomous, remote, and non-invasive time-lapse electrical resistivity tomography. This innovative monitoring approach was combined with conventional point sensors to assess the hydrogeological behavior of 280 m-long experimental covers under real meteorological conditions at an active mining site. The covers with capillary barrier effects (CCBEs) were designed to act as oxygen barriers whereas the covers with low saturated hydraulic conductivity layers (LSHCCs) aimed at limiting the water infiltration rate through the covers. A methodology was proposed to process the daily hydrogeophysical datasets from four 23 m-long instrumented sections and estimate the 2D distribution of moisture content. Hydrogeophysical monitoring suggested that the CCBE was able to maintain high degrees of saturation (above 85%) in the moisture-retaining layer throughout the one-year monitoring period and was not significantly affected by the slopes of the inclined sections, which would make it an efficient oxygen barrier. Larger spatio-temporal changes in moisture content were identified from hydrogeophysical data in the LSHCC. Most of the low hydraulic conductivity layers remained below 85% saturation and the estimated moisture content was at the lowest level in August 2022, which was attributed to the combined effect of low precipitation, evapotranspiration caused by rapid vegetation development, and potential water percolation through the cover. Overall, the methodology proposed in this study allowed the hydrogeological behavior of the covers to be monitored, which was helpful to investigate the performance of the covers. This study provided the first "proof-of-concept" at the pilot scale and under real conditions that the geoelectrical method can be used as a complementary monitoring technique to spatially extend the monitoring of moisture dynamics in mining wastes, which might be useful for geochemical and geotechnical monitoring programs in large-scale mining waste storage facilities.

4.2 Introduction

Mining operations generate two types of wastes during the extraction and processing of the ore : waste rocks and tailings (Bussière and Guittonny, 2021a). Waste rocks are generally coarse material with non-economical mineralization that have been blasted and extracted from the ground to reach the ore deposit. Tailings refer to the rocks extracted from the ore deposit that have been crushed into fine particles and mixed with water and chemicals to extract the metals (Dimech et al., 2022). Large volumes of mining wastes are generated worldwide since the proportion of metals in the ore is generally well below 10% for most

metals (down to a few grams per tons for silver, platinum or gold), and these ore grades are expected to drop in the future due to global ore depletion and increasing demand (Mudd, 2007; Rötzer and Schmidt, 2018). In 2019, it was estimated that over 220 billion tons of tailings have been generated worldwide, and 50 billion tons were expected to be generated over the following five years (**World Mine Tailings Failures**). Tailings and waste rocks are generally stored in large-scale waste facilities that can extend across tens of square kilometers and measure hundreds of meters in height (Kossoff et al., 2014; Vriens et al., 2020a; Dimech et al., 2022), and have been described as "the largest man-made structures on earth" (Bowker and Chambers, 2015).

Mining wastes can represent major environmental concerns for two main reasons : the geotechnical and geochemical instabilities of tailings storage facilities (TSFs) and waste rock piles (WRPs) (Bussière, 2007; Aznar-Sánchez et al., 2018). On the one hand, the poor geotechnical properties of tailings make TSFs vulnerable to failure if the dams are poorly designed and/or exposed to extreme precipitation, earthquakes, or landslides (Azam and Li, 2010); several catastrophic failures have been reported in recent years (Rotta et al., 2020). On the other hand, the sulfides generally present in mining wastes can oxidize when exposed to water and oxygen, which is commonly referred to as acid mine drainage (AMD) generation (Blowes et al., 2003; Plante et al., 2021b). If poorly controlled, AMD can have significant impacts on both surface water and groundwater, decreasing the pH below 7 and increasing the solubility of most metal species (Nordstrom et al., 2015; Rezaie and Anderson, 2020).

In recent years, several reclamation techniques have been developed to manage the risk of AMD, both at the source and over the long term, by controlling water and/or oxygen fluxes from the atmosphere toward the tailings, which significantly reduces the oxidation reaction (Bussière and Guittonny, 2021a). Among other approaches, the construction of covers with capillary barrier effects (CCBEs) at the surface of potentially AMD-generating tailings is particularly promising to control the availability of oxygen to tailings in humid climates (Bussière et al., 2003; Aubertin et al., 1995). CCBEs are based on the capillary barrier effects that develop at the interface between fine and coarse materials under unsaturated conditions, which tend to reduce vertical water flow across this interface (Morel-Seytoux, 1992). In most CCBEs, a layer made of fine materials, referred to as the moisture-retaining layer (MRL), is installed between two layers of coarser materials, referred to as the capillary break layers (Aubertin et al., 1995). The capillary break layers tend to drain rapidly because of their poor water retention capacity, whereas the MRL tends to remain nearly saturated, which in turn greatly reduces oxygen migration (Bussière et al., 2003; Aachib et al., 2004; Demers and Pabst, 2021b). Low saturated hydraulic conductivity covers (LSHCCs) are an alternative

reclamation approach, also referred to as water infiltration barriers or impermeable barriers, which aim to limit water infiltration into the wastes (Maqsoud et al., 2021). The low saturated hydraulic conductivity layer of the LSHCC is generally made of fine-grained soils (clay or fine silt) and/or man-made materials (e.g., geotextile, geomembrane or geosynthetic clay liner), with a suggested saturated hydraulic conductivity less than or equal to 10^{-7} cm/s (Aubertin et al., 2016; Maqsoud et al., 2021).

The performance of CCBEs and LSHCCs has been documented in the literature in recent years across different scales (e.g., numerical studies (Bussière et al., 2003; Fala et al., 2005; Aubertin et al., 2009), laboratory columns (Kalonji-Kabambi et al., 2017; Larochelle et al., 2019), field pilot-scale cells (Bussière et al., 2007), and field large-scale covers (Bussière et al., 2003; Dagenais, 2005)). However, the performance of CCBEs and LSHCCs is dependent on the water budget at a specific mining site and on the cover design (e.g., hydrogeological properties of the material used, thickness of the layers, topography of the cover) (Demers and Pabst, 2021b; Maqsoud et al., 2021). Moreover, the performance can be locally or globally affected by physical processes (e.g., extreme precipitation and droughts, freeze-thaw cycles, or preferential pathways) or biological processes (e.g., evapotranspiration from vegetation, root-water uptake, and root or burrowing animal intrusions), both in the short or long-term (MEND, 2004; Rykaart et al., 2006). As a result, it is generally recommended to construct one or more test covers at the pilot scale to assess the hydrogeological behavior under real meteorological conditions and monitor the performance in the short term (Bussière et al., 2021). More generally, reclamation covers installed on TSFs and WRPs should also be properly monitored over the long term to provide early detection of local or global decreases in cover performance (MEND, 2004).

From a broader perspective, the conventional tools deployed to monitor the geotechnical and geochemical stability of mining wastes are based on local measurements within the material (e.g., moisture sensors, suction sensors, or piezometers) or skin-deep surface observations (e.g., visual inspections, photogrammetry, or remote sensing) (Hui et al., 2018; Clarkson and Williams, 2020). While surface observation generally cover large scales with relatively low spatial resolution, local measurements allow physical parameters to be precisely monitored within a few centimeters around the sensors (Vereecken et al., 2008). As a result, many monitoring stations using dense networks of sensors might be needed to cover TSFs and WRPs, which could represent significant costs for the monitoring programs and produce large amounts of data that could be difficult to handle (Rykaart et al., 2006; Le Borgne et al., 2022). As noted by Robinson et al. (2008b), geophysical techniques provide a promising approach to bridge the gap between local measurements and surface observations since they allow 2D

or 3D imaging of key physical parameter distribution in the subsurface across intermediate scales, which can range from centimetric to kilometeric surveys (Auken et al., 2014; Binley et al., 2015b; Parsekian et al., 2015; Ulusoy et al., 2015; Palacios et al., 2020).

Time-lapse electrical resistivity tomography (TL-ERT) has emerged in recent years as one of the most promising geophysical techniques for subsurface monitoring (Binley et al., 2015b; Dimech et al., 2022). Indeed, TL-ERT is quite robust, cost-effective, and readily deployable for permanent, continuous and remote monitoring for various types of applications such as landslide, permafrost or infrastructure monitoring (Uhlemann et al., 2017b; Falzone et al., 2019; Mollaret et al., 2019; Slater and Binley, 2021; Chambers et al., 2022; Holmes et al., 2022b). As highlighted by the reviews from Dimech et al. (2022) and Martinez-Pagan et al. (2021), ERT has been used in the context of mining wastes to (i) characterize the internal structure of TSFs and WRPs (Anterrieu et al., 2010; Power et al., 2018b; Vásconez-Maza et al., 2019; Gabarrón et al., 2020), (ii) delineate AMD-affected areas (Bortnikova et al., 2013; Tycholiz et al., 2016; Power et al., 2018b; Jodeiri Shokri et al., 2022), (iii) identify AMD pathways (Bortnikova et al., 2018; Hudson et al., 2018; Casagrande et al., 2020; Camarero et al., 2022), and (iv) image moisture content distribution or water table elevation in TSFs and WRPs (Rucker, 2010; Booterbaugh et al., 2015; Epov et al., 2017; Mollehuara-Canales et al., 2020). Moreover, TL-ERT has also been successfully used to track the flow of tracers within mining wastes to help assess their hydrogeological behavior (Greer et al., 2017; Dimech et al., 2019; Hester et al., 2019; Targa et al., 2021) and to monitor potential contaminants or leakage from sealing layers (Binley and Daily, 2003; Martín-Crespo et al., 2010; Cortada et al., 2017; Puttiwongrak et al., 2019; Rey et al., 2020a). Finally, a few studies have reported applications of TL-ERT to monitor (i) the geotechnical stability of TSF dams (Sjödahl et al., 2005, 2008; Coulibaly, 2016; Tresoldi et al., 2020a) and (ii) the performance of reclamation covers installed on TSFs and WRPs (Maqsood et al., 2011; Villain et al., 2015; Dimech et al., 2019). However, the potential that TL-ERT represents as a large-scale complementary monitoring technique remains largely untapped for mining wastes (Dimech et al., 2022), despite recent developments of remote, permanent and automated geoelectrical monitoring systems in many other fields of geosciences (Slater and Binley, 2021; Chambers et al., 2022).

This study presents the results from a pilot-scale experimental investigation at an active mining site where permanent ERT arrays were deployed to continuously monitor moisture content in several multi-layer covers. This paper aims to (i) present and test the methodology followed to predict moisture content distribution using daily ERT measurements, (ii) assess the accuracy of ERT-predicted moisture content distribution using co-located hydrogeolo-

gical sensors, and (iii) test how continuous remote geoelectrical monitoring can be used in conjunction with conventional techniques to assess the performance of mine tailings reclamation covers across large scales. To our knowledge, this survey is one of the first attempts to use permanent, automated, and remote TL-ERT for monitoring mining wastes at the pilot scale. As a result, this study provides a "proof-of-concept" that geoelectrical monitoring is a robust technique that could be successfully combined with conventional techniques to spatially extend the monitoring of moisture dynamics in mining wastes for geochemical or geotechnical monitoring.

4.3 Site description

Canadian Malartic Mine (CMM) is a world-class large-tonnage and low-grade gold deposit located in the Abitibi region, Quebec, Canada (48.11°N, 78.12°W). It is expected that over 620 Mt of waste rocks and nearly 300 Mt of tailings will have been produced by the end of the operations in 2029 (Canadian Malartic, 2020). These wastes will be stored in WRPs (3.7 km²) and in TSFs (6.2 km²), as shown in Figure 4.1a with a satellite view of the mine (Canadian Malartic, 2020). The tailings have average sulfur and carbon contents of 1.2% and 0.6%, respectively. This corresponds to a neutralizing potential ratio below 2 (Plante et al., 2021b), which places the tailings in an uncertainty zone for their AMD generating potential (Plante et al., 2021a). The region is characterized by a cold and temperate continental climate with a typical annual precipitation of 900 mm (Larchevêque et al., 2014; Canadian Malartic Mine, 2015). The mean annual temperature is around 1 °C, with cold winters (mean of -17 °C in January) and hot summers (mean of 17 °C in July) (Canadian Malartic Mine, 2015).

As part of its mine reclamation decision-making process, Canadian Malartic Mine conducted a failure mode and effects analysis exercise. As a result, it was decided that four large-scale field experimental covers would be built in order to address various identified risks, notably in terms of constructability and performance of the covers. Two CCBE-type and two LHSCC-type covers were constructed in 2019 and 2020 in the southwestern portion of the TSF (Figure 4.1a). Each cover was about 18 m-wide and 280 m-long, with an 80 m-long flat section (referred to as "plateau") and a 200 m-long inclined section with a 10% slope. The CCBEs were constructed to evaluate, among other things, the possibility of using mine tailings as a material for the MRL (Design A on Figure 4.1b). The CCBEs were made from two layers of crushed waste rocks (mostly composed of gravels), a MRL made of tailings (a fine-grained material categorized as non-plastic silt, USCS classification, McCarthy (1977)),

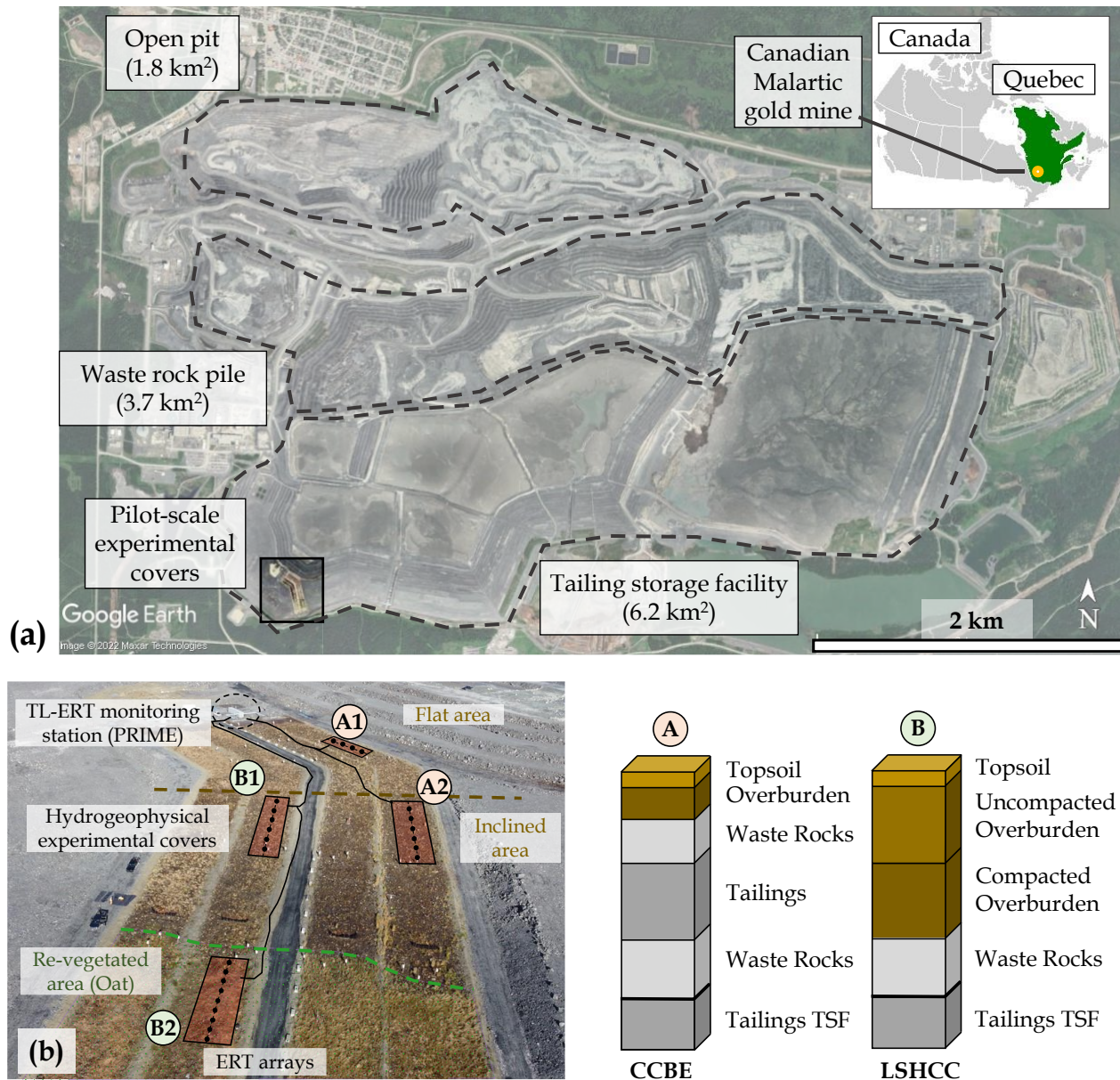


FIGURE 4.1 (a) Satellite view of Canadian Malartic gold mine located in Quebec, Canada (48.11°N, 78.12°W). Identification of the open-pit, WRP and TSF that are planned to be reclaimed. (b) Aerial photography of the four pilot-scale experimental multi-layer covers and simplified composition of the CCBE and LSHCC multi-layer covers investigated in this study.

a layer of uncompacted overburden (clay and silt) and a topsoil layer. The LSHCCs were designed to reduce the net percolation of water toward the tailings (Design B on Figure 4.1b). The LSHCCs were made of a bottom support layer of waste rocks, overlain by a layer of compacted overburden (acting as the low saturated hydraulic conductivity layer), a layer of uncompacted overburden and a final layer of topsoil. It was expected that the lower portion

of the layer of compacted overburden would remain saturated most of the year. Therefore, although the main function of the LSHCC was to reduce the annual net percolation in the tailings, this type of cover could also act as a partial oxygen barrier. The topsoil layer was placed at the top of all covers to promote vegetation development in combination with the uncompacted overburden layer. The hydrogeophysical survey was carried out in four 23 m-long sections of the covers illustrated by rectangles A1, A2, B1, and B2 in Fig. 4.1b.

4.4 Materials and methods

4.4.1 Physico-chemical, hydrogeological, and electrical characterizations

Detailed physico-chemical, hydrogeological, and electrical characterizations were performed on 44, 47, and 8 samples of tailings, overburden, and waste rock materials, respectively. The samples were mostly collected from the 23 m-long hydrogeophysical sections during the construction of the covers, according to a regular sampling grid. The grain size distribution (GSD) presented in Figure 4.2 was determined using laser diffraction for the tailings and overburden samples, and a combination of sieve analysis and laser diffraction for the waste rocks (ASTM D-422). The specific gravity (G_s) was determined for all materials using a helium pycnometer (ASTM D-5550). The sulfur and carbon contents of the samples were determined using a LECO CS-2000 induction furnace (ASTM UOP-703), and were used to compute the acidity and neutralization potentials of the tailings and waste rocks materials (Plante et al., 2021a).

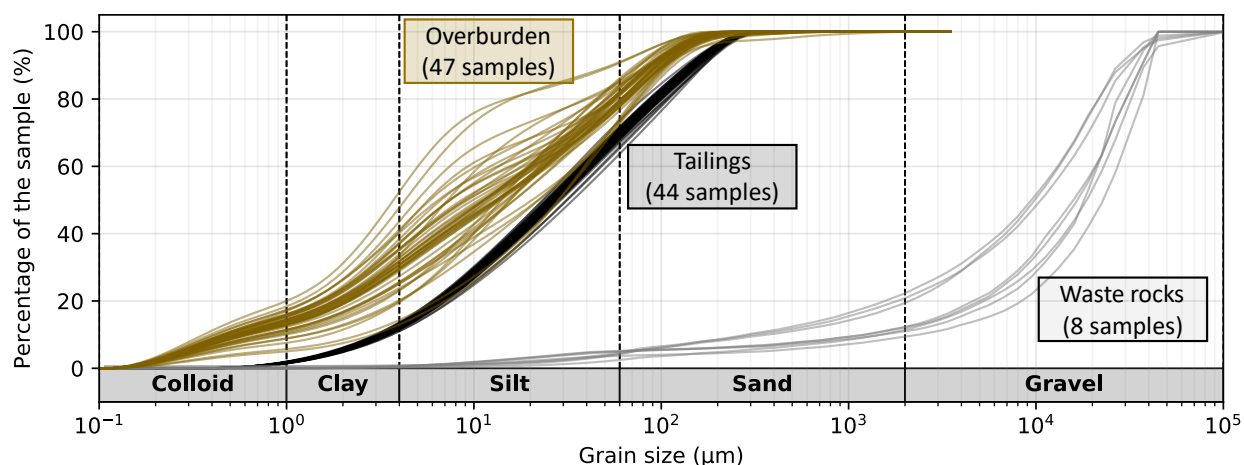


FIGURE 4.2 Grain size distribution (GSD) for the materials used in the experimental covers. Each sample is shown in light brown, black and grey for the overburden, tailings and waste rocks, respectively.

A systematic measurement strategy was carried out during the hydrogeophysical cover section construction in the field to assess material compaction, porosity, and gravimetric and volumetric moisture content (GMC and VWC) using a nucleodensimeter (86 measurements for the tailings and 33 for the overburden). The GMC of the material used for the construction (referred to as "at installation") was also estimated by weighing the wet samples of tailings and overburden collected from the covers during construction, and by weighing the same samples dried in an oven at 60 °C for 48 h (ASTM D-2216). The saturated hydraulic conductivities (k_{sat}) for the tailings and overburden materials were predicted using the modified Kozeny-Carman model (KCM) (Mbonimpa et al., 2002; Chapuis and Aubertin, 2003). Moreover, k_{sat} was also determined in the laboratory using flexible wall permeameters by Dubois-Roy (2021) for overburden samples taken from the experimental covers and by Lavoie-Deraspe (2019) for tailings with a similar grain size distribution as the one used in the experimental covers. Lavoie-Deraspe (2019) also determined k_{sat} of waste rocks with a similar grain size distribution using a rigid wall permeameter (ASTM D-5084). Standard Tempe cells were used to assess the water retention curves for the tailings and overburden (ASTM D-6836). For the Tempe cell tests, the saturated tailings and overburden samples were compacted to a respective porosity of $n = 0.40$ and $n = 0.45$ (estimated porosity based on the nucleodensimeter results of the field covers) in cylindrical molds with a diameter of 8.5 cm and a height of 2.5 cm. Incremental steps of pressure were applied to the top of the Tempe cells using air pressure controllers and high-pressure nitrogen bottles to drive changes in the VWC of the samples. The Tempe cells were weighed after two days at each pressure increment and the pressure-VWC data were used to assess the air-entry value and the residual VWC (θ_r).

The electrical properties of the tailings and overburden samples were characterized using a laboratory apparatus described in Dimech et al. (2023b). As shown in Figure 4.3, a standard Tempe cell was slightly modified to carry out time-lapse ERT in the samples to simultaneously determine moisture content and bulk electrical conductivity (EC) for each pressure increment. The conventional brass cylinder was replaced by a non-conductive polyvinyl chloride (PVC) cylinder that could withstand pressures up to 350 kPa. A PVC cylinder of 6 cm in height and 7.5 cm in internal diameter was used. Six stainless-steel electrodes of 1 cm in diameter were inserted in the PVC cylinder to be in contact with the material sample with a penetration of 5 mm to ensure good electrical contact. The electrodes were connected to a Terrameter LS resistivity meter (ABEM, Sweden) and measurements were carried out during sample drainage. The datasets were used to fit Archie petrophysical models following the methodology presented in Dimech et al. (2023b).

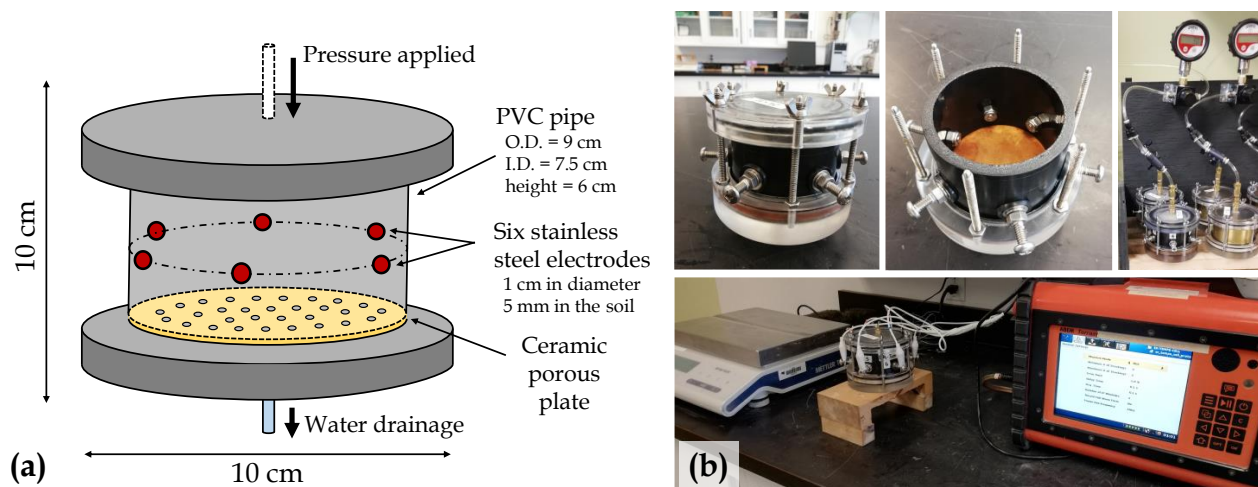


FIGURE 4.3 (a) Schematic view of the modified Tempe Cell used to characterize electrical properties of samples. (b) Photographs showing the modified Tempe Cell, the porous ceramic plate, the six stainless steel electrodes and the ABEM Terrameter LS resistivity meter.

4.4.2 Design, instrumentation, and monitoring of experimental covers

The four 23 m-long sections of the field experimental multi-layer covers were instrumented with a dense network of hydrogeological sensors and geophysical electrodes. As illustrated in Figure 4.1, two hydrogeophysical sections were located in one CCBE : in the plateau section (A1) and at the top of the slope (A2). Similarly, two other sections were located in one LSHCC : at the top of the slope (B1) and at the bottom of the slope (B2). The locations of the four sections were selected in order to assess the potential of geoelectrical measurements to monitor moisture content dynamics in covers for a broad range of field conditions at the pilot scale. Both the multi-layer cover design and the slope were expected to affect the hydrogeological behavior of the field covers (Bussière et al., 2007). Moreover, the bottom part of the slope was re-vegetated in October 2020 and June 2021 using oat seeds as indicated in Fig. 4.1b, which was also expected to play a role in the moisture content distribution.

Figure 4.4 presents the geometry of the multi-layer covers and the location of hydrogeological sensors and electrodes. From bottom to top, the CCBE cover (Design A) consisted of a 0.3 m-thick bottom capillary break layer made of waste rocks (0-100 mm), a 1.0 m-thick MRL of tailings, a 0.5 m-thick upper capillary break layer made of waste rocks (0-50 mm), and a layer of material that supported the growth of vegetation, made of 0.4 m of overburden overlain by 0.1 m of topsoil (Fig. 4.4a). The hydrogeophysical CCBE sections were equipped with hydrogeological monitoring stations located at the center of the sections, connected to vertical profiles of six Teros 12 sensors, which continuously monitor unfrozen volumetric

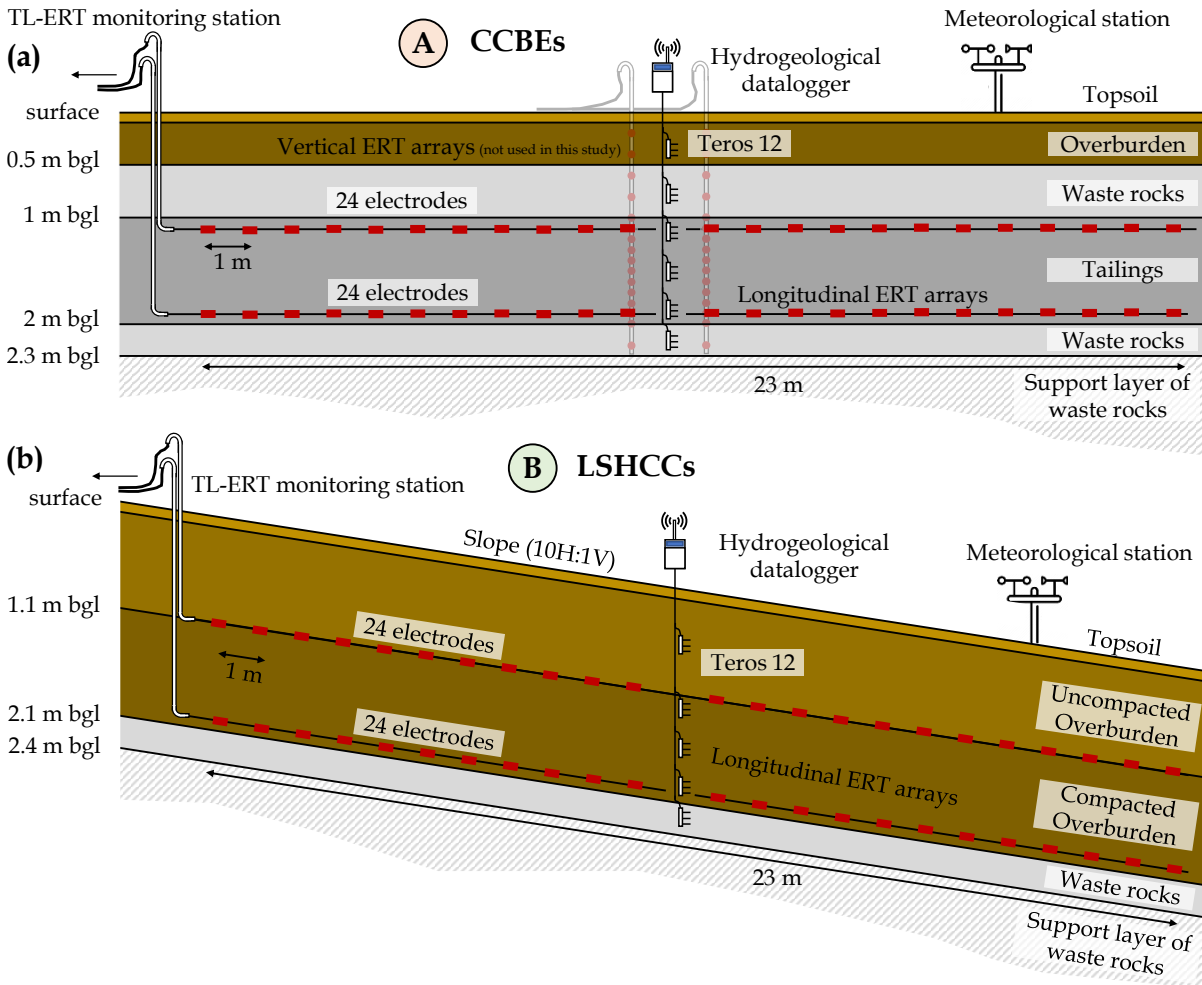


FIGURE 4.4 Geometry of the experimental CCBE (a) and the LSHCC (b) built on the TSF of MCM. The location of hydrogeophysical instruments is presented on the vertical sections (longitudinal profiles of electrodes in red and Teros 12 sensors along a vertical profile in the center of the 23 m-long cover sections).

water content, temperature, bulk EC (two-points method), and pore water EC (MeterGroup (2019)). Two longitudinal profiles of electrodes were also buried within the tailings to protect the electrodes from coarse waste rocks, ensure good electrical grounding, and maximize the resolution within the MRL. The longitudinal profiles were placed, respectively, 0.15 m above the bottom tailings-waste rocks interface and 0.15 m below the top tailings-waste rocks interface. Each longitudinal profile contained 24 flat rectangular stainless-steel electrodes measuring 6 cm x 2.5 cm and separated from each other by 1 m. Two additional vertical arrays of electrodes were also installed around the Teros 12 sensors, represented as vertical profiles shaded in Fig. 4.4a. These arrays were not used in this study and more details are provided in Dimech et al. (2023b).

Similarly, from bottom to top, the LSHCC (Design B) consisted of a 0.3 m-thick support layer made of waste rocks (0-100 mm), a 1.0 m-thick low saturated hydraulic conductivity layer made of compacted overburden, a 1.0 m-thick protective layer made of uncompacted overburden, and a 0.1 m-thick surface layer made of topsoil (Fig. 4.4b). Each LSHCC hydrogeophysical cover section was also equipped with a vertical profile of five Teros 12 hydrogeological sensors and two longitudinal profiles of 24 electrodes with an electrode spacing of 1 m. The electrodes had the same geometry as for the CCBE cover and the location of the two longitudinal profiles was, respectively, 0.15 m above the overburden-waste rocks interface and at the interface between compacted and loose overburden. The Teros 12 specific material calibration curves were obtained in the laboratory for tailings and overburden and the accuracy for moisture content calibrated measurements was $\pm 0.03 \text{ m}^3/\text{m}^3$ (Isabelle, 2022). The Teros 12 sensors were connected to ZL6 autonomous and remote dataloggers powered by solar panels (MeterGroup). Hydrogeological measurements were recorded every 30 minutes and transferred automatically to remote servers once a day.

All electrodes of the four instrumented sections were connected to a PRIME system autonomous resistivity meter developed by the British Geological Survey (PRoactive Infrastructure Monitoring and Evaluation) (Holmes et al., 2020, 2022b; Chambers et al., 2022). Robust 12 AWG solid copper cables were used to connect the electrodes to the PRIME system. The PRIME system was installed in a cabin equipped with a router and an antenna to transfer ERT data to remote servers three times per day, which significantly reduced the need for costly field campaigns while allowing high temporal resolution monitoring. Four sets of ERT data were measured every day for each one of the four hydrogeophysical sections. Meteorological data such as air temperature, precipitation, and relative humidity were also monitored using a meteorological station. The hydrogeophysical datasets presented in this study extended over a one-year period from July 2021 to August 2022.

4.4.3 Construction of pilot-scale field experimental covers

The 280 m-long large-scale experimental covers were constructed from 2019 to 2020 in an inactive area at the southwestern part of the Canadian Malartic Mine TSF. At this location, the maximum TSF elevation was approximately 30 m above the natural ground with a slope of 10% in the inclined areas. The first step was to prepare a 1-3 m-thick base layer made of coarse waste rocks (0-1000 mm) to support the covers. This was done using a mechanical shovel or a bulldozer to flatten the benches in the inclined area and by adding waste rocks directly on the tailings in the plateau area. A 0.3 m-thick layer of finer waste rocks (0-100 mm) was placed on top of the supporting layer to act as a transition layer between the coarse waste

rocks and the overlying fine material.

Figure 4.5 presents the main construction steps. Construction of the tailings layers in the hydrogeophysical cover sections was done in four lifts using a mechanical shovel. The first 0.15 m-thick lift was constructed and proper compaction and flattening was achieved using the mechanical shovel. The prepared electrode profiles were then installed on this flat surface and all electrodes were surveyed. A second 0.35 m-thick lift was then constructed and the material was carefully deposited on the electrode profiles to ensure the electrodes did not move. A third 0.35 m-thick lift was installed for the CCBE to prepare the top electrode level and a final 0.15 m-thick lift completed the 1.0 m-thick MRL. The remaining layers were installed in one lift each by the mechanical shovel. A similar procedure was followed for the LSHCC, with three lifts with respective thicknesses of 0.15 m, 0.35 m and 0.5 m. The 1.0 m-thick uncompacted overburden layer was installed in one lift.

Nucleodensimeter measurements were carried out after the construction of each lift to ensure that proper compaction was achieved. Seven material samples were also collected for each cover section after each lift construction to assess GMC at installation and the spatial variability of the material properties. VWC sensors were installed at the specified depths by excavating a small hole after each lift installation; the needles of the sensors were then inserted into the compacted material and surveyed. They were held in place by backfilling the holes with the material that was previously excavated to ensure representative compaction. The cables were inserted into acrylonitrile-butadiene-styrene (ABS) pipes to protect them from the waste rocks, following the methodology of Boulanger-Martel et al. (2021b).

Electrode cables were also inserted into vertical ABS pipes as shown in Fig. 4.5a. The cables were then connected to the PRIME system using waterproof connection boxes located at the surface of the covers. The connection boxes were also covered by rugged plastic boxes to further protect the electrical connections from potential damage by animals, water infiltration, and snow (Fig. 4.5a). The PRIME system was installed in a monitoring station, powered by two 105 Ah 12 V batteries which were charged by an electrical line and heated during the winter season. The batteries were sufficient to maintain system operation for a few weeks in case the power line failed. In total, approximately 800 electrodes were installed in the four hydrogeophysical cover sections following a 3D grid similar to that described in Martin et al. (2017) and Dimech et al. (2019). For each section, five 23 m-long profiles separated by 1.5 m were installed at two different elevations to define two 23 m x 6 m longitudinal planes of electrodes separated by a vertical distance of 0.7 m. Only the 256 electrodes from the central profiles (Fig. 4.4 and top left photograph of Fig. 4.5a) were connected to the PRIME system for this pilot study.

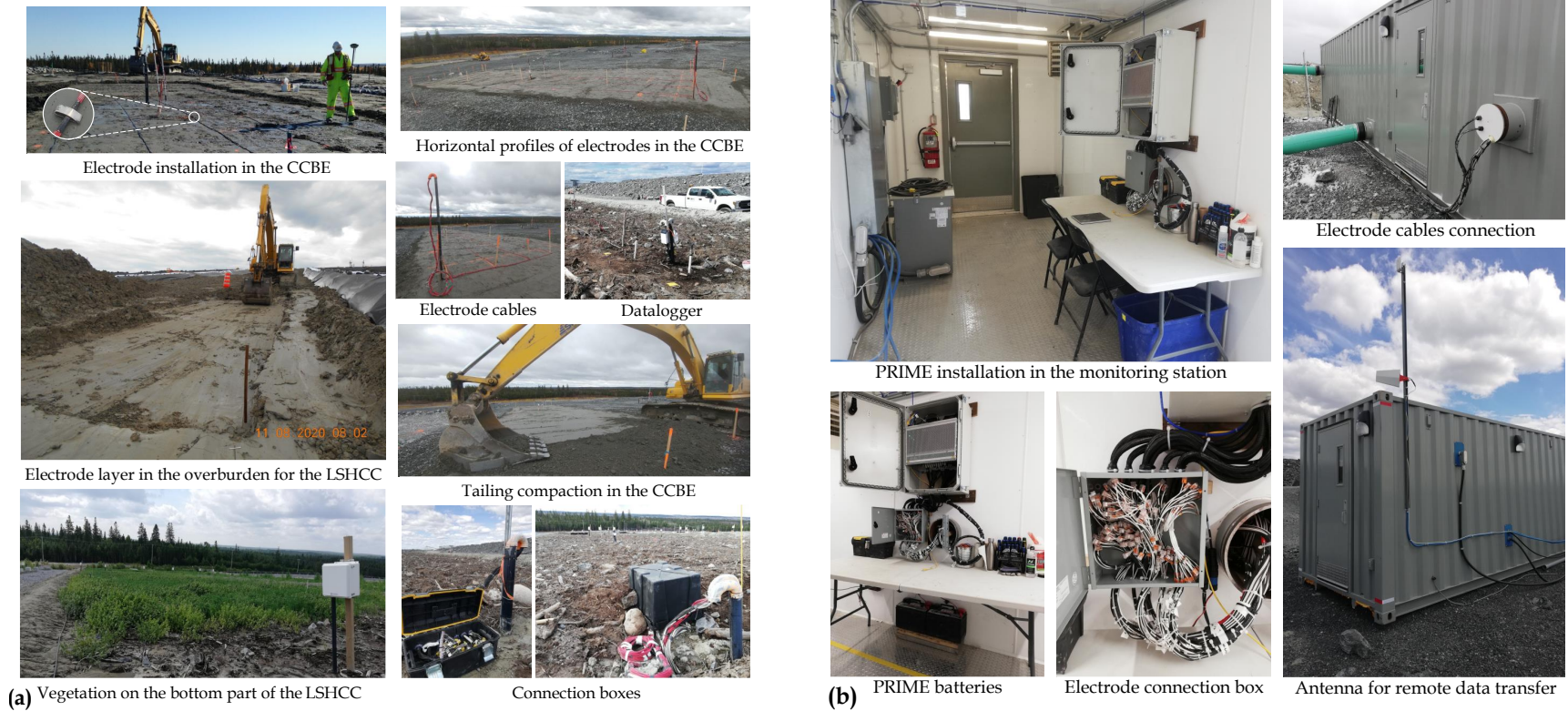


FIGURE 4.5 (a) Photographs showing the different steps of pilot-scale experimental CCBE and LSHCC construction at the TSF of Canadian Malartic Mine. (b) Photographs showing the main components of the geoelectrical monitoring station, including the PRIME resistivity meter, the electrode cables, the batteries, the router, and the antenna.

4.4.4 Time-lapse ERT data acquisition and processing

ERT measurement protocols

A Wenner-type measurement configuration was used in this study to provide a strong signal/noise ratio. The spacing between electrodes ranged from 1 m to 5 m and both bottom and top electrodes were used separately to carry out measurements, as shown by the top panel in Figure 4.6. ERT datasets contained 150 measurements for each experimental cover section, and took less than 10 minutes to be collected. Sensitivity analysis showed high sensitivity was achieved in the tailings layer for the CCBE, and both in the compacted overburden and loose overburden for the LSHCC. Lower sensitivity was observed in the waste rocks layers and little to no sensitivity was achieved in the overburden layer at the top of the CCBE. Figure 4.6 also presents the temporal evolution of raw conductance measured using the top electrode profiles and Wenner configurations with electrode spacings of 2 m and 5 m from June 2021 to July 2022. Each strong precipitation event (i.e., precipitation greater than 20 mm/day) was followed by an increase in conductance. On the contrary, long periods without precipitation corresponded to a decrease in conductance, especially during the summer and winter periods. Four ERT datasets were recorded autonomously each day for each cover section with a time interval of 6 hours (data acquisition from 0 to 2 AM, from 6 to 8 AM, from 0 to 2 PM, and from 6 to 8 PM). An additional set of reciprocal ERT measurements was recorded during the night (from 2 to 4 AM) for data quality assessment. For this pilot study, one dataset per day was used to reduce the total number of inversions. As a result, only the direct and reciprocal datasets recorded during the night were processed.

ERT data error assessment and filtering

ERT datasets were recorded along with a daily set of reciprocal measurements, for which the current and potential electrodes were interchanged (Tso et al., 2017). As reported in Uhlemann et al. (2016a), any difference between direct and reciprocal measurements can be used to assess ERT data quality. ERT data with reciprocal error greater than 10% were removed from the datasets (Tso et al., 2019). Moreover, Hampel filtering was applied to each time-series to identify and remove any temporal outliers (Hampel, 1974). The filtered measurements were then replaced in their respective time-series using spatio-temporal inverse distance weighting interpolation to obtain ERT datasets with the same number of measurements for each snapshot (Uhlemann et al., 2016a). This procedure yielded 397 full datasets, each containing 150 measurements, for each of the four multi-layer hydrogeophysical cover sections, which corresponded to a total of $\simeq 240,000$ data points to be inverted.

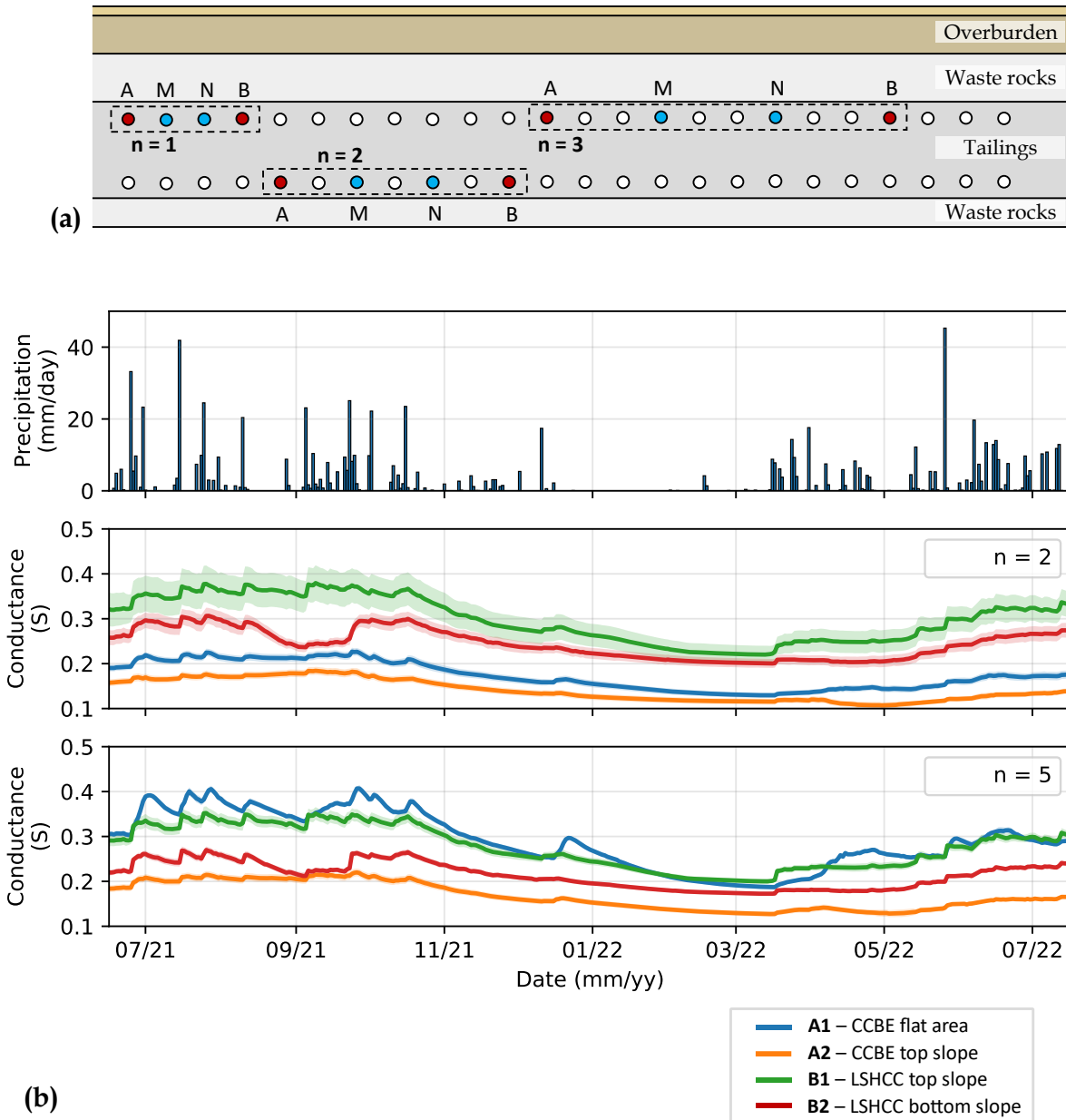


FIGURE 4.6 (a) Wenner measurement protocol used in the experimental covers with electrode spacing ranging from 1 m to 5 m. (b) Raw conductance time-series measured with the PRIME system for an electrode spacing of 2 m and 5 m with the top electrodes of each cover (mean of all measurements).

Time-lapse ERT data inversions

ERT datasets were inverted using pyGIMLi/BERT, a smoothness-constrained least-squares inversion open-access software (Rücker et al., 2017). 2D unstructured meshes were defined according to the known geometry of the covers (see Dimech et al. (2023b)). The meshes

contained 10,600 and 11,400 triangular cells for the CCBE and the LSHCC, respectively. Anisotropic spatial smoothing was applied within each layer to allow greater variations of inverted bulk EC along the vertical direction (as opposed to smooth variations in the horizontal direction). No spatial smoothing constraint was applied at the interface between two successive layers to enable sharp contrasts between two different materials. The normalized χ^2 defined in Johnson et al. (2012b) was used to assess the misfit error between modeled and measured data weighted by their respective measurement errors. Most of the χ^2 values obtained by the inversions ranged between 0.6 and 1.4, which denoted that ERT datasets were appropriately fitted.

Temperature and pore water corrections

Both temperature and pore water EC can have significant effects on the subsurface bulk EC (Hayley et al., 2010; Dimech et al., 2023b). As reported in Dimech et al. (2022), this is especially true for long-term monitoring surveys in areas where significant seasonal changes in air temperature can be observed. A similar observation can be made if significant changes in interstitial pore fluid geochemistry are typically monitored, such as in mining wastes. In such cases, the inverted bulk EC models need to be corrected to standard temperature and standard pore water EC to properly convert bulk EC into moisture content and avoid misinterpretation of geoelectrical monitoring results.

The inverted bulk EC distribution σ was corrected to a standard temperature T_{std} of 25 °C using :

$$\sigma_{T_{\text{std}}} = \sigma \cdot \left[\frac{1}{1 + \delta T \cdot (T - T_{\text{std}})} \right] \quad (4.1)$$

where $\sigma_{T_{\text{std}}}$ is the corrected bulk EC and δT is the fractional change in σ per degree Celsius. A value of $\delta T = 0.02 \text{ } ^\circ\text{C}^{-1}$ was used in this study, which means that bulk EC increases by a factor of 2% for a temperature increase of 1 °C (Hayley et al., 2010; Uhlemann et al., 2017b). The temperature measured by the Teros 12 sensors was used to determine the vertical profiles of temperature for the monitoring period for each multi-layer cover section. Figure 4.7 presents the spatio-temporal variations of temperature measured by the Teros 12 sensors in the CCBE experimental cover section on the plateau. This temperature model was assumed to be representative of the 23 m-long instrumented cell and was used to correct the inverted bulk EC values using Equation 4.2. Since the maximum amplitude of variation of temperature was close to 10 °C in the tailings layer, such a seasonal temperature variation would have affected bulk EC in the tailings up to a factor of 20% if not properly accounted

for (e.g., Dimech et al. (2023b)).

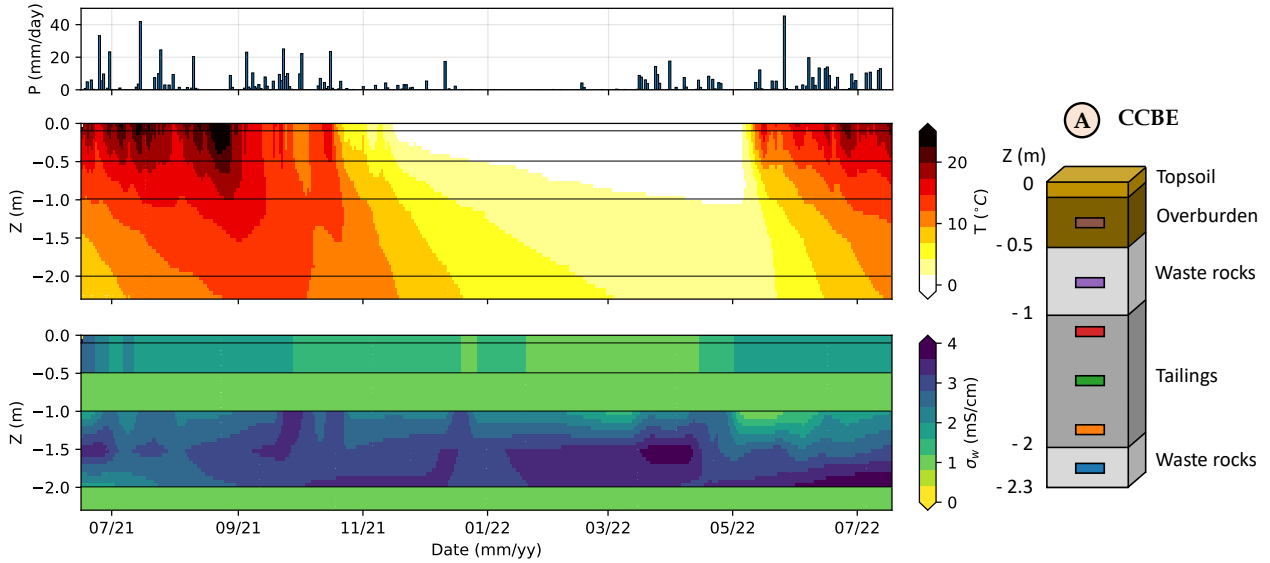


FIGURE 4.7 Precipitation data, spatio-temporal variation of temperature measured by the Teros 12 sensors, and spatio-temporal variation of pore water electrical conductivity derived from the Teros 12 measurements at the center of the CCBE experimental cover section on the plateau.

The inverted bulk EC was also corrected to a standard pore water EC $\sigma_{w \text{ std}}$ of 4.0 mS/cm using :

$$\sigma_{\sigma_{w \text{ std}}} = \sigma \cdot \left[\frac{\sigma_{w \text{ std}}}{\sigma_w} \right] \quad (4.2)$$

where $\sigma_{\sigma_{w \text{ std}}}$ is the corrected bulk EC and σ_w is the pore fluid EC normalized at 25 °C. The pore water EC values were calculated from the moisture content, bulk EC, and temperature data recorded by the Teros 12 sensors using a semi-empirical relationship developed in Hilhorst (2000) (see Dimech et al. (2019) for details). The accuracy of pore water EC determined from this relationship was expected to be around $\pm 20\%$ in media with a moisture content greater than $0.10 \text{ m}^3/\text{m}^3$. The Teros 12 measurements were used to assess the spatio-temporal variations of pore water EC along a vertical profile at the center of each hydrogeophysical cover section as shown in Figure 4.7. The pore water EC was fixed at 0.5 mS/cm in the waste rocks since the relationship could not be applied (moisture content less than $0.10 \text{ m}^3/\text{m}^3$ most of the time). The pore water EC model estimated at the center of the hydrogeophysical cover sections was assumed to be representative of the 23 m-long cover section to be used to correct the inverted bulk EC.

Conversion into moisture content

The Archie model was used to convert the inverted bulk EC to VWC expressed in m^3/m^3 (Archie et al., 1942). The Archie relationship is generally expressed as :

$$\sigma = \sigma_w \cdot n^{m_A} \cdot S_w^{n_A} \quad (4.3)$$

where σ_w is the pore fluid EC, n is the porosity (-), and S_w is the saturation ($\text{VWC} = n \cdot S_w$). The parameters m_A and n_A are unitless, commonly referred to as the cementation exponent and the saturation exponent, respectively (Glover, 2016). Equation 4.3 can be rearranged to convert the corrected bulk EC (σ_{corr}) at standard temperature and standard pore fluid EC ($\sigma_{w \text{ std}}$) into VWC using :

$$\text{VWC} = \left[\frac{\sigma_{\text{corr}}}{\sigma_{w \text{ std}}} \right]^{\frac{1}{n_A}} \cdot n^{1-m_A/n_A} \quad (4.4)$$

4.5 Results

4.5.1 Physico-chemical, hydrogeological, and electrical properties

Table 4.1 summarizes the results from the multi-component characterization approach carried out on material samples. The dry density and GSD obtained for the tailings and waste rocks materials were typical of these materials (e.g., Bussière (2007); Sylvain et al. (2019); Lavoie-Deraspe (2019)). Notably, the 44 tailings samples shared similar properties with low standard deviations, which denoted the homogeneity of the MRL in the CCBE. By comparison, a greater variability was reported among the samples of overburden for the LSHCC. However, systematic sampling showed that the properties were randomly distributed in the LSHCC and no spatial correlation was evidenced. Systematic sampling and systematic nucleodensimeter measurements provided similar results in terms of GMC. GMC at installation was 0.21 ± 0.01 for the tailings layer and 0.27 ± 0.07 for the overburden layer. The *in situ* porosity calculated from nucleodensimeter data was $n = 0.39 \pm 0.02$ and $n = 0.46 \pm 0.06$ for the tailings and overburden layers, respectively. Notably, a slight difference in porosity was observed between the plateau and the inclined sections of the CCBE ($n = 0.38$ and $n = 0.41$, respectively).

The saturated hydraulic conductivity predicted from basic geotechnical properties were in good agreement with permeameter experiments (see Table 4.1). Similarly, the water retention curves (WRC) obtained from the conventional Tempe cells were consistent with those determined from the modified electrical resistivity Tempe cells (see Fig. 4.3) and allowed

the determination of the unsaturated hydraulic properties in terms of saturated and residual volumetric water content (θ_{sat} and θ_r), air-entry value (AEV), noted ψ_a , and suction at residual moisture content ψ_r (Boulanger-Martel et al., 2021a). As expected, the waste rocks (0-100 mm) had a high saturated hydraulic conductivity (k_{sat} around 10^{-1} cm/s) and low water retention capacity (e.g., Kalonji-Kabambi et al. (2017)). In this study, the waste rocks with grades 0-100 mm and 0-50 mm were supposed to exhibit similar hydrogeological behaviors. On the contrary, the fine materials exhibited lower saturated hydraulic conductivities (k_{sat} around 10^{-5} and 10^{-6} cm/s for tailings and overburden, respectively) and higher water retention capacities (ψ_a around 20-30 kPa for tailings and around 60-100 kPa for overburden). Such strong contrasts between coarse and fine materials suggested that capillary barrier effects would be likely to develop at the interface between the waste rocks and tailings for the CCBE and between the waste rocks and the compacted overburden materials for the LSHCC (Aubertin et al., 1995; Bussière et al., 2003).

The electrical resistivity Tempe cells allowed the electrical properties of the tailings and overburden materials to be determined. The parameters of the Archie petrophysical model were optimized to fit the experimental measurements of bulk EC and moisture content in the modified Tempe cells following the methodology presented in Dimech et al. (2023b). The tailings were compacted to a porosity of $n = 0.40$ in the Tempe cell to reproduce similar conditions as in the field CCBE ($n = 0.45$ for the overburden). The values $m_A = 1.2$ and $n_A = 3.5$ provided the best fit to the experimental data for the tailings at a reference temperature of 25 °C and a reference pore water EC of 4 mS/cm ($m_A = 0.5$ and $n_A = 3.4$ for the overburden). The petrophysical relationship could not be determined for the waste rock samples given that the Tempe cell was too small to fit the coarse particles while respecting a ratio of 6 :1 between the diameter of the cell and the larger particle size (Peregoedova, 2012). As a result, an a-priori Archie model was defined for the waste rocks with a porosity of $n = 0.35$ (Lavoie-Deraspe, 2019) and Archie parameters of $m_A = n_A = 2$. This assumption was not expected to impact the hydrogeological interpretations since the waste rocks layers were generally less than $0.15 \text{ m}^3/\text{m}^3$, and an accurate determination of moisture content was not necessary in these layers (as opposed to moisture content measurements in the MRL of the CCBE).

TABLEAU 4.1 Summary of the physico-chemical, hydrogeological, and electrical properties of materials :

Property (unit)	Tailings ($n = 44$)	Compacted overburden ($n = 47$)	Waste rocks (0-100 mm) ($n = 8$)
Physical			
C_u (-)	12 ± 1	35 ± 9	16 ± 3
D_{10} (μm)	3.3 ± 0.2	0.6 ± 0.2	$1,488 \pm 447$
D_{30} (μm)	11.1 ± 0.6	7.7 ± 1.2	$9,631 \pm 2, 137$
D_{60} (μm)	40.6 ± 2.7	18.0 ± 10.7	$22,948 \pm 3, 747$
G_s (g/cm^3)	2.76 ^(a)	2.70 ^(b)	2.77
Chemical			
Sulfur content (%)	1.22 ± 0.08	-	0.51 ± 0.12
Carbon content (%)	0.55 ± 0.03	-	0.23 ± 0.05
Acidity potential ($\text{kg CaCO}_3/\text{t}$)	38 ± 3	-	16 ± 4
Neutralization potential ($\text{kg CaCO}_3/\text{t}$)	45 ± 2	-	19 ± 4
Neutralizing potential ratio (-)	1.2 ± 0.1	-	1.2 ± 0.1
Hydrogeological			
GMC at installation ^(c) (kg/kg)	0.21 ± 0.02	0.24 ± 0.06	-
VWC at installation ^(c) (m^3/m^3)	0.36 ± 0.03	0.34 ± 0.05	-
Porosity n at installation ^(c) (-)	0.39 ± 0.02	0.46 ± 0.06	-
GMC at installation ^(d) (kg/kg)	0.21 ± 0.01	0.27 ± 0.07	-
MKC predicted k_{sat} ^(e) (cm/s)	3×10^{-5}	4×10^{-6}	8×10^{-1}
k_{sat} (cm/s)	7×10^{-5} ^(a)	5×10^{-7} ^(b)	5×10^{-1} ^(a)
θ_{sat} (m^3/m^3)	0.40	0.45	0.35 ^(a)
θ_r (m^3/m^3)	0.05	0.05	0.01 ^(a)
Air-entry value ψ_a (kPa)	20-30	60-100	< 0.1 ^(a)
Residual suction ψ_r (kPa)	600-1,000	1,500-2,000	< 1 ^(a)
Electrical ^(f)			
Porosity n (-)	0.40	0.45	0.35 ^(g)
Cementation exponent m_A (-)	1.2	0.5	2 ^(g)
Saturation exponent n_A (-)	3.5	3.4	2 ^(g)

^(a) Analysis carried out in Lavoie-Deraspe (2019) for similar tailings and waste rocks from Canadian Malartic Mine. ^(e) Laboratory analysis carried out in Dubois-Roy (2021) for overburden material of the LSHCC. ^(c)

Porosity calculated from nucleodensimeter field measurements during the cover construction. ^(d) Laboratory determination of GMC in wet samples dried in the oven. ^(e) Hydraulic conductivity predicted for fine materials using the modified Kozeny-Carman model (Mbonimpa et al., 2002). ^(f) Archie petrophysical models with a reference pore water EC of 4 mS/cm, a reference temperature of 25 °C. ^(g) A-priori Archie petrophysical model for the waste rocks samples (not calibrated in the laboratory).

4.5.2 Moisture content dynamics from the hydrogeological sensors

The daily precipitation and moisture content dynamics measured by the hydrogeological sensors in the four experimental cover sections are shown in Figure 4.8. As expected, VWC was much lower (typically less than $0.15 \text{ m}^3/\text{m}^3$) in the waste rocks layers (blue and purple sensors for CCBE and blue sensor for LSHCC) when compared to the fine materials. In particular, almost no temporal variations in VWC were observed in the bottom waste rocks layers, which suggested limited percolation rates from the overlying layers in the CCBE sections. VWC remained between 0.30 and $0.40 \text{ m}^3/\text{m}^3$ in the tailings layer of the CCBE section on the plateau and greater than $0.35 \text{ m}^3/\text{m}^3$ in the inclined area during the one-year monitoring period. Each significant precipitation event (i.e., greater than 20 mm/day) was followed by a sharp increase in VWC at the top of the tailings layer in the plateau section, whereas VWC was mostly stable in the rest of the MRL and in the inclined area. Finally, VWC in the overburden layer of the CCBE remained near $0.30 \text{ m}^3/\text{m}^3$ throughout the year and VWC slightly increased after each precipitation event. A sharp decrease in VWC was observed during winter in the overburden layer of the plateau section. This was interpreted as a partial freezing of the pore water in this superficial layer, given that the Teros 12 sensors measured unfrozen water content, which was consistent with the measured temperature near $0 \text{ }^\circ\text{C}$ at the same location during winter. The moisture content dynamics of the CCBE located in the inclined area was similar to the CCBE in the plateau section, which suggested that the slope did not significantly affect the hydrogeological behavior of these covers. Nonetheless, the MRL in the inclined section seemed to be slightly less affected by precipitation than the MRL in the plateau section, which suggested that a fraction of the precipitation was laterally diverted within the top waste rocks layer toward the bottom of the slope (e.g., Bussi re et al. (2003)). Overall, moisture content dynamics monitored in the CCBEs were consistent with the expected behavior for that type of multi-layer cover, and suggested that capillary barrier effects were present at the top and at the bottom of the tailings layers (e.g., Nicholson et al. (1989); Aubertin et al. (1995)).

VWC remained between 0.30 and 0.45 m^3/m^3 in the compacted overburden material at the top of the slope of the LSHCC. In comparison, the compacted overburden material at the bottom of the slope was slightly less wet in the hydrogeophysical section, with VWC ranging from 0.25 to 0.38 m^3/m^3 . The high and steady VWC values observed at the bottom of the compacted overburden layers suggested that a capillary barrier effect developed at the interface between the waste rocks and the compacted overburden. On the contrary, significant changes in VWC were observed in the uncompacted overburden material and at the top of the compacted overburden layers in the LSHCC, with variations of up to 0.15 m^3/m^3 between the wettest and driest periods. These variations suggested that the top part of the LSHCC was more affected by vertical drainage, evaporation, or evapotranspiration (or a combination of these three components) than the compacted overburden material at greater depths in the covers. VWC in the transition layer of waste rocks was higher near the bottom of the slope than near the top part of the slope. Strong increases in VWC were recorded in the waste rock layers of the LSHCC following each significant precipitation event, and the temporal variations of VWC in the bottom waste rocks layers were stronger at the bottom of the slope of the LSHCC, both in terms of absolute values and amplitude of variation.

4.5.3 Time-lapse electrical resistivity tomography results

Spatial distribution of moisture content from inverted conductivity

Electrical resistivity tomography in the field multi-layer covers allowed the monitoring of moisture content dynamics to extend spatially across the 23 m-long cover sections. Figure 4.9 presents the distribution of VWC predicted by inversion for the four cover sections on July 1st, 2021 (left panel) and on August 28th, 2021 (right panel). As indicated by the dashed lines on Fig. 4.8, July 1st, 2021 corresponded to a wet period, with cumulative rain of $\simeq 55$ mm during the previous week (blue dashed line) whereas August 28th, 2021 corresponded to a dry period with cumulative rain of < 1 mm during the previous two weeks and $\simeq 40$ mm during the previous month (red dashed line).

The VWC distribution predicted from geoelectrical monitoring was consistent with hydrogeological measurements for both dates shown on Fig. 4.9. VWC was high in the MRL composed of tailings for the CCBE (between 0.30 and 0.40 m^3/m^3) and of overburden for the LSHCC (between 0.25 and 0.45 m^3/m^3). In the meantime, VWC was less than 0.10 m^3/m^3 in the waste rocks, which suggested that the capillary barrier effects at the interface between fine and coarse materials were effective. Higher VWC values were predicted from ERT inversions in July after the strong precipitation events, as opposed to August, which seemed to be more

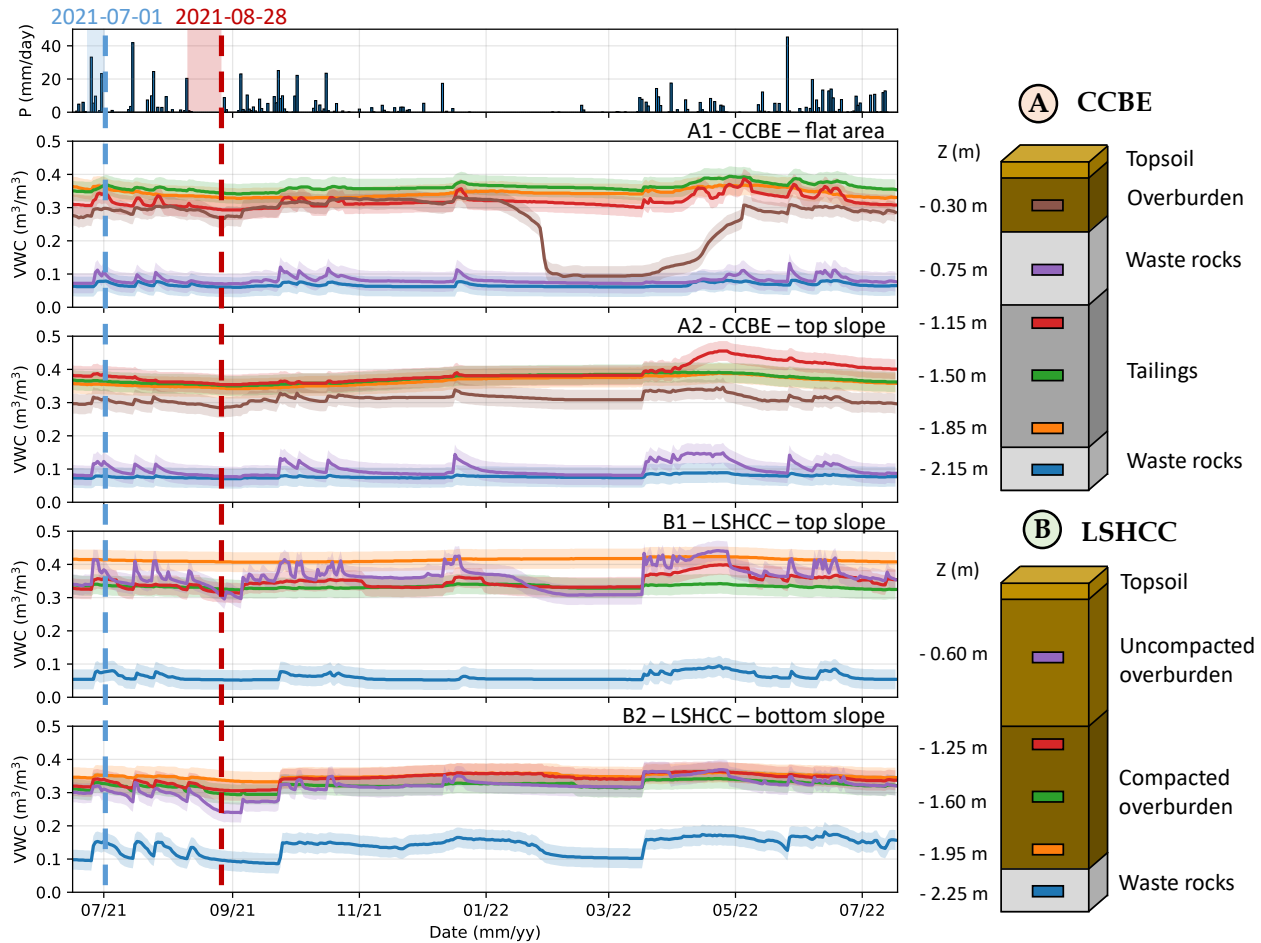


FIGURE 4.8 Daily precipitation and unfrozen volumetric water content measured by the Teros 12 sensors for the four cover sections. The vertical dashed lines correspond to the wet and dry dates referred to in Fig. 4.9

affected by the drought, particularly in the overburden material of the LSHCC. ERT inversions produced VWC distributions that were globally smooth in the longitudinal direction and showed stronger changes in the vertical direction (Fig. 4.9). This was consistent with the inversion anisotropic smoothing and with the increase of suction with elevation expected in such multi-layer covers (Bussi ere et al., 2007). Nonetheless, some horizontal variations in VWC were noted for the LSHCC, which might have been caused by the higher variability in hydrogeological properties for the overburden material evidenced by the systematic characterization. For instance, higher VWC values were predicted from ERT inversions at the left upslope part of the profile for the top slope LSHCC (as opposed to the right bottom slope part of the profile).

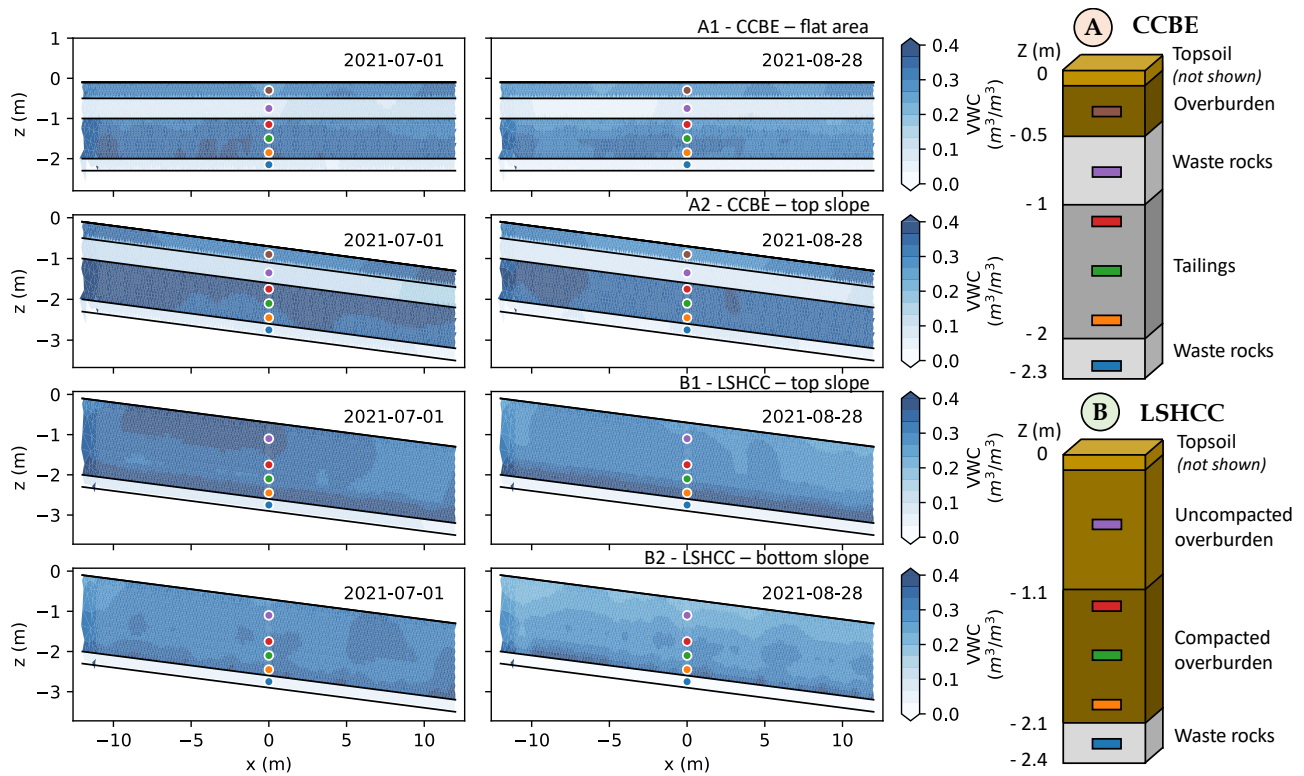


FIGURE 4.9 VWC distribution derived from inverted resistivity models using the Archie-based resistivity-to-VWC relationship in the CCBEs (first and second panels) and in the LSHCCs (third and fourth panels) for the two dates identified on Fig. 4.8 corresponding to wet and dry conditions (the 0.1 m-thick layer of topsoil at the top of the covers is not shown in these plots).

Spatio-temporal dynamics of moisture content

The complex spatio-temporal dynamics of VWC in the four experimental covers during Summer 2021 was further investigated using the relative variation of VWC. Figure 4.10 presents the VWC distribution on July 25th, 2021 before significant precipitation events (55 mm in one week) on the top panel. This date was considered as a baseline for the calculation of relative variations of VWC during the precipitation event (following week) and during the following months (drier conditions).

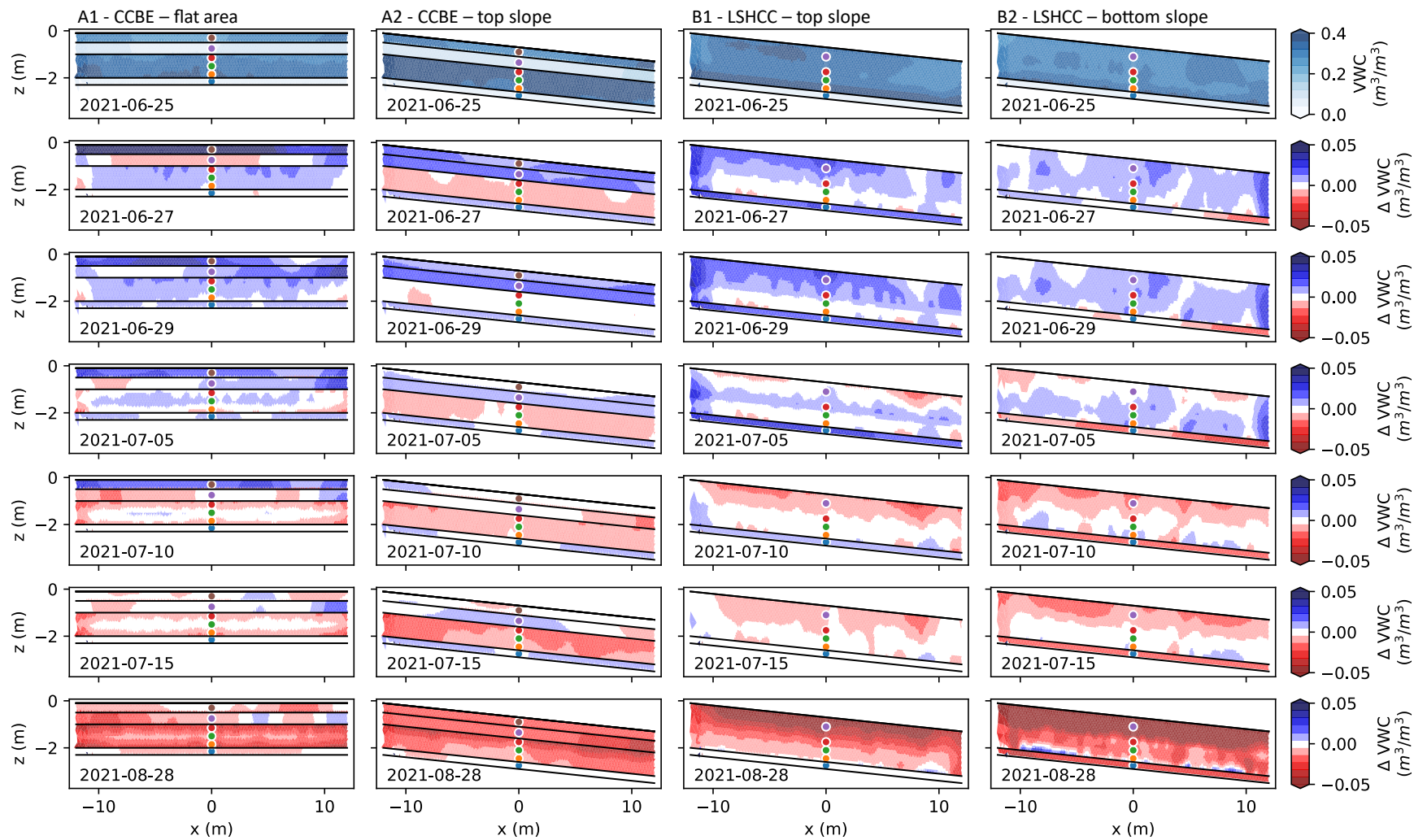


FIGURE 4.10 Spatio-temporal dynamics of VWC in the field experimental CCBEs (two vertical panels on the left) and in the LSHCCs (two vertical panels on the right) at selected dates. As shown in Fig. 4.8, the last week of June 2021 was particularly wet while drier conditions were recorded during August 2021.

Different hydrogeological behaviors were identified for each cover section. For the CCBEs, only the top layers were affected by the precipitation with a VWC increase greater than $0.05 \text{ m}^3/\text{m}^3$ in the overburden and top waste rocks layers. The top of the tailings was also slightly affected by the precipitation with an increase in VWC around $0.05 \text{ m}^3/\text{m}^3$ in the plateau section (Design A1) while almost no variations were recorded in the tailings layer in the inclined area (Design A2). Such different behaviors were interpreted to be caused by the slope, which could have increased the lateral deviation of precipitation toward the bottom of the slope at the interface between the top waste rocks layer and the tailings, thus reducing the amount of water percolating into the tailings. However, the decrease in VWC associated with drier conditions (August 28th, 2021) was similar for the two CCBE sections, with a decrease less than $0.05 \text{ m}^3/\text{m}^3$, which was consistent with the hydrogeological sensor measurements located at the center of the covers (colored dots on Fig. 4.10).

Greater spatio-temporal changes were observed in the LSHCCs; the largest variations in VWC were in the upper part of the uncompacted overburden layer, with a relative increase in VWC around $0.03 \text{ m}^3/\text{m}^3$ following precipitation events and a relative decrease in VWC greater than $0.05 \text{ m}^3/\text{m}^3$ during the dry period. By contrast, the 1 m-thick layer of compacted overburden did not show significant variations after precipitation, particularly for the cell located at the top of the slope (Design B1). Nonetheless, the decrease in VWC that was recorded at the end of August 2021 affected both the uncompacted and the compacted overburden layers. Overall, no lateral trends in the VWC temporal variations were obvious for any of the experimental hydrogeophysical covers sections (e.g., preferential flow in a specific area, lateral deviation of water, or heterogeneity in the material).

Accuracy of ERT-predicted moisture content

The accuracy of the geoelectrical results was investigated in the four cover sections by comparing the VWC measured by the Teros 12 sensors and the VWC predicted by ERT at the same locations. Following the methodology described in Dimech et al. (2023b), the ERT-predicted VWC values were extracted from the 2D inverted conductivity models at the sensor location, knowing their volume of investigation (approximately 1 L). The left panel of Figure 4.11 compares the temporal evolution of the measured VWC (dashed lines) and the ERT-predicted VWC (solid lines) at the location of sensors in the tailings layers for the CCBEs and in the overburden material for the LSHCCs. The right panel shows the comparison between measured VWC (horizontal axis) and ERT-predicted VWC (vertical axis). Overall, the ERT-predicted VWC matched the hydrogeological measurements well, both in absolute value and relative temporal variations. Indeed, most of the ERT-predicted VWC values were close to

the black solid line that represents a perfect fit between predicted and measured VWC (right panel of Fig. 4.11). The difference between the two datasets was less than $\pm 0.05 \text{ m}^3/\text{m}^3$ and the root mean square errors ranged from 0.01 to 0.03 m^3/m^3 . These results were consistent with previous results from a multiscale accuracy assessment study in the CCBE located in the plateau section, which reported similar accuracy (Dimech et al., 2023b).

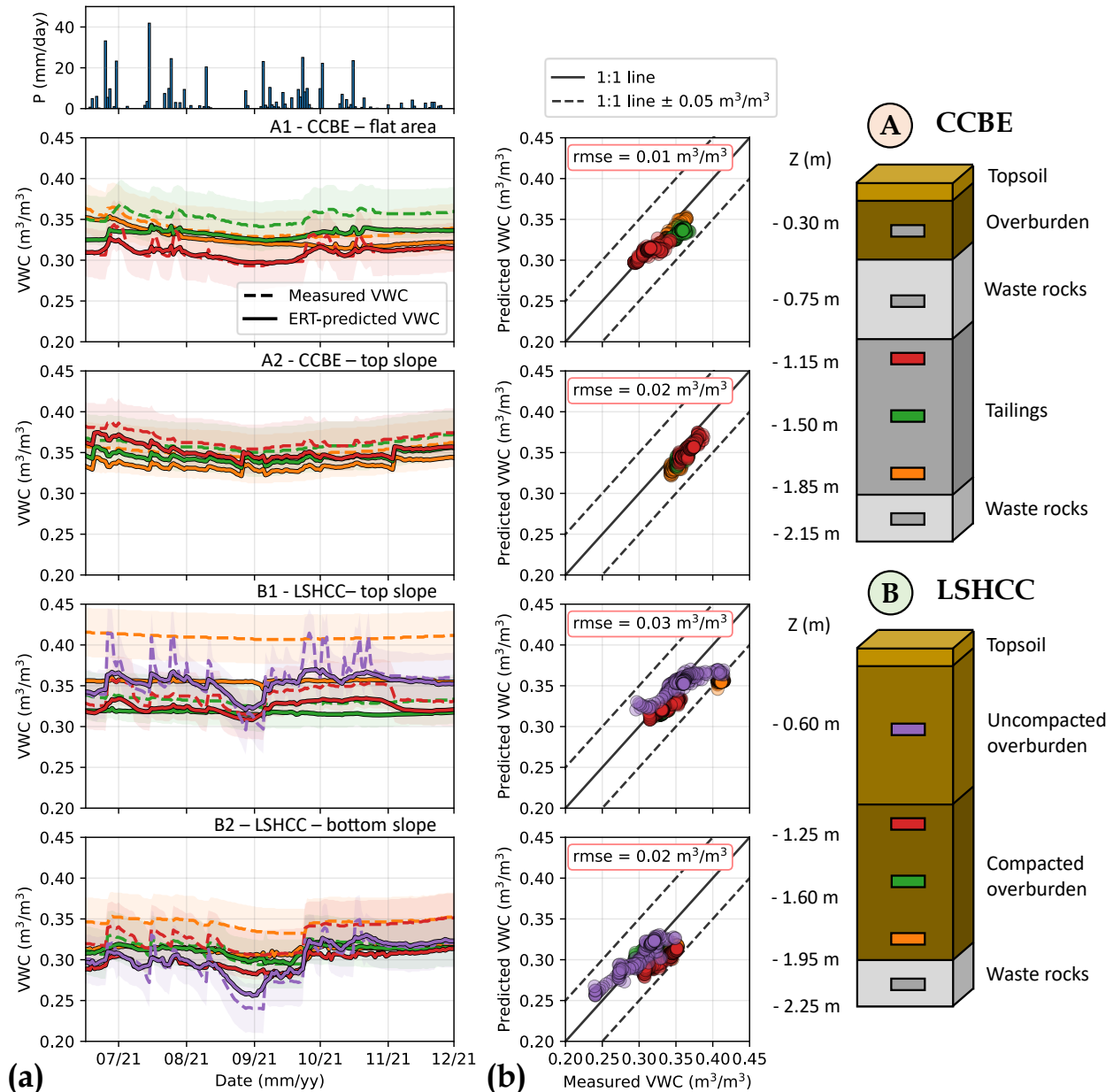


FIGURE 4.11 Accuracy of ERT-predicted VWC using the VWC measured by the hydrogeological sensors at the center of the covers as a reference for the four experimental multi-layer covers. (a) Temporal evolution and (b) comparison of measured (dashed lines) and ERT-predicted (solid line) VWC.

Spatio-temporal dynamics of the degree of saturation during one year

The hydrogeophysical monitoring data allowed 2D imaging of VWC dynamics for each experimental hydrogeophysical cover section over a period of 400 days, which revealed the hydrogeological behavior of the multi-layer covers. The VWC distribution predicted from geoelectrical data was converted into saturation degree, given that this property is generally determinant for the performance assessment of the covers. In the CCBEs, the degree of saturation was calculated using an estimated porosity of 0.38 and 0.41 for the tailings layer in the plateau section and in the inclined section, respectively (cf. Table 4.1). Similarly, an estimated porosity of 0.46 was used to calculate the degree of saturation in the overburden layers (compacted and uncompacted) of the LSHCCs for both sections (top and bottom parts of the slope).

The left panel of Figure 4.12 presents the 2D imaging of the calculated degree of saturation for the hydrogeophysical cover sections in July 2022 using a simplified color code. The degree of saturation was mostly greater than 85% in the MRL of the CCBE sections, whereas the degree of saturation was more heterogeneously distributed in the LSHCC sections. For the LSHCCs, the highest values (greater than 90%) were observed at the bottom of the compacted overburden layer at the top of the slope (section B1) and the lowest values (less than 75%) were reported in the uncompacted overburden layer at the surface of the LSHCCs, particularly at the bottom of the slope (section B2). The right panel of Fig. 4.12 assesses which surface of the fine-grained material (tailings or overburden) remained at a specific interval of degree of saturation for a given period of time (in% of the total surface considered). Finally, the pie-charts summarize the cumulative portions of the fine-grained material layers for each interval of degree of saturation during the one-year period (e.g., 34% and 53% of the MRL with a saturation degree greater than 90% for the CCBEs in the plateau and inclined sections, respectively).

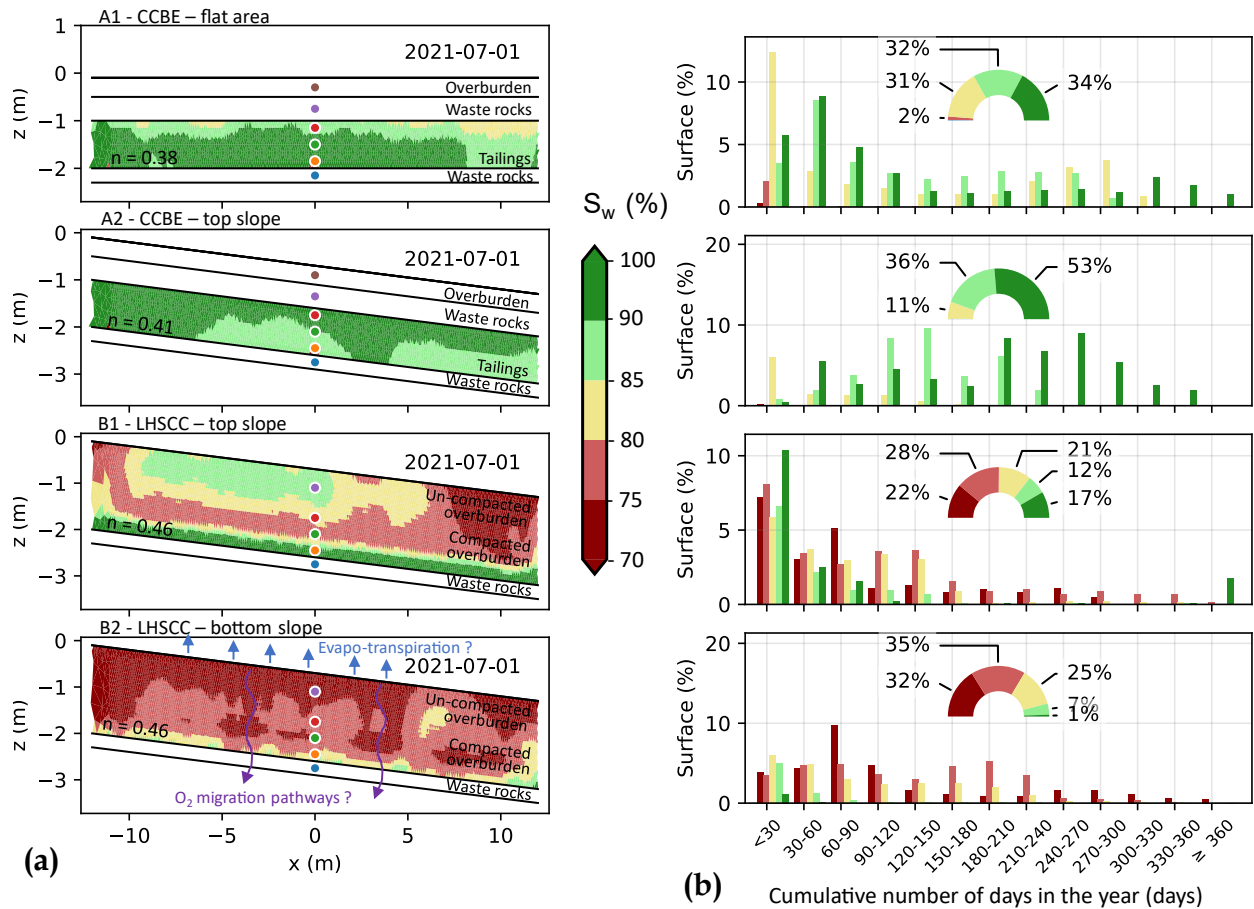


FIGURE 4.12 (a) Distribution of the degree of saturation predicted from ERT measurements for the four experimental cover sections. (b) Surface percentage of the fine-grained layers at different intervals of degrees of saturation for a given period of time and summary for the one-year monitoring period.

4.6 Discussion

4.6.1 Performance assessment of the multi-layer covers from hydrogeophysical monitoring data

Performance of the covers with capillary barrier effects (CCBEs)

The CCBEs were designed to act as oxygen barriers thanks to the high water retention capacity of a MRL (Nicholson et al., 1989; Demers and Pabst, 2021b). Therefore, the performance of the CCBE can be assessed from the degree of saturation of the MRL using a threshold value of 85%, which is generally considered to define an efficient CCBE (Aubertin et al., 1998; Aachib et al., 2004; Bussière et al., 2007; Demers and Pabst, 2021b). Moreover, the performance of the CCBE was considered uncertain for degrees of saturation between 80%

to 90% (yellow and light green colors on Fig. 4.12). This allowed to take into account the uncertainties associated with the calculated degree of saturation, given that an accuracy of $\pm 0.02 \text{ m}^3/\text{m}^3$ in terms of VWC corresponds to an accuracy of $\pm 5\%$ in terms of degree of saturation (considering a porosity of $n = 0.40$).

Good performance was achieved throughout the monitoring period in the CCBE hydrogeophysical sections since the MRL maintained an estimated degree of saturation greater than 85% most of the time. The two sections of CCBEs investigated in this study showed similar behavior, which suggested that the slope did not greatly affect the performance of the CCBE. Fig. 4.12 shows that the CCBE section located at the top of the slope (Design A2) presented the best performance. The ERT-predicted degree of saturation in the MRL of the CCBE located on the plateau section was occasionally in the uncertainty zone, between 80% and 85% for short periods of time during the driest periods of the year in the top part of the MRL. The slight difference in performance between the two sections of the CCBE could be explained, at least in part, by variations inherent to such large-scale construction.

From a broader perspective, the hydrogeological behavior of the CCBE sections was consistent with previous field CCBEs (e.g., Dagenais et al. (2005); Bussière et al. (2009); Maqsoud et al. (2011); Kalonji-Kabambi et al. (2017)), which suggested that capillary barrier effects were likely to occur at the interface between tailings and waste rocks (Nicholson et al., 1989). This type of reclamation covers using tailings and waste rocks is promising since no natural materials are needed for the construction (e.g., natural sand, silt, or clay from nearby borrow pits), which reduces the environmental impact of reclamation and provides logistical and economic benefits (Aubertin et al., 1995; Bussière et al., 2007; Larochelle et al., 2019). Bussière et al. (2003) and Bussière et al. (2006) also demonstrated that the performance of CCBEs installed along inclined slopes would be lower in the upper part of the slope, which suggests that the lower part of the field experimental CCBE (not instrumented with geophysical instruments) would achieve an even better performance. Nonetheless, more investigation might be necessary to assess the impact of vegetation and climate change on long-term CCBE performance since these two elements have been reported to potentially play a role for such covers (e.g., Hotton et al. (2019); Proteau et al. (2020b,a); Bussière and Guittonny (2021b)).

Hydrogeological behavior of the low saturated hydraulic conductivity covers (LSHCCs)

For the LSHCCs, both hydrogeological and geophysical monitoring results suggested greater spatio-temporal variations in moisture content and a lower degree of saturation within the

overburden material (compacted and uncompacted). The greater variations were located at the bottom of the slope (Design B2). At this location, nearly 90% of the compacted overburden layer remained below 80% throughout the year (50% of the layer at the top of the slope). The lowest degrees of saturation within the compacted and uncompacted overburden material were recorded in August and September 2021, during a dry period (< 1 mm of rain during the last two weeks of August 2021). These observations would be helpful in the future to assess the performance of the LSHCC sections, which is generally defined as their ability to reduce the net percolation of water toward the mining wastes (Maqsoud et al., 2021). Indeed, the degree of saturation in the LSHCC would likely affect the storage capacity and the evapotranspiration of the overburden layers following each precipitation and drought event, which both play a role in the assessment of the reduction of water infiltration through the cover (Maqsoud et al., 2021). In particular, these datasets could be used in the future to calibrate hydrogeological numerical models, which would allow the ability of the LSHCCs to control water infiltration to be assessed (e.g., Bussière et al. (2003); Pabst et al. (2017); Power et al. (2017)).

Higher water accumulation could have been expected at the bottom of the slope, following the results from Bussière et al. (2003), which was not the case in this study for the LSHCC. This observation could be explained, at least in part, by the presence of vegetation in the lowest part of the slope (see Fig. 4.1), which might have modified the water budget by adding evapotranspiration for this area, as it has been documented for CCBEs (e.g., Bussière and Guittonny (2021b)). These field results also highlighted the impact of the top waste rocks layer placed above the fine-material layer in a CCBE that acts as an evaporation barrier (not present in the LSHCCs), which explains the lower saturation. Lastly, the larger variability in overburden physical properties evidenced by systematic sampling and multi-physical characterization did not seem to play a major role in the LSHCC hydrogeological behavior. Although the imaged distribution of VWC was slightly less homogeneous than in the tailings, no clear spatial trends were evidenced in the overburden material, such as potential preferential flow or strong anomalies of VWC in the material, as has been documented in previous work using ERT for heterogeneous materials (e.g., Beauvais et al. (2004); Bechtold et al. (2012b)).

As mentioned above, the main function of the LSHCC is to reduce the infiltration rate toward the tailings. Unfortunately, the resolution of geoelectrical imaging was too low in the waste rocks to properly assess the amount of water percolating through the interface between the compacted overburden material and the waste rocks. Nonetheless, the strong variations in moisture content monitored by the sensors in the waste rocks layer at the bottom of the cover

suggested that a non negligible portion of the precipitation infiltrated toward the tailings, which could be explained in part by the saturated hydraulic conductivity estimated for the overburden material (around 10^{-6} cm/s) and the higher variability in material properties. Finally, hydrogeophysical monitoring of the flow of tracers (e.g., conductive water or using heat as a proxy with hot water Hübner et al. (2017); Dimech et al. (2019); Robert et al. (2019)) in the LSHCCs could be a promising avenue to extract more information from TL-ERT and further investigate the hydrogeological behavior and water movement in these covers.

4.6.2 Advantages of TL-ERT for multi-layer cover performance monitoring

Pilot-scale proof-of-concept of performance assessment using geoelectrical monitoring

This study addresses the reliability of geoelectrical monitoring for the performance assessment of multi-layer covers at the pilot scale under field conditions. The proposed methodology allowed the prediction of VWC from ERT, given that the temperature, pore water conductivity, and petrophysical relationships were properly accounted for. In particular, the ERT-predicted VWC was similar to the measured VWC, both in terms of absolute value and temporal variations, with root mean square errors between measured and predicted VWC ranging from 0.01 to 0.03 m³/m³, which corresponds to an accuracy in terms of degrees of saturation ranging from $\pm 2.5\%$ to $\pm 7.5\%$ (assuming a porosity of 0.40). Such accuracy is similar to the accuracy of the hydrogeological sensors used in this study. Although to our knowledge this study was the first of its kind for mining waste monitoring, similar accuracy values for ERT-predicted VWC have been reported for other types of applications (e.g., Garré et al. (2011); Beff et al. (2013); Dietrich et al. (2014); Fan et al. (2015)). As noted previously, the ability to accurately assess moisture content would likely play a major role for a broader application of geoelectrical monitoring for mining reclamation given that only small changes in the degree of saturation of an oxygen barrier can strongly affect its performance (Demers and Pabst, 2021b; Dimech et al., 2022). The methodology presented in this study could be applied to active, closed, or abandoned mining sites to provide continuous and remote monitoring of the moisture content in mine tailings, which could help operators to assess the geotechnical and/or geochemical stability of the mine wastes over the long term.

Spatial resolution, lateral extension and monitoring costs of time-lapse ERT

The spatial imaging capacity of ERT is a strong advantage of this monitoring technique since it allows the mapping of key physical parameters of the subsurface in 2D or 3D across large

scales (Chambers et al., 2014b; Uhlemann et al., 2017b; Dimech et al., 2019). Although the surface of the experimental cover sections monitored using TL-ERT was relatively small for this pilot study (23 m-long profiles), several recent studies presented field cases where wider areas have been monitored using non-invasive, continuous, and remote monitoring (up to several hundreds of meters) for other types of applications (Auken et al., 2014; Chambers et al., 2022; Holmes et al., 2022a). As discussed in Dimech et al. (2022), this perspective is promising for monitoring large structures such as mining waste storage facilities to spatially extend the performance assessment and provide complementary data to traditional local hydrogeological sensors. As a result, the integration of geoelectrical imaging techniques within traditional surveillance programs could allow large-scale monitoring at reduced costs (Bussi ere et al., 2021; Tresoldi et al., 2021). ERT arrays could be deployed permanently in the storage facilities across profiles that could measure up to several hundreds of meters to yield autonomous and continuous monitoring of the moisture content in mine wastes (in combination with hydrogeological sensors for moisture content, suction, temperature, and pore water EC). This would allow, for instance, the quantification and monitoring of the performance of the cover to act as an oxygen barrier, and provide early warning for areas where the performance does not meet the design criteria or where too much water is detected for geotechnical stability assessment (e.g., Tresoldi et al. (2020c); Dimech et al. (2021)). In particular, the recent development of autonomous, off-grid, remote resistivity meters such as the PRIME system used in this study (Chambers et al., 2022; Holmes et al., 2022b) is likely to play a role in the development of geoelectrical monitoring applications since hundreds of electrodes can be used with a single resistivity meter, which in turn improves the spatial resolution and increases the area covered while ensuring high temporal resolution (e.g., one or more images per day) (Slater and Binley, 2021; Chambers et al., 2022). As discussed by Dimech et al. (2022), permanent geoelectrical monitoring could also play a major role in the near future for the autonomous surveillance of the geotechnical stability of tailings dams across large scales. Following the example of Tresoldi et al. (2021) and Gunn et al. (2015), permanent ERT arrays could be installed within the dams to track potential seepage, and provide early warnings to the operators if anomalous water accumulation, which could threaten the stability of the dams, is detected.

4.6.3 Limitations and challenges of TL-ERT for monitoring of multi-layer cover performance

Strong influence of temperature, pore water conductivity, and porosity on ERT results

Since ERT is based on low-frequency electrical measurements, several components contribute simultaneously to the electrical conductivity in the subsurface (Dimech et al., 2022). As a result, the relationship between bulk electrical conductivity and volumetric water content is dependent on temperature and water electrical conductivity, which can vary simultaneously in the material and must be properly taken into account (Hayley et al., 2007; Ma et al., 2011; Dimech et al., 2019). Although the temperature and pore water EC correction presented in this study was used to correct these effects, Dimech et al. (2023b) demonstrated that not taking into account these variations reduces the accuracy of moisture content predictions by a factor of 10. Such conclusions highlight the importance of using complementary hydrogeological sensors to monitor temperature and pore water conductivity at different locations, which will be needed to correct the ERT datasets (Dimech et al., 2022). However, high uncertainties could be associated with the extrapolation of local temperature and pore water EC data in the imaging domain, especially for pore water EC, which can vary sharply in mining wastes, both in space and time (e.g., Dimech et al. (2019)). In addition, the Teros 12 sensors measure bulk EC using a two-points method, which is less reliable than four-points measurements, especially at lower moisture content as discussed by Hen-Jones et al. (2017a). Moreover, the calculation of pore water EC based on Teros 12 data has a rather low accuracy ($\pm 20\%$) when moisture content is lower than $0.10 \text{ m}^3/\text{m}^3$, and even lower accuracy for drier media (Hilhorst, 2000; MeterGroup, 2019). Local variations of porosity in the material are also likely to occur in such covers (cf. Table 4.1), which can be explained by changes in the material properties, water content of the initial material, precipitation events occurring during construction, additional compaction by heavy machinery, or variations in the compaction from the mechanical shovel. As a result, the degree of saturation could be locally under or over-estimated, which could impact the performance assessment. As discussed in Wagner and Uhlemann (2021), the integration of other geophysical methods could help reduce this ambiguity, as it has successfully been done for permafrost imaging using electrical and seismic co-located characterization (Hauck et al., 2011; Wagner et al., 2019; Mollaret et al., 2020). For instance, active seismic, ground penetrating radar or electromagnetic surveys could be carried out frequently where ERT arrays are installed (Wagner and Uhlemann, 2021). Permanent passive seismic or fiber-optic arrays could also be installed alongside ERT arrays to carry out monitoring, although only a few examples are reported in the literature (Daley

et al., 2013; Olivier et al., 2017; Pevzner et al., 2021; Wu et al., 2021).

Uncertainties associated with ERT inversions and petrophysical models

In this study, most of the geoelectrical data processing (i.e., pre-processing, inversion, and conversion of bulk EC to VWC using petrophysical relationship) was done independently from the hydrogeological measurements. As a result, the hydrogeological and physical constraints associated with this kind of multi-layered unsaturated media might not be fully represented by the numerical solution from the inversion, which is neither perfect nor unique (Samouëlian et al., 2005; Loke, 2018) and depends on the spatio-temporal regularization constraints applied (Johnson et al., 2012a; Loke et al., 2022). For instance, some artifacts could be present in the inverted distribution of bulk EC, especially in areas of low sensitivity such as at the boundaries of the imaged volume, or due to the complex geometries of these media (Nimmer et al., 2008; Dimech et al., 2017; Hojat et al., 2020). Moreover, the inverted results might differ locally from the hydrogeological measurements because of the difference in volume of investigation. Indeed, the sensors only sample a small volume (typically less than 1 L), whereas ERT measurements provide information averaged across larger volumes (typically several m³) (Robinson et al., 2008b). The latter could explain some differences between the measured and ERT-predicted VWC temporal evolution reported at some locations in this study (Fig. 4.11), especially close to the surface (purple sensor in the LSHCC), where rapid variations of VWC were captured by the sensors but were not well resolved by geoelectrical monitoring (spatio-temporal smoothing). In this regard, Dimech et al. (2022) identified several alternative data processing (e.g., coupled hydrogeo-physical inversion) and assimilation techniques (e.g., Ensemble Kalman Filters) that are promising to combine hydrogeological data alongside numerical modeling tools (e.g., hydrogeo-thermal, transport flow, and geophysical modeling) and geoelectrical datasets to provide more realistic distributions of VWC in the subsurface (Camporese et al., 2015; Kang et al., 2018, 2019; Tso et al., 2020; Isabelle, 2022). Finally, some uncertainties remain associated with the petrophysical models in tailings, mainly because of the potential effects of mineralogy on solid matrix conduction and the importance of the electrical double layer on surface conduction for clay-like materials (Revil et al., 2012; Booterbaugh et al., 2015; Mollehuara-Canales et al., 2020).

4.7 Conclusion

This study presented the first pilot-scale application of autonomous and remote time-lapse geoelectrical monitoring of moisture dynamics within experimental engineered multi-layer

covers on mine tailings. We presented the methodology followed to install the hydrogeophysical instruments, record daily ERT measurements, and obtain 2D distributions of bulk EC for which temperature and pore EC variations were taken into account. The petrophysical models calibrated in the laboratory were used to convert bulk EC into 2D distributions of volumetric water content. This approach provided data that were combined with conventional moisture sensors to assess the hydrogeological behavior of the covers. In particular, the 2D distributions of moisture content were used to assess the ability of the covers to act as oxygen barriers to control the risk of acid mine drainage generation. This study provided a "proof-of-concept" demonstration of how continuous geophysical monitoring can be used to help assess the performance of mine tailings reclamation covers across larger scales. Both hydrogeological and geophysical datasets were consistent, with a root mean square error between 0.01 and 0.03 m³/m³. Despite some limitations specifically identified for the application of TL-ERT in mining wastes, the high accuracy, high temporal resolution, and large-scale monitoring capacity of TL-ERT make it promising for monitoring the geochemical and geotechnical stability of mining waste storage facilities in the near future. Geoelectrical monitoring could be combined with conventional sensors to spatially extend the monitoring of these large structures to help control the risk of environmental contamination and provide early warning to prevent catastrophic failures.

CHAPITRE 5 DISCUSSION GÉNÉRALE

Les chapitres précédents ont permis de répondre à l'objectif général du projet qui consistait à développer et tester à l'échelle pilote une approche de surveillance de la teneur en eau volumique dans des recouvrements miniers par tomographie de résistivité électrique (c.f., Section 1.2). Cette thèse a permis de poser les bases théoriques de la méthode électrique appliquée au suivi des recouvrements tout en démontrant sa faisabilité par la mise en application d'une preuve de concept à l'échelle pilote par les actions suivantes :

- (i) en identifiant dans la littérature les meilleures pratiques développées en termes d'instrumentation, de collecte de données automatisée à distance et pour le traitement et l'interprétation des données hydrogéophysiques (Chap. 2) ;
- (ii) en proposant un dispositif de laboratoire permettant de calibrer la relation entre la conductivité électrique, la teneur en eau et la succion dans des résidus (Chap. 3) ;
- (iii) en estimant la précision de la teneur en eau calculée à partir des données de résistivité électrique à différentes échelles en laboratoire et sur le terrain (Chap. 3) ;
- (iv) en illustrant la faisabilité de la méthode électrique pour imager la teneur en eau volumique à l'échelle pilote dans des recouvrements en continu (Chap. 4).

L'objectif de la discussion est d'élargir le cadre des travaux réalisés dans cette thèse pour proposer un guide de conception de dispositifs de surveillance impliquant la tomographie de résistivité électrique dans les systèmes de recouvrements. Ce guide méthodologique s'appuie sur les observations issues de la revue bibliographique présentée au chapitre 2 mais aussi sur les résultats et conclusions des essais réalisés en laboratoire et sur le terrain présentés aux chapitres 3 et 4. Ainsi, les aspects méthodologiques et les résultats présentés aux chapitres 2 à 4 ou dans le cadre de conférences, qui sont jugés pertinents pour illustrer les éléments du guide de conception, sont abordés et complétés par des éléments issus de la littérature.

Ce guide a pour vocation d'être utilisé comme base de travail pour orienter le choix de qui-conque serait intéressé.e à effectuer le suivi d'un recouvrement mis en place sur site minier actif, en fermeture ou abandonné. Il a été inspiré par les travaux de l'IRME et du MEND qui traitent des approches de suivi de la performance *in situ* des recouvrements en restauration minière, notamment par MEND (2004) et par Bussière et al. (2021), qui aborde succinctement la question de la conception d'un système de suivi temporel de la performance de recouvrements en utilisant l'approche électrique.

5.1 Guide méthodologique proposé pour appliquer la surveillance électrique sur des aires de stockage de rejets miniers à pleine échelle

La Figure 5.1 résume les six principales étapes du guide de conception proposé pour orienter la mise en place d'un dispositif de suivi temporel par la méthode électrique dans les systèmes de recouvrement. De manière globale, le choix du dispositif de suivi électrique devrait être spécifique pour chaque site minier et chaque mode de restauration des rejets miniers. Dans ce sens, le choix d'un dispositif de suivi électrique s'approche de la conception d'un programme de suivi de performance utilisant des instruments de mesures conventionnels (e.g., sondes hydrogéologiques, piézomètres, voir MEND (2004) et Bussière et al. (2021)) et requiert "de l'expérience, du bon sens, et une bonne compréhension du site et de ses particularités" et de notions de physique, de programmation et de sciences de données (Bussière et al., 2021). Chacune des six étapes de la Figure 5.1 est détaillée ci-après.

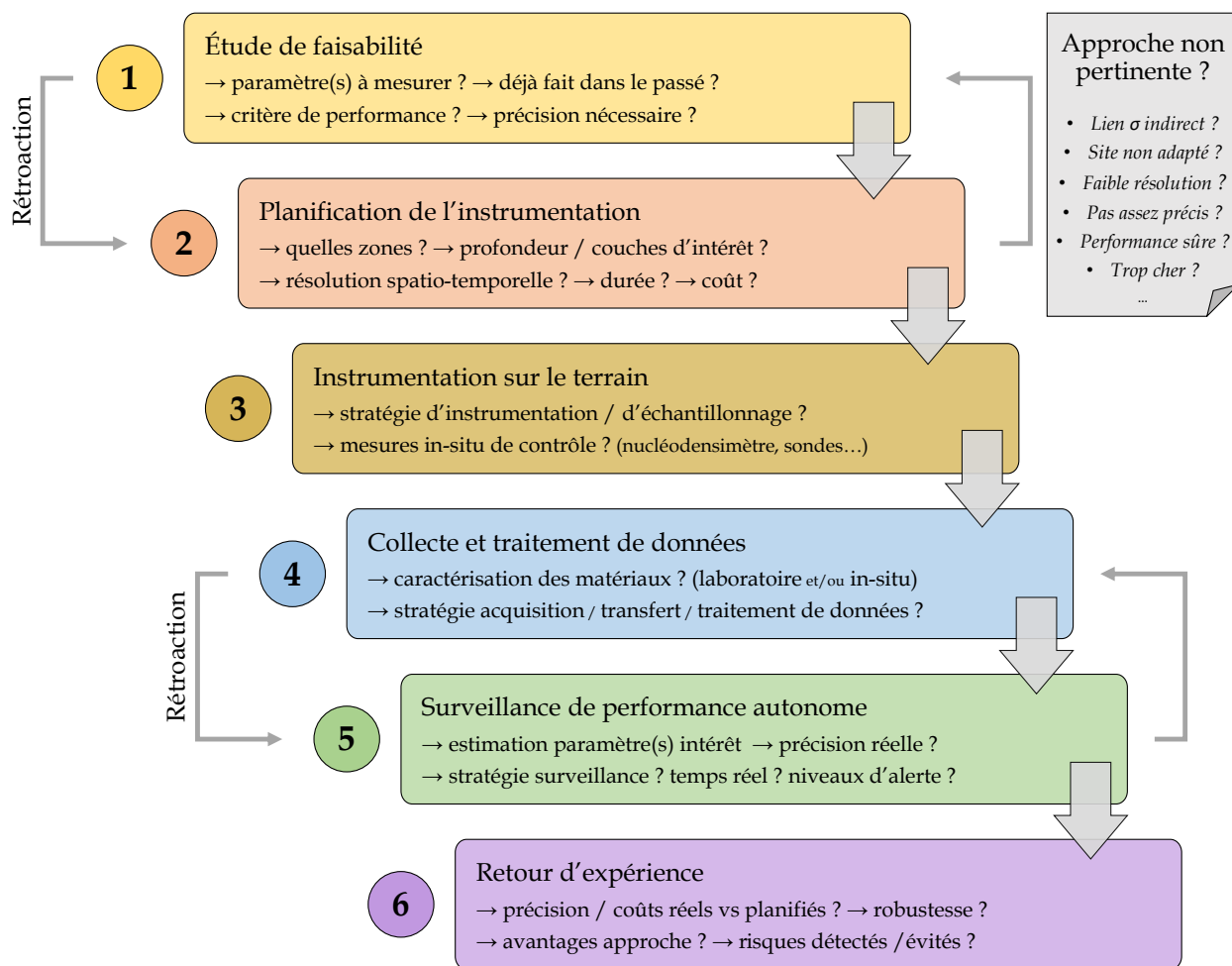


FIGURE 5.1 Guide de conception de dispositif de suivi électrique dans les recouvrements.

5.1.1 Étape 1 : Étude de faisabilité

La première étape qui devrait être suivie dans la conception d'un système de suivi des systèmes de recouvrements miniers impliquant la méthode électrique consiste à identifier clairement le cahier des charges du suivi, c'est à dire, de répondre aux questions :

- **Question 1.1** : Quels sont le ou les paramètres physiques qui devraient être estimés dans le système de recouvrement à partir de l'imagerie électrique ?
- **Question 1.2** : Existe-t-il une relation directe et/ou des relations empiriques entre chacun de ces paramètres physiques et la conductivité électrique du milieu ?
- **Question 1.3** : Est-ce que d'autres paramètres physiques qui affectent également la conductivité électrique risquent de varier fortement dans le temps et/ou l'espace ?
- **Question 1.4** : Si oui, est-il possible de mesurer ces paramètres et/ou de prédire leur évolution spatio-temporelle au sein du recouvrement pour corriger leur effet ?
- **Question 1.5** : Est-ce que ce type de suivi a déjà été réalisé par le passé, sur un site minier ou dans un autre contexte ? de manière continue ou discontinue dans le temps ?
- **Question 1.6** : Est-il possible de quantifier la performance du recouvrement à partir du ou des paramètres imagés ? Si oui, comment les relier à la performance ?
- **Question 1.7** : Si oui, quel est le niveau de précision nécessaire pour être capable de détecter une baisse de performance du recouvrement à partir des données électriques ?

À titre d'exemple, la Figure 5.2 résume la démarche identifiée dès le début du projet de thèse pour effectuer le suivi de performance des CEBCs expérimentales construites à la mine Canadian Malartic. Ce schéma est largement inspiré par les travaux du BGS (*British Geological Survey* en Angleterre) qui a développé une approche similaire pour la surveillance de la teneur en eau dans les glissements de terrain et les infrastructures routières et ferroviaires (e.g., Chambers et al. (2014a); Gunn et al. (2015); Uhlemann et al. (2017a); Whiteley et al. (2019); Holmes et al. (2020, 2022b); Chambers et al. (2022)).

Comme discuté dans les chapitres 3 et 4, le principal paramètre physique qui permet de quantifier la performance de la CEBC est le degré de saturation dans la couche de rétention d'eau constituée de résidus miniers (réponse à la **Question 1.1**) (Demers and Pabst, 2021b). Il existe plusieurs relations semi-empiriques reliant le degré de saturation à la conductivité électrique dans le milieu, telles que les relations d'Archie (Archie et al., 1942), de Waxman-Smits (Waxman and Smits, 1968) ou d'Archie généralisé (Glover, 2010) qui peuvent être calibrées

en laboratoire (**Question 1.2**). Ceci fait de la conductivité un bon marqueur pour imager le degré de saturation dans la couche de rétention d'eau comme illustré par la figure 5.2. Comme décrit dans le chapitre 3, les variations spatio-temporelle de température, de conductivité du fluide interstitiel et de porosité dans les résidus ont été identifiées comme potentiels défis pour estimer précisément le degré de saturation et des sondes hydrogéologiques ont été installées pour prendre en compte ces variations (**Questions 1.3 et 1.4**).

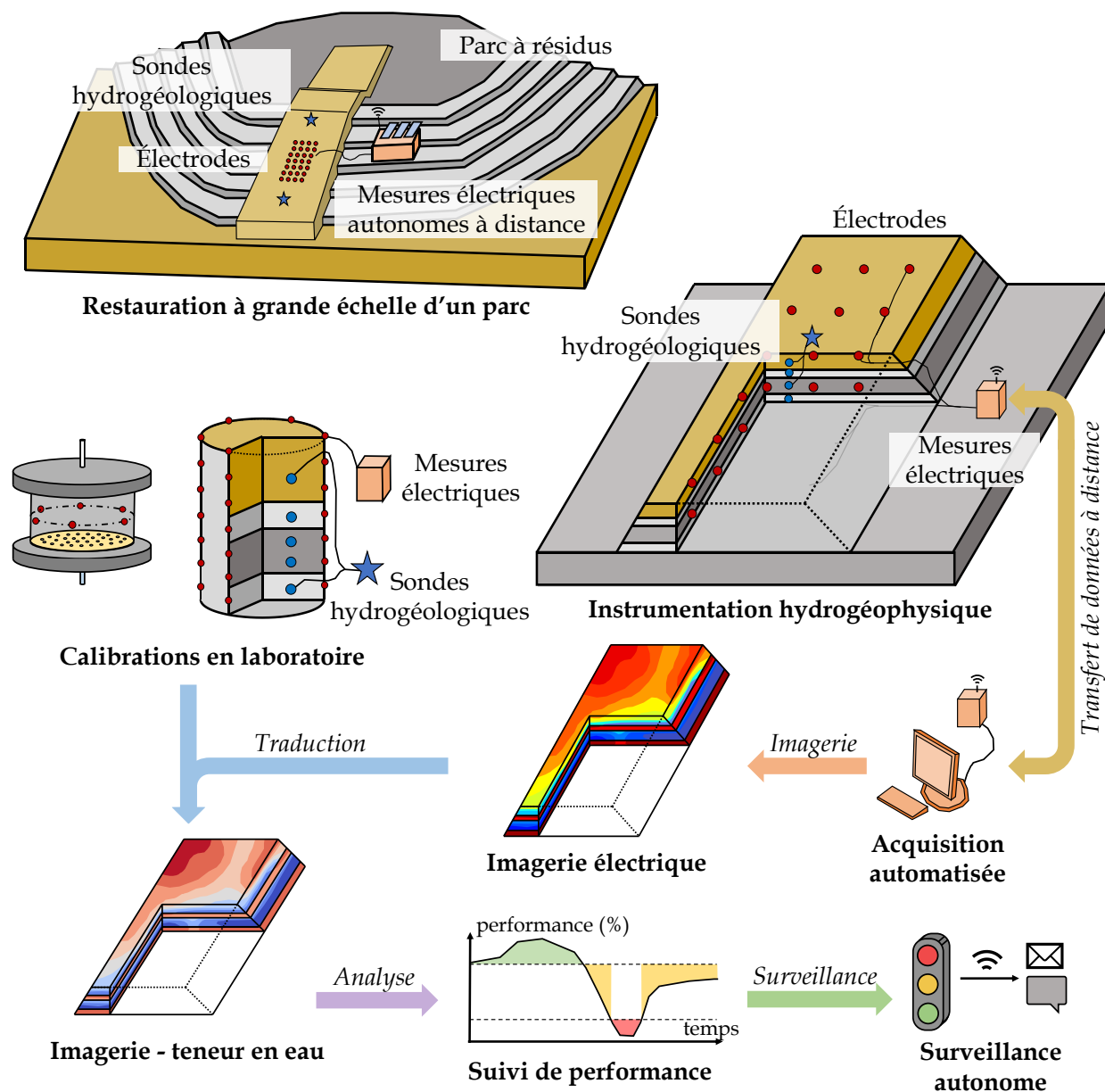


FIGURE 5.2 Approche méthodologique proposée dans cette thèse pour effectuer la surveillance de la performance de CEBC à l'échelle pilote par la méthode électrique.

Comme mentionné plus haut, la méthode électrique est fréquemment employée pour estimer la teneur en eau dans le milieu, notamment dans le contexte du suivi des glissements de terrain (Uhlemann et al., 2017a), de la stabilité des infrastructures (Chambers et al., 2014a) ou de l'agriculture par exemple (Michot et al., 2003) (**Question 1.5**). Les Figures 2.6 à 2.10 ainsi que les Tableaux 2.1 à 2.6 pourront être utiles à celles et ceux qui voudront identifier les paramètres physiques qui ont déjà été imagés et/ou surveillés dans le temps avec la méthode électrique, dans les recouvrements miniers et d'autres domaines (Chap. 2). Les bases de données sont également disponibles en accès libre sur un **site web interactif**.

Pour finir, une valeur limite cible de 85% de saturation est généralement considérée comme critère de performance pour que la couche de rétention joue son rôle de barrière à l'oxygène (Demers and Pabst, 2021b) et une précision de $\pm 5\%$ sur l'estimation du degré de saturation a été considérée comme suffisante dans un premier temps pour identifier une perte de performance anormale de la CEBC (**Questions 1.6 et 1.7**). Il est intéressant de noter qu'il existe des approches plus avancées pour effectuer des études de faisabilité numériques, comme l'approche proposée par Robinson et al. (2019) présentée sur la Figure 5.3. Des modélisations hydrogéologiques sont utilisées pour générer des données ERT synthétiques qui sont bruitées et inversées pour évaluer la capacité de l'ERT à imager les phénomènes modélisés.

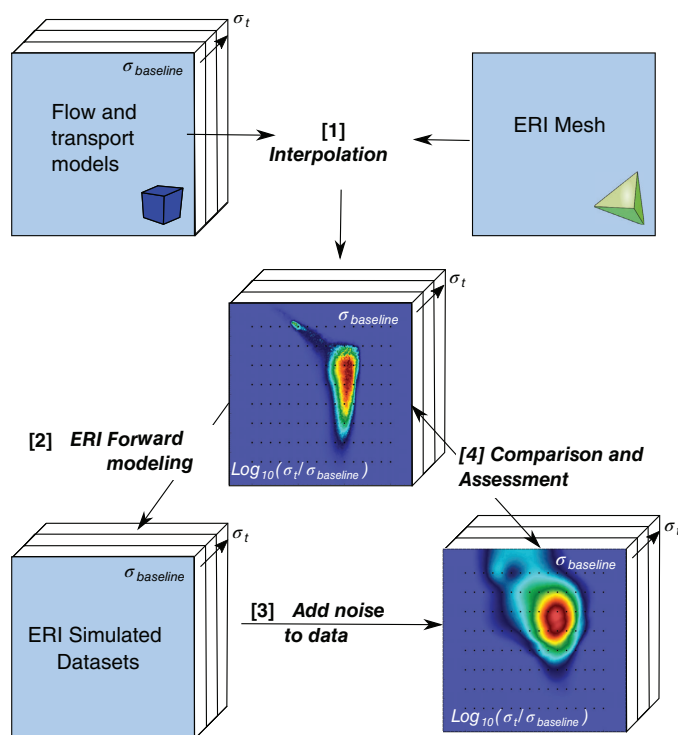


FIGURE 5.3 Méthodologie proposée par Robinson et al. (2019) pour effectuer une étude de faisabilité pour le suivi temporel par la méthode électrique à partir de modélisations.

5.1.2 Étape 2 : Planification de l'instrumentation

La deuxième étape proposée par le guide de conception (Fig. 5.1) consiste à planifier l'instrumentation de terrain, qui dépend directement de l'objectif du suivi identifié à l'étape 1 et dépend de chaque site minier. Cette étape permet de déterminer toutes les caractéristiques de l'instrumentation géophysique qui sera mise en place pour un système de recouvrement spécifique, notamment en répondant aux questions suivantes :

- **Question 2.1** : Quelles sont la ou les zones du parc/halde qui devraient être surveillées avec la méthode électrique ? Quelle devrait être l'étendue de la zone surveillée ?
- **Question 2.2** : Quelles sont les options envisageables pour la mise en place des électrodes ? (en surface, en forage, dans des tranchées ou pendant la construction ?)
- **Question 2.3** : Quelle est la profondeur d'investigation nécessaire pour le suivi électrique ? Quelles sont les couches d'intérêt jouant un rôle dans le recouvrement ?
- **Question 2.4** : Quelle serait la résolution spatio-temporelle idéale pour le suivi électrique ? Pendant combien de temps la surveillance devra-t-elle être effectuée ?
- **Question 2.5** : Les coûts d'instrumentation, d'installation et du résistivimètre sont-ils satisfaisants ? (connaissant le nombre d'électrodes et la longueur de câbles nécessaires)

Bien que les méthodes géophysiques puissent être employées pour investiguer des volumes considérablement plus grands que les mesures ponctuelles (e.g., profils d'électrodes de plusieurs centaines de mètres de longueur ; Auken et al. (2014); Binley et al. (2015b); Ulusoy et al. (2015)), ces approches n'en restent pas moins limitées en termes de surface d'investigation et seront généralement incapables de couvrir la totalité d'un parc à résidus mesurant plusieurs kilomètres carrés par exemple. Il est donc nécessaire de faire des choix concernant les zones du parc ou de la halde qui seront instrumentées et surveillées dans le temps.

De même que pour un programme de surveillance de performance utilisant des instruments de mesure conventionnels, un programme de suivi impliquant la méthode électrique devrait être focalisé sur les zones les plus à risques (MEND, 2004; Bussière et al., 2021). On peut penser par exemple (i) aux zones localisées en haut de pente où la performance d'un recouvrement de type CEBC peut être moins bonne (Bussière et al., 2003, 2006), (ii) dans les zones où la nappe sera la plus profonde pour une CEBC (Ethier, 2018; Demers and Pabst, 2021b), (iii) dans des zones où la végétation et/ou les intrusions animales seront les plus importantes (Proteau et al., 2020a; Bussière and Guittony, 2021b), (iv) dans une zone où la variabilité des

matériaux utilisés pour la construction ne permet pas de se fier uniquement à des instruments ponctuels (Fala et al., 2013; Lahmira et al., 2017) ou encore (v) dans une zone du parc où l'on s'attend à ce que la nappe soit particulièrement haute et doit être surveillée du point de vue géotechnique (Booterbaugh et al., 2015). C'est cette approche qui a été suivie pour identifier les zones à instrumenter sur les recouvrements construits à la mine Canadian Malartic pour cette thèse (voir Chap. 4) afin de comparer la performance des recouvrements dans la zone du plateau, en haut et en bas de pente, avec ou sans végétation (**Question 2.1**).

La Figure 5.4 illustre les choix et les solutions qui peuvent être prises pendant la planification de l'instrumentation électrique pour répondre aux **Questions 2.2** et **2.3** pour différentes fonctions de suivi. Dans l'**exemple A**, le suivi de la hauteur de la nappe peut être effectué dans la totalité du parc à résidus, et plus particulièrement près des digues. Pour cet exemple, la profondeur d'investigation devrait être assez grande, et des électrodes de surface pourraient être combinées avec des électrodes en forage et installées directement dans les résidus miniers (e.g. Clément et al. (2010); al Hagrey and Petersen (2011); Rucker (2014)).

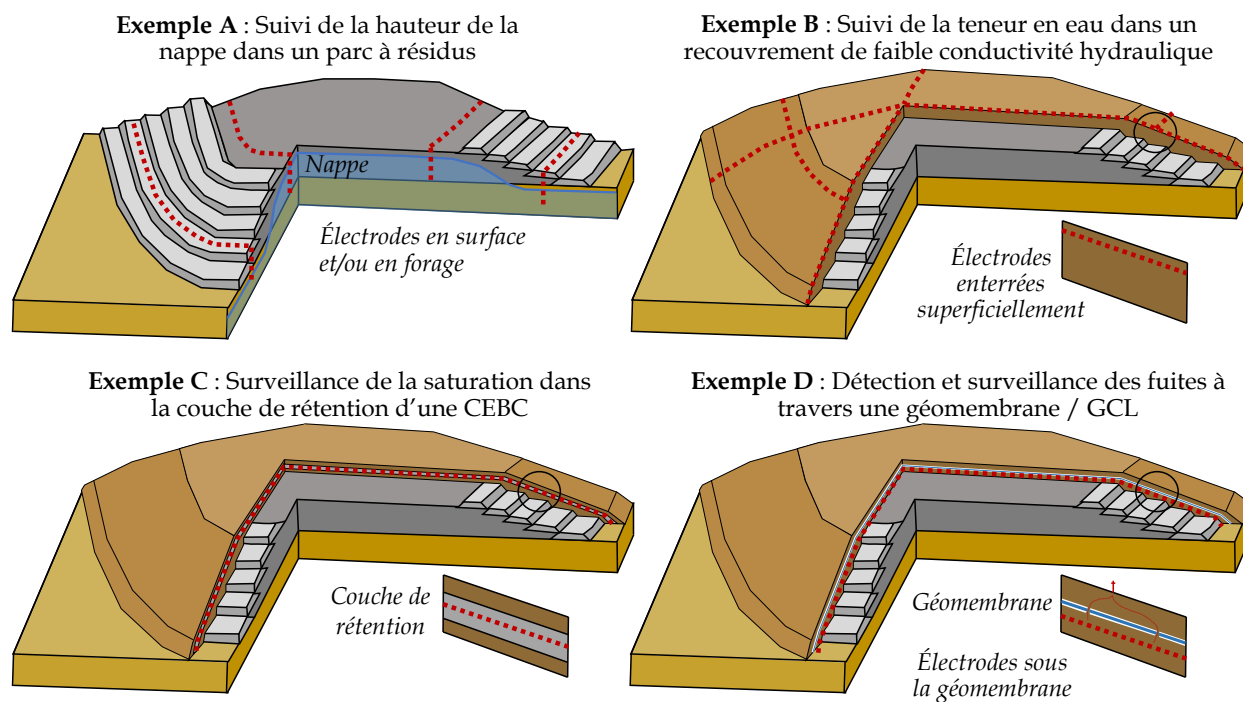


FIGURE 5.4 Exemples de quatre systèmes de suivi électrique à grande échelle ayant différentes fonctions, résolutions spatio-temporelle et profondeurs d'investigation, avec des électrodes installées en surface, en forage ou enterrées dans le recouvrement lors de sa construction.

Pour les **exemples B** et **C**, qui représentent les recouvrements expérimentaux instrumentés à la mine Canadian Malartic présentés dans le chapitre 4, la profondeur d'investigation n'est pas

un enjeu significatif puisque les mesures électriques ne sont importantes que dans les couches du recouvrement ayant un rôle, comme la couche de rétention d'eau d'une CEBC mesurant typiquement 1 m de haut par exemple (Demers and Pabst, 2021b). Pour ces scénarios, les électrodes pourraient être enterrées dans les couches d'intérêt lors de la construction des recouvrements (approche suivie dans le cadre des travaux de terrain de cette thèse), ou à partir de la surface dans des tranchées creusées pour enterrer superficiellement les électrodes si l'instrumentation géophysique est réalisée après la construction des recouvrements.

Enfin, l'**exemple D** illustre une application de la méthode électrique servant à détecter et cartographier d'éventuels défauts dans une géomembrane installée sur un parc à résidus pour empêcher l'eau et l'oxygène d'atteindre les résidus (Maqsood et al., 2021; Rarison et al., 2023). Dans ce cas, les électrodes pourraient être installées sous la membrane et quelques électrodes de surface pourraient être utilisées pour détecter des liens électriques à travers la membrane, qui permettraient de cartographier les défauts d'installation et les perforations éventuelles de la membrane. Cette dernière méthode a déjà été appliquée avec succès pour détecter des fuites de contaminants provenant de sites d'enfouissement (Ling et al., 2019; Mary et al., 2022) et de fuites dans des barrages (Zhao et al., 2021, 2023).

La résolution spatio-temporelle d'un suivi électrique est un élément crucial qui devrait être étudié et défini de façon appropriée (voir Figure 2.4, Rucker (2014)), et ce pour chaque dispositif de suivi électrique et pour chaque site minier et recouvrement particulier. Selon les définitions proposées dans le chapitre 2, la résolution spatiale correspond à la dimension de la plus petite anomalie qui peut être imagée par la méthode électrique (Friedel, 2003), et dépendra notamment de la position et de l'espacement des électrodes, de la distance entre l'anomalie à détecter et les électrodes, du protocole de mesure employé et de la nature du milieu. À titre d'exemple, il sera impossible de détecter une anomalie de faibles dimensions et présentant un faible contraste de conductivité électrique si l'espacement entre les électrodes est grand et/ou que les électrodes sont situées loin de cette anomalie (e.g., Friedel (2003)).

Cependant, il n'existe pas de règle précise et il est généralement recommandé de recourir à des études numériques de sensibilité pour caractériser la résolution spatiale d'un dispositif de mesures électriques spécifique, et pour une anomalie donnée (e.g., Wilkinson et al. (2012b); Uhlemann et al. (2018b)). C'est la démarche qui a été suivie au début de ce projet de doctorat pour identifier la disposition d'électrodes qui permettrait de maximiser la résolution dans la couche de résidus constituant la couche de rétention d'eau de la CEBC, et qui est présentée dans la Figure 5.5 (**Question 2.4**). Des modèles représentant la CEBC et les propriétés hydrogéologiques et électriques des matériaux ont été utilisés pour simuler des mesures électriques synthétiques en utilisant différentes configurations d'électrodes (e.g.,

plusieurs profils longitudinaux d'électrodes, différentes localisation des profils d'électrodes, différents espacements d'électrodes). Les données ERT synthétiques ont ensuite été perturbées puis inversées et converties en distributions de teneur en eau, qui ont été comparées aux distributions de teneur en eau initiales. Un espacement de 1 m entre chaque électrode a ainsi été choisi pour maximiser la résolution dans les sections expérimentales de recouvrements de 23 m de long (échelle pilote). Néanmoins, les résultats montrés dans le chapitre 4 suggèrent que cet espacement aurait pu être plus grand (jusqu'à 5 m) tout en conservant une résolution satisfaisante, ce qui serait une avenue intéressante pour augmenter l'étendue des mesures électriques dans les recouvrements. De même, il serait intéressant de comparer le scénario mis en place dans les CEBCs expérimentales et décrit au chapitre 4 (deux profils en haut et en bas de la couche de rétention) avec un scénario impliquant un unique profil d'électrodes au centre de la couche de rétention. En combinant ces deux modifications (séparation de 5 m et unique profil d'électrodes), la zone couverte par 48 électrodes passerait de 23 m à 235 m de long. Finalement, une résolution temporelle de quatre images par jour a été choisie dans le cadre du projet pilote de la thèse (c.f. Chap. 4) mais cette fréquence d'imagerie aurait pu être réduite à une image par jour ou moins (**Question 2.4**).

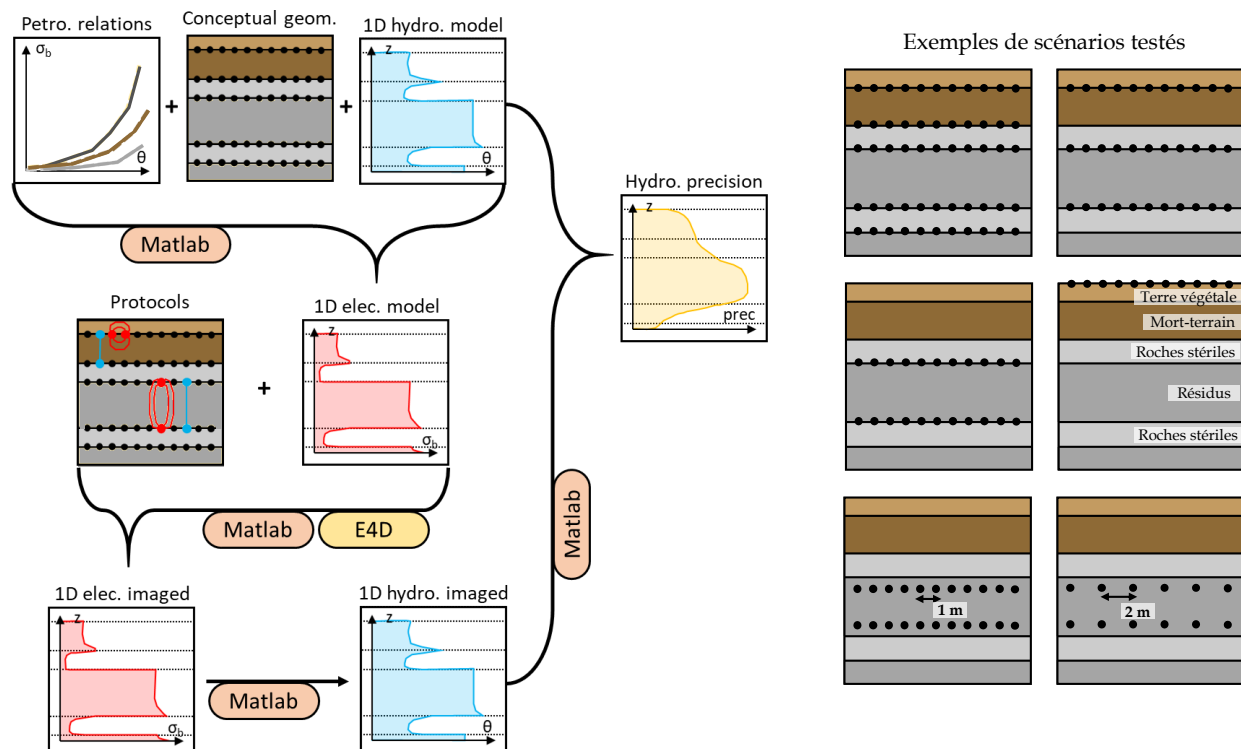


FIGURE 5.5 Approche méthodologique suivie au début de la thèse pour identifier la configuration d'électrodes maximisant la résolution spatiale de l'imagerie de teneur en eau dans la couche de rétention de la CEBC construite à la mine Canadian Malartic.

Wagner et al. (2015a), Uhlemann et al. (2018a) et Jiang et al. (2021a,b) ont proposé des approches prometteuses permettant de déterminer le nombre et la position optimales d'électrodes nécessaires pour maximiser la résolution de l'imagerie électrique dans une zone donnée. Cette approche, présentée par la Figure 5.6, est très intéressante dans le contexte de la surveillance électrique des recouvrements miniers à grande échelle puisqu'elle permettrait de réduire le nombre d'électrodes au minimum nécessaire, tout en assurant une bonne résolution spatiale, ce qui permettrait d'augmenter les surfaces couvertes par l'imagerie électrique pour le même nombre d'électrodes et/ou de réduire les coûts d'instrumentation électrique.

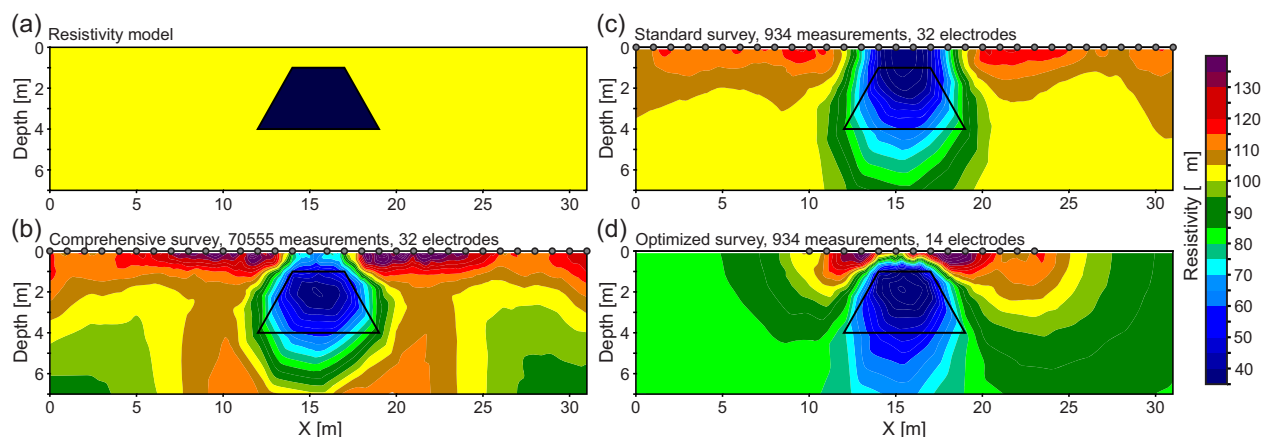


FIGURE 5.6 Optimisation simultanée de protocoles de mesures et de la localisation / du nombre d'électrodes tel que proposé par Uhlemann et al. (2018b).

Le coût d'un dispositif de suivi électrique est un paramètre à prendre en compte très tôt dans le processus de conception d'un programme de surveillance de stabilité et/ou de performance de restauration. À cette étape de conception, les questions précédentes devraient permettre d'avoir une idée du nombre d'électrodes nécessaires, de la distance entre les électrodes, des modes de mise en place des électrodes ainsi que de la distance entre les électrodes et le résistivimètre autonome. À titre d'exemple, le Tableau 5.1 résume les ordres de grandeur de coûts d'instrumentation pour les 256 électrodes installées dans les quatre cellules expérimentales tel que présenté dans le chapitre 4 (**Question 2.5**). Au total, l'instrumentation géophysique a coûté environ 10 000 \$ (en excluant l'appareil de mesures), dont la majorité a été utilisée pour connecter les électrodes de la LSHCC et de la CEBC au container instrumenté (extensions représentées sur la figure 5.7). Notons que le résistivimètre autonome (40 000 \$) représente les 4/5 du coût total, ce qui devrait être ramené à la durée totale d'utilisation pour un suivi sur le long terme. Même si ces coûts peuvent sembler importants, ils restent raisonnables sachant que les coûts de construction de recouvrements sont de l'ordre de 150 à 400 k\$ par hectare. Par ailleurs, ces coûts sont aussi considérablement plus faible que pour un

programme d'instrumentation à grande échelle en considérant que chaque sonde hydrogéologique (ponctuelle) coûte entre 250 \$ et > 1 000 \$ (sans compter les dispositifs d'acquisition pouvant être très dispendieux). Il est cependant important de mentionner que le dispositif d'instrumentation électrique a été conçu spécifiquement pour ce projet de recherche à partir de matériaux de base (câbles monobrins et rondelles d'acier inoxydable) et que la conception d'un nouveau dispositif ou l'achat d'un dispositif existant dans le commerce pourraient être plus dispendieux. Par ailleurs, des coûts supplémentaires pourraient être nécessaires pour l'installation des électrodes dans des tranchées ou des forages (non considérés ici). Par ailleurs, la récente démocratisation de la méthode électrique va probablement faire diminuer les coûts des résistivimètres autonomes qui vont probablement être capables d'utiliser de plus en plus d'électrodes (Binley and Slater, 2020; Clement et al., 2020; Slater and Binley, 2021). La revue des résistivimètres autonomes et de leurs récents développements, effectuée au chapitre 2, pourrait être utile pour quiconque serait intéressé.e à choisir un dispositif d'acquisition électrique. Les dispositifs instrumentaux (câbles et électrodes) sont relativement robustes puisqu'il existe dans la littérature des exemples de sites instrumentés et suivis par imagerie électrique depuis plus de vingt ans (e.g., Mollaret et al. (2019)).

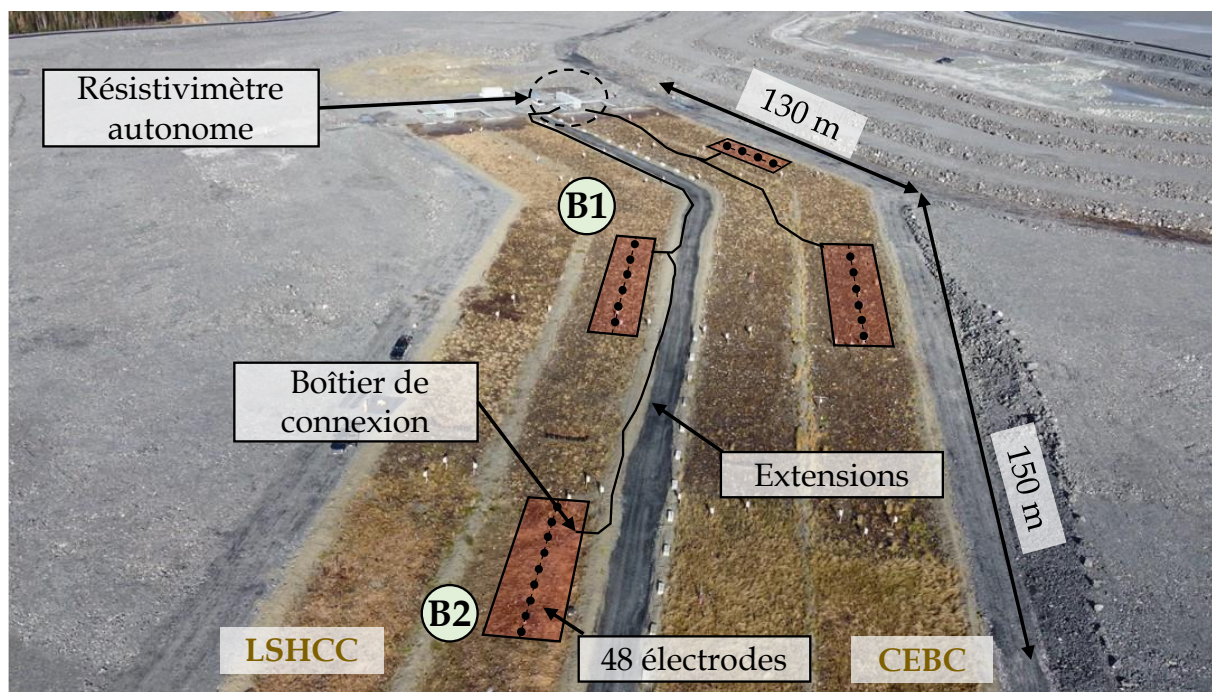


FIGURE 5.7 Vue par drone des recouvrements expérimentaux à grande échelle construits à la mine Canadian Malartic. Les principales composantes du dispositif de suivi électrique à l'échelle pilote dont les coûts sont résumés au Tableau 5.1 sont identifiées.

TABLEAU 5.1 Synthèse des coûts d'instrumentation électrique sur les recouvrements

Matériel	Coût unitaire	Quantité	Total
Électrode en acier inoxydable	$\simeq 3$ \$	300 unités	$\simeq 1\,000$ \$
Câble cuivre 18 AWG (solid)	$\simeq 0.2$ \$/m	$\simeq 5\,000$ m	$\simeq 1\,000$ \$
Boîtiers de connexion étanches	$\simeq 250$ \$	4 unités	$\simeq 1\,000$ \$
Extensions 22 AWG - 25 paires	$\simeq 10$ \$/m	$\simeq 700$ m	$\simeq 7\,000$ \$
Résistivimètre autonome Batteries, panneaux solaires	$\simeq 40\,000$ \$	1 unité	$\simeq 40\,000$ \$

5.1.3 Étape 3 : Instrumentation sur le terrain

La troisième étape, qui consiste à mettre en place l'instrumentation sur le terrain, peut commencer dès lors qu'une solution de dispositif de suivi électrique satisfaisante a été trouvée à la suite des étapes 1 et 2 (processus itératif pour trouver un compromis entre coût, étendue spatiale, nombre d'électrodes et résolution spatio-temporelle). Les aspects importants qui doivent être abordés à cette étape sont présentés sous la forme des questions suivantes :

- **Question 3.1** : Quelles seront les propriétés des matériaux dans lesquels les électrodes seront installées ? (granulométrie grossière ? roches anguleuses ? conditions acides ?)
- **Question 3.2** : Quelle est la meilleure méthodologie pour installer les électrodes, sans nuire à la construction des recouvrements ni à la gestion des parcs/haldes ?
- **Question 3.3** : Quels sont le ou les paramètres qui doivent être mesurés localement pour être pris en compte dans l'imagerie électrique ? (c.f., **Questions 1.3** et **1.4**)
- **Question 3.4** : Quels instruments devraient être installés pour mesurer ces paramètres et où les installer dans les recouvrements ? (c.f., **Questions 1.3** et **1.4**)
- **Question 3.5** : Quelle est la stratégie d'échantillonnage à mettre en place lors de l'instrumentation pour assurer un contrôle adéquat de la variabilité des matériaux ?
- **Question 3.6** : Quelle sont les mesures de contrôle *in situ* à effectuer lors de l'instrumentation ? (nucléodensimètre, porosité en place, arpentage, teneur en eau ?)

La première question à laquelle il faudrait répondre à l'étape d'instrumentation sur le terrain consiste à savoir si les électrodes, câbles, boîtiers de connexions et connexions électriques

seront adaptés aux conditions de terrain. En effet, la nature des matériaux dans lesquels vont être installées les électrodes peut grandement influencer la durabilité du système de suivi électrique. Il serait par exemple risqué d'installer des électrodes ou des câbles dans des matériaux coupants et/ou anguleux et/ou de grandes dimensions (e.g. blocs métriques dans les haldes à stériles (Bussi re, 2007; Aubertin et al., 2016)) et on pr f rera dans ces cas favoriser les couches de matériaux plus fins et plus humides permettant de minimiser la r sistance de contact entre les  lectrodes et le milieu (Peter-Borie et al., 2011; Gance et al., 2016; Watlet et al., 2018).   titre d'exemple, les profils d' lectrodes ont  t  install s   l'int rieur de couches de matériaux fins (r sids et mort-terrain) dans les recouvrements exp rimentaux de la mine Canadian Malartic, et un "coussin protecteur" de 15 cm d' paisseur de matériaux fins a m me  t  mis en place pour offrir une protection aux câbles et  lectrodes, qui auraient  t  en contact avec les roches st riles (voir Chap. 4) (**Question 3.1**).

Certains param tres de conception des  lectrodes peuvent am liorer la r sistance de contact avec le milieu pour des matériaux grossier, avec des teneurs en eau faibles ou susceptibles de geler. L' tude de Tomařkovi ov  et al. (2016) a par exemple permis de comparer les trois mod les d' lectrodes pr sent s dans la Figure 5.8 (en haut) dans un contexte arctique, soit une  lectrode standard (simple tige de m tal), une  lectrode plate (*plate electrode* en anglais) et une  lectrode en c tes de maille (*mesh electrode*). Comme attendu, cette derni re offrait la plus grande asp rit  et la plus grande surface de contact avec le milieu, ce qui avait pour cons quence de r duire la r sistance de contact, et donc d'am liorer le rapport signal sur bruit des mesures. Par ailleurs, plus la surface de contact des  lectrodes utilis es augmente, meilleur sera le contact avec le milieu comme illustr  par la figure 5.8 avec des  lectrodes plates mesurant 20 cm de c t  (Arosio et al., 2017) (en bas   gauche) et avec des  lectrodes install es le long d'un tube de forage (Ogilvy et al., 2009) (en bas   droite). Finalement, le fait d'enterrer les  lectrodes dans le milieu augmente encore davantage le contact  lectrique, tout en prot geant les  lectrodes et les câbles des animaux, en maintenant en place les  lectrodes en tout temps et en r duisant l'impact du gel en surface en hiver. C'est la strat gie d'installation qui a  t  favoris e pour ce projet pilote pour les raisons  voqu es (**Questions 3.2**).

Il est recommand  de mettre en place des instruments de mesures compl mentaires dans les recouvrements qui permettront de mesurer localement certains param tres comme la temp rature, la teneur en eau et la conductivit   lectrique de l'eau interstitielle, qui peuvent affecter simultan ment la conductivit   lectrique (Archie et al., 1942; Waxman and Smits, 1968). Une  tude de sensibilit  pr sent e dans le chapitre 3 a d montr  notamment que la pr cision de l'estimation de la teneur en eau volumique  tait diminu e d'un ordre de grandeur sur le terrain si la fluctuation temporelle de la temp rature et de la conductivit   lectrique du

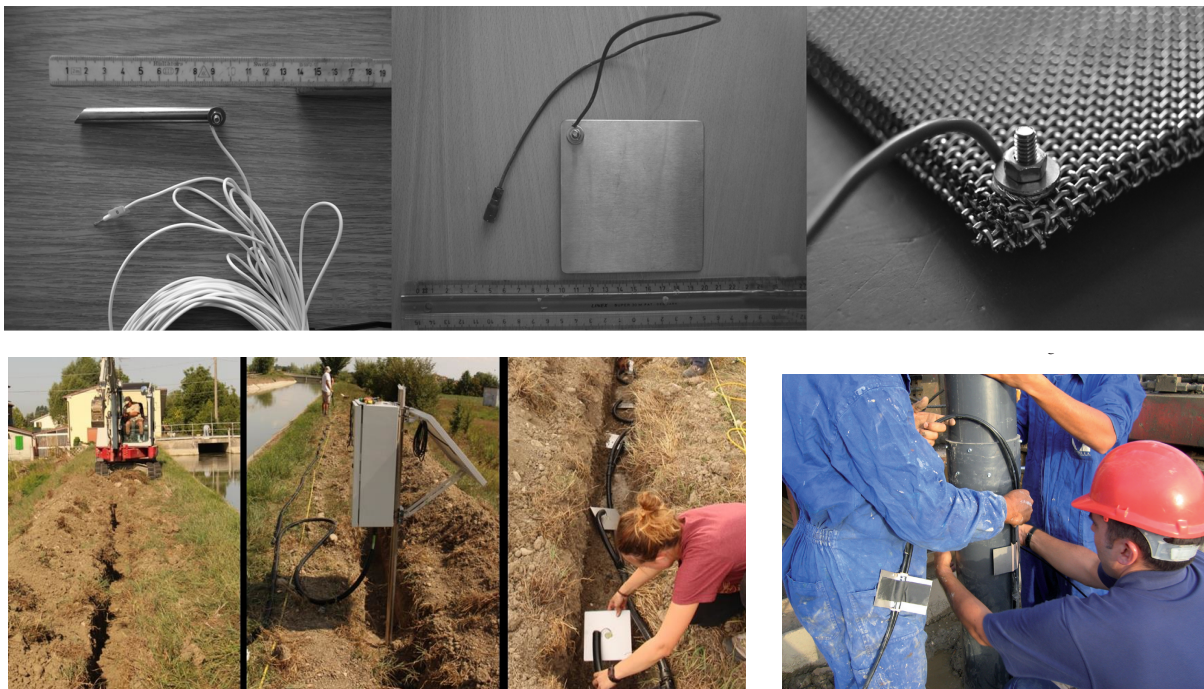


FIGURE 5.8 Influence de la forme, de la taille de l'électrode et de sa mise en place dans le milieu sur la résistance de contact. Photographies tirées de Tomaškovičová et al. (2016) (en haut), (Arosio et al., 2017) (en bas à gauche) et Ogilvy et al. (2009) (en bas à droite).

fluide n'étaient pas prise en compte. Ainsi, il est important de répondre aux **Questions 3.3** et **3.4** afin de caractériser les variations spatio-temporelles de ces paramètres pour pouvoir les prendre en compte et corriger leur effet sur l'imagerie électrique. À titre d'exemple, il a été décidé d'installer un profil vertical comportant 5 à 6 sondes Teros 12 pour chacune des quatre sections de recouvrement mesurant 23 m de long (voir chapitres 3 et 4).

Il est important de mentionner ici que cette approche présente une limitation importante dans la mesure où l'avantage de l'instrumentation électrique est de réduire le nombre de capteurs ponctuels nécessaires. Or, on pourrait imaginer un milieu dans lequel la conductivité électrique du fluide interstitiel est très variable dans l'espace, par exemple à cause de la minéralogie des rejets qui pourrait varier fortement d'un endroit à un autre de manière aléatoire (e.g., suivant la déposition aléatoire de matériel par les camions). Pour ce cas précis, il faudrait donc installer un grand nombre de sondes mesurant la conductivité électrique du fluide interstitiel localement si on voulait estimer la teneur en eau avec précision par la méthode électrique, ce qui ne serait pas réaliste. Dans un cas comme celui-ci, l'interprétation des mesures géophysiques ne pourrait pas être quantitative, et on devrait se limiter à une description qualitative des tendances générales de conductivité électrique du milieu. Par

conséquent, on est obligé de poser l'hypothèse que les mesures hydrogéologiques "de contrôle" réalisées au centre des sections des recouvrements par les sondes hydrogéologiques doivent être représentatives de l'ensemble de la section instrumentée, ce qui est plausible pour la température, mais moins certain pour la conductivité électrique du fluide interstitiel.

Finalement, il est crucial de réaliser un échantillonnage des matériaux adapté (**Question 3.5**) ainsi que d'effectuer des mesures de contrôle *in situ* (**Question 3.6**) pendant l'instrumentation géophysique des recouvrements (Bussière et al., 2021). D'une part, des campagnes d'échantillonnage et de mesures de contrôle systématiques permettront d'estimer les paramètres d'intérêt du milieu lors de l'installation (e.g., porosité, compaction, teneur en eau massique) et d'estimer la variabilité spatiale de ces propriétés. D'autre part, les échantillons de matériel pourront être utilisés pour calibrer les relations pétrophysiques reliant la conductivité électrique avec le paramètre d'intérêt à surveiller (voir Chap. 3). Ainsi, une campagne d'échantillonnage systématique a été mise en place pour chacune des quatre sections instrumentées : un échantillon était prélevé tous les 4 m le long du profil instrumenté à trois hauteurs différentes dans la couche de rétention d'eau de la CEBC et dans la couche de faible conductivité hydraulique de la LSHCC (7 échantillons par niveau, soit environ une centaine d'échantillons au total). De même, des mesures au nucléodensimètre ont été effectuées tous les 4 m et à trois niveaux différents dans chaque section. Ces mesures ont joué un rôle important pour la caractérisation du comportement hydrogéologique des recouvrements (i) puisqu'elles ont permis de démontrer qu'il n'existait aucune corrélation spatiale dans la variabilité des matériaux et (ii) puisque la porosité *in situ* a pu être prise en compte section par section pour calculer le degré de saturation à partir des données électriques.

5.1.4 Étape 4 : Collecte et traitement de données

La quatrième étape de mise en oeuvre d'instrumentation géophysique consiste à acquérir les données de laboratoire et de terrain permettant d'effectuer le suivi électrique des zones instrumentées. Les recherches bibliographiques ainsi que l'expérience acquise pendant la réalisation des essais de laboratoire et de terrain présentés dans cette thèse ont permis d'identifier les aspects les plus importants de cette phase cruciale d'un projet de suivi électrique, qui sont regroupés dans les questions suivantes :

- **Question 4.1** : Quel dispositif expérimental de laboratoire permettrait de relier le paramètre d'intérêt et la conductivité électrique ? (c.f., **Question 1.1**)
- **Question 4.2** : Existe-t-il dans la littérature un modèle semi-empirique reliant ce paramètre et la conductivité qui soit applicable aux matériaux ? (c.f., **Question 1.2**)

- **Question 4.3** : Est-il possible de vérifier que la relation calibrée à petite échelle demeure valide à l'échelle du terrain avec des mesures de contrôle *in situ* ?
- **Question 4.4** : Quelle est la meilleure approche d'acquisition, de transfert et de gestion des données électriques ? (protocole de mesure ? fréquence de mesure et de transfert ?)
- **Question 4.5** : Quelle est la stratégie de traitement de données qui minimise le temps de calcul tout en maximisant l'information obtenue à partir des données électriques ?

Il existe dans la littérature un grand nombre d'articles présentant différents dispositifs expérimentaux qui permettent notamment d'établir des relations entre conductivité électrique, teneur en eau, succion, conductivité du fluide interstitiel, température, indice des vides et autres paramètres physiques (e.g., Comina et al. (2008); Calamita et al. (2012); Kibria et al. (2018); Derfouf et al. (2019); Holmes et al. (2022b)). Le dispositif de laboratoire inspiré par les cellules Tempe qui a été proposé au chapitre 3 pourrait être appliqué de manière standardisée dans les matériaux des recouvrements pour calibrer la relation entre conductivité électrique, teneur en eau et succion (ainsi que la température si on le place dans une chambre à température contrôlée) (**Question 4.1**). Il existe par ailleurs d'autres dispositifs du même genre, dont deux exemplaires sont présentés par la Figure 5.9, servant à calibrer la relation entre l'indice des vides, la pression et la conductivité électrique (appelés "oedomètres électriques"). Les données expérimentales peuvent ainsi être utilisées pour calibrer les paramètres d'un modèle semi-empirique identifié dans la littérature, en suivant la méthodologie présentée dans le chapitre 3 avec le modèle d'Archie, ou utilisées pour identifier une relation purement empirique (e.g., Bryson (2005); Crawford and Bryson (2018)) (**Question 4.2**).

Il existe plusieurs approches possibles pour valider que les relations déterminées à l'échelle du laboratoire demeurent applicables sur le terrain afin de répondre à la **Question 4.3**. L'approche décrite dans le chapitre 3 est basée sur la comparaison entre la conductivité électrique inversée et la teneur en eau volumique mesurée au même endroit et au même instant par une sonde hydrogéologique. Cette approche a été également appliquée par plusieurs auteurs (e.g., Garré et al. (2012); Fan et al. (2015); Wicki and Hauck (2022)) et a notamment comme avantage de reposer sur une estimation précise de la teneur en eau volumique et sur une estimation volumique de la conductivité électrique représentative des mesures à grande échelle, par opposition à la mesure de la conductivité électrique qui pourrait être obtenue à partir de sondes hydrogéologiques (Hen-Jones et al., 2017b). L'utilisation de pénétromètres coniques (CPT pour *cone penetration testing*) équipés d'électrodes en acier inoxydable, tels que présenté sur la Figure 5.10, pourrait être une approche très intéressante pour mesurer simultanément la conductivité électrique *in situ* et plusieurs autres paramètres d'intérêt géo-

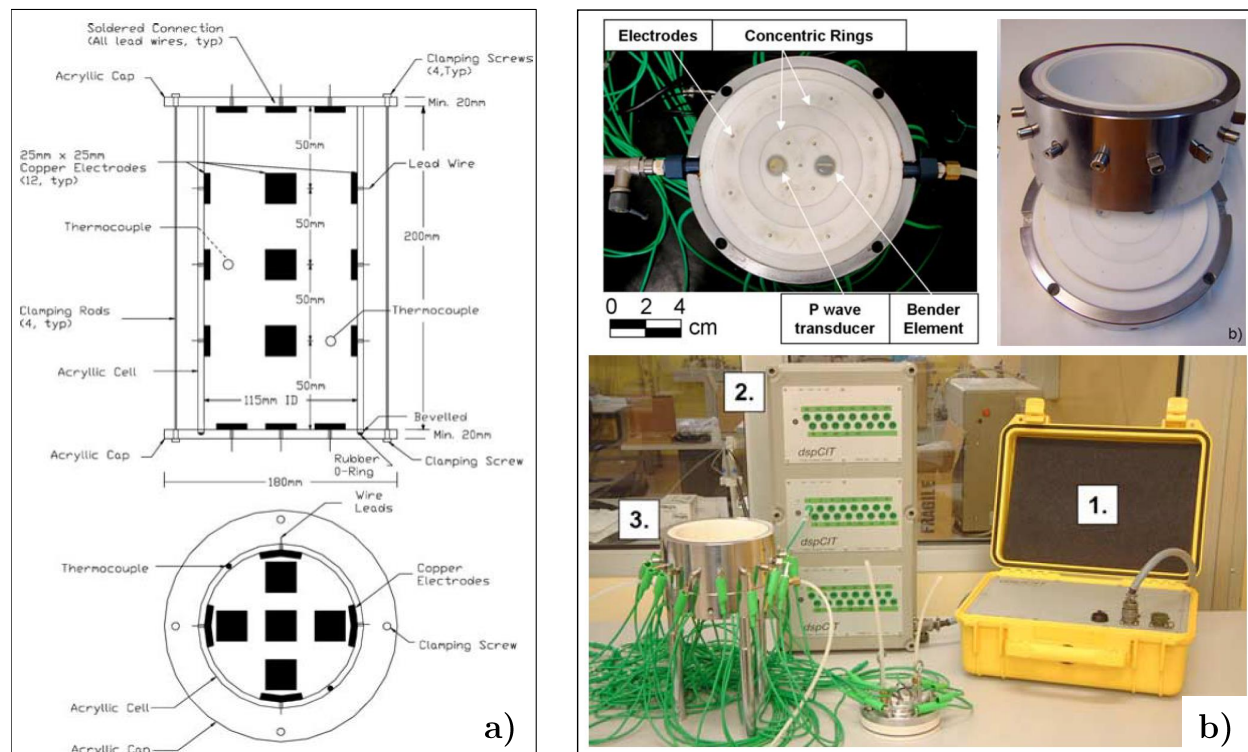


FIGURE 5.9 Dispositifs de laboratoire normés pour caractériser la relation entre l'indice des vides et la conductivité électrique (tiré de Bryson and Bathe (2009) et Comina et al. (2008)).

techniques dans les matériaux des recouvrements, et ainsi établir des relations empiriques *in situ* entre les différents paramètres (e.g., Morey et al. (1999); Friedel et al. (2006); Robertson and Cabal (2008); Booterbaugh et al. (2015)).

La revue de littérature proposée au chapitre 2 a permis d'identifier les paramètres d'acquisition et du traitement de données qui ont le plus d'impact sur la qualité des résultats obtenus par un suivi temporel électrique. La revue a également permis d'identifier les meilleures pratiques disponibles dans la littérature. Cette méthodologie a été appliquée pour l'acquisition et le traitement des données de laboratoire et de terrain tel que présenté dans les chapitres 3 et 4 et devrait être reproduite pour appliquer cette méthode à un cas d'application réel à grande échelle. Il convient par exemple d'identifier un protocole de mesure adapté au site, à la disposition d'électrodes et aux objectifs du suivi électrique en termes de résolution spatio-temporelle (**Question 4.4**). Comme décrit à la section 2.3.2, le protocole de mesure devrait permettre un bon compromis entre résolution spatiale et durée d'acquisition dans un contexte de suivi temporel. Comme illustré à la Figure 5.11, le choix du protocole de type Wenner a été effectué pour le suivi des recouvrements expérimentaux à la mine Canadian Malartic pour maximiser la sensibilité dans la couche de résidus (couche d'intérêt de la CEBC) et assurer le

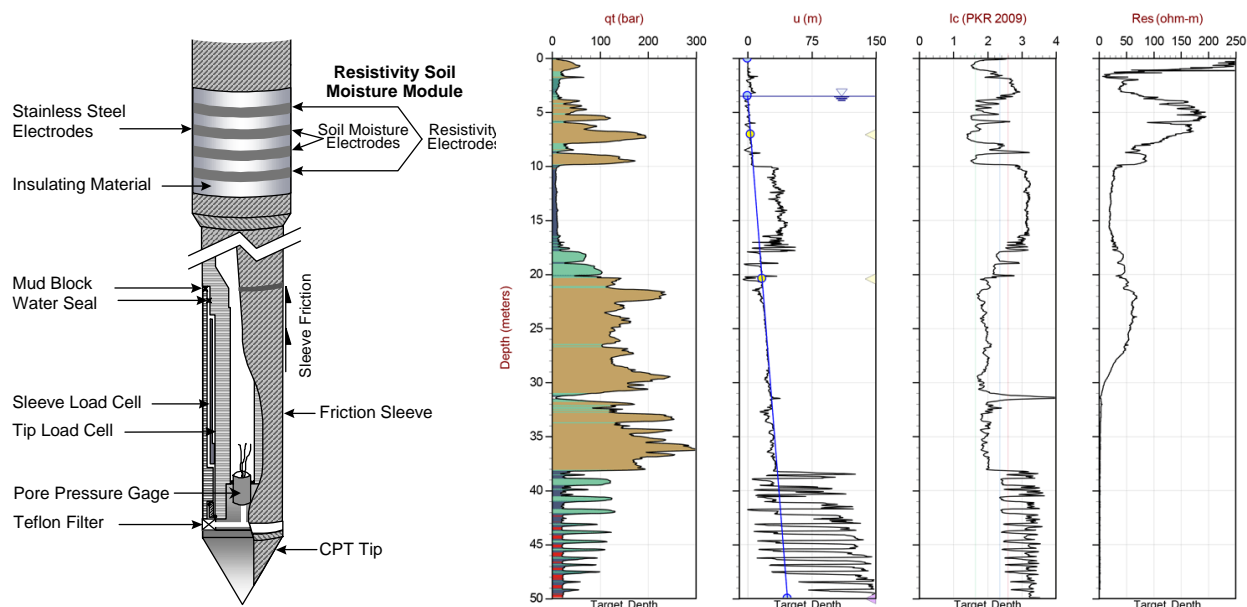


FIGURE 5.10 Schéma simplifié d'un pénétromètre conique (CPT) équipé d'électrodes, tiré de Morey et al. (1999). Résultats typiques d'une investigation à 50 m de profondeur avec un CPT équipé d'électrodes, soit la résistance à la pénétration, la pression interstitielle, l'indice de la qualité des sols I_c et la résistivité électrique, tiré du site web de ConeTec, accès le 26/02/2023.

meilleur rapport signal sur bruit. Cette démarche a permis d'assurer une bonne qualité des données, avec 90 % des données dont la différence entre mesures directes et réciproques était plus faible que 1 % (e.g., Tso et al. (2017); Uhlemann et al. (2016a, 2017b)).

La durée d'acquisition n'était pas un enjeu majeur dans le cas du suivi des recouvrements expérimentaux à l'échelle pilote. Par conséquent, quatre mesures directes étaient effectuées par jour pour chacune des quatre sections, et un jeu de données réciproque était enregistré par jour. Les données étaient par ailleurs transférées par courrier électronique trois fois par jour par le PRIME (Chambers et al., 2022), tel que décrit dans le chapitre 4. Il existe néanmoins plusieurs approches pour réduire la durée des protocoles de mesure si la durée d'acquisition est un enjeu. On peut par exemple favoriser les protocoles qui utilisent la capacité multi-canaux de la plupart des résistivimètres (comme le protocole dipôle-dipôle). Il est également possible d'utiliser des protocoles optimisés qui maximisent la résolution tout en minimisant le nombre de configurations nécessaires, ce qui pourrait par exemple être attrayant pour des dispositifs utilisant un grand nombre d'électrodes (Loke et al., 2014b).

En revanche, la durée nécessaire pour effectuer le traitement des données électriques peut devenir un enjeu dans le cadre d'un suivi temporel autonome avec une haute résolution

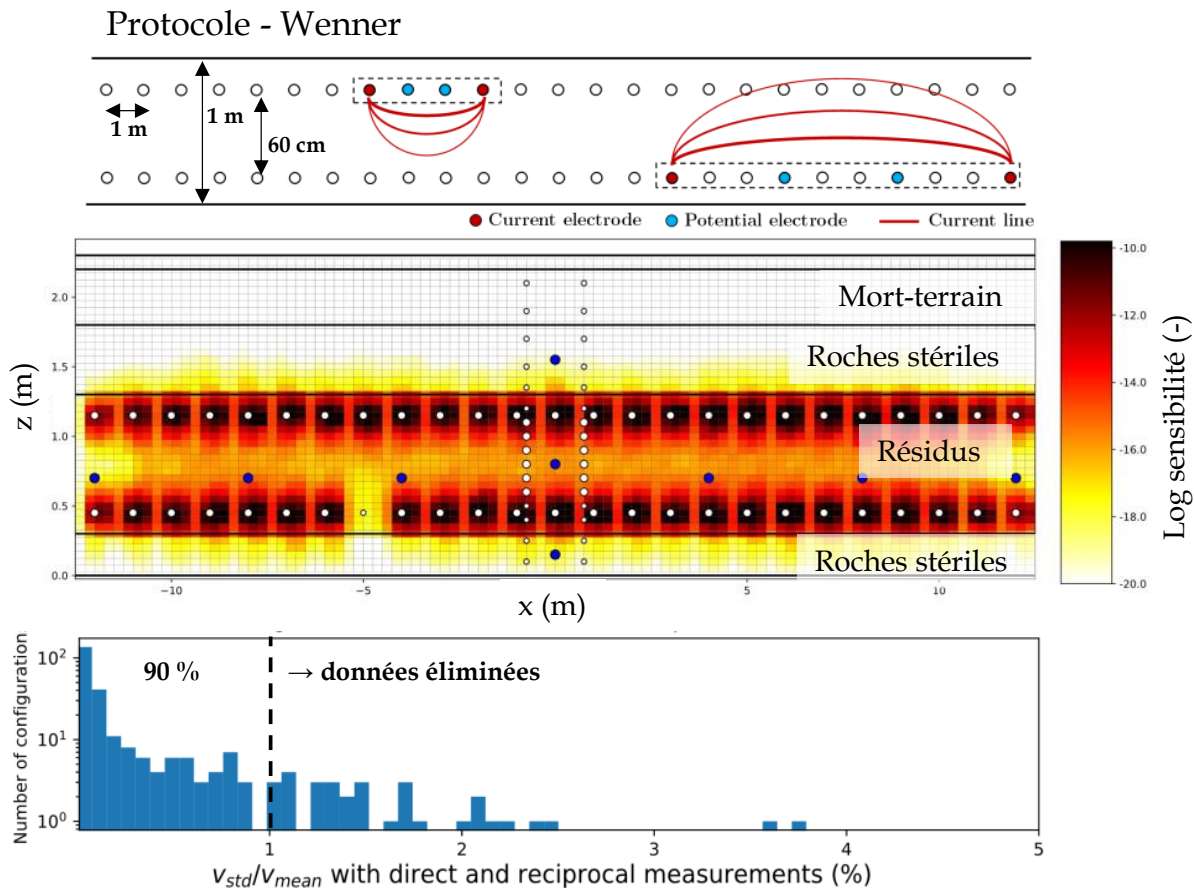


FIGURE 5.11 Choix du protocole de type Wenner dans les recouvrements expérimentaux de la mine Canadian Malartic pour maximiser la sensibilité et le rapport signal sur bruit.

spatio-temporelle. À titre d'exemple, différents scénarios ont été testés dans le cadre de l'inversion des données de terrain obtenues à la mine Canadian Malartic pour identifier le meilleur compromis entre complexité du modèle utilisé pour l'inversion, et le temps nécessaire pour effectuer chaque inversion (**Question 4.5**). La Figure 5.12 présente trois modèles de complexité croissante utilisés avec le logiciel E4D comme modèle pour l'inversion de la première campagne de données non automatisées en juillet 2020 (Johnson et al., 2017). On remarque que la précision de la teneur en eau volumique prédite par la méthode électrique est meilleure quand l'inversion est régularisée, c'est à dire quand on permet au modèle inversé des contrastes forts de conductivité électrique entre les couches qui composent la CEBC. L'utilisation de modèles plus précis représente cependant un coût en terme de nombre d'éléments, ce qui correspond à des durées de temps de calcul pour l'inversion plus importantes.

C'est dans cette optique que le choix du logiciel d'inversion a été orienté vers pygimli en 2D (Rücker et al., 2017) plutôt que l'approche initiale utilisant E4D en 3D (Johnson et al., 2017).

Comme le montre la Figure 5.13, le modèle 2D utilisé pour inverser les données électriques dans la CEBC présente à la fois une bonne résolution spatiale (cellules triangulaires de petites tailles aux interfaces entre les couches et proche des électrodes), et un faible nombre de cellules (augmentation de la taille des cellules loin des électrodes). Comme rapporté dans le chapitre 4, le maillage 2D de la CEBC comprend environ 10 000 cellules triangulaires et chaque inversion dure moins de 20 secondes, ce qui marque une amélioration considérable par rapport au modèle de 500 000 éléments tétraédriques de E4D présenté à la figure 5.12.

Pour finir, le chapitre 4 présente la démarche qui a été développée pour estimer la distribution spatio-temporelle de la température et de la conductivité du fluide interstitiel dans les recouvrements expérimentaux à l'aide des profils verticaux de sondes de teneur en eau volumique. Les relations semi-empiriques de Hayley et al. (2007, 2010) et Archie et al. (1942) ont ensuite été utilisées pour corriger leur effet sur la conductivité électrique du milieu. Cette démarche devrait être reproduite pour n'importe quelle application de la méthode électrique sur le long terme quand le milieu investigué est affecté par les précipitations et par les variations annuelles de température (Uhlemann et al., 2016a). À titre d'exemple, une augmentation de 10 °C dans le milieu (courant dans les recouvrements au Québec) correspondrait à une augmentation de 20 % de la conductivité électrique (Ma et al., 2011).

5.1.5 Étape 5 : Surveillance de performance autonome

La dernière étape de traitement de données consiste à convertir les résultats du suivi électrique obtenus à l'issue de l'étape 4 en paramètres d'intérêt pour effectuer une surveillance de performance. Les questions qui devraient être abordées à cette étape sont les suivantes ;

- **Question 5.1** : Quelle est la précision réelle du ou des paramètres d'intérêt prédits à l'aide de la méthode électrique et des modèles pétrophysiques calibrés précédemment ?
- **Question 5.2** : Est-il pertinent de définir des valeurs seuils définissant des niveaux d'alerte ? Si oui, comment les définir ? Est-il souhaitable d'intégrer la notion de durée ?
- **Question 5.3** : À quelle fréquence est-il souhaitable d'effectuer un suivi et pour quelle durée ? Sous quelle forme et à qui devraient être présentés les résultats ?
- **Question 5.4** : Pour un suivi en temps réel, que faire en cas de dépassement de seuil critique ? Qui prévenir et comment ? Quelles actions devraient être prises et par qui ?

Dans un premier temps, les données électriques temporelles peuvent être converties en utilisant les relations pétrophysiques calibrées en laboratoire et validées à l'échelle de terrain

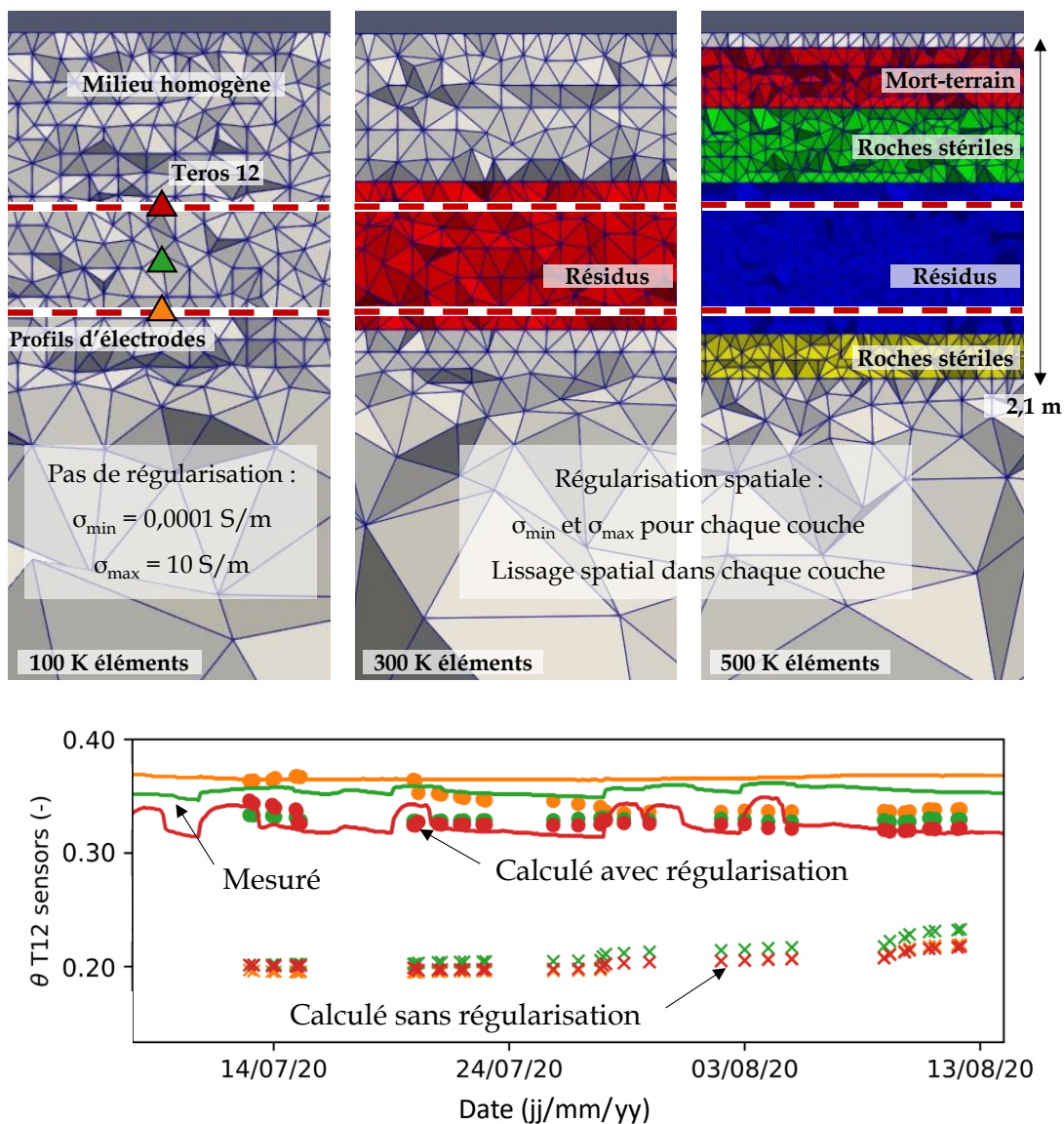


FIGURE 5.12 Effet de la régularisation sur la précision des résultats d'inversion (CEBC).

pour estimer la distribution spatio-temporelle du paramètre d'intérêt. Il est alors possible de comparer les valeurs prédites par la méthode électrique avec les valeurs mesurées par les instruments de mesures conventionnels s'ils ont été installés dans le milieu. C'est la démarche qui a été suivie dans les recouvrements expérimentaux de la mine Canadian Malartic puisque les mesures de teneur en eau volumique effectuées par les sondes hydrogéologiques installées au centre des cellules ont été comparées à la teneur en eau volumique estimée par la méthode électrique. Cette approche a permis de quantifier l'écart-type entre les deux jeux de données qui était proche de $0.02 \text{ m}^3/\text{m}^3$, ce qui correspondait à une précision de $\pm 5 \%$ en termes de degré de saturation, en considérant une porosité de 0.40 (voir chapitre 4) (réponse à la

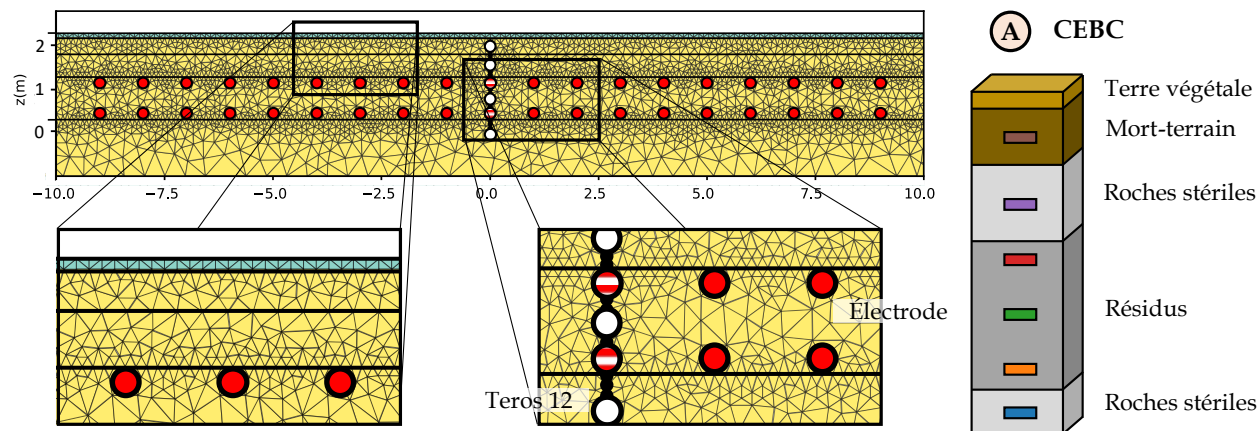


FIGURE 5.13 Maillage 2D utilisé pour effectuer les inversions avec pygimli dans la CEBC.

Question 5.1).

Dans les cas de figure pour lesquels le paramètre d'intérêt estimé par la méthode électrique peut directement être utilisé pour quantifier la performance d'un recouvrement, il est alors possible de suivre l'évolution spatio-temporelle de la performance de la section du recouvrement instrumentée. À titre d'exemple, la valeur de 85 % de saturation a été utilisée comme valeur cible pour la performance de la CEBC expérimentale (Chap. 4). Les zones de la couche de rétention dont le degré de saturation était supérieur à 90 % ont été identifiées comme performantes, et celles dont le degré de saturation était inférieur à 80 % ont été identifiées comme moins performantes afin de prendre en compte l'incertitude de ± 5 %. Aucun seuil critique n'a été défini pour le cas d'application à l'échelle pilote, mais une valeur de 80 % de saturation dans la couche de rétention d'une CEBC pourrait par exemple être utilisée pour identifier une baisse de performance, et une valeur de 70 % de saturation, maintenue pendant une certaine période de temps, pourrait être considérée comme seuil d'alerte pour avertir les utilisateurs d'une baisse critique de la performance de la CEBC (**Question 5.2**).

La Figure 5.14 résume les résultats du suivi de performance de la CEBC instrumentée à la mine Canadian Malartic pendant une période d'un an. Ce type de résultats pourraient être intégrés à des rapports périodiques rendant compte des différentes données mesurées dans le cadre d'un programme de suivi de la performance des recouvrements. On pourrait par exemple envisager que la distribution de degré de saturation puisse être calculée chaque semaine et un rapport hebdomadaire pourrait ainsi être envoyé aux personnes responsables du suivi. Des rapports plus complets pourraient aussi être préparés tous les quatre mois. Finalement, un rapport annuel synthétisant l'ensemble des données de suivi pourrait être généré et utilisé pour quantifier la performance globale de la CEBC. De tels rapports quantifiant

la performance de recouvrements seraient notamment utiles pour comparer la performance d'une année sur l'autre, pour plusieurs scénarios de restauration et plusieurs sites. Une telle approche s'intégrerait bien aux recommandations en termes de rapports de suivi de performance proposées par Bussière et al. (2021) et par le rapport du MEND *Field performance monitoring and sustainable performance of cover systems* (MEND, 2004) (**Question 5.3**).

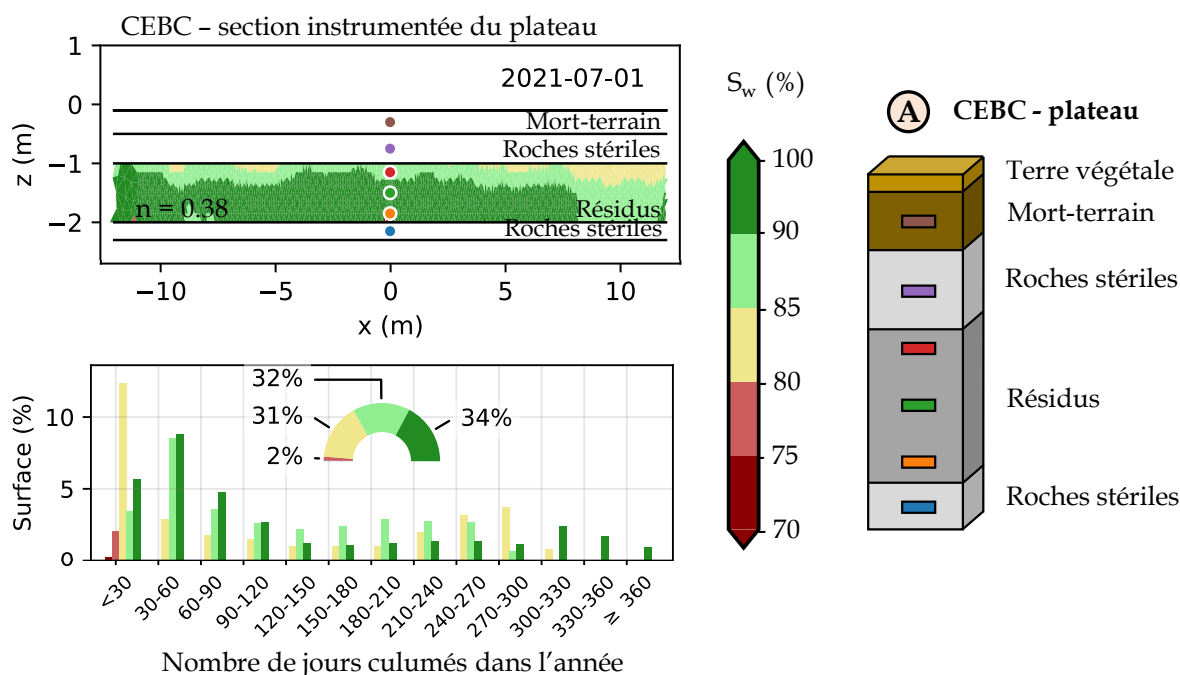


FIGURE 5.14 Évaluation de la performance de la CEBC à l'échelle pilote dans la section dite "plateau" à partir des mesures électriques (adapté de Dimech et al. (2023a), chapitre 4).

La revue de littérature présentée dans le chapitre 2 a mis en évidence l'utilisation de plus en plus fréquente des mesures électriques continues dans le cadre de systèmes d'alerte précoce (EWS pour *early warning system*), notamment pour les glissements de terrain (Budler; Whiteley et al., 2019) les infrastructures routières et ferroviaires (Chambers et al., 2014a; Gunn et al., 2015) ou la migration de contaminants ou d'eau salée dans les aquifères (Chen et al., 2018a; Puttiwongrak et al., 2019; Denham et al., 2020). Il est intéressant de noter que plusieurs des principales composantes d'un EWS décrites dans la Figure 5.15 sont cohérentes avec ce guide, et cette approche pourrait être appliquée pour la surveillance en temps réel de la performance des recouvrements en restauration minière (e.g., Tresoldi et al. (2020b, 2021)) (**Question 5.4**).

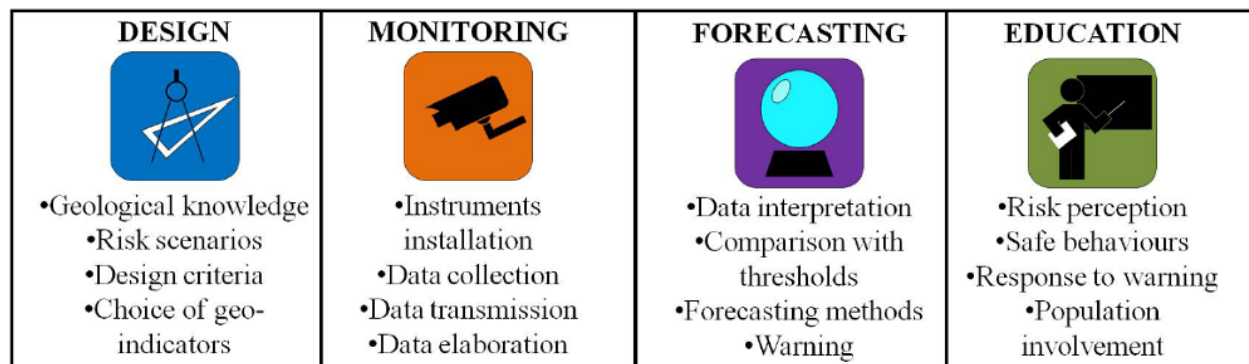
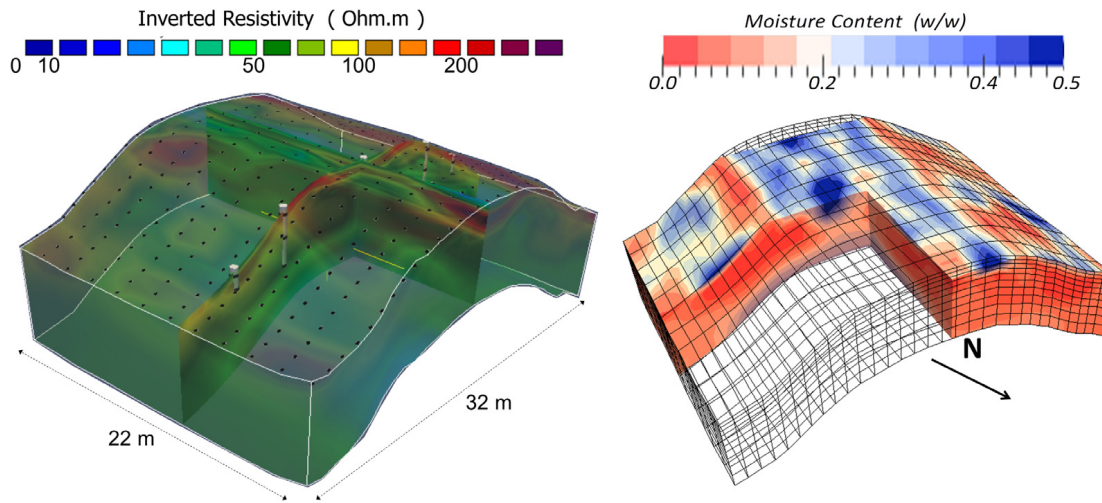


FIGURE 5.15 Principales composantes d'un système d'alerte précoce (EWS pour *Early Warning System* en anglais) tiré de Budler (2017), adapté de Intrieri et al. (2013).

À titre d'exemple, il serait possible de traiter quotidiennement les nouvelles données électrique effectuées et transférées de façon autonome par le résistivimètre PRIME installé sur le parc à résidus de la mine Canadian Malartic. Ces données pourraient être utilisées pour estimer en temps réel le niveau de performance des sections instrumentées de la CEBC et envoyer un message d'alerte par courrier électronique aux opérateur.rice.s concerné.e.s si les seuils critiques précédemment définis sont dépassés (e.g., Versteeg and Johnson (2013); Slater and Binley (2021); Chambers (2021); Chambers et al. (2022)). Ce type d'approche, déjà envisagés dans plusieurs domaines liés aux infrastructures permettrait notamment de détecter en amont des enjeux de perte de performance de recouvrements, et pourraient être utilisés pour guider des campagnes de caractérisation ou de contrôle plus précises sur le terrain à l'emplacement des anomalies détectées. La Figure 5.16 présente un exemple de ce type d'approche innovante basée sur l'imagerie de la teneur en eau dans un talus de voie ferrée à partir de la méthode électrique pour identifier les zones à risques d'instabilités physiques et alerter les opérateur.rice.s compétent.e.s (Chambers et al., 2014a; Gunn et al., 2015, 2018).

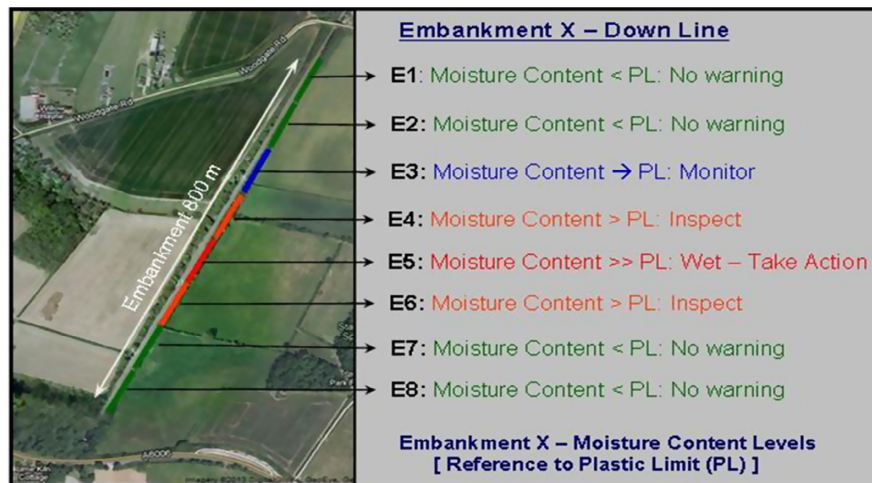
5.1.6 Étape 6 : Retour d'expérience

Pour finir, il serait pertinent d'effectuer un retour d'expérience sur l'utilisation de la méthode électrique pour effectuer le suivi d'un recouvrement installé sur un parc à résidus ou d'une halde à stériles actifs, abandonnés ou restaurés. En effet, il n'existe, à la connaissance de l'auteur et lors de l'écriture de ces lignes, aucun document dans la littérature scientifique ou technique permettant d'établir la pertinence et la faisabilité de l'application de la méthode électrique sur un site à pleine échelle comme méthode de suivi sur le long terme dans le contexte des rejets miniers. Dans ce sens, les futures applications réelles sur des sites miniers apporteront de nombreuses informations qui permettront d'identifier les enjeux et les

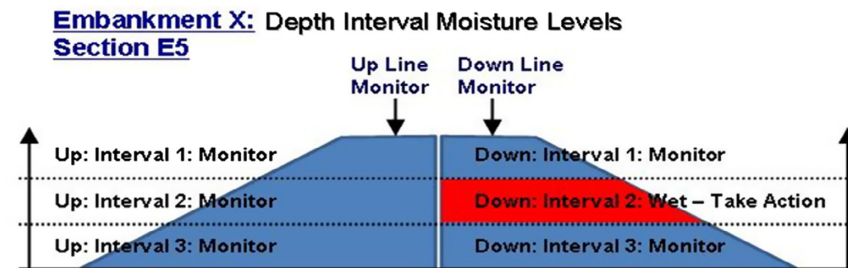


(a) Lensoidal distribution of the high resistivity materials under the crest and across the flanks of the embankment.

(b) Moisture content distribution after rainfall event in February 2011 showing infiltration into crest.



(a) Linear route monitoring system showing Down Line moisture levels and warnings.



(b) Moisture level section monitor indicating Action State on Down Line – Mid-Interval.

FIGURE 5.16 Exemple de surveillance automatisée d’un talus de voie ferrée à l’aide de la méthode électrique autonome (tiré de Chambers et al. (2014a) et Gunn et al. (2015)). Les imageries de teneur en eau réalisées à l’aide de la méthode électrique sont comparées à des valeurs seuils pour alerter les opérateurs en cas de dépassement et localiser les anomalies.

avantages de la méthode et pour améliorer les pratiques. Cette étape pourrait permettre de répondre aux questions suivantes ;

- **Question 6.1** : La mise en application de la méthode électrique a-t-elle permis d'estimer les paramètres d'intérêt ciblés au début du projet ? Si oui, avec quelle précision ?
- **Question 6.2** : A-t-il été possible de relier ces paramètres à la performance des recouvrements en restauration minière ?
- **Question 6.3** : Les choix d'instrumentation pris à l'étape 2 ont-ils été justifiés ? (robustesse des équipements, profondeur d'investigation, résolution spatio-temporelle ?)
- **Question 6.4** : Les coûts d'instrumentation et d'opération ont-ils été correctement estimés à l'étape de planification du projet ? Si non, pour quelle(s) raison(s) ?
- **Question 6.5** : La méthodologie de surveillance intégrant l'approche électrique a-t-elle permis d'identifier des problèmes de perte de performance dans les ouvrages ?
- **Question 6.6** : Si oui, est-ce que l'instrumentation conventionnelle aurait pu permettre de détecter ces problématiques ? Quelles ont été les actions prises ? Par qui ?
- **Question 6.7** : Quels ont été les avantages / limitations de l'approche électrique pour le suivi ? Quel aspect devrait être amélioré pour de futures applications ?

Il n'existe que peu d'applications de la méthode de suivi électrique proposée au contexte des rejets miniers comme discuté dans le chapitre 2. La mise en application de cette dernière étape permettra donc d'apporter de nouveaux éléments qui seront pertinents pour améliorer les pratiques, notamment pour répondre aux défis spécifiques posés par le contexte minier, qui ont été synthétisés à la section 2.5.2. À titre d'exemple, il n'existe que peu d'informations dans la littérature concernant la durabilité des électrodes et câbles utilisés en géophysique dans des résidus miniers et des conditions potentiellement acides.

CHAPITRE 6 CONCLUSION ET RECOMMANDATIONS

La surface considérable occupée par les aires de stockage de rejets miniers qui doivent être restaurées pour contrôler les risques de génération de contaminants rend nécessaire le développement de techniques de suivi applicables à grande échelle, et qui pourront être combinées aux outils de mesure conventionnels ponctuels. Cette thèse a permis de développer et tester à l'échelle de terrain une approche géophysique innovante de suivi de la teneur en eau volumique dans les systèmes de recouvrements en restauration minière.

Dans un premier temps, une revue de littérature exhaustive a permis de poser les bases théoriques de la méthode électrique appliquée pour le suivi temporel et d'identifier les meilleures pratiques concernant la planification, l'instrumentation ainsi que l'acquisition, le traitement et l'interprétation des données électriques. La base de données comprenant près de 650 articles présentant des applications de la méthode électrique en suivi temporel a mis en évidence la récente popularisation de cette technique depuis 2010, et en particulier la diversification des champs d'application (e.g., suivi du pergélisol, des glissements de terrain, de la végétation ou des gaz). Néanmoins, il a été surprenant de constater le faible nombre d'études utilisant cette technique de suivi dans le contexte des rejets miniers (moins de 3% des études de la base de données). Ce constat est d'autant plus frappant que de nombreuses études ont appliqué avec succès la tomographie de résistivité électrique comme technique d'imagerie pour la caractérisation des rejets miniers et la détection de contaminants. Par conséquent, la revue de littérature a montré que la méthode électrique est prometteuse en tant que méthode de suivi temporel des rejets miniers de manière non-invasive et applicable à grande échelle.

Par ailleurs, la revue de littérature a également permis d'identifier les principaux développements de la méthode électrique au cours des dernières années, notamment en ce qui concerne le perfectionnement des résistivimètres autonomes capables d'effectuer des mesures électrique quotidiennement en utilisant plusieurs centaines d'électrodes et de transférer les données à distance de manière autonome. Ces récents progrès techniques, mais aussi numériques et logiciels, sont très utiles pour l'application de la méthode au contexte des rejets miniers et pour répondre à plusieurs défis potentiels, soit (i) la complexité que représente son application sur des sites miniers, souvent en conditions éloignées, (ii) la nécessité d'effectuer un suivi de haute résolution spatio-temporelle, couvrant de grandes étendues et pendant de longues périodes et (iii) l'importance de quantifier les paramètres physiques suivis avec précision dans des milieux où d'autres paramètres influençant la conductivité électrique sont également susceptibles de varier. Par conséquent, les travaux de doctorat présentés dans cette thèse se sont concentrés

sur la mise en place d'une méthodologie permettant d'évaluer et de maximiser la précision de la teneur en eau volumique estimée à partir de la méthode électrique au laboratoire et sur le terrain ainsi que sur la mise en place d'une "preuve de concept" à l'échelle pilote dans des systèmes de recouvrement expérimentaux en conditions réelles à la Mine Canadian Malartic.

Dans un deuxième temps, un dispositif de laboratoire adapté à partir de cellules Tempe a été proposé et testé pour établir la relation pétrophysique reliant teneur en eau volumique et conductivité électrique dans des matériaux fins. La mesure simultanée de ces deux paramètres dans les résidus miniers au fur et à mesure que la pression dans la cellule augmentait a permis de calibrer un modèle semi-empirique d'Archie utilisé afin de convertir la conductivité électrique mesurée en teneur en eau volumique avec une précision de $\pm 0.02 \text{ m}^3/\text{m}^3$. Ce dispositif est prometteur pour la détermination des relations pétrophysiques dans les matériaux fins puisqu'il est peu coûteux, facilement reproductible et réalisable en conditions contrôlées (porosité, température et conductivité du fluide interstitiel). Dans un troisième temps, deux autres montages de laboratoire et deux dispositifs de mesure sur le terrain ont ensuite été instrumentés afin de suivre simultanément la teneur en eau volumique et la conductivité électrique pour différentes conditions hydrogéologiques. Au laboratoire d'abord, une chaudière remplie des résidus de la mine Canadian Malartic et une colonne représentant une couverture avec effet de barrière capillaire (CEBC) miniature ont été instrumentées avec des sondes de teneur en eau et des électrodes géophysiques et ont été respectivement soumises à des cycles de mouillage et séchage par la surface ainsi qu'à un drainage effectué par la base. Sur le terrain ensuite, une section de 23 m de long d'une CEBC expérimentale a été instrumentée à l'aide de sondes de teneur en eau, de profils verticaux d'électrodes éloignées de 10 cm (haute résolution) et de profils horizontaux d'électrodes séparées par 1 m (plus basse résolution). Ces expériences ont permis d'établir des relations pétrophysiques *in situ* à quatre échelles différentes qui ont été utilisées pour estimer la teneur en eau volumique dans les résidus miniers à partir des mesures électriques avec une précision variant de ± 0.02 à $\pm 0.04 \text{ m}^3/\text{m}^3$ dépendamment des expériences. Cette méthodologie a permis de valider que la relation déterminée à petite échelle dans les cellules Tempe modifiées restait valide à plus grande échelle, ce qui était un élément important pour pouvoir appliquer la méthode électrique pour le suivi de la teneur en eau volumique dans les systèmes de recouvrements sur le terrain.

Ces expériences réalisées dans différentes conditions hydrogéologiques et à différentes échelles ont permis de développer et de tester une méthodologie de traitement de données permettant de maximiser la précision des estimations de teneur en eau volumique prédites à partir de l'imagerie électrique dans les systèmes de recouvrements. Les sondes hydrogéologiques installées à proximité des électrodes géophysiques ont été utilisées pour estimer la distribution

spatio-temporelle de la température et de la conductivité électrique du fluide interstitiel dans les systèmes de recouvrement. L'effet de ces paramètres physiques sur la conductivité électrique du milieu a ainsi pu être pris en compte à l'aide de relations semi-empiriques pour corriger les valeurs de conductivité électrique *in-situ* à une température de référence de 25°C et à une conductivité électrique du fluide interstitiel de référence de 4 mS/cm, valeurs obtenues pour les expériences de laboratoire. Ces corrections ont joué un rôle majeur pour le suivi hydrogéophysique réalisé en conditions réelles ; à titre d'exemple, les variations de température mesurées dans les systèmes de recouvrements expérimentaux de la Mine Canadian Malartic de $\pm 10^\circ\text{C}$ entre l'été et l'hiver ont causé une variation de conductivité électrique du milieu de $\pm 20\%$. Ainsi, il a été démontré que ne pas prendre en compte les variations de ces deux paramètres physiques dans les résidus de la CEBC instrumentée sur le terrain aurait diminué la précision de l'estimation de teneur en eau volumique d'un ordre de grandeur.

La méthode de suivi électrique a ensuite été appliquée dans des systèmes de recouvrements expérimentaux construits à la Mine Canadian Malartic en conditions réelles et à l'échelle pilote ; soit une CEBC conçue pour jouer un rôle de barrière à oxygène et un recouvrement comprenant une couche de faible perméabilité (nommé LSHCC) conçu pour réduire l'infiltration d'eau vers les résidus. Quatre sections de 23 m de long ont été instrumentées et suivies en continu avec des sondes hydrogéologiques et des électrodes connectées à un résistivimètre autonome effectuant quatre images par jour et transférant les données à distance. Les données électriques ont été inversées et converties en distributions spatio-temporelles de teneur en eau volumique à l'aide des modèles pétrophysiques calibrés en laboratoire. La précision de la teneur en eau volumique prédite par la méthode électrique variait de ± 0.01 à $\pm 0.03 \text{ m}^3/\text{m}^3$, (i.e., précision entre $\pm 2.5\%$ et $\pm 7.5\%$ en termes de degré de saturation), dépendamment des sections instrumentées pour la période de suivi (juin 2021 à juillet 2022).

Le suivi hydrogéophysique dans les quatre sections instrumentées a mis en évidence des comportements hydrogéologiques différents entre les deux types de systèmes de recouvrements. Dans les sections de CEBC, la teneur en eau volumique est restée élevée tout au long de l'année dans les couches de rétention d'eau constituées de résidus miniers tandis que des variations temporelles plus importantes ont été observées dans les autres couches de la CEBC. En particulier, la détermination de la porosité *in situ* lors de la construction des recouvrements a permis de convertir la distribution de teneur en eau volumique en degré de saturation dans la couche de rétention d'eau. Ceci a permis de quantifier la performance des sections de CEBC, en utilisant un critère de performance de 85% de saturation, couramment utilisé en restauration minière. Cette approche a montré qu'au moins 90% de la couche de rétention d'eau de la CEBC en haut de pente est restée à un degré de saturation supérieur à 85% tout

au long de la période de suivi (respectivement 70% pour la section de CEBC sur le plateau). Ces résultats de terrain à l'échelle pilote ont donc démontré l'efficacité d'un recouvrement de type CEBC à maintenir un haut degré de saturation pour bloquer les flux d'oxygène provenant de l'atmosphère pour le parc à résidus de la Mine Canadian Malartic.

Des variations spatio-temporelles de teneur en eau volumique plus importantes ont été observées dans les sections instrumentées des recouvrements de type LSHCC, pour lesquelles de plus faibles valeurs de teneur en eau volumique ont été mesurées tout au long de la période de suivi. Plus précisément, les couches constituées de mort-terrain ont été fortement affectées par les précipitations et les périodes de sécheresse, avec des valeurs de teneur en eau volumique minimales aussi basses que $0.25 \text{ m}^3/\text{m}^3$, ce qui correspond à un degré de saturation d'environ 60% pour une porosité *in situ* de 0.45. Ces valeurs ont été mesurées pendant l'été 2021 en bas de pente, pendant une période particulièrement sèche, alors que l'on pouvait observer à cet endroit une croissance rapide de végétation qui a certainement affecté le bilan hydrique en augmentant l'évapo-transpiration. Par ailleurs, les sondes hydrogéologiques localisées dans les couches de roches stériles sous-jacentes ont mesuré d'importantes variations de teneur en eau volumique, ce qui semble indiquer qu'au moins une partie de l'eau s'est infiltré à travers la couche de mort-terrain et a percolé vers les résidus du parc.

La mise en place d'un suivi combinant des instruments ponctuels et la méthode de tomographie de résistivité électrique dans des systèmes de recouvrements expérimentaux à la Mine Canadian Malartic a donc permis de démontrer la faisabilité, la précision et la pertinence de cette approche innovante. Les données hydrogéophysiques ont permis d'imager en continu dans l'espace et le temps la teneur en eau volumique dans les couches d'intérêt des recouvrements, ce qui a permis de quantifier la performance des sections de CEBC, et de fournir des données qui pourront être utilisées pour raffiner l'estimation du bilan hydrique pour les LSHCCs à l'aide de modèles numériques. L'ensemble des observations et des résultats obtenus par ce projet de doctorat ont ensuite été combinés pour élaborer un guide de conception en six étapes qui pourra orienter quiconque serait intéressé.e à inclure la méthode de suivi électrique à un programme de surveillance de performance d'un système de recouvrement à pleine échelle. En particulier, ce guide devrait être suivi pour identifier en amont les objectifs du suivi électrique dans les systèmes de recouvrement ainsi que la précision, l'étendue spatiale et la résolution spatio-temporelle minimales qui seraient nécessaires. Il permet également d'identifier les meilleures stratégies à mettre en place pour l'acquisition, le traitement et l'interprétation des données, et pose les bases de l'intégration de l'approche électrique dans les systèmes d'alerte précoce qui pourront être mis en place à l'avenir pour détecter efficacement une perte de performance dans les systèmes de recouvrement.

Pour conclure, plusieurs recommandations peuvent être proposées pour poursuivre les travaux de doctorat présentés dans cette thèse, et ainsi améliorer et permettre une éventuelle démocratisation de l'application de la méthode électrique au suivi temporel de la performance des systèmes de recouvrements en restauration minière.

Recommandation 1 : Test de la méthode à pleine échelle en conditions réelles.

Dans le cadre de ce projet de doctorat, la méthode électrique a été appliquée à l'échelle pilote ($\simeq 30$ m) et dans des conditions idéales qui ne pourront probablement pas être reproduites à pleine échelle (i.e., électrodes espacées de 1 m, deux niveaux d'électrodes dans chaque couche d'intérêt, installation au fur et à mesure de la construction et mise en place minutieuse du matériel des recouvrements sur les instruments). Il serait donc pertinent d'identifier des stratégies d'instrumentation applicables à pleine échelle qui permettraient d'obtenir une résolution spatio-temporelle ainsi qu'une précision équivalentes à ce qui a été présenté dans les recouvrements pilotes.

Recommandation 2 : Amélioration des modèles pétrophysiques pour les résidus.

Le modèle semi-empirique d'Archie a été employé dans cette thèse pour décrire la relation entre conductivité électrique du milieu et teneur en eau volumique. Bien que les résultats soient satisfaisants, ce modèle demeure assez simplifié et nécessite une calibration de laboratoire spécifique pour chaque type de résidus miniers. Il serait intéressant de raffiner ce type de modèle en caractérisant différents échantillons de résidus afin de développer des méthodes de prédiction des propriétés pétrophysiques à partir des données physiques, granulométriques et minéralogiques des résidus, comme c'est le cas en hydrogéologie par exemple.

Recommandation 3 : Assimilation des données hydrogéophysiques et modèles numériques.

La méthodologie suivie pour cette étude se base sur l'inversion des données électriques puis leur conversion en teneur en eau volumique en corrigeant l'effet de la température et de la conductivité électrique du fluide interstitiel. Il serait pertinent de développer des approches de traitement de données comme les filtres de Kalman d'ensemble (EnKFs) qui permettraient de prendre en compte simultanément les données hydrogéologiques ponctuelles, les données électriques volumiques ainsi que des modélisations numériques afin d'améliorer la prédiction de la teneur en eau volumique dans les recouvrements. Cette approche a été développée par Isabelle (2022) et testée en 1D avec une CEBC à petite échelle en laboratoire. Une approche similaire devrait ainsi être développée et testée en 2D avec les données de terrain obtenues dans les recouvrements expérimentaux de la Mine Canadian Malartic pour estimer en temps réel la teneur en eau volumique dans les recouvrements et calibrer des modèles numériques reproduisant leur comportement hydrogéologique à partir de données réelles.

RÉFÉRENCES

- M. Aachib, M. Mbonimpa, and M. Aubertin. Measurement and prediction of the oxygen diffusion coefficient in unsaturated media, with applications to soil covers. *Water, air, and soil pollution*, 156(1) :163–193, 2004.
- F. Abdulsamad, A. Revil, A. S. Ahmed, A. Coperey, M. Karaoulis, S. Nicaise, and L. Peyras. Induced polarization tomography applied to the detection and the monitoring of leaks in embankments. *Engineering Geology*, 254 :89–101, 2019.
- B. S. Acharya, T. Halihan, C. B. Zou, and R. E. Will. Vegetation controls on the spatio-temporal heterogeneity of deep moisture in the unsaturated zone : A hydrogeophysical evaluation. *Scientific Reports*, 7(1) :1–10, 2017.
- J. Acosta, P. Martínez-Pagán, S. Martínez-Martínez, A. Faz, R. Zornoza, and D. Carmona. Assessment of environmental risk of reclaimed mining ponds using geophysics and geochemical techniques. *Journal of Geochemical Exploration*, 147 :80–90, 2014.
- J. A. Acosta, M. Gabarrón, M. Martínez-Segura, S. Martínez-Martínez, Á. Faz, A. Pérez-Pastor, M. D. Gómez-López, and R. Zornoza. Soil water content prediction using electrical resistivity tomography (ert) in mediterranean tree orchard soils. *Sensors*, 22(4) :1365, 2022.
- A. Adler and W. R. Lionheart. Uses and abuses of eiders : an extensible software base for eit. *Physiological measurement*, 27(5) :S25, 2006.
- . Agnico Eagle Mine Laronde. Mise à jour du plan de restauration – laronde et bousquet 2 - révision 5 (version 2021). page 383, 2021. URL https://gestim.mines.gouv.qc.ca/documents/001_D0_Plan_restoration_LaRonde_2021-02-25_0000056103.pdf.
- G. Agricola and H. Hoover. *De Re Metallica. Translated from the First Latin Edition of 1556 by Herbert Clark Hoover*. London, 1556/1912.
- S. Al Hagrey. Electrical resistivity imaging of tree trunks. *Near Surface Geophysics*, 4(3) : 179–187, 2006.
- S. A. al Hagrey and T. Petersen. Numerical and experimental mapping of small root zones using optimized surface and borehole resistivity tomography. *Geophysics*, 76(2) :G25–G35, 2011.
- S. A. al Hagrey, R. Meissner, U. Werban, W. Rabbel, and A. Ismaeil. Hydro-, bio-geophysics. *The leading edge*, 23(7) :670–674, 2004. ISSN 1070-485X.
- A. Almpanis, J. Gerhard, and C. Power. Mapping and monitoring of dnapl source zones with combined direct current resistivity and induced polarization : A field-scale numerical investigation. *Water Resources Research*, 57(11) :e2021WR031366, 2021.

- A. Amazirh, O. Merlin, S. Er-Raki, Q. Gao, V. Rivalland, Y. Malbeteau, S. Khabba, and M. J. Escorihuela. Retrieving surface soil moisture at high spatio-temporal resolution from a synergy between sentinel-1 radar and landsat thermal data : A study case over bare soil. *Remote sensing of environment*, 211 :321–337, 2018.
- O. Anterrieu, M. Chouteau, and M. Aubertin. Geophysical characterization of the large-scale internal structure of a waste rock pile from a hard rock mine. *Bulletin of engineering geology and the environment*, 69(4) :533–548, 2010. ISSN 1435-9529.
- G. E. Archie et al. The electrical resistivity log as an aid in determining some reservoir characteristics. *Transactions of the AIME*, 146(01) :54–62, 1942.
- D. Arosio, S. Munda, G. Tresoldi, M. Papini, L. Longoni, and L. Zanzi. A customized resistivity system for monitoring saturation and seepage in earthen levees : installation and validation. *Open Geosciences*, 9(1) :457–467, 2017.
- ASTM. *Standard Test Method for Capillary-Moisture Relationships for Coarse- and Medium-Textured Soils by Porous-Plate Apparatus*. ASTM International, 2000.
- ASTM. *Standard Test Methods for Determination of the Soil Water Characteristic Curve for Desorption Using Hanging Column, Pressure Extractor, Chilled Mirror Hygrometer, or Centrifuge*. ASTM International, 2016.
- M. Aubertin, R. Chapuis, M. Aachib, B. Bussière, J. Ricard, and L. Tremblay. *Évaluation en laboratoire de barrières sèches construites à partir de résidus miniers*. École Polytechnique de Montréal, 1995.
- M. Aubertin, J.-F. Ricard, and R. P. Chapuis. A predictive model for the water retention curve : application to tailings from hard-rock mines. *Canadian Geotechnical Journal*, 35 (1) :55–69, 1998.
- M. Aubertin, M. Mbonimpa, B. Bussière, and R. Chapuis. A model to predict the water retention curve from basic geotechnical properties. *Canadian Geotechnical Journal*, 40(6) : 1104–1122, 2003. ISSN 0008-3674.
- M. Aubertin, O. Fala, J. Molson, A. Gamache-Rochette, B. Lahmira, V. Martin, R. Lefebvre, B. Bussière, R. P. Chapuis, and M. Chouteau. Évaluation du comportement hydrogéologique et géochimique des haldes à stériles. *Symposium Rouyn-Noranda : L'Environnement et les Mines*, pages 15–18, 2005.
- M. Aubertin, E. Cifuentes, S. Apithy, B. Bussière, J. Molson, and R. Chapuis. Analyses of water diversion along inclined covers with capillary barrier effects. *Canadian Geotechnical Journal*, 46(10) :1146–1164, 2009. ISSN 0008-3674.

- M. Aubertin, B. Bussière, T. Pabst, M. James, and M. Mbonimpa. Review of the reclamation techniques for acid-generating mine wastes upon closure of disposal sites. *Geo-Chicago 2016*, pages 343–358, 2016.
- M. Audebert, R. Clément, S. Moreau, C. Duquennoi, S. Loisel, and N. Touze-Foltz. Understanding leachate flow in municipal solid waste landfills by combining time-lapse ert and subsurface flow modelling—part i : Analysis of infiltration shape on two different waste deposit cells. *Waste management*, 55 :165–175, 2016.
- E. Auken, L. Pellerin, N. B. Christensen, and K. Sørensen. A survey of current trends in near-surface electrical and electromagnetic methods. *Geophysics*, 71(5) :G249–G260, 2006.
- E. Auken, J. Doetsch, G. Fiandaca, A. V. Christiansen, A. Gazoty, A. G. Cahill, and R. Jakobsen. Imaging subsurface migration of dissolved co2 in a shallow aquifer using 3-d time-lapse electrical resistivity tomography. *Journal of Applied Geophysics*, 101 :31–41, 2014.
- A. S. Awoh, M. Mbonimpa, and B. Bussière. Water covers. *Hard Rock Mine Reclamation : From Prediction to Management of Acid Mine Drainage*, page 135, 2021.
- S. Azam and Q. Li. Tailings dam failures : a review of the last one hundred years. *Geotechnical news*, 28(4) :50–54, 2010.
- J. Aznar-Sánchez, J. García-Gómez, J. Velasco-Muñoz, and A. Carretero-Gómez. Mining Waste and Its Sustainable Management : Advances in Worldwide Research. *Minerals*, 8(7) : 284, 2018.
- A. Bakulin, I. Silvestrov, and R. Pevzner. Surface seismics with das : An emerging alternative to modern point-sensor acquisition. *The Leading Edge*, 39(11) :808–818, 2020.
- K. Banerjee, S. Sharma, A. Sarangi, and D. Sengupta. Delineation of subsurface structures using resistivity, vlf and radiometric measurement around a u-tailings pond and its hydrogeological implication. *Physics and Chemistry of the Earth, Parts A/B/C*, 36(16) : 1345–1352, 2011.
- A. Beauvais, M. Ritz, J.-C. Parisot, C. Bantsimba, and M. Dukhan. Combined ert and gpr methods for investigating two-stepped lateritic weathering systems. *Geoderma*, 119(1-2) : 121–132, 2004.
- M. Bechtold, J. Vanderborght, L. Weihermüller, M. Herbst, T. Günther, O. Ippisch, R. Kasteel, and H. Vereecken. Upward transport in a three-dimensional heterogeneous laboratory soil under evaporation conditions. *Vadose Zone Journal*, 11(2), 2012a.
- M. Bechtold, J. Vanderborght, L. Weihermüller, M. Herbst, T. Günther, O. Ippisch, R. Kasteel, and H. Vereecken. Upward transport in a three-dimensional heterogeneous laboratory soil under evaporation conditions. *Vadose Zone Journal*, 11(2), 2012b. ISSN 1539-1663.

- L. Beff, T. Günther, B. Vandoorne, V. Couvreur, and M. Javaux. Three-dimensional monitoring of soil water content in a maize field using electrical resistivity tomography. *Hydrology and Earth System Sciences*, 17(2) :595–609, 2013.
- N. Belabid, F. Zhao, L. Brocca, Y. Huang, and Y. Tan. Near-real-time flood forecasting based on satellite precipitation products. *Remote Sensing*, 11(3) :252, 2019.
- A. K. Benson and C. L. Addams. Detecting the presence of acid mine drainage using hydrogeological, geochemical, and geophysical data ; applications to contrasting conditions at mine sites in little cottonwood and american fork canyons, utah. *Environmental Geosciences*, 5(1) :17–27, 1998.
- E. M. Benyassine, A. Lachhab, A. Dekayir, J. C. Parisot, and M. Rouai. An application of electrical resistivity tomography to investigate heavy metals pathways. *Journal of Environmental and Engineering Geophysics*, 22(4) :315–324, 2017.
- P. Bergmann, C. Schmidt-Hattenberger, D. Kiessling, C. Rücker, T. Labitzke, J. Hennings, G. Baumann, and H. Schütt. Surface-downhole electrical resistivity tomography applied to monitoring of co2 storage at ketzin, germany. *Geophysics*, 77(6) :B253–B267, 2012.
- P. Bergmann, M. Diersch, J. Götz, M. Ivandic, A. Ivanova, C. Juhlin, J. Kummerow, A. Lieb-scher, S. Lueth, S. Meekes, et al. Review on geophysical monitoring of co2 injection at ketzin, germany. *Journal of Petroleum Science and Engineering*, 139 :112–136, 2016.
- J. Bergström. *Geophysical methods for investigating and monitoring the integrity of sealing layers on mining waste deposits*. PhD thesis, Luleå tekniska universitet, 1998.
- C. L. Bérubé, G. R. Olivo, M. Chouteau, S. Perrouty, P. Shamsipour, R. J. Enkin, W. A. Morris, L. Feltrin, and R. Thiémonge. Predicting rock type and detecting hydrothermal alteration using machine learning and petrophysical properties of the canadian malartic ore and host rocks, pontiac subprovince, québec, canada. *Ore Geology Reviews*, 96 :130–145, 2018.
- C. L. Bérubé, G. R. Olivo, M. Chouteau, and S. Perrouty. Mineralogical and textural controls on spectral induced polarization signatures of the canadian malartic gold deposit : Applications to mineral exploration mineralogical controls on sip. *Geophysics*, 84(2) :B135–B151, 2019.
- A. Besson, I. Cousin, A. Dorigny, M. Dabas, and D. King. The temperature correction for the electrical resistivity measurements in undisturbed soil samples : Analysis of the existing conversion models and proposal of a new model. *Soil Science*, 173(10) :707–720, 2008. ISSN 0038-075X.
- J. Bethune, J. Randell, R. L. Runkel, and K. Singha. Non-invasive flow path characterization in a mining-impacted wetland. *Journal of contaminant hydrology*, 183 :29–39, 2015.

- D. Bevc and H. F. Morrison. Borehole-to-surface electrical resistivity monitoring of a salt water injection experiment. *Geophysics*, 56(6) :769–777, 1991.
- G. Bièvre, L. Oxarango, T. Günther, D. Goutaland, and M. Massardi. Improvement of 2d ert measurements conducted along a small earth-filled dyke using 3d topographic data and 3d computation of geometric factors. *Journal of Applied Geophysics*, 153 :100–112, 2018.
- A. Binley and W. Daily. The performance of electrical methods for assessing the integrity of geomembrane liners in landfill caps and waste storage ponds. *Journal of Environmental & Engineering Geophysics*, 8(4) :227–237, 2003.
- A. Binley and L. Slater. *Resistivity and Induced Polarization : Theory and Applications to the Near-Surface Earth*. Cambridge University Press, 2020. doi : 10.1017/9781108685955.
- A. Binley, S. S. Hubbard, J. A. Huisman, A. Revil, D. A. Robinson, K. Singha, and L. D. Slater. The emergence of hydrogeophysics for improved understanding of subsurface processes over multiple scales. *Water resources research*, 51(6) :3837–3866, 2015a.
- A. Binley, S. S. Hubbard, J. A. Huisman, A. Revil, D. A. Robinson, K. Singha, and L. D. Slater. The emergence of hydrogeophysics for improved understanding of subsurface processes over multiple scales. *Water resources research*, 51(6) :3837–3866, 2015b. ISSN 1944-7973.
- G. Blanchy, S. Saneiyani, J. Boyd, P. McLachlan, and A. Binley. Resipy, an intuitive open source software for complex geoelectrical inversion/modeling. *Computers & Geosciences*, 137 :104423, 2020a.
- G. Blanchy, C. W. Watts, J. Richards, J. Bussell, K. Huntenburg, D. L. Sparkes, M. Stalham, M. J. Hawkesford, W. R. Whalley, and A. Binley. Time-lapse geophysical assessment of agricultural practices on soil moisture dynamics. *Vadose Zone Journal*, 19(1) :e20080, 2020b.
- D. Blowes, C. Ptacek, J. Jambor, and C. Weisener. The geochemistry of acid mine drainage. *Environmental geochemistry*, 9 :149–204, 2003.
- D. Blowes, C. Ptacek, J. Jambor, C. Weisener, D. Paktunc, and W. Gould. Treatise on geochemistry. *The geochemistry of acid mine drainage*, pages 131–90, 2014.
- A. P. Booterbaugh, L. R. Bentley, and C. A. Mendoza. Geophysical characterization of an undrained dyke containing an oil sands tailings pond, alberta, canada. *Journal of Environmental and Engineering Geophysics*, 20(4) :303–317, 2015.
- S. Bortnikova, N. Yurkevich, E. Bessonova, Y. Karin, and O. Saeva. The combination of geoelectrical measurements and hydro-geochemical studies for the evaluation of groundwater pollution in mining tailings areas. In *Threats to the Quality of Groundwater Resources*, pages 239–256. Springer, 2013.

- S. Bortnikova, V. Olenchenko, O. Gaskova, N. Yurkevich, N. Abrosimova, E. Shevko, A. Edelev, T. Korneeva, I. Provornaya, and L. Eder. Characterization of a gold extraction plant environment in assessing the hazardous nature of accumulated wastes (kemerovo region, russia). *Applied Geochemistry*, 93 :145–157, 2018.
- S. Bortnikova, O. Gaskova, N. Yurkevich, O. Saeva, and N. Abrosimova. Chemical treatment of highly toxic acid mine drainage at a gold mining site in southwestern siberia, russia. *Minerals*, 10(10) :867, 2020.
- V. Boulanger-Martel, B. Bussière, and J. Côté. Insulation covers with capillary barrier effects to control sulfide oxidation in the arctic. *Canadian Geotechnical Journal*, 58(4) : 583–594, 2021a.
- V. Boulanger-Martel, B. Bussière, and J. Côté. Thermal behaviour and performance of two field experimental insulation covers to control sulfide oxidation at meadowbank mine, nunavut. *Canadian Geotechnical Journal*, 58(3) :427–440, 2021b.
- V. Bouzaglou, E. Crestani, P. Salandin, E. Gloaguen, and M. Camporese. Ensemble kalman filter assimilation of ert data for numerical modeling of seawater intrusion in a laboratory experiment. *Water*, 10(4) :397, 2018.
- L. N. Bowker and D. M. Chambers. The risk, public liability, & economics of tailings storage facility failures. *Earthwork Act*, pages 1–56, 2015.
- J. Boyd, G. Blanchy, S. Saneiyani, and A. Binley. 3d geoelectrical problems with resipy, an open source graphical user interface for geoelectrical data processing. *Fast Times*, 24(4) : 85–92, 2019.
- J. Boyd, J. Chambers, P. Wilkinson, M. Peppas, A. Watlet, M. Kirkham, L. Jones, R. Swift, P. Meldrum, S. Uhlemann, et al. A linked geomorphological and geophysical modelling methodology applied to an active landslide. *Landslides*, 18(8) :2689–2704, 2021.
- A. Boyle, P. B. Wilkinson, J. E. Chambers, P. I. Meldrum, S. Uhlemann, and A. Adler. Jointly reconstructing ground motion and resistivity for ert-based slope stability monitoring. *Geophysical Journal International*, 212(2) :1167–1182, 2018.
- L. Brillante, B. Bois, O. Mathieu, V. Bichet, D. Michot, and J. Lévêque. Monitoring soil volume wetness in heterogeneous soils by electrical resistivity. a field-based pedotransfer function. *Journal of hydrology*, 516 :56–66, 2014.
- L. Brillante, O. Mathieu, B. Bois, C. Van Leeuwen, and J. Lévêque. The use of soil electrical resistivity to monitor plant and soil water relationships in vineyards. *Soil*, 1(1) :273–286, 2015.

- L. Brillante, B. Bois, J. Leveque, and O. Mathieu. Variations in soil-water use by grapevine according to plant water status and soil physical-chemical characteristics—a 3d spatio-temporal analysis. *European journal of agronomy*, 77 :122–135, 2016a.
- L. Brillante, B. Bois, O. Mathieu, and J. Lévêque. Electrical imaging of soil water availability to grapevine : a benchmark experiment of several machine-learning techniques. *Precision agriculture*, 17(6) :637–658, 2016b.
- L. Brocca, S. Hasenauer, T. Lacava, F. Melone, T. Moramarco, W. Wagner, W. Dorigo, P. Matgen, J. Martínez-Fernández, P. Llorens, et al. Soil moisture estimation through ascats and amsr-e sensors : An intercomparison and validation study across europe. *Remote Sensing of Environment*, 115(12) :3390–3408, 2011.
- A. Brovelli and G. Cassiani. A combination of the hashin-shtrikman bounds aimed at modeling electrical conductivity and permittivity of variably saturated porous media. *Geophysical Journal International*, 180(1) :225–237, 2010.
- P. Brunet, R. Clément, and C. Bouvier. Monitoring soil water content and deficit using electrical resistivity tomography (ert)—a case study in the cevennes area, france. *Journal of Hydrology*, 380(1-2) :146–153, 2010.
- L. S. Bryson. Evaluation of geotechnical parameters using electrical resistivity measurements. pages 1–12, 2005.
- L. S. Bryson and A. Bathe. Determination of selected geotechnical properties of soil using electrical conductivity testing. *Geotechnical Testing Journal*, 32(3) :1–10, 2009.
- J. Budler. Improved geoelectrical imaging of water content dynamics applied to landslide monitoring.
- J. Budler. *Improved Geoelectrical Imaging of Water Content Dynamics Applied to Landslide Monitoring*. PhD thesis, 2017.
- L. Busato, J. Boaga, M. T. Perri, B. Majone, A. Bellin, and G. Cassiani. Hydrogeophysical characterization and monitoring of the hyporheic and riparian zones : The vermigliana creek case study. *Science of the Total Environment*, 648 :1105–1120, 2019.
- G. Buselli and K. Lu. Groundwater contamination monitoring with multichannel electrical and electromagnetic methods. *Journal of Applied Geophysics*, 48(1) :11–23, 2001.
- B. Bussière and M. Guittonny. *Hard Rock Mine Reclamation : From Prediction to Management of Acid Mine Drainage*. CRC Press, 2021a.
- B. Bussière and M. Guittonny. Long-term evolution of reclamation performance. *Hard Rock Mine Reclamation : From Prediction to Management of Acid Mine Drainage*, 2021b.

- B. Bussière and G. W. Wilson. Store-and-release covers. *Hard Rock Mine Reclamation : From Prediction to Management of Acid Mine Drainage*, page 115, 2021.
- B. Bussière, M. Aubertin, and R. P. Chapuis. The behavior of inclined covers used as oxygen barriers. *Canadian Geotechnical Journal*, 40(3) :512–535, 2003.
- B. Bussière, M. Aubertin, M. Mbonimpa, J. W. Molson, and R. P. Chapuis. Field experimental cells to evaluate the hydrogeological behaviour of oxygen barriers made of silty materials. *Canadian Geotechnical Journal*, 44(3) :245–265, 2007.
- B. Bussière, T. Pabst, V. Boulanger-Martel, M. Guittonny, B. Plante, C. M. Neculita, S. Awoh, M. Mbonimpa, I. Demers, A. Maqsoud, A. Dimech, and P.-L. Labonté-Raymond. Monitoring the performance of mine site reclamation. *Hard Rock Mine Reclamation : From Prediction to Management of Acid Mine Drainage*, 2021.
- B. Bussière. Colloquium 2004 : Hydrogeotechnical properties of hard rock tailings from metal mines and emerging geoenvironmental disposal approaches. *Canadian Geotechnical Journal*, 44(9) :1019–1052, 2007. doi : 10.1139/T07-040.
- B. Bussière, A. Maqsoud, M. Aubertin, J. Martschuk, J. McMullen, and M. Julien. Results from the monitoring program at the LTA site : hydraulic behavior of the cover. *Proceedings of the 105th Annual General Meeting of CIM-ICM, Montréal, Que*, pages 4–7, 2003.
- B. Bussière, A. Maqsoud, M. Aubertin, J. Martschuk, J. McMullen, and M. Julien. Performance of the oxygen limiting cover at the LTA site, Malartic, Quebec. *CIM Bulletin*, 1(6) : 1–11, 2006.
- B. Bussière, R. Potvin, A.-M. Dagenais, M. Aubertin, A. Maqsoud, and J. Cyr. Restauration du site minier Lorraine, Latulipe, Québec : Résultats de 10 ans de suivi. *Déchets Sci Et Tech*, 54 :49–64, 2009.
- J. Cai, W. Wei, X. Hu, and D. A. Wood. Electrical conductivity models in saturated porous media : A review. *Earth-Science Reviews*, 171 :419–433, 2017.
- G. Calamita, L. Brocca, A. Perrone, S. Piscitelli, V. Lapenna, F. Melone, and T. Moramarco. Electrical resistivity and tdr methods for soil moisture estimation in central italy test-sites. *Journal of Hydrology*, 454 :101–112, 2012.
- G. Calvo, G. Mudd, A. Valero, and A. Valero. Decreasing ore grades in global metallic mining : A theoretical issue or a global reality? *Resources*, 5(4) :36, 2016.
- P. L. Camarero, C. A. Moreira, D. A. Targa, B. G. Duz, and H. G. Pereira. Analysis of acid drainage flow zones in a rocky massif in a uranium mine from structural and geophysical diagnoses. *Mine Water and the Environment*, 41(2) :303–316, 2022.

- M. Camporese, G. Cassiani, R. Deiana, P. Salandin, and A. Binley. Coupled and uncoupled hydrogeophysical inversions using ensemble Kalman filter assimilation of ert-monitored tracer test data. *Water Resources Research*, 51(5) :3277–3291, 2015.
- D. Campos, M. Chouteau, M. Aubertin, and B. Bussière. Using geophysical methods to image the internal structure of mine waste rock piles. *9th EAGE/EEGS Meeting*, 2003.
- . Canadian Malartic. Canadian malartic reclamation plan - revision 3 (version 2020). page 3068, 2020. URL https://gestim.mines.gouv.qc.ca/documents/010a_DO_PDR_Plan_restauracion_Canadian_Malartic_2020_0000055517.pdf.
- . Canadian Malartic Mine. Canadian malartic reclamation plan - revision 2. page 127, 2015. doi : https://gestim.mines.gouv.qc.ca/documents/009_PDR_Canadian_Malartic_MAJ2015_extension_2016-04-14_0000055515.pdf.
- A. M. Carey, G. B. Paige, B. J. Carr, and M. Dogan. Forward modeling to investigate inversion artifacts resulting from time-lapse electrical resistivity tomography during rainfall simulations. *Journal of Applied Geophysics*, 145 :39–49, 2017.
- S. Carrière, J. Ruffault, F. Pimont, C. Doussan, G. Simioni, K. Chalikakis, J.-M. Limousin, I. Scotti, F. Courdier, C.-B. Cakpo, et al. Impact of local soil and subsoil conditions on inter-individual variations in tree responses to drought : insights from electrical resistivity tomography. *Science of the Total Environment*, 698 :134247, 2020.
- S. D. Carriere, K. Chalikakis, C. Danquigny, R. Clement, and C. Emblanch. Feasibility and limits of electrical resistivity tomography to monitor water infiltration through karst medium during a rainy event. In *Hydrogeological and environmental investigations in Karst systems*, pages 45–55. Springer, 2015.
- C. R. Carrigan, X. Yang, D. J. LaBrecque, D. Larsen, D. Freeman, A. L. Ramirez, W. Daily, R. Aines, R. Newmark, J. Friedmann, et al. Electrical resistance tomographic monitoring of co2 movement in deep geologic reservoirs. *International Journal of Greenhouse Gas Control*, 18 :401–408, 2013.
- M. F. S. Casagrande, C. A. Moreira, D. A. Targa, and H. L. C. Alberti. Integration of geophysical methods in the study of acid drainage in uranium mining waste. *Brazilian Journal of Geophysics*, 36(4) :439–450, 2018.
- M. F. S. Casagrande, C. A. Moreira, and D. A. Targa. Study of generation and underground flow of acid mine drainage in waste rock pile in an uranium mine using electrical resistivity tomography. *Pure and Applied Geophysics*, 177(2) :703–721, 2020.
- G. Cassiani, V. Bruno, A. Villa, N. Fusi, and A. M. Binley. A saline trace test monitored via time-lapse surface electrical resistivity tomography. *Journal of Applied Geophysics*, 59 (3) :244–259, 2006.

- G. Cassiani, J. Boaga, M. Rossi, M. Putti, G. Fadda, B. Majone, and A. Bellin. Soil–plant interaction monitoring : Small scale example of an apple orchard in trentino, north-eastern italy. *Science of the Total Environment*, 543 :851–861, 2016.
- D. Caterina, A. F. Orozco, and F. Nguyen. Long-term ert monitoring of biogeochemical changes of an aged hydrocarbon contamination. *Journal of Contaminant Hydrology*, 201 : 19–29, 2017.
- D. Chambers. *Post-mount polley : tailings dam safety in British Columbia*. MiningWatch Canada, 2016.
- J. Chambers. Geophysical monitoring of natural and engineered slopes : towards improved early warning of landslides. In *Engineering and Mining Geophysics 2021*, volume 2021, pages 1–7. European Association of Geoscientists & Engineers, 2021.
- J. Chambers, D. Gunn, P. Wilkinson, R. Ogilvy, G. Ghataora, M. Burrow, and R. T. Smith. *Non-invasive time-lapse imaging of moisture content changes in earth embankments using electrical resistivity tomography (ERT)*. CRC Press, 2008.
- J. Chambers, P. Wilkinson, O. Kuras, J. Ford, D. Gunn, P. Meldrum, C. Pennington, A. Weller, P. Hobbs, and R. Ogilvy. Three-dimensional geophysical anatomy of an active landslide in Lias Group mudrocks, Cleveland Basin, UK. *Geomorphology*, 125(4) :472–484, 2011. ISSN 0169-555X.
- J. Chambers, D. Gunn, P. Wilkinson, P. Meldrum, E. Haslam, S. Holyoake, M. Kirkham, O. Kuras, A. Merritt, and J. Wragg. 4d electrical resistivity tomography monitoring of soil moisture dynamics in an operational railway embankment. *Near Surface Geophysics*, 12(1) : 61–72, 2014a.
- J. Chambers, D. Gunn, P. Wilkinson, P. Meldrum, E. Haslam, S. Holyoake, M. Kirkham, O. Kuras, A. Merritt, and J. Wragg. 4d electrical resistivity tomography monitoring of soil moisture dynamics in an operational railway embankment. *Near Surface Geophysics*, 12(1) : 61–72, 2014b. ISSN 1873-0604.
- J. Chambers, J. Holmes, J. Whiteley, J. Boyd, P. Meldrum, P. Wilkinson, O. Kuras, R. Swift, H. Harrison, S. Glendinning, et al. Long-term geoelectrical monitoring of landslides in natural and engineered slopes. *The Leading Edge*, 41(11) :768–776, 2022.
- R. P. Chapuis and M. Aubertin. On the use of the Kozeny Carman equation to predict the hydraulic conductivity of soils. *Canadian Geotechnical Journal*, 40(3) :616–628, 2003. ISSN 0008-3674.
- G. Chen, Y. Ye, N. Yao, N. Hu, J. Zhang, and Y. Huang. A critical review of prevention, treatment, reuse, and resource recovery from acid mine drainage. *Journal of Cleaner Production*, 329 :129666, 2021.

- T.-T. Chen, Y.-C. Hung, M.-W. Hsueh, Y.-H. Yeh, and K.-W. Weng. Evaluating the application of electrical resistivity tomography for investigating seawater intrusion. *Electronics*, 7(7) :107, 2018a.
- Y. Chen, Z. Wei, M. Irfan, J. Xu, and Y. Yang. Laboratory investigation of the relationship between electrical resistivity and geotechnical properties of phosphate tailings. *Measurement*, 126 :289–298, 2018b.
- C.-C. Chung, C.-P. Lin, S.-H. Yang, J.-Y. Lin, and C.-H. Lin. Investigation of non-unique relationship between soil electrical conductivity and water content due to drying-wetting rate using tdr. *Engineering Geology*, 252 :54–64, 2019.
- M. O. Cimpoiășu, O. Kuras, T. Pridmore, and S. J. Mooney. Potential of geoelectrical methods to monitor root zone processes and structure : A review. *Geoderma*, 365 :114232, 2020.
- L. Clarkson and D. Williams. Critical review of tailings dam monitoring best practice. *International Journal of Mining, Reclamation and Environment*, 34(2) :119–148, 2020.
- L. Clarkson, D. Williams, and J. Seppälä. Real-time monitoring of tailings dams. *Georisk : Assessment and Management of Risk for Engineered Systems and Geohazards*, 15(2) :113–127, 2021.
- R. Clement and S. Moreau. How should an electrical resistivity tomography laboratory test cell be designed? numerical investigation of error on electrical resistivity measurement. *Journal of Applied Geophysics*, 127 :45–55, 2016.
- R. Clément, M. Descloitres, T. Günther, L. Oxarango, C. Morra, J.-P. Laurent, and J.-P. Gourc. Improvement of electrical resistivity tomography for leachate injection monitoring. *Waste Management*, 30(3) :452–464, 2010.
- R. Clement, Y. Fargier, V. Dubois, J. Gance, E. Gros, and N. Forquet. Ohmpi : An open source data logger for dedicated applications of electrical resistivity imaging at the small and laboratory scale. *HardwareX*, 8 :e00122, 2020.
- R. Cockett, S. Kang, L. J. Heagy, A. Pidlisecky, and D. W. Oldenburg. Simpeg : An open source framework for simulation and gradient based parameter estimation in geophysical applications. *Computers & Geosciences*, 85 :142–154, 2015.
- C. Comina, S. Foti, G. Musso, and E. Romero. Eit oedometer : an advanced cell to monitor spatial and time variability in soil with electrical and seismic measurements. *Geotechnical Testing Journal*, 31(5) :404–412, 2008.
- C. Comina, N. Giordano, G. Ghidone, and F. Fischanger. Time-lapse 3d electric tomography for short-time monitoring of an experimental heat storage system. *Geosciences*, 9(4) :167, 2019.

- D. D. Corona-Lopez, S. Sommer, S. A. Rolfe, F. Podd, and B. D. Grieve. Electrical impedance tomography as a tool for phenotyping plant roots. *Plant methods*, 15(1) :49, 2019.
- U. Cortada, J. Martínez, J. Rey, M. C. Hidalgo, and S. Sandoval. Assessment of tailings pond seals using geophysical and hydrochemical techniques. *Engineering Geology*, 223 : 59–70, 2017.
- D. Corwin and E. Scudiero. Review of soil salinity assessment for agriculture across multiple scales using proximal and/or remote sensors. *Advances in Agronomy*, page 1, 2019.
- R. M. Cosentini, G. Della Vecchia, S. Foti, and G. Musso. Estimation of the hydraulic parameters of unsaturated samples by electrical resistivity tomography. *Géotechnique*, 62 (7) :583–594, 2012.
- A. Costall, B. Harris, and J. Pigois. Electrical resistivity imaging and the saline water interface in high-quality coastal aquifers. *Surveys in geophysics*, 39(4) :753–816, 2018.
- A. Costall, B. Harris, B. Teo, R. Schaa, F. Wagner, and J. Pigois. Groundwater throughflow and seawater intrusion in high quality coastal aquifers. *Scientific reports*, 10(1) :1–33, 2020.
- Y. Coulibaly. Auscultation de la digue Nord-Ouest du parc à résidus miniers no. 1 de Doyon dans une perspective d'évaluation de la stabilité pendant la phase de restauration. Master's thesis, École Polytechnique de Montréal, 2016.
- Y. Coulibaly, T. Belem, and L. Cheng. Numerical analysis and geophysical monitoring for stability assessment of the Northwest tailings dam at Westwood Mine. *International Journal of Mining Science and Technology*, 27(4) :701–710, 2017. ISSN 2095-2686.
- C. A. Cravotta III. Dissolved metals and associated constituents in abandoned coal-mine discharges, pennsylvania, usa. part 2 : geochemical controls on constituent concentrations. *Applied Geochemistry*, 23(2) :203–226, 2008.
- M. M. Crawford and L. S. Bryson. Assessment of active landslides using field electrical measurements. *Engineering Geology*, 233 :146–159, 2018.
- M. M. Crawford, L. S. Bryson, E. W. Woolery, and Z. Wang. Long-term landslide monitoring using soil-water relationships and electrical data to estimate suction stress. *Engineering Geology*, 251 :146–157, 2019.
- B. Cabbage, D. F. Rucker, B. Zaebst, J. Gillis, and J. Cain. Geophysical heap characterization throughout construction and operations of the carlota mine. *Proceedings of Heap Leach Mining Solutions*, pages 18–20, 2016.
- A. Cultrera, D. Serazio, A. Zurutuza, A. Centeno, O. Txoperena, D. Etayo, A. Cordon, A. Redo-Sanchez, I. Arnedo, M. Ortolano, et al. Mapping the conductivity of graphene with electrical resistance tomography. *Scientific reports*, 9(1) :1–9, 2019.

- D. C. G. da Rocha, M. A. da Silva Braga, and C. T. Rodrigues. Geophysical methods for br tailings dam research and monitoring in the mineral complex of tapira-minas gerais, brazil. *Brazilian Journal of Geophysics*, 37(3) :275–289, 2019.
- B. Dafflon, Y. Wu, S. S. Hubbard, J. T. Birkholzer, T. M. Daley, J. D. Pugh, J. E. Peterson, and R. C. Trautz. Monitoring co2 intrusion and associated geochemical transformations in a shallow groundwater system using complex electrical methods. *Environmental science & technology*, 47(1) :314–321, 2013.
- B. Dafflon, R. Oktem, J. Peterson, C. Ulrich, A. P. Tran, V. Romanovsky, and S. S. Hubbard. Coincident aboveground and belowground autonomous monitoring to quantify covariability in permafrost, soil, and vegetation properties in arctic tundra. *Journal of Geophysical Research : Biogeosciences*, 122(6) :1321–1342, 2017.
- A.-M. Dagenais. *Techniques de contrôle du drainage minier acide basées sur les effets capillaires*. PhD thesis, École polytechnique, 2005.
- A.-M. Dagenais, M. Aubertin, B. Bussière, L. Bernier, and J. Cyr. Monitoring at the Lorraine mine site : a follow up on the remediation plan. *2001 National Association of Abandoned Mine Land Programs Annual Conference : Land Reborn : Tolls for the 21st Century, Athens, Ohio. Proceedings on CD-Rom*, 2001.
- A.-M. Dagenais, M. Aubertin, B. Bussière, and V. Martin. Large scale applications of covers with capillary barrier effects to control the production of acid mine drainage. *Proceedings of post-mining*, pages 16–17, 2005.
- A.-M. Dagenais, M. Mbonimpa, B. Bussière, and M. Aubertin. A modified oxygen consumption test to evaluate gas flux through oxygen barrier cover systems. *Geotechnical testing journal*, 35(1) :150–158, 2012.
- T. Dahlin, P. Aronsson, and M. Thörnelöf. Soil resistivity monitoring of an irrigation experiment. *Near Surface Geophysics*, 12(1) :35–44, 2014.
- T. M. Daley, B. M. Freifeld, J. Ajo-Franklin, S. Dou, R. Pevzner, V. Shulakova, S. Kashikar, D. E. Miller, J. Goetz, J. Hennings, et al. Field testing of fiber-optic distributed acoustic sensing (das) for subsurface seismic monitoring. *The Leading Edge*, 32(6) :699–706, 2013.
- M. Darijani and C. G. Farquharson. Inversion of magnetic and frequency-domain electromagnetic data for investigating lithologies associated with gold mineralization in the canadian malartic area, québec, canada. *Canadian Journal of Earth Sciences*, 58(5) :413–432, 2021.
- F. Day-Lewis, E. White, C. Johnson, J. Lane Jr, and M. Belaval. Continuous resistivity profiling to delineate submarine groundwater discharge—Examples and limitations. *The Leading Edge*, 25(6) :724–728, 2006. ISSN 1070-485X.

- F. D. Day-Lewis, C. D. Johnson, K. Singha, and J. W. Lane Jr. Best practices in electrical resistivity imaging : Data collection and processing, and application to data from corinna, maine. *EPA report, Boston, MA*, 2008.
- L. De Carlo, A. Battilani, D. Solimando, and M. C. Caputo. Application of time-lapse ert to determine the impact of using brackish wastewater for maize irrigation. *Journal of Hydrology*, page 124465, 2019.
- G. De Donno and E. Cardarelli. VEMI : a flexible interface for 3d tomographic inversion of time-and frequency-domain electrical data in EIDORS. *Near Surface Geophysics*, 15(1) : 43–58, 2017. ISSN 1873-0604.
- G. De Donno, L. Di Giambattista, and L. Orlando. High-resolution investigation of masonry samples through gpr and electrical resistivity tomography. *Construction and Building Materials*, 154 :1234–1249, 2017.
- R. De Franco, G. Biella, L. Tosi, P. Teatini, A. Lozej, B. Chiozzotto, M. Giada, F. Rizzetto, C. Claude, A. Mayer, et al. Monitoring the saltwater intrusion by time lapse electrical resistivity tomography : The chioggia test site (venice lagoon, italy). *Journal of Applied Geophysics*, 69(3-4) :117–130, 2009.
- L. B. B. de Melo, B. M. Silva, D. S. Peixoto, T. P. A. Chiarini, G. C. de Oliveira, and N. Curi. Effect of compaction on the relationship between electrical resistivity and soil water content in oxisol. *Soil and Tillage Research*, 208 :104876, 2021.
- P. De Vita, R. Di Maio, and E. Piegari. A study of the correlation between electrical resistivity and matric suction for unsaturated ash-fall pyroclastic soils in the campania region (southern italy). *Environmental Earth Sciences*, 67(3) :787–798, 2012.
- J. Deceuster, O. Kaufmann, and M. Van Camp. Automated identification of changes in electrode contact properties for long-term permanent ert monitoring experiments. *Geophysics*, 78(2) :E79–E94, 2013.
- D. Delforge, A. Watlet, O. Kaufmann, M. Van Camp, and M. Vanclooster. Time-series clustering approaches for subsurface zonation and hydrofacies detection using a real time-lapse electrical resistivity dataset. *Journal of Applied Geophysics*, 184 :104203, 2021.
- I. Demers and T. Pabst. Alternative and innovative integrated mine waste management approaches. *Hard Rock Mine Reclamation : From Prediction to Management of Acid Mine Drainage*, 2021a.
- I. Demers and T. Pabst. Covers with capillary barrier effects. *Hard Rock Mine Reclamation : From Prediction to Management of Acid Mine Drainage*, page 167, 2021b.
- Y. Deng, X. Shi, H. Xu, Y. Sun, J. Wu, and A. Revil. Quantitative assessment of electrical resistivity tomography for monitoring dnaps migration–comparison with high-resolution

- light transmission visualization in laboratory sandbox. *Journal of hydrology*, 544 :254–266, 2017.
- M. E. Denham, M. B. Amidon, H. M. Wainwright, B. Dafflon, J. Ajo-Franklin, and C. A. Eddy-Dilek. Improving long-term monitoring of contaminated groundwater at sites where attenuation-based remedies are deployed. *Environmental Management*, 66(6) :1142–1161, 2020.
- F.-E. M. Derfouf, Z.-S. Li, N. Abou-Bekr, S. Taibi, and J.-M. Fleureau. A new osmotic oedometer with electrical resistivity technique for monitoring water exchanges. *Geotechnical Testing Journal*, 43(3) :588–606, 2019.
- A. Dey and H. Morrison. Resistivity modelling for arbitrarily shaped two-dimensional structures. *Geophysical prospecting*, 27(1) :106–136, 1979.
- T. Dezert, Y. Fargier, S. P. Lopes, and P. Côte. Geophysical and geotechnical methods for fluvial levee investigation : A review. *Engineering Geology*, 260 :105206, 2019.
- M. G. Di Giuseppe and A. Troiano. Monitoring active fumaroles through time-lapse electrical resistivity tomograms : an application to the pisciarelli fumarolic field (campi flegrei, italy). *Journal of Volcanology and Geothermal Research*, 375 :32–42, 2019.
- J. Dick, D. Tetzlaff, J. Bradford, and C. Soulsby. Using repeat electrical resistivity surveys to assess heterogeneity in soil moisture dynamics under contrasting vegetation types. *Journal of Hydrology*, 559 :684–697, 2018. ISSN 0022-1694.
- S. Dietrich, P. A. Weinzettel, and M. Varni. Infiltration and drainage analysis in a heterogeneous soil by electrical resistivity tomography. *Soil Science Society of America Journal*, 78(4) :1153–1167, 2014.
- A. Dimech. Monitoring water infiltration in an experimental mine waste rock pile using 3d time-lapse electrical resistivity tomography [*Imagerie de l'écoulement de l'eau dans une halde à stériles expérimentale par tomographie 3D de résistivité électrique*]. Master's thesis, École Polytechnique de Montréal, 2018.
- A. Dimech, M. Chouteau, E. Chou, M. Aubertin, V. Martin, B. Bussière, and B. Plante. Monitoring water infiltration in an experimental waste rock pile with time-lapse ert and multi-parameter data collection. *Symposium on the Application of Geophysics to Engineering and Environmental Problems 2017*, pages 195–203, 2017. doi : 10.4133/SAGEEP.30-009.
- A. Dimech, M. Chouteau, B. Bussière, V. Martin, M. Aubertin, and B. Plante. 3d time-lapse geoelectrical monitoring of moisture content in an experimental waste rock pile : validation using hydrogeological data. *FastTIMES Special Issue Mine Site and Mining Geophysics*, 2018. doi : 10.4133/sageep.31-009.

- A. Dimech, M. Chouteau, M. Aubertin, B. Bussière, V. Martin, and B. Plante. Three-dimensional time-lapse geoelectrical monitoring of water infiltration in an experimental mine waste rock pile. *Vadose Zone Journal*, 18(1), 2019. doi : 10.2136/vzj2018.05.0098.
- A. Dimech, L. Cheng, B. Bussière, M. Chouteau, A. Isabelle, G. Fabien-Ouellet, P. Meldrum, P. Wilkinson, and J. Chambers. Using time-lapse electrical resistivity tomography to extend spatially the performance monitoring of large-scale experimental reclamation covers. *Symposium 2021 - Mines and the environment*, 2021.
- A. Dimech, L. Cheng, M. Chouteau, J. Chambers, S. Uhlemann, P. Wilkinson, P. Meldrum, B. Mary, G. Fabien-Ouellet, and A. Isabelle. A review on applications of time-lapse electrical resistivity tomography over the last 30 years : perspectives for mining waste monitoring. *Surveys in Geophysics*, 2022. doi : 10.1007/s10712-022-09731-2.
- A. Dimech, B. Bussière, L. Cheng, M. Chouteau, G. Fabien-Ouellet, N. Chevé, A. Isabelle, P. Wilkinson, P. Meldrum, and J. Chambers. Monitoring moisture dynamics in multi-layer cover systems for mine tailings reclamation using autonomous and remote time-lapse electrical resistivity tomography. *Submitted to Canadian Geotechnical Journal*, 2023a.
- A. Dimech, A. Isabelle, K. Sylvain, C. Liu, L. Cheng, B. Bussière, M. Chouteau, G. Fabien-Ouellet, C. Bérubé, P. Wilkinson, P. Meldrum, and J. Chambers. A multiscale accuracy assessment of moisture content predictions using time-lapse electrical resistivity tomography in mine tailings. *Submitted to Scientific Reports*, 2023b.
- M. M. P. F. do Nascimento, C. A. Moreira, B. G. Duz, and A. J. T. da Silveira. Geophysical diagnosis of diversion channel infiltration in a uranium waste rock pile. *Mine Water and the Environment*, pages 1–17, 2022.
- J. Doetsch, N. Linde, T. Vogt, A. Binley, and A. G. Green. Imaging and quantifying salt-tracer transport in a riparian groundwater system by means of 3d ERT monitoring. *Geophysics*, 77(5) :B207–B218, 2012. ISSN 0016-8033.
- W. Dorigo, W. Wagner, C. Albergel, F. Albrecht, G. Balsamo, L. Brocca, D. Chung, M. Ertl, M. Forkel, A. Gruber, et al. Esa cci soil moisture for improved earth system understanding : State-of-the art and future directions. *Remote Sensing of Environment*, 203 :185–215, 2017.
- F. Dubois-Roy. Caractérisation hydrogéotechnique préliminaire de la cellule expérimentale de mort-terrain (2m) de la mine canadienne malartic. *Research Institute of Mines and Environment*, 2021.
- A. Ebraheem, M. Hamburger, E. Bayless, and N. Krothe. A study of acid mine drainage using earth resistivity measurements. *Groundwater*, 28(3) :361–368, 1990. ISSN 0017-467X.

- O. El-Saadawy, A. Gaber, A. Othman, A. Z. Abotalib, M. El Bastawesy, and M. Attwa. Modeling flash floods and induced recharge into alluvial aquifers using multi-temporal remote sensing and electrical resistivity imaging. *Sustainability*, 12(23) :10204, 2020.
- A. Elghali, M. Benzaazoua, B. Bussière, and T. Genty. Spatial mapping of acidity and geochemical properties of oxidized tailings within the former eagle/telbel mine site. *Minerals*, 9(3) :180, 2019.
- M. Epov, N. Yurkevich, S. Bortnikova, Y. G. Karin, and O. Saeva. Analysis of mine waste by geochemical and geophysical methods (a case study of the mine tailing dump of the salair ore-processing plant). *Russian Geology and Geophysics*, 58(12) :1543–1552, 2017.
- M.-P. Ethier. *Évaluation de la performance d'un système de recouvrement monocouche avec nappe surélevée pour la restauration d'un parc à résidus miniers abandonné*. PhD thesis, Université du Québec en Abitibi-Témiscamingue, 2018.
- M.-P. Ethier, B. Bussière, M. Aubertin, A. Maqsoud, I. Demers, and S. Broda. In situ evaluation of performance of reclamation measures implemented on abandoned reactive tailings disposal site. *Canadian Geotechnical Journal*, 55(12) :1742–1755, 2018.
- B. Etzelmüller, M. Guglielmin, C. Hauck, C. Hilbich, M. Hoelzle, K. Isaksen, J. Noetzli, M. Oliva, and M. Ramos. Twenty years of european mountain permafrost dynamics—the pace legacy. *Environmental Research Letters*, 15(10) :104070, 2020.
- I. Fabregat, F. Gutiérrez, C. Roqué, X. Comas, M. Zarroca, D. Carbonel, J. Guerrero, and R. Linares. Reconstructing the internal structure and long-term evolution of hazardous sinkholes combining trenching, electrical resistivity imaging (eri) and ground penetrating radar (gpr). *Geomorphology*, 285 :287–304, 2017.
- O. Fala, J. Molson, M. Aubertin, and B. Bussière. Numerical modelling of flow and capillary barrier effects in unsaturated waste rock piles. *Mine Water and the Environment*, 24(4) : 172–185, 2005. ISSN 1025-9112.
- O. Fala, J. Molson, M. Aubertin, I. Dawood, B. Bussière, and R. Chapuis. A numerical modelling approach to assess long-term unsaturated flow and geochemical transport in a waste rock pile. *International Journal of Mining, Reclamation and Environment*, 27(1) : 38–55, 2013. ISSN 1748-0930.
- I. H. Falcon-Suarez, K. Livo, B. Callow, H. Marin-Moreno, M. Prasad, and A. I. Best. Geophysical early warning of salt precipitation during geological carbon sequestration. *Scientific reports*, 10(1) :1–14, 2020.
- S. Falzone, J. Robinson, and L. Slater. Characterization and monitoring of porous media with electrical imaging : a review. *Transport in Porous Media*, 130(1) :251–276, 2019.

- B. Fan, X. Liu, Q. Zhu, G. Qin, J. Li, H. Lin, and L. Guo. Exploring the interplay between infiltration dynamics and critical zone structures with multiscale geophysical imaging : A review. *Geoderma*, 374 :114431, 2020.
- J. Fan, A. Scheuermann, A. Guyot, T. Baumgartl, and D. A. Lockington. Quantifying spatiotemporal dynamics of root-zone soil water in a mixed forest on subtropical coastal sand dune using surface ert and spatial tdr. *Journal of Hydrology*, 523 :475–488, 2015.
- M. Farzamian, G. Vieira, F. Monteiro Santos, B. Yaghoobi Tabar, C. Hauck, M. C. Paz, I. Bernando, M. Ramos, and M. A. de Pablo. Detailed detection of fast changes in the active layer using quasi-continuous electrical resistivity tomography (deception island, antarctica). *The Cryosphere Discuss.*, <https://doi.org/10.5194/tc-2019-39>, in review, 2019.
- N. Florsch, M. Llubes, and F. Téreygeol. Induced polarization 3d tomography of an archaeological direct reduction slag heap. *Near Surface Geophysics*, 10(6) :567–574, 2012.
- R. Fortier, A.-M. LeBlanc, M. Allard, S. Buteau, and F. Calmels. Internal structure and conditions of permafrost mounds at Umiujaq in Nunavik, Canada, inferred from field investigation and electrical resistivity tomography. *Canadian Journal of Earth Sciences*, 45(3) : 367–387, 2008. ISSN 0008-4077.
- H. French and A. Binley. Snowmelt infiltration : monitoring temporal and spatial variability using time-lapse electrical resistivity. *Journal of Hydrology*, 297(1-4) :174–186, 2004. ISSN 0022-1694.
- H. K. French, C. Hardbattle, A. Binley, P. Winship, and L. Jakobsen. Monitoring snowmelt induced unsaturated flow and transport using electrical resistivity tomography. *Journal of Hydrology*, 267(3-4) :273–284, 2002.
- S. Friedel. Resolution, stability and efficiency of resistivity tomography estimated from a generalized inverse approach. *Geophysical Journal International*, 153(2) :305–316, 2003.
- S. Friedel, A. Thielen, and S. M. Springman. Investigation of a slope endangered by rainfall-induced landslides using 3d resistivity tomography and geotechnical testing. *Journal of Applied Geophysics*, 60(2) :100–114, 2006.
- S. P. Friedman. Soil properties influencing apparent electrical conductivity : a review. *Computers and electronics in agriculture*, 46(1-3) :45–70, 2005.
- Y. Fu, R. Horton, T. Ren, and J. Heitman. A general form of archie’s model for estimating bulk soil electrical conductivity. *Journal of Hydrology*, 597 :126160, 2021.
- A. Furman, T. P. Ferré, and G. L. Heath. Spatial focusing of electrical resistivity surveys considering geologic and hydrologic layering. *Geophysics*, 72(2) :F65–F73, 2007.

- M. Gabarrón, P. Martínez-Pagán, M. A. Martínez-Segura, M. C. Bueso, S. Martínez-Martínez, Á. Faz, and J. A. Acosta. Electrical resistivity tomography as a support tool for physicochemical properties assessment of near-surface waste materials in a mining tailing pond (el gorguel, se spain). *Minerals*, 10(6) :559, 2020.
- J. Gance, J.-P. Malet, R. Supper, P. Sailhac, D. Ottowitz, and B. Jochum. Permanent electrical resistivity measurements for monitoring water circulation in clayey landslides. *Journal of Applied Geophysics*, 126 :98–115, 2016. ISSN 0926-9851.
- S. Garré, M. Javaux, J. Vanderborght, L. Pagès, and H. Vereecken. Three-dimensional electrical resistivity tomography to monitor root zone water dynamics. *Vadose Zone Journal*, 10(1) :412–424, 2011.
- S. Garré, T. Günther, J. Diels, and J. Vanderborght. Evaluating experimental design of ert for soil moisture monitoring in contour hedgerow intercropping systems. *Vadose Zone Journal*, 11(4) :vzj2011–0186, 2012.
- S. Garré, I. Coteur, C. Wongleecharoen, T. Kongkaew, J. Diels, and J. Vanderborght. Noninvasive monitoring of soil water dynamics in mixed cropping systems : A case study in ratchaburi province, thailand. *Vadose Zone Journal*, 12(2) :1–12, 2013.
- S. Garré, D. Hyndman, B. Mary, and U. Werban. Geophysics conquering new territories : The rise of “agrogeophysics”. *Vadose Zone Journal*, (a) :e20115, 2021.
- S. Gascoin, M. Grizonnet, M. Bouchet, G. Salgues, and O. Hagolle. Theia snow collection : High-resolution operational snow cover maps from sentinel-2 and landsat-8 data. *Earth System Science Data*, 11(2) :493–514, 2019.
- D. Gervais, C. Roy, A. Thibault, C. Pednault, and D. Doucet. Technical report on the mineral resource and mineral reserve estimates for the canadian malartic property. *Mine Canadian Malartic*, 460, 2014.
- P.-L. Giertzuch, J. Doetsch, A. Shakas, M. Jalali, B. Brixel, and H. Maurer. Four-dimensional tracer flow reconstruction in fractured rock through borehole ground-penetrating radar (gpr) monitoring. *Solid Earth*, 12(7) :1497–1513, 2021.
- N. Giordano, C. Comina, and G. Mandrone. Laboratory scale geophysical measurements aimed at monitoring the thermal affected zone in underground thermal energy storage (utes) applications. *Geothermics*, 61 :121–134, 2016.
- P. Glover. What is the cementation exponent ? a new interpretation. *The Leading Edge*, 28 (1) :82–85, 2009.
- P. Glover. 11.04–geophysical properties of the near surface earth : Electrical properties. *Treatise on geophysics*, pages 89–137, 2015.

- P. W. Glover. A generalized archie's law for n phases. *Geophysics*, 75(6) :E247–E265, 2010.
- P. W. Glover. Archie's law—a reappraisal. *Solid Earth*, 7(4) :1157–1169, 2016.
- P. W. Glover. A new theoretical interpretation of archie's saturation exponent. *Solid Earth*, 8(4) :805–816, 2017.
- R. M. González, C. R. Cánovas, M. Olías, and F. Macías. Rare earth elements in a historical mining district (south-west spain) : Hydrogeochemical behaviour and seasonal variability. *Chemosphere*, 253 :126742, 2020.
- G. Grandjean, C. Hibert, F. Mathieu, E. Garel, and J.-P. Malet. Monitoring water flow in a clay-shale hillslope from geophysical data fusion based on a fuzzy logic approach. *Comptes Rendus Geoscience*, 341(10-11) :937–948, 2009.
- S. Grebby, A. Sowter, J. Gluyas, D. Toll, D. Gee, A. Athab, and R. Girindran. Advanced analysis of satellite data reveals ground deformation precursors to the brumadinho tailings dam collapse. *Communications Earth & Environment*, 2(1) :2, 2021.
- B. M. Greer, T. J. Burbey, C. E. Zipper, and E. T. Hester. Electrical resistivity imaging of hydrologic flow through surface coal mine valley fills with comparison to other landforms. *Hydrological processes*, 31(12) :2244–2260, 2017.
- N. Greggio, B. Giambastiani, E. Balugani, C. Amaini, and M. Antonellini. High-resolution electrical resistivity tomography (ert) to characterize the spatial extension of freshwater lenses in a salinized coastal aquifer. *Water*, 10(8) :1067, 2018.
- S. Grellier, R. Guérin, H. Robain, A. Bobachev, F. Vermeersch, and A. Tabbagh. Monitoring of leachate recirculation in a bioreactor landfill by 2-d electrical resistivity imaging. *Journal of Environmental & Engineering Geophysics*, 13(4) :351–359, 2008.
- M. Guittonny-Larchevêque, B. Bussière, and C. Pednault. Tree–substrate water relations and root development in tree plantations used for mine tailings reclamation. *Journal of environmental quality*, 45(3) :1036–1045, 2016a.
- M. Guittonny-Larchevêque, Y. Meddeb, and D. Barrette. Can graminoids used for mine tailings revegetation improve substrate structure? *Botany*, 94(11) :1053–1061, 2016b.
- D. Gunn, J. Chambers, S. Uhlemann, P. Wilkinson, P. Meldrum, T. Dijkstra, E. Haslam, M. Kirkham, J. Wragg, and S. Holyoake. Moisture monitoring in clay embankments using electrical resistivity tomography. *Construction and Building Materials*, 92 :82–94, 2015. ISSN 0950-0618.
- D. Gunn, J. Chambers, B. Dashwood, A. Lacinska, T. Dijkstra, S. Uhlemann, R. Swift, M. Kirkham, A. Milodowski, J. Wragg, et al. Deterioration model and condition monitoring of aged railway embankment using non-invasive geophysics. *Construction and Building Materials*, 170 :668–678, 2018.

- T. Günther and T. Martin. Spectral two-dimensional inversion of frequency-domain induced polarization data from a mining slag heap. *Journal of Applied Geophysics*, 135 :436–448, 2016.
- T. Günther, C. Rücker, and K. Spitzer. Three-dimensional modelling and inversion of dc resistivity data incorporating topography—ii. inversion. *Geophysical Journal International*, 166(2) :506–517, 2006.
- T. Günther, C. Rücker, and K. Spitzer. Three-dimensional modelling and inversion of DC resistivity data incorporating topography—II. Inversion. *Geophysical Journal International*, 166(2) :506–517, 2006. ISSN 1365-246X.
- F. R. Hampel. The influence curve and its role in robust estimation. *Journal of the american statistical association*, 69(346) :383–393, 1974.
- M. Hardie, J. Ridges, N. Swarts, and D. Close. Drip irrigation wetting patterns and nitrate distribution : comparison between electrical resistivity (eri), dye tracer, and 2d soil–water modelling approaches. *Irrigation science*, 36(2) :97–110, 2018.
- M. Hasan, Y. Shang, H. Meng, P. Shao, and X. Yi. Application of electrical resistivity tomography (ert) for rock mass quality evaluation. *Scientific Reports*, 11(1) :1–19, 2021.
- C. Hauck. *Geophysical methods for detecting permafrost in high mountains*. PhD thesis, ETH Zurich, 2001.
- C. Hauck, D. V. Mühlh, and H. Maurer. Using DC resistivity tomography to detect and characterize mountain permafrost. *Geophysical prospecting*, 51(4) :273–284, 2003. ISSN 1365-2478.
- C. Hauck, M. Böttcher, and H. Maurer. A new model for estimating subsurface ice content based on combined electrical and seismic data sets. *The Cryosphere*, 5(2) :453–468, 2011. ISSN 1994-0416.
- M. Hayashi. Temperature-electrical conductivity relation of water for environmental monitoring and geophysical data inversion. *Environmental monitoring and assessment*, 96(1) : 119–128, 2004.
- K. Hayley, L. R. Bentley, M. Gharibi, and M. Nightingale. Low temperature dependence of electrical resistivity : Implications for near surface geophysical monitoring. *Geophysical research letters*, 34(18), 2007.
- K. Hayley, L. Bentley, and A. Pidlisecky. Compensating for temperature variations in time-lapse electrical resistivity difference imaging. *Geophysics*, 75(4) :WA51–WA59, 2010.
- K. Hayley, A. Pidlisecky, and L. Bentley. Simultaneous time-lapse electrical resistivity inversion. *Journal of Applied Geophysics*, 75(2) :401–411, 2011.

- L. J. Heagy, R. Cockett, S. Kang, G. K. Rosenkjaer, and D. W. Oldenburg. A framework for simulation and inversion in electromagnetics. *Computers & Geosciences*, 107 :1–19, 2017.
- J. Heenan, L. D. Slater, D. Ntarlagiannis, E. A. Atekwana, B. Z. Fathepure, S. Dalvi, C. Ross, D. D. Werkema, and E. A. Atekwana. Electrical resistivity imaging for long-term autonomous monitoring of hydrocarbon degradation : Lessons from the deepwater horizon oil spill. *Geophysics*, 80(1) :B1–B11, 2015.
- R. Hen-Jones, P. Hughes, R. Stirling, S. Glendinning, J. Chambers, D. Gunn, and Y. Cui. Seasonal effects on geophysical–geotechnical relationships and their implications for electrical resistivity tomography monitoring of slopes. *Acta Geotechnica*, 12(5) :1159–1173, 2017a.
- R. Hen-Jones, P. Hughes, R. Stirling, S. Glendinning, J. Chambers, D. Gunn, and Y. Cui. Seasonal effects on geophysical–geotechnical relationships and their implications for electrical resistivity tomography monitoring of slopes. *Acta Geotechnica*, 12(5) :1159–1173, 2017b.
- R. D. Henderson, F. D. Day-Lewis, E. Abarca, C. F. Harvey, H. N. Karam, L. Liu, and J. W. Lane. Marine electrical resistivity imaging of submarine groundwater discharge : sensitivity analysis and application in waquoit bay, massachusetts, usa. *Hydrogeology Journal*, 18(1) : 173–185, 2010.
- T. Hermans, A. Vandenbohede, L. Lebbe, and F. Nguyen. A shallow geothermal experiment in a sandy aquifer monitored using electric resistivity tomography. *Geophysics*, 77(1) :B11–B21, 2012. ISSN 0016-8033.
- T. Hermans, F. Nguyen, T. Robert, and A. Revil. Geophysical methods for monitoring temperature changes in shallow low enthalpy geothermal systems. *Energies*, 7(8) :5083–5118, 2014.
- T. Hermans, F. Nguyen, M. Klepikova, A. Dassargues, and J. Caers. Uncertainty quantification of medium-term heat storage from short-term geophysical experiments using bayesian evidential learning. *Water Resources Research*, 54(4) :2931–2948, 2018.
- T. Herring, E. Cey, and A. Pidlisecky. Electrical resistivity of a partially saturated porous medium at subzero temperatures. *Vadose Zone Journal*, 18(1) :1–11, 2019.
- T. Herring, A. Pidlisecky, and E. Cey. Removing the effects of temperature on electrical resistivity tomography data collected in partially frozen ground : Limitations and considerations for field applications. *Vadose Zone Journal*, 20(5) :e20146, 2021.
- E. T. Hester, K. L. Little, J. D. Buckwalter, C. E. Zipper, and T. J. Burbey. Variability of subsurface structure and infiltration hydrology among surface coal mine valley fills. *Science of the total environment*, 651 :2648–2661, 2019.

- M. Hilhorst. A pore water conductivity sensor. *Soil Science Society of America Journal*, 64 (6) :1922–1925, 2000. ISSN 1435-0661.
- A. Hojat, D. Arosio, V. I. Ivanov, M. H. Loke, L. Longoni, M. Papini, G. Tresoldi, and L. Zanzi. Quantifying seasonal 3d effects for a permanent electrical resistivity tomography monitoring system along the embankment of an irrigation canal. *Near Surface Geophysics*, 18(Geoelectrical Monitoring) :427–443, 2020.
- J. Holmes, J. Chambers, P. Meldrum, P. Wilkinson, J. Boyd, P. Williamson, D. Huntley, K. Sattler, D. Elwood, V. Sivakumar, et al. Four-dimensional electrical resistivity tomography for continuous, near-real-time monitoring of a landslide affecting transport infrastructure in british columbia, canada. *Near Surface Geophysics*, 2020.
- J. Holmes, J. Chambers, P. Wilkinson, B. Dashwood, D. Gunn, M. Cimpoiaşu, M. Kirkham, S. Uhlemann, P. Meldrum, O. Kuras, et al. 4d electrical resistivity tomography for assessing the influence of vegetation and subsurface moisture on railway cutting condition. *Engineering Geology*, 307 :106790, 2022a.
- J. Holmes, J. Chambers, P. Wilkinson, P. Meldrum, M. Cimpoiaşu, J. Boyd, D. Huntley, P. Williamson, D. Gunn, B. Dashwood, et al. Application of petrophysical relationships to electrical resistivity models for assessing the stability of a landslide in british columbia, canada. *Engineering Geology*, 301 :106613, 2022b.
- G. Hotton, B. Bussière, T. Pabst, É. Bresson, and P. Roy. Influence of climate change on the ability of a cover with capillary barrier effects to control acid generation. *Hydrogeology Journal*, pages 1–17, 2019.
- E. Hudson, B. Kulesa, P. Edwards, T. Williams, and R. Walsh. Integrated hydrological and geophysical characterisation of surface and subsurface water contamination at abandoned metal mines. *Water, Air, & Soil Pollution*, 229(8) :1–14, 2018.
- S. Hui, L. Charlebois, and C. Sun. Real-time monitoring for structural health, public safety, and risk management of mine tailings dams. *Canadian Journal of Earth Sciences*, 55(3) : 221–229, 2018.
- D. Huntley, P. Bobrowsky, M. Hendry, R. Macciotta, D. Elwood, K. Sattler, M. Best, J. Chambers, and P. Meldrum. Application of multi-dimensional electrical resistivity tomography datasets to investigate a very slow-moving landslide near ashcroft, british columbia, canada. *Landslides*, 16(5) :1033–1042, 2019.
- R. Hübner, K. Heller, T. Günther, and A. Kleber. Monitoring hillslope moisture dynamics with surface ERT for enhancing spatial significance of hydrometric point measurements. *Hydrology and Earth System Sciences*, 19(1) :225–240, 2015. ISSN 1027-5606.

- R. Hübner, T. Günther, K. Heller, U. Noell, and A. Kleber. Impacts of a capillary barrier on infiltration and subsurface stormflow in layered slope deposits monitored with 3-D ERT and hydrometric measurements. *Hydrology and Earth System Sciences*, 21(10) :5181, 2017. ISSN 1607-7938.
- C. Inauen, J. Chambers, A. Watlet, J. Whiteley, D. Gunn, B. Dashwood, P. Wilkinson, A. Brooks, O. Neal, D. Scott, D. Caterina, I. Isunza Manrique, X. Piquet, and A. Dimech. Landfill characterization with a multi-method geophysical approach—a case study from emersons green, uk. In *25th European Meeting of Environmental and Engineering Geophysics*, volume 2019, pages 1–5. European Association of Geoscientists & Engineers, 2019.
- E. Intrieri, G. Gigli, N. Casagli, and F. Nadim. Brief communication " landslide early warning system : toolbox and general concepts". *Natural hazards and earth system sciences*, 13(1) : 85–90, 2013.
- A. Isabelle. Hydrogeophysical data assimilation using ensemble kalman filters to predict moisture content in mining reclamation covers [*Assimilation de données hydrogéophysiques par filtre de Kalman d'ensemble pour l'estimation de la teneur en eau en restauration minière*]. Master's thesis, École Polytechnique de Montréal, 2022.
- M. James, M. Aubertin, and B. Bussière. On the use of waste rock inclusions to improve the performance of tailings impoundments. In *Proceedings of the 18th International Conference Soil Mechanics and Geotechnical Engineering, Paris, France*, pages 2–6, 2013.
- D. H. Jayawickreme, R. L. Van Dam, and D. W. Hyndman. Hydrological consequences of land-cover change : Quantifying the influence of plants on soil moisture with time-lapse electrical resistivity. *Geophysics*, 75(4) :WA43–WA50, 2010.
- K. H. Jensen and J. C. Refsgaard. Hobe : The danish hydrological observatory. *Vadose Zone Journal*, 17(1) :1–24, 2018.
- L. Jiang, G. Tian, B. Wang, X. Guo, X. He, A. Zou, H. Chen, T. Yang, and A. Abd El-Raouf. Application of three-dimensional electrical resistivity tomography in urban zones by arbitrary electrode distribution survey design. *Journal of Applied Geophysics*, 194 :104460, 2021a.
- L. Jiang, B. Wang, G. Tian, X. He, A. Zou, X. Guo, H. Chen, and A. A. El-Raouf. Strategy for optimization of arbitrary electrode distribution for 3d electrical resistivity tomography in urban zones. *Pure and Applied Geophysics*, 178(9) :3601–3618, 2021b.
- B. Jodeiri Shokri, F. Shafaei, F. Doulati Ardejani, A. Mirzaghobanali, and S. Entezam. Use of time-lapse 2d and 3d geoelectrical inverse models for monitoring acid mine drainage—a case study. *Soil and Sediment Contamination : An International Journal*, pages 1–24, 2022.

- C. Jodry, S. P. Lopes, Y. Fargier, M. Sanchez, and P. Cote. 2d-ert monitoring of soil moisture seasonal behaviour in a river levee : A case study. *Journal of Applied Geophysics*, 167 :140–151, 2019.
- S. Johansson, T. Dahlin, et al. Seepage monitoring in an earth embankment dam by repeated resistivity measurements. *European Journal of Engineering and Environmental Geophysics*, 1(3) :229–247, 1996.
- T. C. Johnson, R. J. Versteeg, A. Ward, F. D. Day-Lewis, and A. Revil. Improved hydrogeophysical characterization and monitoring through parallel modeling and inversion of time-domain resistivity and induced-polarization data. *Geophysics*, 75(4) :WA27–WA41, 2010. ISSN 0016-8033.
- T. C. Johnson, L. D. Slater, D. Ntarlagiannis, F. D. Day-Lewis, and M. Elwaseif. Monitoring groundwater-surface water interaction using time-series and time-frequency analysis of transient three-dimensional electrical resistivity changes. *Water Resources Research*, 48(7), 2012a.
- T. C. Johnson, R. J. Versteeg, M. Rockhold, L. D. Slater, D. Ntarlagiannis, W. J. Greenwood, and J. Zachara. Characterization of a contaminated wellfield using 3d electrical resistivity tomography implemented with geostatistical, discontinuous boundary, and known conductivity constraints. *Geophysics*, 77(6) :EN85–EN96, 2012b.
- T. C. Johnson, R. J. Versteeg, F. D. Day-Lewis, W. Major, and J. W. Lane Jr. Time-lapse electrical geophysical monitoring of amendment-based biostimulation. *Groundwater*, 53(6) : 920–932, 2015.
- T. C. Johnson, G. E. Hammond, and X. Chen. PFLOTRAN-E4d : A parallel open source PFLOTRAN module for simulating time-lapse electrical resistivity data. *Computers & Geosciences*, 99 :72–80, 2017. ISSN 0098-3004.
- A. Johnston, R. L. Runkel, A. Navarre-Sitchler, and K. Singha. Exploration of diffuse and discrete sources of acid mine drainage to a headwater mountain stream in colorado, usa. *Mine Water and the Environment*, 36(4) :463–478, 2017.
- D. Jougnot, N. Linde, E. B. Haarder, and M. C. Looms. Monitoring of saline tracer movement with vertically distributed self-potential measurements at the hobe agricultural test site, vouldund, denmark. *Journal of Hydrology*, 521 :314–327, 2015.
- A. Kalonji-Kabambi, B. Bussière, and I. Demers. Hydrogeological behaviour of covers with capillary barrier effects made of mining materials. *Geotechnical and Geological Engineering*, 35(3) :1199–1220, 2017.

- A. Kalonji-Kabambi, B. Bussière, and I. Demers. Hydrogeochemical behavior of reclaimed highly reactive tailings, part 2 : Laboratory and field results of covers made with mine waste materials. *Minerals*, 10(7) :589, 2020.
- X. Kang, X. Shi, Y. Deng, A. Revil, H. Xu, and J. Wu. Coupled hydrogeophysical inversion of dnapl source zone architecture and permeability field in a 3d heterogeneous sandbox by assimilation time-lapse cross-borehole electrical resistivity data via ensemble kalman filtering. *Journal of Hydrology*, 567 :149–164, 2018.
- X. Kang, X. Shi, A. Revil, Z. Cao, L. Li, T. Lan, and J. Wu. Coupled hydrogeophysical inversion to identify non-gaussian hydraulic conductivity field by jointly assimilating geochemical and time-lapse geophysical data. *Journal of Hydrology*, 578 :124092, 2019.
- M. Karaoulis, P. Tsourlos, J.-H. Kim, and A. Revil. 4d time-lapse ERT inversion : Introducing combined time and space constraints. *Near Surface Geophysics*, 12(1) :25–34, 2014. ISSN 1873-0604.
- K. K. Karkkainen, A. H. Sihvola, and K. I. Nikoskinen. Effective permittivity of mixtures : numerical validation by the fdtd method. *IEEE Transactions on Geoscience and Remote Sensing*, 38(3) :1303–1308, 2000.
- M. Keuschnig, M. Krautblatter, I. Hartmeyer, C. Fuß, and L. Schrott. Automated electrical resistivity tomography testing for early warning in unstable permafrost rock walls around alpine infrastructure. *Permafrost and Periglacial Processes*, 28(1) :158–171, 2017.
- T. A. Khan and S. H. Ling. Review on electrical impedance tomography : Artificial intelligence methods and its applications. *Algorithms*, 12(5) :88, 2019.
- G. Kibria, S. Hossain, and M. S. Khan. Determination of consolidation properties using electrical resistivity. *Journal of Applied Geophysics*, 152 :150–160, 2018.
- D. Kiessling, C. Schmidt-Hattenberger, H. Schuett, F. Schilling, K. Krueger, B. Schoebel, E. Danckwardt, J. Kummerow, C. Group, et al. Geoelectrical methods for monitoring geological co2 storage : First results from cross-hole and surface–downhole measurements from the co2sink test site at ketzin (germany). *International Journal of Greenhouse Gas Control*, 4(5) :816–826, 2010.
- H. G. Kiflu. Improved 2d and 3d resistivity surveys using buried electrodes and optimized arrays : The multi-electrode resistivity implant technique (MERIT). 2016.
- J.-H. Kim, M.-J. Yi, S.-G. Park, and J. G. Kim. 4-D inversion of DC resistivity monitoring data acquired over a dynamically changing earth model. *Journal of Applied Geophysics*, 68 (4) :522–532, 2009. ISSN 0926-9851.
- A. King and J. McNeill. *Applications of Geophysical Methods for Monitoring Acid Mine Drainage*. Canada Centre for Mineral and Energy Technology, 1994.

- P. H.-M. Kinnunen and A. H. Kaksonen. Towards circular economy in mining : Opportunities and bottlenecks for tailings valorization. *Journal of cleaner production*, 228 :153–160, 2019.
- D. R. Klazinga, C. M. Steelman, A. L. Endres, and B. L. Parker. Geophysical response to simulated methane migration in groundwater based on a controlled injection experiment in a sandy unconfined aquifer. *Journal of Applied Geophysics*, 168 :59–70, 2019.
- G. Kłosowski, T. Rymarczyk, and A. Gola. Increasing the reliability of flood embankments with neural imaging method. *Applied Sciences*, 8(9) :1457, 2018.
- C. Kneisel, C. Hauck, R. Fortier, and B. Moorman. Advances in geophysical methods for permafrost investigations. *Permafrost and Periglacial Processes*, 19(2) :157–178, 2008. ISSN 1045-6740.
- J. Koestel, A. Kemna, M. Javaux, A. Binley, and H. Vereecken. Quantitative imaging of solute transport in an unsaturated and undisturbed soil monolith with 3-D ERT and TDR. *Water Resources Research*, 44(12), 2008. ISSN 1944-7973.
- J. Koestel, R. Kasteel, A. Kemna, O. Esser, M. Javaux, A. Binley, and H. Vereecken. Imaging brilliant blue stained soil by means of electrical resistivity tomography. *Vadose Zone Journal*, 8(4) :963–975, 2009. ISSN 1539-1663.
- D. Kossoff, W. Dubbin, M. Alfredsson, S. Edwards, M. Macklin, and K. A. Hudson-Edwards. Mine tailings dams : characteristics, failure, environmental impacts, and remediation. *Applied Geochemistry*, 51 :229–245, 2014.
- M. Krautblatter, S. Verleysdonk, A. Flores-Orozco, and A. Kemna. Temperature-calibrated imaging of seasonal changes in permafrost rock walls by quantitative electrical resistivity tomography (zugspitze, german/austrian alps). *Journal of Geophysical Research : Earth Surface*, 115(F2), 2010.
- T. Kremer, C. Vieira, and A. Maineult. ERT monitoring of gas injection into water saturated sands : Modeling and inversion of cross-hole laboratory data. *Journal of Applied Geophysics*, 2018. ISSN 0926-9851.
- A. S. Kuhl, A. D. Kendall, R. L. Van Dam, and D. W. Hyndman. Quantifying soil water and root dynamics using a coupled hydrogeophysical inversion. *Vadose Zone Journal*, 17 (1) :1–13, 2018.
- O. Kuras, R. Ogilvy, P. Meldrum, J. Gisbert, S. Jorreto, I. Francés, A. Vallejos, F. S. Martos, J. Calaforra, and A. P. Bosch. Monitoring coastal aquifers with Automated time-Lapse Electrical Resistivity Tomography (ALERT) : Initial results from the Andarax delta, SE Spain. *Gestion Intégrée des Ressources en Eaux et Défis du Développement Durable*, 2006.

- O. Kuras, J. D. Pritchard, P. I. Meldrum, J. E. Chambers, P. B. Wilkinson, R. D. Ogilvy, and G. P. Wealthall. Monitoring hydraulic processes with automated time-lapse electrical resistivity tomography (alert). *Comptes Rendus Geoscience*, 341(10-11) :868–885, 2009.
- O. Kuras, P. B. Wilkinson, P. I. Meldrum, L. S. Oxby, S. Uhlemann, J. E. Chambers, A. Binley, J. Graham, N. T. Smith, and N. Atherton. Geoelectrical monitoring of simulated subsurface leakage to support high-hazard nuclear decommissioning at the Sellafield Site, UK. *Science of the Total Environment*, 566 :350–359, 2016. ISSN 0048-9697.
- P.-L. Labonté-Raymond, T. Pabst, B. Bussière, and É. Bresson. Impact of climate change on extreme rainfall events and surface water management at mine waste storage facilities. *Journal of Hydrology*, 590 :125383, 2020.
- D. LaBrecque and W. Daily. Assessment of measurement errors for galvanic-resistivity electrodes of different composition. *Geophysics*, 73(2) :F55–F64, 2008.
- D. J. LaBrecque and X. Yang. Difference inversion of ert data : A fast inversion method for 3-d in situ monitoring. *Journal of Environmental & Engineering Geophysics*, 6(2) :83–89, 2001.
- A. Lachhab, E. M. Benyassine, M. Rouai, A. Dekayir, J. C. Parisot, and M. Boujamaoui. Integration of multi-geophysical approaches to identify potential pathways of heavy metals contamination—a case study in zeida, morocco. *Journal of Environmental and Engineering Geophysics*, 25(3) :415–423, 2020.
- C. Lafrenière-Bérubé. *Intégration des signatures pétrophysiques et minéralogiques de l’empreinte hydrothermale du gisement d’or Canadian Malartic*. PhD thesis, École Polytechnique de Montréal, 2018.
- B. Lahmira, R. Lefebvre, M. Aubertin, and B. Bussière. Effect of material variability and compacted layers on transfer processes in heterogeneous waste rock piles. *Journal of contaminant hydrology*, 204 :66–78, 2017.
- E. Laloy, M. Javaux, M. Vanclooster, C. Roisin, and C. Biielders. Electrical resistivity in a loamy soil : Identification of the appropriate pedo-electrical model. *Vadose Zone Journal*, 10(3) :1023–1033, 2011.
- M. Larchevêque, A. Desrochers, B. Bussière, and D. Cimon. Planting trees in soils above non-acid-generating wastes of a boreal gold mine. *Ecoscience*, 21(3-4) :217–231, 2014.
- C. G. Larochelle, B. Bussière, and T. Pabst. Acid-generating waste rocks as capillary break layers in covers with capillary barrier effects for mine site reclamation. *Water, Air, & Soil Pollution*, 230(3) :1–16, 2019.

- J. Lavoie-Deraspe. Étude du comportement hydrogéologique de couvertures avec effets de barrière capillaire sur une halde à stériles de grande dimension. Master's thesis, Polytechnique Montréal, 2019.
- V. Le Borgne, A. Siamaki, and A. Dulmage. Review of modern recommendations for monitoring of tailings storage facilities. *Tailings and Mine Waste Conference, Hyatt Regency – Denver Tech Center*, 2022.
- T. Lebourg, S. Binet, E. Tric, H. Jomard, and S. El Bedoui. Geophysical survey to estimate the 3d sliding surface and the 4d evolution of the water pressure on part of a deep seated landslide. *Terra Nova*, 17(5) :399–406, 2005.
- J. Lee and J. C. Santamarina. Electrical resistivity tomography in cylindrical cells—guidelines for hardware pre-design. *Geotechnical Testing Journal*, 33(1) :23–32, 2010.
- P. Lehmann, F. Gambazzi, B. Suski, L. Baron, A. Askarinejad, S. M. Springman, K. Holliger, and D. Or. Evolution of soil wetting patterns preceding a hydrologically induced landslide inferred from electrical resistivity survey and point measurements of volumetric water content and pore water pressure. *Water Resources Research*, 49(12) :7992–8004, 2013.
- D. P. Lesmes and S. P. Friedman. Relationships between the electrical and hydrogeological properties of rocks and soils. In *Hydrogeophysics*, pages 87–128. Springer, 2005.
- N. Lesparre, F. Nguyen, A. Kemna, T. Robert, T. Hermans, M. Daoudi, and A. Flores-Orozco. A new approach for time-lapse data weighting in electrical resistivity tomography. *Geophysics*, 82(6) :E325–E333, 2017. ISSN 0016-8033.
- N. Lesparre, T. Robert, F. Nguyen, A. Boyle, and T. Hermans. 4d electrical resistivity tomography (ert) for aquifer thermal energy storage monitoring. *Geothermics*, 77 :368–382, 2019.
- Q.-m. Li, H.-n. Yuan, and M.-h. Zhong. Safety assessment of waste rock dump built on existing tailings ponds. *Journal of Central South University*, 22(7) :2707–2718, 2015.
- S. Li, L. Yuan, H. Yang, H. An, and G. Wang. Tailings dam safety monitoring and early warning based on spatial evolution process of mud-sand flow. *Safety science*, 124 :104579, 2020.
- C. Ling and Q. Zhang. Evaluation of surface water and groundwater contamination in a msw landfill area using hydrochemical analysis and electrical resistivity tomography : a case study in sichuan province, southwest china. *Environmental monitoring and assessment*, 189 (4) :140, 2017.
- C. Ling, A. Revil, Y. Qi, F. Abdulsamad, P. Shi, S. Nicaise, and L. Peyras. Application of the mise-à-la-masse method to detect the bottom leakage of water reservoirs. *Engineering Geology*, 261 :105272, 2019.

- B. Liu, Z. Liu, S. Li, K. Fan, L. Nie, and X. Zhang. An improved time-lapse resistivity tomography to monitor and estimate the impact on the groundwater system induced by tunnel excavation. *Tunnelling and Underground Space Technology*, 66 :107–120, 2017.
- M. Loke, J. Chambers, D. Rucker, O. Kuras, and P. Wilkinson. Recent developments in the direct-current geoelectrical imaging method. *Journal of Applied Geophysics*, 95 :135–156, 2013.
- M. Loke, T. Dahlin, and D. Rucker. Smoothness-constrained time-lapse inversion of data from 3d resistivity surveys. *Near Surface Geophysics*, 12(1) :5–24, 2014a.
- M. Loke, P. Wilkinson, J. Chambers, and M. Strutt. Optimized arrays for 2d cross-borehole electrical tomography surveys. *Geophysical Prospecting*, 62(1) :172–189, 2014b. ISSN 1365-2478.
- M. Loke, P. Wilkinson, S. Uhlemann, J. Chambers, and L. Oxby. Computation of optimized arrays for 3-D electrical imaging surveys. *Geophysical Journal International*, 199(3) :1751–1764, 2014c. ISSN 1365-246X.
- M. Loke, H. Kiflu, P. Wilkinson, D. Harro, and S. Kruse. Optimized arrays for 2d resistivity surveys with combined surface and buried arrays. *Near Surface Geophysics*, 13(5) :505–517, 2015a.
- M. Loke, P. Wilkinson, J. Chambers, S. Uhlemann, and J. Sorensen. Optimized arrays for 2-D resistivity survey lines with a large number of electrodes. *Journal of Applied Geophysics*, 112 :136–146, 2015b. ISSN 0926-9851.
- M. Loke, P. Wilkinson, J. Chambers, S. Uhlemann, T. Dijkstra, and T. Dahlin. The use of asymmetric time constraints in 4-d ert inversion. *Journal of Applied Geophysics*, 197 : 104536, 2022.
- M. H. Loke. Tutorial : 2-d and 3-d electrical imaging surveys, 2018.
- M. H. Loke, I. Acworth, and T. Dahlin. A comparison of smooth and blocky inversion methods in 2d electrical imaging surveys. *Exploration geophysics*, 34(3) :182–187, 2003.
- M. Long, S. Donohue, J.-S. L’Heureux, I.-L. Solberg, J. S. Rønning, R. Limacher, P. O’Connor, G. Sauvin, M. Rømøen, and I. Lecomte. Relationship between electrical resistivity and basic geotechnical parameters for marine clays. *Canadian Geotechnical Journal*, 49(10) : 1158–1168, 2012.
- J. López, M. Reig, X. Vecino, and J. Cortina. Arsenic impact on the valorisation schemes of acidic mine waters of the iberian pyrite belt : Integration of selective precipitation and spiral-wound nanofiltration processes. *Journal of hazardous materials*, 403 :123886, 2021.

- M. López-Sánchez, L. Mansilla-Plaza, and M. Sánchez-de laOrden. Geometric factor and influence of sensors in the establishment of a resistivity-moisture relation in soil samples. *Journal of Applied Geophysics*, 145 :1–11, 2017.
- D. Lumbroso, M. R. Collell, G. Petkovsek, M. Davison, Y. Liu, C. Goff, and M. Wetton. Damsat : An eye in the sky for monitoring tailings dams. *Mine Water and the Environment*, 40(1) :113–127, 2021.
- Z. Luo, H. Guan, and X. Zhang. The temperature effect and correction models for using electrical resistivity to estimate wood moisture variations. *Journal of Hydrology*, 578 : 124022, 2019.
- Z. Luo, Z. Deng, K. Singha, X. Zhang, N. Liu, Y. Zhou, X. He, and H. Guan. Temporal and spatial variation in water content within living tree stems determined by electrical resistivity tomography. *Agricultural and Forest Meteorology*, 291 :108058, 2020.
- C. Lyu, Q. Sun, and W. Zhang. Real-time geoelectric monitoring of seepage into sand and clay layer. *Groundwater Monitoring & Remediation*, 39(4) :80–88, 2019a.
- Z. Lyu, J. Chai, Z. Xu, Y. Qin, and J. Cao. A comprehensive review on reasons for tailings dam failures based on case history. *Advances in Civil Engineering*, 2019, 2019b.
- R. Ma, A. McBratney, B. Whelan, B. Minasny, and M. Short. Comparing temperature correction models for soil electrical conductivity measurement. *Precision Agriculture*, 12 (1) :55–66, 2011.
- C. K. J. Macleod, M. W. Humphreys, W. R. Whalley, L. Turner, A. Binley, C. W. Watts, L. Skøt, A. Joynes, S. Hawkins, I. P. King, et al. A novel grass hybrid to reduce flood generation in temperate regions. *Scientific reports*, 3(1) :1–7, 2013.
- P. Madejón, D. Caro-Moreno, C. M. Navarro-Fernández, S. Rossini-Oliva, and T. Marañón. Rehabilitation of waste rock piles : Impact of acid drainage on potential toxicity by trace elements in plants and soil. *Journal of Environmental Management*, 280 :111848, 2021.
- S. Maghsoudy, F. D. Ardejani, J. Molson, M. Amini, and L. Ebrahimi. Application of geoelectrical tomography in coupled hydro-mechanical–chemical investigations in heap leaching. *Mine Water and the Environment*, 38(1) :197–212, 2019.
- G. Mainali. *Monitoring of tailings dams with geophysical methods*. PhD thesis, Luleå tekniska universitet, 2006.
- G. Mainali, E. Nordlund, S. Knutsson, and H. Thunehed. Tailings dams monitoring in swedish mines using self-potential and electrical resistivity methods. *Electronic Journal of Geotechnical Engineering*, 20 :5859–5875, 2015.

- A. Maqsoud, B. Bussiere, M. Aubertin, M. Chouteau, and M. Mbonimpa. Field investigation of a suction break designed to control slope-induced desaturation in an oxygen barrier. *Canadian Geotechnical Journal*, 48(1) :53–71, 2011. ISSN 0008-3674.
- A. Maqsoud, B. Bussière, M. Aubertin, and M. Mbonimpa. Predicting hysteresis of the water retention curve from basic properties of granular soils. *Geotechnical and Geological Engineering*, 30(5) :1147–1159, 2012.
- A. Maqsoud, B. Bussière, and M. Mbonimpa. Low saturated hydraulic conductivity covers. *Hard Rock Mine Reclamation : From Prediction to Management of Acid Mine Drainage*, 2021.
- M. Markovaara-Koivisto, T. Valjus, T. Tarvainen, T. Huotari, J. Lerssi, M. Eklund, et al. Preliminary volume and concentration estimation of the aijala tailings pond—evaluation of geophysical methods. *Resources Policy*, 59(C) :7–16, 2018.
- R. Markovic, M. Bessho, N. Masuda, Z. Stevanovic, D. Bozic, T. Apostolovski Trujic, and V. Gardic. New approach of metals removal from acid mine drainage. *Applied Sciences*, 10(17) :5925, 2020.
- T. Martin, K. Kuhn, T. Günther, and R. Kniess. Geophysical exploration of a historical stamp mill dump for the volume estimation of valuable residues. *Journal of Environmental and Engineering Geophysics*, 25(2) :275–286, 2020.
- V. Martin, B. Bussière, B. Plante, T. Pabst, M. Aubertin, F. Medina, M.-L. B. Lanoix, A. Dimech, J. Dubuc, and B. Poaty. Controlling water infiltration in waste rock piles : Design, construction, and monitoring of a large-scale in-situ pilot test pile. *70th Canadian Geotechnical Conference, Ottawa, Ontario, Canada*, 2017.
- V. Martin, T. Pabst, B. Bussière, B. Plante, and M. Aubertin. A new approach to control contaminated mine drainage generation from waste rock piles : Lessons learned after 4 years of field monitoring. *Proceedings of GeoEnvironmental Engineering 2019 Concordia Montréal*, 2019.
- T. Martín-Crespo, C. De Ignacio-San José, D. Gómez-Ortiz, S. Martín-Velázquez, and J. Lillo-Ramos. Monitoring study of the mine pond reclamation of mina concepción, iberian pyrite belt (spain). *Environmental Earth Sciences*, 59(6) :1275, 2010.
- T. Martín-Crespo, D. Gómez-Ortiz, S. Martín-Velázquez, P. Martínez-Pagán, C. De Ignacio, J. Lillo, and Á. Faz. Geoenvironmental characterization of unstable abandoned mine tailings combining geophysical and geochemical methods (cartagena-la union district, spain). *Engineering Geology*, 232 :135–146, 2018.

- T. Martín-Crespo, D. Gómez-Ortiz, and S. Martín-Velázquez. Geoenvironmental characterization of sulfide mine tailings. In *Applied Geochemistry with Case Studies on Geological Formations, Exploration Techniques and Environmental Issues*. IntechOpen, 2019.
- T. Martín-Crespo, D. Gómez-Ortiz, S. Martín-Velázquez, P. Martínez-Pagán, C. de Ignacio-San José, J. Lillo, and Á. Faz. Abandoned mine tailings affecting riverbed sediments in the cartagena–la union district, mediterranean coastal area (spain). *Remote Sensing*, 12(12) : 2042, 2020.
- J. Martínez, J. Rey, M. Hidalgo, and J. Benavente. Characterizing abandoned mining dams by geophysical (eri) and geochemical methods : the linares-la carolina district (southern spain). *Water, Air, & Soil Pollution*, 223(6) :2955–2968, 2012.
- J. Martinez, J. Rey, M. Hidalgo, J. Garrido, and D. Rojas. Influence of measurement conditions on the resolution of electrical resistivity imaging : The example of abandoned mining dams in the la carolina district (southern spain). *International Journal of Mineral Processing*, 133 :67–72, 2014.
- J. Martínez, M. Hidalgo, J. Rey, J. Garrido, C. Kohfahl, J. Benavente, and D. Rojas. A multidisciplinary characterization of a tailings pond in the linares-la carolina mining district, spain. *Journal of Geochemical Exploration*, 162 :62–71, 2016.
- P. Martínez-Pagán, Á. Faz Cano, E. Aracil, and J. M. Arocena. Electrical resistivity imaging revealed the spatial properties of mine tailing ponds in the sierra minera of southeast spain. *Journal of Environmental & Engineering Geophysics*, 14(2) :63–76, 2009.
- P. Martinez-Pagan, D. Gómez-Ortiz, T. Martín-Crespo, S. Martín-Velázquez, and M. Martinez-Segura. Electrical resistivity imaging applied to tailings ponds : An overview. *Mine Water and the Environment*, pages 1–13, 2021.
- M. A. Martínez-Segura, M. D. Váscenez-Maza, and M. C. García-Nieto. Volumetric characterisation of waste deposits generated during the production of fertiliser derived from phosphoric rock by using lidar and electrical resistivity tomography. *Science of The Total Environment*, 716 :137076, 2020.
- B. Mary and G. Blanchy. Cags : Catalog of agrogeophysical studies. 2021. doi : 10.5281/zenodo.4058524.
- B. Mary, G. Saracco, L. Peyras, M. Vennetier, P. Mériaux, and C. Camerlynck. Mapping tree root system in dikes using induced polarization : Focus on the influence of soil water content. *Journal of Applied Geophysics*, 135 :387–396, 2016.
- B. Mary, D. Vanella, S. Consoli, and G. Cassiani. Assessing the extent of citrus trees root apparatus under deficit irrigation via multi-method geo-electrical imaging. *Scientific reports*, 9(1) :1–10, 2019.

- B. Mary, L. Peruzzo, J. Boaga, N. Cenni, M. Schmutz, Y. Wu, S. S. Hubbard, and G. Cassiani. Time-lapse monitoring of root water uptake using electrical resistivity tomography and mise-à-la-masse : a vineyard infiltration experiment. *Soil*, 6(1) :95–114, 2020.
- B. Mary, L. Peruzzo, Y. Wu, and G. Cassiani. Advanced potential field analysis applied to mise-à-la-masse surveys for leakage detection. *Journal of Geophysical Research : Solid Earth*, 127(11) :e2022JB024747, 2022.
- M. Masi, F. Ferdos, G. Losito, and L. Solari. Monitoring of internal erosion processes by time-lapse electrical resistivity tomography. *Journal of Hydrology*, 589 :125340, 2020.
- C. Massari, L. Brocca, T. Moramarco, Y. Trambly, and J.-F. D. Lescot. Potential of soil moisture observations in flood modelling : Estimating initial conditions and correcting rainfall. *Advances in Water Resources*, 74 :44–53, 2014.
- M. Mbonimpa, M. Aubertin, R. Chapuis, and B. Bussière. Practical pedotransfer functions for estimating the saturated hydraulic conductivity. *Geotechnical & Geological Engineering*, 20(3) :235–259, 2002. ISSN 0960-3182.
- M. Mbonimpa, M. Aubertin, M. Aachib, and B. Bussière. Diffusion and consumption of oxygen in unsaturated cover materials. *Canadian Geotechnical Journal*, 40(5) :916–932, 2003.
- M. Mbonimpa, V. Boulanger-Martel, B. Bussière, and A. Maqsoud. Water, gas, and heat movement in cover materials. *Hard Rock Mine Reclamation : From Prediction to Management of Acid Mine Drainage*, 2021.
- W. McCarter, J. Blewett, T. Chrisp, and G. Starrs. Electrical property measurements using a modified hydraulic oedometer. *Canadian geotechnical journal*, 42(2) :655–662, 2005.
- D. McCarthy. *Essentials of soil mechanics and foundations*. Reston Publishing Company Virginia, 1977.
- P. McLachlan, J. E. Chambers, S. S. Uhlemann, and A. Binley. Geophysical characterisation of the groundwater–surface water interface. *Advances in water resources*, 109 :302–319, 2017.
- P. McLachlan, J. Chambers, S. Uhlemann, J. Sorensen, and A. Binley. Electrical resistivity monitoring of river–groundwater interactions in a chalk river and neighbouring riparian zone. *Near Surface Geophysics*, 18(Geoelectrical Monitoring) :385–398, 2020.
- . MDDEP. Directive 019 sur l’industrie minière, mddep (ministère du développement durable, de l’environnement et des parcs), devenu le melccfp (ministère de l’environnement, de la lutte contre les changements climatiques, de la faune et des parcs), québec. 2012. URL https://www.environnement.gouv.qc.ca/milieu_ind/directive019/directive019.pdf.

Z. Medina-Cetina and F. Nadim. Stochastic design of an early warning system. *Georisk*, 2(4) :223–236, 2008.

. MELCC. Guide de caractérisation des résidus miniers et du minerai, melcc (ministère de l'environnement et de la lutte contre les changements climatiques), devenu le melccfp (ministère de l'environnement, de la lutte contre les changements climatiques, de la faune et des parcs), québec. 2020. URL <https://www.environnement.gouv.qc.ca/Industriel/secteur-minier/guide-caracterisation-minerai.pdf>.

MEND. 2.22.4 - field performance of the les terrains aurifères composite dry covers. *Canadian Mine Environment Neutral Drainage Program*, 2000.

MEND. Project 2.21.4 - design, construction and performance monitoring of cover systems for waste rock and tailings. *Canadian Mine Environment Neutral Drainage Program*, 2004.

A. Merritt, J. Chambers, P. Wilkinson, L. West, W. Murphy, D. Gunn, and S. Uhlemann. Measurement and modelling of moisture—electrical resistivity relationship of fine-grained unsaturated soils and electrical anisotropy. *Journal of Applied Geophysics*, 124 :155–165, 2016.

A. Merritt, J. Chambers, W. Murphy, P. Wilkinson, L. West, S. Uhlemann, P. Meldrum, and D. Gunn. Landslide activation behaviour illuminated by electrical resistance monitoring. *Earth Surface Processes and Landforms*, 43(6) :1321–1334, 2018. ISSN 0197-9337.

MeterGroup. Teros 12 datasheet. 2019.

B. Mewes, C. Hilbich, R. Delaloye, and C. Hauck. Resolution capacity of geophysical monitoring regarding permafrost degradation induced by hydrological processes. *The Cryosphere*, 11(6) :2957–2974, 2017.

D. Michot, Y. Benderitter, A. Dorigny, B. Nicoullaud, D. King, and A. Tabbagh. Spatial and temporal monitoring of soil water content with an irrigated corn crop cover using surface electrical resistivity tomography. *Water Resources Research*, 39(5), 2003. ISSN 1944-7973.

D. Michot, Z. Thomas, and I. Adam. Nonstationarity of the electrical resistivity and soil moisture relationship in a heterogeneous soil system : a case study. *Soil*, 2(2) :241–255, 2016.

C. R. Miller, P. S. Routh, T. R. Brosten, and J. P. McNamara. Application of time-lapse ert imaging to watershed characterization. *Geophysics*, 73(3) :G7–G17, 2008.

A. Mojica, I. Díaz, C. A. Ho, F. Ogden, R. Pinzón, J. Fábrega, D. Vega, and J. Hendrickx. Study of seasonal rainfall infiltration via time-lapse surface electrical resistivity tomography : Case study of gamboa area, panama canal watershed. *Air, Soil and Water Research*, 6 : ASWR–S12306, 2013.

- C. Mollaret, C. Hilbich, C. Pellet, A. Flores-Orozco, R. Delaloye, and C. Hauck. Mountain permafrost degradation documented through a network of permanent electrical resistivity tomography sites. *The Cryosphere*, 13(10) :2557–2578, 2019.
- C. Mollaret, F. M. Wagner, C. Hilbich, C. Scapozza, and C. Hauck. Petrophysical joint inversion applied to alpine permafrost field sites to image subsurface ice, water, air, and rock contents. *Frontiers in Earth Science*, 8, 2020.
- R. Mollehuara-Canales, E. Kozlovskaya, J. P. Lunkka, H. Guan, E. Banks, and K. Moio. Geoelectric interpretation of petrophysical and hydrogeological parameters in reclaimed mine tailings areas. *Journal of Applied Geophysics*, 181 :104139, 2020.
- R. Mollehuara-Canales, E. Kozlovskaya, J. Lunkka, K. Moio, and D. Pedretti. Non-invasive geophysical imaging and facies analysis in mining tailings. *Journal of Applied Geophysics*, 192 :104402, 2021a.
- R. Mollehuara-Canales, E. Kozlovskaya, J. Lunkka, K. Moio, and D. Pedretti. Non-invasive geophysical imaging and facies analysis in mining tailings. *Journal of Applied Geophysics*, 192 :104402, 2021b.
- M. Monego, G. Cassiani, R. Deiana, M. Putti, G. Passadore, and L. Altissimo. A tracer test in a shallow heterogeneous aquifer monitored via time-lapse surface electrical resistivity tomography. *Geophysics*, 75(4) :WA61–WA73, 2010. ISSN 0016-8033.
- C. Monterroso and F. Macías. Prediction of the acid generating potential of coal mining spoils. *International Journal of Surface Mining, Reclamation and Environment*, 12(1) :5–9, 1998.
- C. A. Moreira, M. F. S. Casagrande, F. M. de Siqueira Büchi, and D. A. Targa. Hydrogeological characterization of a waste rock pile and bedrock affected by acid mine drainage from geophysical survey. *SN Applied Sciences*, 2(7) :1–12, 2020.
- H. Morel-Seytoux. The capillary barrier effect at the interface of two soil layers with some contrast in properties. hydrowar report 92.4. *Hydrology Days Publications*, 57 :94027–3926, 1992.
- R. M. Morey, S. M. Conklin, S. P. Farrington, et al. Tomographic site characterization using cpt, ert, and gpr. Technical report, Federal Energy Technology Center Morgantown (FETC-MGN), Morgantown, WV . . . , 1999.
- A. K. M. Morita, N. de Souza Pelinson, V. R. Elis, and E. Wendland. Long-term geophysical monitoring of an abandoned dumpsite area in a guarani aquifer recharge zone. *Journal of contaminant hydrology*, 230 :103623, 2020.
- G. M. Mudd. Global trends in gold mining : Towards quantifying environmental and resource sustainability. *Resources Policy*, 32(1-2) :42–56, 2007.

- J. B. Murton, O. Kuras, M. Krautblatter, T. Cane, D. Tschofen, S. Uhlemann, S. Schober, and P. Watson. Monitoring rock freezing and thawing by novel geoelectrical and acoustic techniques. *Journal of Geophysical Research : Earth Surface*, 121(12) :2309–2332, 2016. ISSN 2169-9011.
- C. Nai, X. Sun, Z. Wang, Y. Xu, Y. Liu, J. Liu, L. Dong, Q. Huang, and Y. Wang. Complex resistivity characteristics of saltwater-intruded sand contaminated by heavy metal. *Scientific Reports*, 9(1) :1–10, 2019.
- N. T. Nassar, G. W. Lederer, J. L. Brainard, A. J. Padilla, and J. D. Lessard. Rock-to-metal ratio : A foundational metric for understanding mine wastes. *Environmental Science & Technology*, 2022.
- A. Neyamadpour. 3d electrical resistivity tomography as an aid in investigating gravimetric water content and shear strength parameters. *Environmental Earth Sciences*, 78(19) :1–14, 2019.
- F. Nguyen, A. Kemna, A. Antonsson, P. Engesgaard, O. Kuras, R. Ogilvy, J. Gisbert, S. Jorreto, and A. Pulido-Bosch. Characterization of seawater intrusion using 2d electrical imaging. *Near Surface Geophysics*, 7(5-6) :377–390, 2009.
- R. V. Nicholson, R. W. Gillham, J. A. Cherry, and E. J. Reardon. Reduction of acid generation in mine tailings through the use of moisture-retaining cover layers as oxygen barriers. *Canadian geotechnical journal*, 26(1) :1–8, 1989.
- W. Nikonow, D. Rammlmair, and M. Furche. A multidisciplinary approach considering geochemical reorganization and internal structure of tailings impoundments for metal exploration. *Applied Geochemistry*, 104 :51–59, 2019.
- R. E. Nimmer, J. L. Osiensky, A. M. Binley, and B. C. Williams. Three-dimensional effects causing artifacts in two-dimensional, cross-borehole, electrical imaging. *Journal of Hydrology*, 359(1-2) :59–70, 2008. ISSN 0022-1694.
- A. Nivorlis, T. Dahlin, M. Rossi, N. Höglund, and C. Sparrenbom. Multidisciplinary characterization of chlorinated solvents contamination and in-situ remediation with the use of the direct current resistivity and time-domain induced polarization tomography. *Geosciences*, 9(12) :487, 2019.
- K. Noborio. Measurement of soil water content and electrical conductivity by time domain reflectometry : a review. *Computers and electronics in agriculture*, 31(3) :213–237, 2001.
- D. K. Nordstrom. Mine waters : acidic to circumneutral. *Elements*, 7(6) :393–398, 2011.
- D. K. Nordstrom, C. N. Alpers, C. J. Ptacek, and D. W. Blowes. Negative ph and extremely acidic mine waters from iron mountain, california. *Environmental Science & Technology*, 34(2) :254–258, 2000.

- D. K. Nordstrom, D. W. Blowes, and C. J. Ptacek. Hydrogeochemistry and microbiology of mine drainage : an update. *Applied Geochemistry*, 57 :3–16, 2015.
- R. Ogilvy, P. Meldrum, O. Kuras, P. Wilkinson, J. Chambers, M. Sen, A. Pulido-Bosch, J. Gisbert, S. Jorreto, and I. Frances. Automated monitoring of coastal aquifers with electrical resistivity tomography. *Near Surface Geophysics*, 7(5-6) :367–375, 2009.
- G. A. Oldenborger and A.-M. LeBlanc. Monitoring changes in unfrozen water content with electrical resistivity surveys in cold continuous permafrost. *Geophysical Journal International*, 215(2) :965–977, 2018.
- D. W. Oldenburg and Y. Li. Estimating depth of investigation in dc resistivity and ip surveys. *Geophysics*, 64(2) :403–416, 1999.
- V. Olenchenko, D. Kucher, S. Bortnikova, O. Gas'kova, A. Edelev, and M. Gora. Vertical and lateral spreading of highly mineralized acid drainage solutions (ur dump, salair) : electrical resistivity tomography and hydrogeochemical data. *Russian Geology and Geophysics*, 57 (4) :617–628, 2016.
- L. A. Oliveira, M. A. Braga, G. Prosdocimi, A. de Souza Cunha, L. Santana, and F. da Gama. Improving tailings dam risk management by 3d characterization from resistivity tomography technique : Case study in são paulo–brazil. *Journal of Applied Geophysics*, page 104924, 2023.
- G. Olivier, F. Brenguier, T. de Wit, and R. Lynch. Monitoring the stability of tailings dam walls with ambient seismic noise. *The Leading Edge*, 36(4) :350a1–350a6, 2017.
- J. R. Owen, D. Kemp, É. Lébre, K. Svobodova, and G. P. Murillo. Catastrophic tailings dam failures and disaster risk disclosure. *International Journal of Disaster Risk Reduction*, 42 :101361, 2020.
- T. Pabst. Elevated water table with monolayer covers. *Hard Rock Mine Reclamation : From Prediction to Management of Acid Mine Drainage*, page 167, 2021.
- T. Pabst, M. Aubertin, B. Bussière, and J. Molson. Experimental and numerical evaluation of single-layer covers placed on acid-generating tailings. *Geotechnical and Geological Engineering*, 35(4) :1421–1438, 2017.
- M. Paepen, D. Hanssens, P. D. Smedt, K. Walraevens, and T. Hermans. Combining resistivity and frequency domain electromagnetic methods to investigate submarine groundwater discharge in the littoral zone. *Hydrology and Earth System Sciences*, 24(7) :3539–3555, 2020.
- A. Palacios, J. J. Ledo, N. Linde, L. Luquot, F. Bellmunt, A. Folch, A. Marcuello, P. Queralt, P. A. Pezard, L. Martínez, et al. Time-lapse cross-hole electrical resistivity tomography (chert) for monitoring seawater intrusion dynamics in a mediterranean aquifer. *Hydrology and Earth System Sciences*, 24(4) :2121–2139, 2020.

- E. Palis, T. Lebourg, E. Tric, J.-P. Malet, and M. Vidal. Long-term monitoring of a large deep-seated landslide (la clapiere, south-east french alps) : initial study. *Landslides*, 14(1) : 155–170, 2017.
- C. J. B. Paria, J. P. B. Gamarra, and E. L. Pereira. Geophysical-geotechnical investigation of an old tailings dam from a mine in the peruvian highland. *Brazilian Journal of Geophysics*, 38(1) :20–31, 2020.
- I. Park, C. B. Tabelin, S. Jeon, X. Li, K. Seno, M. Ito, and N. Hiroyoshi. A review of recent strategies for acid mine drainage prevention and mine tailings recycling. *Chemosphere*, 219 : 588–606, 2019.
- A. Parsekian, K. Singha, B. J. Minsley, W. S. Holbrook, and L. Slater. Multiscale geophysical imaging of the critical zone. *Reviews of Geophysics*, 53(1) :1–26, 2015.
- D. Peng, Q. Xu, X. Zhang, H. Xing, S. Zhang, K. Kang, X. Qi, Y. Ju, and K. Zhao. Hydrological response of loess slopes with reference to widespread landslide events in the heifangtai terrace, nw china. *Journal of Asian Earth Sciences*, 171 :259–276, 2019.
- A. Peregoedova. Étude expérimentale des propriétés hydrogéologiques des roches stériles à une échelle intermédiaire de laboratoire. 2012.
- M. Perri, G. Cassiani, I. Gervasio, R. Deiana, and A. Binley. A saline tracer test monitored via both surface and cross-borehole electrical resistivity tomography : Comparison of time-lapse results. *Journal of Applied Geophysics*, 79 :6–16, 2012. ISSN 0926-9851.
- A. Perrone. Lessons learned by 10 years of geophysical measurements with civil protection in basilicata (italy) landslide areas. *Landslides*, pages 1–10, 2020.
- A. Perrone, V. Lapenna, and S. Piscitelli. Electrical resistivity tomography technique for landslide investigation : a review. *Earth-Science Reviews*, 135 :65–82, 2014.
- M. Peter-Borie, C. Sirieix, V. Naudet, and J. Riss. Electrical resistivity monitoring with buried electrodes and cables : noise estimation with repeatability tests. *Near Surface Geophysics*, 9(4) :369–380, 2011. ISSN 1873-0604.
- A. Petit, A. Cerepi, O. Le Roux, C. Loisy, S. Kennedy, A. Estublier, S. Noirez, B. Garcia, et al. Study of water transfer dynamics in a carbonate vadose zone from geophysical properties. *Pure and Applied Geophysics*, 178(6) :2257–2285, 2021.
- R. Pevzner, R. Isaenkov, S. Yavuz, A. Yurikov, K. Tertyshnikov, P. Shashkin, B. Gurevich, J. Correa, S. Glubokovskikh, T. Wood, et al. Seismic monitoring of a small co2 injection using a multi-well das array : Operations and initial results of stage 3 of the co2crc otway project. *International Journal of Greenhouse Gas Control*, 110 :103437, 2021.
- J. Pierwoła. Using geoelectrical imaging to recognize zn-pb post-mining waste deposits. *Polish Journal of Environmental Studies*, 24(5), 2015.

- J. Pierwoła, M. Szuszkiewicz, J. Cabala, K. Jochymczyk, B. Żogała, and T. Magiera. Integrated geophysical and geochemical methods applied for recognition of acid waste drainage (awd) from zn-pb post-flotation tailing pile (olkusz, southern poland). *Environmental Science and Pollution Research*, 27(14) :16731–16744, 2020.
- T. Planès, M. Mooney, J. Rittgers, M. Parekh, M. Behm, and R. Snieder. Time-lapse monitoring of internal erosion in earthen dams and levees using ambient seismic noise. *Géotechnique*, 66(4) :301–312, 2016.
- B. Plante, G. Schudel, and M. Benzaazoua. Prediction of acid mine drainage. *Hard Rock Mine Reclamation : From Prediction to Management of Acid Mine Drainage*, 2021a.
- B. Plante, G. Schudel, and M. Benzaazoua. Generation of acid mine drainage. *Hard Rock Mine Reclamation : From Prediction to Management of Acid Mine Drainage*, 2021b.
- J. Poisson, M. Chouteau, M. Aubertin, and D. Campos. Geophysical experiments to image the shallow internal structure and the moisture distribution of a mine waste rock pile. *Journal of Applied Geophysics*, 67(2) :179–192, 2009. ISSN 0926-9851.
- C. Power, J. I. Gerhard, P. Tsourlos, P. Soupios, K. Simyrdanis, and M. Karaoulis. Improved time-lapse electrical resistivity tomography monitoring of dense non-aqueous phase liquids with surface-to-horizontal borehole arrays. *Journal of applied geophysics*, 112 :1–13, 2015. ISSN 0926-9851.
- C. Power, M. Ramasamy, D. MacAskill, J. Shea, J. MacPhee, D. Mayich, F. Baechler, and M. Mkandawire. Five-year performance monitoring of a high-density polyethylene (hdpe) cover system at a reclaimed mine waste rock pile in the sydney coalfield (nova scotia, canada). *Environmental Science and Pollution Research*, 24(34) :26744–26762, 2017.
- C. Power, M. Ramasamy, and M. Mkandawire. Performance assessment of a single-layer moisture store-and-release cover system at a mine waste rock pile in a seasonally humid region (nova scotia, canada). *Environmental monitoring and assessment*, 190(4) :1–20, 2018a.
- C. Power, P. Tsourlos, M. Ramasamy, A. Nivorlis, and M. Mkandawire. Combined DC resistivity and induced polarization (DC-IP) for mapping the internal composition of a mine waste rock pile in Nova Scotia, Canada. *Journal of Applied Geophysics*, 150 :40–51, 2018b. ISSN 0926-9851.
- M. Priegnitz, J. Thaler, E. Spangenberg, C. Rücker, and J. M. Schicks. A cylindrical electrical resistivity tomography array for three-dimensional monitoring of hydrate formation and dissociation. *Review of Scientific Instruments*, 84(10) :104502, 2013. ISSN 0034-6748.

- A. Proteau, M. Guittonny, B. Bussière, and A. Maqsood. Aboveground and belowground colonization of vegetation on a 17-year-old cover with capillary barrier effect built on a boreal mine tailings storage facility. *Minerals*, 10(8) :704, 2020a.
- A. Proteau, M. Guittonny, B. Bussière, and A. Maqsood. Oxygen migration through a cover with capillary barrier effects colonized by roots. *Canadian Geotechnical Journal*, (ja), 2020b.
- A. Puttiwongrak, T. Suteerasak, P. K. Mai, K. Hashimoto, J. C. Gonzalez, R. Rattanakom, and K. Prueksakorn. Application of multi-monitoring methods to investigate the contamination levels and dispersion of pb and zn from tin mining in coastal sediments at saphan hin, phuket, thailand. *Journal of Cleaner Production*, 218 :108–117, 2019.
- Y. Qi, A. Soueid Ahmed, A. Revil, A. Ghorbani, F. Abdulsamad, N. Florsch, and J. Bonenfant. Induced polarization response of porous media with metallic particles—part 7 : Detection and quantification of buried slag heaps. *Geophysics*, 83(5) :E277–E291, 2018.
- S. Qiang, X. Shi, X. Kang, and A. Revil. Optimized arrays for electrical resistivity tomography survey using bayesian experimental design. *Geophysics*, 87(4) :E189–E203, 2022.
- A. Ramirez, W. Daily, D. LaBrecque, E. Owen, and D. Chesnut. Monitoring an underground steam injection process using electrical resistance tomography. *Water Resources Research*, 29(1) :73–87, 1993. ISSN 1944-7973.
- R. F. M. Rarison, M. Mbonimpa, B. Bussière, and S. Pouliot. Properties of hdpe geomembrane exhumed 20 years after installation in a mine reclamation cover system. *International Journal of Geosynthetics and Ground Engineering*, 9(1) :1, 2023.
- H. Rasul, L. Zou, and B. Olofsson. Monitoring of moisture and salinity content in an operational road structure by electrical resistivity tomography. *Near Surface Geophysics*, 16(4) :423–444, 2018.
- K. Raymond, N. Seigneur, D. Su, and K. U. Mayer. Investigating the influence of structure and heterogeneity in waste rock piles on mass loading rates—a reactive transport modeling study. *Frontiers in Water*, 3 :39, 2021.
- K. E. Raymond, N. Seigneur, D. Su, B. Poaty, B. Plante, B. Bussière, and K. U. Mayer. Numerical modeling of a laboratory-scale waste rock pile featuring an engineered cover system. *Minerals*, 10(8) :652, 2020.
- A. Revil, M. Karaoulis, T. Johnson, and A. Kemna. Some low-frequency electrical methods for subsurface characterization and monitoring in hydrogeology. *Hydrogeology Journal*, 20 (4) :617–658, 2012.
- A. Revil, M. Skold, M. Karaoulis, M. Schmutz, S. S. Hubbard, T. L. Mehlhorn, and D. B. Watson. Hydrogeophysical investigations of the former s-3 ponds contaminant plumes, oak

ridge integrated field research challenge site, tennessee. *Geophysics*, 78(4) :EN29–EN41, 2013.

A. Revil, P. Kessouri, and C. Torres-Verdín. Electrical conductivity, induced polarization, and permeability of the fontainebleau sandstone. *Geophysics*, 79(5) :D301–D318, 2014.

A. Revil, A. S. Ahmed, and S. Matthai. Transport of water and ions in partially water-saturated porous media. part 3. electrical conductivity. *Advances in water resources*, 121 : 97–111, 2018.

J. Rey, J. Martínez, M. Hidalgo, R. Mendoza, and S. Sandoval. Assessment of tailings ponds by a combination of electrical (ert and ip) and hydrochemical techniques (linares, southern spain). *Mine Water and the Environment*, pages 1–10, 2020a.

N. J. Rey, I. Demers, B. Bussière, M. Mbonimpa, and M. Gagnon. A geochemical evaluation of a monolayer cover with an elevated water table for the reclamation of the doyon-westwood tailings ponds, canada. *Environmental Earth Sciences*, 79(2) :1–14, 2020b.

S. Rezaei, I. Shooshpasha, and H. Rezaei. Reconstruction of landslide model from ert, geotechnical, and field data, nargeschal landslide, iran. *Bulletin of Engineering Geology and the Environment*, 78(5) :3223–3237, 2019.

B. Rezaie and A. Anderson. Sustainable resolutions for environmental threat of the acid mine drainage. *Science of The Total Environment*, page 137211, 2020.

J. Rhoades, N. Manteghi, P. Shouse, and W. Alves. Soil electrical conductivity and soil salinity : New formulations and calibrations. *Soil Science Society of America Journal*, 53 (2) :433–439, 1989.

A. Ritter and R. Munoz-Carpena. Performance evaluation of hydrological models : Statistical significance for reducing subjectivity in goodness-of-fit assessments. *Journal of Hydrology*, 480 :33–45, 2013.

T. Robert, C. Paulus, P.-Y. Bolly, E. Koo Seen Lin, and T. Hermans. Heat as a proxy to image dynamic processes with 4d electrical resistivity tomography. *Geosciences*, 9(10) :414, 2019.

P. Robertson and K. Cabal. Guide to cone penetration testing for geo-environmental engineering. *Gregg Drilling & Testing Inc*, 2008.

D. Robinson, A. Binley, N. Crook, F. Day-Lewis, T. Ferré, V. Grauch, R. Knight, M. Knoll, V. Lakshmi, R. Miller, et al. Advancing process-based watershed hydrological research using near-surface geophysics : A vision for, and review of, electrical and magnetic geophysical methods. *Hydrological Processes : An International Journal*, 22(18) :3604–3635, 2008a.

- D. Robinson, C. Campbell, J. Hopmans, B. K. Hornbuckle, S. B. Jones, R. Knight, F. Ogden, J. Selker, and O. Wendroth. Soil moisture measurement for ecological and hydrological watershed-scale observatories : A review. *Vadose Zone Journal*, 7(1) :358–389, 2008b.
- J. Robinson, T. Johnson, and M. Rockhold. Feasibility assessment of long-term electrical resistivity monitoring of a nitrate plume. *Groundwater*, 2019.
- A. Romero-Ruiz, N. Linde, T. Keller, and D. Or. A review of geophysical methods for soil structure characterization. *Reviews of Geophysics*, 56(4) :672–697, 2018.
- H. R. Roodposhti, M. K. Hafizi, M. R. S. Kermani, and M. R. G. Nik. Electrical resistivity method for water content and compaction evaluation, a laboratory test on construction material. *Journal of Applied Geophysics*, 168 :49–58, 2019.
- H. Rosqvist, V. Leroux, T. Dahlin, M. Svensson, M. Lindsjö, C.-H. Månsson, and S. Johansson. Mapping landfill gas migration using resistivity monitoring. In *Proceedings of the Institution of Civil Engineers-Waste and Resource Management*, volume 164, pages 3–15. ICE Publishing, 2011.
- L. H. S. Rotta, E. Alcantara, E. Park, R. G. Negri, Y. N. Lin, N. Bernardo, T. S. G. Mendes, and C. R. Souza Filho. The 2019 brumadinho tailings dam collapse : Possible cause and impacts of the worst human and environmental disaster in brazil. *International Journal of Applied Earth Observation and Geoinformation*, 90 :102119, 2020.
- N. Rötzer and M. Schmidt. Decreasing metal ore grades—is the fear of resource depletion justified? *Resources*, 7(4) :88, 2018.
- C. Rücker, T. Günther, and K. Spitzer. Three-dimensional modelling and inversion of dc resistivity data incorporating topography—i. modelling. *Geophysical Journal International*, 166(2) :495–505, 2006.
- D. Rucker. Moisture estimation within a mine heap : An application of cokriging with assay data and electrical resistivity. *Geophysics*, 75(1) :B11–B23, 2010.
- D. Rucker. Investigating motion blur and temporal aliasing from time-lapse electrical resistivity. *Journal of Applied Geophysics*, 111 :1–13, 2014.
- D. F. Rucker. Deep well rinsing of a copper oxide heap. *Hydrometallurgy*, 153 :145–153, 2015.
- D. F. Rucker, D. R. Glaser, T. Osborne, and W. C. Maehl. Electrical resistivity characterization of a reclaimed gold mine to delineate acid rock drainage pathways. *Mine Water and the Environment*, 28(2) :146–157, 2009a. ISSN 1025-9112.
- D. F. Rucker, M. McNeill, A. Schindler, and G. Noonan. Monitoring of a secondary recovery application of leachate injection into a heap. *Hydrometallurgy*, 99(3-4) :238–248, 2009b.

- D. F. Rucker, A. Schindler, M. T. Levitt, and D. R. Glaser. Three-dimensional electrical resistivity imaging of a gold heap. *Hydrometallurgy*, 98(3-4) :267–275, 2009c.
- D. F. Rucker, N. Crook, J. Winterton, M. McNeill, C. A. Baldyga, G. Noonan, and J. B. Fink. Real-time electrical monitoring of reagent delivery during a subsurface amendment experiment. *Near Surface Geophysics*, 12(1) :151–163, 2014.
- D. F. Rucker, R. J. Zaebst, J. Gillis, J. C. Cain IV, and B. Teague. Drawing down the remaining copper inventory in a leach pad by way of subsurface leaching. *Hydrometallurgy*, 169 :382–392, 2017.
- M. Rykaart, D. Hockley, and M. P. Michel Noel. Findings of international review of soil cover design and construction practices for mine waste closure. In *International Conference on Acid Rock Drainage (ICARD)*. St. Louis MO, 2006.
- T. Rymarczyk, G. Kłosowski, E. Kozłowski, and P. Tchórzewski. Comparison of selected machine learning algorithms for industrial electrical tomography. *Sensors*, 19(7) :1521, 2019.
- C. Rücker and T. Günther. The simulation of finite ERT electrodes using the complete electrode model. *Geophysics*, 76(4) :F227–F238, 2011. ISSN 0016-8033.
- C. Rücker, T. Günther, and F. M. Wagner. pyGIMLi : An open-source library for modelling and inversion in geophysics. *Computers & Geosciences*, 109 :106–123, 2017. ISSN 0098-3004.
- T. Sakaki and T. H. Illangasekare. Comparison of height-averaged and point-measured capillary pressure–saturation relations for sands using a modified tempe cell. *Water resources research*, 43(12), 2007.
- J. Saladich, L. Rivero, I. Queralt, R. Lovera, X. Font, M. Himi, A. Casas, and A. Sendros. Geophysical evaluation of the volume of a mine tailing dump (osor, girona, ne spain) using ert. In *Near Surface Geoscience 2016-22nd European Meeting of Environmental and Engineering Geophysics*, volume 2016, pages cp–495. European Association of Geoscientists & Engineers, 2016.
- A. Samouëlian, G. Richard, I. Cousin, R. Guerin, A. Bruand, and A. Tabbagh. Three-dimensional crack monitoring by electrical resistivity measurement. *European Journal of Soil Science*, 55(4) :751–762, 2004.
- A. Samouëlian, I. Cousin, A. Tabbagh, A. Bruand, and G. Richard. Electrical resistivity survey in soil science : a review. *Soil and Tillage research*, 83(2) :173–193, 2005.
- W. R. Sandlin, J. B. Langman, K. V. Waynant, M. Mukhopadhyay, T. Thuneman, and J. G. Moberly. Comparison of aptes-functionalized silica fiber and clinoptilolite for reducing iron concentrations in an acidic iron (ii) sulfate solution : Potential passive treatment substrates. *Mine Water and the Environment*, 39(4) :797–807, 2020.

- S. Saneiyan, D. Ntarlagiannis, J. Ohan, J. Lee, F. Colwell, and S. Burns. Induced polarization as a monitoring tool for in-situ microbial induced carbonate precipitation (micp) processes. *Ecological engineering*, 127 :36–47, 2019.
- A. Scaini, M. Audebert, C. Hissler, F. Fenicia, L. Gourdol, L. Pfister, and K. J. Beven. Velocity and celerity dynamics at plot scale inferred from artificial tracing experiments and time-lapse ERT. *Journal of hydrology*, 546 :28–43, 2017. ISSN 0022-1694.
- C. Schlumberger. *Study of underground electrical prospecting*. 1920.
- C. Schmidt-Hattenberger, P. Bergmann, T. Labitzke, F. Wagner, and D. Rippe. Permanent crosshole electrical resistivity tomography (ert) as an established method for the long-term co2 monitoring at the ketzin pilot site. *International Journal of Greenhouse Gas Control*, 52 :432–448, 2016.
- C. Schmidt-Hattenberger, P. Bergmann, T. Labitzke, J. Pommerencke, D. Rippe, F. Wagner, and B. Wiese. Monitoring the complete life-cycle of a co2 storage reservoir—demonstration of applicability of geoelectrical imaging. *Energy Procedia*, 114 :3948–3955, 2017.
- B. F. Schwartz, M. E. Schreiber, and T. Yan. Quantifying field-scale soil moisture using electrical resistivity imaging. *Journal of Hydrology*, 362(3-4) :234–246, 2008.
- P. N. Sen. Resistivity of partially saturated carbonate rocks with microporosity. *Geophysics*, 62(2) :415–425, 1997.
- F. Shafaei, H. Ramazi, B. J. Shokri, and F. D. Ardejani. Detecting the source of contaminant zones down-gradient of the alborz sharghi coal washing plant using geo-electrical methods, northeastern iran. *Mine Water and the Environment*, 35(3) :381–388, 2016.
- L. Sherrod, W. Sauck, and D. D. Werkema Jr. A low-cost, in situ resistivity and temperature monitoring system. *Groundwater Monitoring & Remediation*, 32(2) :31–39, 2012.
- S. Shin, S. Park, and J.-H. Kim. Time-lapse electrical resistivity tomography characterization for piping detection in earthen dam model of a sandbox. *Journal of Applied Geophysics*, 170 :103834, 2019.
- B. J. Shokri, F. D. Ardejani, and A. Moradzadeh. Mapping the flow pathways and contaminants transportation around a coal washing plant using the vlf-em, geo-electrical and ip techniques—a case study, ne iran. *Environmental Earth Sciences*, 75(1) :62, 2016a.
- B. J. Shokri, F. D. Ardejani, H. Ramazi, and A. Moradzadeh. Predicting pyrite oxidation and multi-component reactive transport processes from an abandoned coal waste pile by comparing 2d numerical modeling and 3d geo-electrical inversion. *International Journal of Coal Geology*, 164 :13–24, 2016b.

- J. B. Shokri, F. Shafaei, D. F. Ardejani, A. Mirzaghobanali, and S. Entezam. Use of time-lapse 2d and 3d geoelectrical inverse models for monitoring acid mine drainage—a case study. *Soil and Sediment Contamination : An International Journal*, pages 1–24, 2022.
- K. Simyrdanis, N. Papadopoulos, P. Soupios, S. Kirkou, and P. Tsourlos. Characterization and monitoring of subsurface contamination from olive oil mills’ waste waters using electrical resistivity tomography. *Science of The Total Environment*, 637 :991–1003, 2018.
- K. Singha and S. M. Gorelick. Saline tracer visualized with three-dimensional electrical resistivity tomography : Field-scale spatial moment analysis. *Water Resources Research*, 41 (5), 2005. ISSN 1944-7973.
- K. Singha, F. D. Day-Lewis, T. Johnson, and L. D. Slater. Advances in interpretation of subsurface processes with time-lapse electrical imaging. *Hydrological Processes*, 29(6) : 1549–1576, 2015. ISSN 0885-6087.
- P. Sjö Dahl, T. Dahlin, and S. Johansson. Using resistivity measurements for dam safety evaluation at enemossen tailings dam in southern sweden. *Environmental geology*, 49(2) : 267–273, 2005.
- P. Sjö Dahl, T. Dahlin, S. Johansson, and M. Loke. Resistivity monitoring for leakage and internal erosion detection at hällby embankment dam. *Journal of Applied Geophysics*, 65 (3-4) :155–164, 2008.
- P. Sjö Dahl, T. Dahlin, and S. Johansson. Embankment dam seepage evaluation from resistivity monitoring data. *Near Surface Geophysics*, 7(5-6) :463–474, 2009.
- L. Slater. Near surface electrical characterization of hydraulic conductivity : From petrophysical properties to aquifer geometries—a review. *Surveys in Geophysics*, 28(2-3) :169–197, 2007.
- L. Slater and A. Binley. Advancing hydrological process understanding from long-term resistivity monitoring systems. *Wiley Interdisciplinary Reviews : Water*, 8(3) :e1513, 2021.
- J. A. Smethurst, A. Smith, S. Uhlemann, C. Wooff, J. Chambers, P. Hughes, S. Lenart, H. Saroglou, S. M. Springman, H. Löfroth, et al. Current and future role of instrumentation and monitoring in the performance of transport infrastructure slopes. *Quarterly Journal of Engineering Geology and Hydrogeology*, 50(3) :271–286, 2017.
- . SNC Lavalin. Révision du plan de réaménagement et de restauration du site des opérations minières de mine raglan (version 2018 - 653645-1000-4eer-0001). page 279, 2018. URL https://gestim.mines.gouv.qc.ca/documents/001_Plan_restoration_Raglan_2018-05-15_0000046333.pdf.
- . SNC Lavalin. Révision du plan de réaménagement et de restauration du site minier Éléonore (version 2020 - 658524-0000-4eer-0001). page 757, 2020.

URL https://gestim.mines.gouv.qc.ca/documents/004_D0_Plan_restauracion_Eleonore_V01_2020-09-16_0000049580.pdf.

. SNC Lavalin. Plan de réaménagement et de restauration du site de doyon/grand-duc (version 2021 - 680588-0000-40er-0002). page 155, 2021a. URL https://gestim.mines.gouv.qc.ca/documents/2021-12-08_D0_Plan_restauracion_Doyon_0000053846.pdf.

. SNC Lavalin. Révision du plan de réaménagement et de restauration du site de westwood (version 2021 - 680588-4000-40er-0001). page 198, 2021b. URL https://gestim.mines.gouv.qc.ca/documents/2021-12-08_D0_Plan_restauracion_Westwood_0000053847.pdf.

P. Soupios and E. Kokinou. Environmental Geophysics : Techniques, advantages and limitations. *Principles, applications and emerging technologies*, page 1, 2016.

C. M. Steelman, C. S. Kennedy, D. C. Capes, and B. L. Parker. Electrical resistivity dynamics beneath a fractured sedimentary bedrock riverbed in response to temperature and groundwater–surface water exchange. *Hydrology and Earth System Sciences*, 21(6) : 3105, 2017.

M. Steiner, T. Katona, J. Fellner, and A. F. Orozco. Quantitative water content estimation in landfills through joint inversion of seismic refraction and electrical resistivity data considering surface conduction. *Waste Management*, 149 :21–32, 2022.

P. Stummer, H. Maurer, and A. G. Green. Experimental design : Electrical resistivity data sets that provide optimum subsurface information. *Geophysics*, 69(1) :120–139, 2004.

H. Sun, Y. Wang, Y. Zhao, P. Zhang, Y. Song, M. He, C. Zhang, Y. Tong, J. Zhou, L. Qi, et al. Assessing the value of electrical resistivity derived soil water content : insights from a case study in the critical zone of the chinese loess plateau. *Journal of Hydrology*, 589 : 125132, 2020.

R. Supper, A. Römer, B. Jochum, G. Bieber, and W. Jaritz. A complex geo-scientific strategy for landslide hazard mitigation—from airborne mapping to ground monitoring. *Advances in Geosciences*, 14 :195–200, 2008.

R. Supper, D. Ottowitz, B. Jochum, J.-H. Kim, A. Römer, I. Baron, S. Pfeiler, M. Lovisolo, S. Gruber, and F. Vecchiotti. Geoelectrical monitoring : an innovative method to supplement landslide surveillance and early warning. *Near Surface Geophysics*, 12(1) :133–150, 2014.

K. Sylvain, T. Pabst, and A. Dimech. Waste rock valorization in monolayer covers with elevated water table. Proceedings of GeoEnvironmental Engineering 2019 Concordia Montréal, 2019.

- C.-S. Tang, D.-Y. Wang, C. Zhu, Q.-Y. Zhou, S.-K. Xu, and B. Shi. Characterizing drying-induced clayey soil desiccation cracking process using electrical resistivity method. *Applied Clay Science*, 152 :101–112, 2018.
- D. A. Targa, C. A. Moreira, P. L. Camarero, M. F. S. Casagrande, and H. L. C. Alberti. Structural analysis and geophysical survey for hydrogeological diagnosis in uranium mine, poços de caldas (brazil). *SN Applied Sciences*, 1(4) :1–12, 2019.
- D. A. Targa, C. A. Moreira, and M. F. S. Casagrande. Hydrogeological analysis of sulfide tailings at a uranium mine using geophysical and hydrochemical methods. *Mine Water and the Environment*, 40(3) :671–689, 2021.
- A. Tejero-Andrade, G. Cifuentes, R. E. Chávez, A. E. López-González, and C. Delgado-Solórzano. L-and corner-arrays for 3d electric resistivity tomography : an alternative for geophysical surveys in urban zones. *Near Surface Geophysics*, 13(4) :355–368, 2015.
- D. Thayer, A. D. Parsekian, K. Hyde, H. Speckman, D. Beverly, B. Ewers, M. Covalt, N. Fantello, T. Kelleners, N. Ohara, et al. Geophysical measurements to determine the hydrologic partitioning of snowmelt on a snow-dominated subalpine hillslope. *Water Resources Research*, 54(6) :3788–3808, 2018.
- S. Thober, R. Kumar, J. Sheffield, J. Mai, D. Schäfer, and L. Samaniego. Seasonal soil moisture drought prediction over europe using the north american multi-model ensemble (nmme). *Journal of Hydrometeorology*, 16(6) :2329–2344, 2015.
- S. S. Thompson, B. Kulesa, D. I. Benn, and J. R. Mertes. Anatomy of terminal moraine segments and implied lake stability on ngozumpa glacier, nepal, from electrical resistivity tomography (ert). *Scientific Reports*, 7(1) :1–12, 2017.
- P. Tildy, B. Neduczka, P. Nagy, A. I. Kanli, and C. Hegymegi. Time lapse 3d geoelectric measurements for monitoring of in-situ remediation. *Journal of Applied Geophysics*, 136 : 99–113, 2017. ISSN 0926-9851.
- S. Tomaškovičová, T. Ingeman-Nielsen, A. V. Christiansen, I. Brandt, T. Dahlin, and B. Elberling. Effect of electrode shape on grounding resistances—part 2 : Experimental results and cryospheric monitoring. *Geophysics*, 81(1) :WA169–WA182, 2016.
- S. Tomiyama and T. Igarashi. The potential threat of mine drainage to groundwater resources. *Current Opinion in Environmental Science & Health*, page 100347, 2022.
- G. C. Topp, J. Davis, and A. P. Annan. Electromagnetic determination of soil water content : Measurements in coaxial transmission lines. *Water resources research*, 16(3) :574–582, 1980. ISSN 1944-7973.
- L. Toran, B. Hughes, J. Nyquist, and R. Ryan. Freeze core sampling to validate time-lapse resistivity monitoring of the hyporheic zone. *Groundwater*, 51(4) :635–640, 2013.

- L. M. Trento, P. Tsourlos, and J. I. Gerhard. Time-lapse electrical resistivity tomography mapping of dnapl remediation at a star field site. *Journal of Applied Geophysics*, 184 : 104244, 2021.
- G. Tresoldi, D. Arosio, A. Hojat, L. Longoni, M. Papini, and L. Zanzi. Long-term hydrogeophysical monitoring of the internal conditions of river levees. *Engineering Geology*, 259 : 105139, 2019.
- G. Tresoldi, A. Hojat, L. Cordova, L. Zanzi, et al. Permanent geoelectrical monitoring of tailings dams using the autonomous g. re. ta system. In *Tailings and Mining Wastes '20*, pages 729–739, 2020a.
- G. Tresoldi, A. Hojat, L. Cordova, L. Zanzi, et al. The latest installation of g. re. ta along the tailings dam of a copper mine in chile. In *GELMON 2020; 5th International Workshop on Geoelectric Monitoring; Book of Abstracts*, pages 12–12. Berichte der Geologischen Bundesanstalt, 139, 2020b.
- G. Tresoldi, A. Hojat, L. Zanzi, and A. Certo. Introducing g. re. ta—an innovative georesistivimeter for long-term monitoring of earthen dams and unstable slopes. In *Proceedings of the 2020 International Symposium on Slope Stability in Open Pit Mining and Civil Engineering*, pages 487–498. Australian Centre for Geomechanics, 2020c.
- G. Tresoldi, A. Hojat, L. Zanzi, et al. G. re. ta solution to monitor the integrity of tailings dams. In *7th International Conference on Tailings Management*, pages 1–8, 2021.
- A. Troiano, R. Isaia, M. G. Di Giuseppe, F. D. Tramparulo, and S. Vitale. Deep electrical resistivity tomography for a 3d picture of the most active sector of campi flegrei caldera. *Scientific reports*, 9(1) :1–10, 2019.
- C.-H. M. Tso, O. Kuras, P. B. Wilkinson, S. Uhlemann, J. E. Chambers, P. I. Meldrum, J. Graham, E. F. Sherlock, and A. Binley. Improved characterisation and modelling of measurement errors in electrical resistivity tomography (ert) surveys. *Journal of Applied Geophysics*, 146 :103–119, 2017.
- C.-H. M. Tso, O. Kuras, and A. Binley. On the field estimation of moisture content using electrical geophysics : The impact of petrophysical model uncertainty. *Water Resources Research*, 55(8) :7196–7211, 2019.
- C.-H. M. Tso, T. C. Johnson, X. Song, X. Chen, O. Kuras, P. Wilkinson, S. Uhlemann, J. Chambers, and A. Binley. Integrated hydrogeophysical modelling and data assimilation for geoelectrical leak detection. *Journal of Contaminant Hydrology*, 234 :103679, 2020.
- G. Turner, M. Ingham, H. Bibby, and H. Keys. Resistivity monitoring of the tephra barrier at crater lake, mount ruapehu, new zealand. *Journal of applied geophysics*, 73(3) :243–250, 2011.

- C. Tycholiz, I. Ferguson, B. Sherriff, M. Cordeiro, R. S. Ranjan, and M. Pérez-Flores. Geophysical delineation of acidity and salinity in the central manitoba gold mine tailings pile, manitoba, canada. *Journal of Applied Geophysics*, 131 :29–40, 2016.
- S. Uhlemann, P. B. Wilkinson, J. E. Chambers, H. Maurer, A. J. Merritt, D. A. Gunn, and P. I. Meldrum. Interpolation of landslide movements to improve the accuracy of 4d geoelectrical monitoring. *Journal of Applied Geophysics*, 121 :93–105, 2015. ISSN 0926-9851.
- S. Uhlemann, A. Smith, J. Chambers, N. Dixon, T. Dijkstra, E. Haslam, P. Meldrum, A. Merritt, D. Gunn, and J. Mackay. Assessment of ground-based monitoring techniques applied to landslide investigations. *Geomorphology*, 253 :438–451, 2016a. ISSN 0169-555X.
- S. Uhlemann, J. Sorensen, A. House, P. Wilkinson, C. Roberts, D. Gooddy, A. M. Binley, and J. Chambers. Integrated time-lapse geoelectrical imaging of wetland hydrological processes. *Water Resources Research*, 52(3) :1607–1625, 2016b. ISSN 1944-7973.
- S. Uhlemann, J. Chambers, P. Wilkinson, H. Maurer, A. Merritt, P. Meldrum, O. Kuras, D. Gunn, A. Smith, and T. Dijkstra. Four-dimensional imaging of moisture dynamics during landslide reactivation. *Journal of Geophysical Research : Earth Surface*, 122(1) :398–418, 2017a.
- S. Uhlemann, J. Chambers, P. Wilkinson, H. Maurer, A. Merritt, P. Meldrum, O. Kuras, D. Gunn, A. Smith, and T. Dijkstra. Four-dimensional imaging of moisture dynamics during landslide reactivation. *Journal of Geophysical Research : Earth Surface*, 122(1) :398–418, 2017b. ISSN 2169-9011.
- S. Uhlemann, P. B. Wilkinson, H. Maurer, F. M. Wagner, T. C. Johnson, and J. E. Chambers. Optimized survey design for electrical resistivity tomography : combined optimization of measurement configuration and electrode placement. *Geophysical Journal International*, 214(1) :108–121, 2018a.
- S. Uhlemann, P. B. Wilkinson, H. Maurer, F. M. Wagner, T. C. Johnson, and J. E. Chambers. Optimized survey design for electrical resistivity tomography : combined optimization of measurement configuration and electrode placement. *Geophysical Journal International*, 214(1) :108–121, 2018b. ISSN 0956-540X.
- S. Uhlemann, B. Dafflon, J. Peterson, C. Ulrich, I. Shirley, S. Michail, and S. Hubbard. Geophysical monitoring shows that spatial heterogeneity in thermohydrological dynamics reshapes a transitional permafrost system. *Geophysical Research Letters*, 48(6) : e2020GL091149, 2021.

- Í. Ulusoy, T. Dahlin, and B. Bergman. Time-lapse electrical resistivity tomography of a water infiltration test on johannishus esker, sweden. *Hydrogeology Journal*, 23(3) :551–566, 2015.
- D. Vanella, J. M. Ramírez-Cuesta, D. S. Intrigliolo, and S. Consoli. Combining electrical resistivity tomography and satellite images for improving evapotranspiration estimates of citrus orchards. *Remote Sensing*, 11(4) :373, 2019.
- D. Vanella, J. M. Ramírez-Cuesta, A. Sacco, G. Longo-Minnolo, G. L. Cirelli, and S. Consoli. Electrical resistivity imaging for monitoring soil water motion patterns under different drip irrigation scenarios. *Irrigation Science*, 39(1) :145–157, 2021.
- M. D. Vásconez-Maza, M. A. Martínez-Segura, M. C. Bueso, Á. Faz, M. C. García-Nieto, M. Gabarrón, and J. A. Acosta. Predicting spatial distribution of heavy metals in an abandoned phosphogypsum pond combining geochemistry, electrical resistivity tomography and statistical methods. *Journal of hazardous materials*, 374 :392–400, 2019.
- M. D. Vásconez-Maza, M. C. Bueso, A. Faz, J. Acosta, and M. A. Martínez-Segura. Assessing the behaviour of heavy metals in abandoned phosphogypsum deposits combining electrical resistivity tomography and multivariate analysis. *Journal of Environmental Management*, 278 :111517, 2020.
- J. P. Verdon, S. A. Horne, A. Clarke, A. L. Stork, A. F. Baird, and J.-M. Kendall. Microseismic monitoring using a fiber-optic distributed acoustic sensor arraymicroseismic monitoring using a das array. *Geophysics*, 85(3) :KS89–KS99, 2020.
- H. Vereecken, J. Huisman, H. Bogena, J. Vanderborght, J. Vrugt, and J. Hopmans. On the value of soil moisture measurements in vadose zone hydrology : A review. *Water resources research*, 44(4), 2008. ISSN 1944-7973.
- R. Versteeg and D. Johnson. Efficient electrical hydrogeophysical monitoring through cloud-based processing, analysis, and result access. *The Leading Edge*, 32(7) :776–783, 2013. ISSN 1070-485X.
- L. Villain, N. Sundström, N. Perttu, L. Alakangas, and B. Öhlander. Evaluation of the effectiveness of backfilling and sealing at an open-pit mine using ground penetrating radar and geoelectrical surveys, kimheden, northern sweden. *Environmental Earth Sciences*, 73 (8) :4495–4509, 2015.
- A. Voss, P. Hosseini, M. Pour-Ghaz, M. Vauhkonen, and A. Seppänen. Three-dimensional electrical capacitance tomography—a tool for characterizing moisture transport properties of cement-based materials. *Materials & Design*, 181 :107967, 2019.
- B. Vriens, B. Plante, N. Seigneur, and H. Jamieson. Mine waste rock : Insights for sustainable hydrogeochemical management. *Minerals*, 10(9) :728, 2020a.

- B. Vriens, N. Seigneur, K. U. Mayer, and R. D. Beckie. Scale dependence of effective geochemical rates in weathering mine waste rock. *Journal of Contaminant Hydrology*, 234 : 103699, 2020b.
- F. Wagner, C. Mollaret, T. Günther, A. Kemna, and C. Hauck. Quantitative imaging of water, ice and air in permafrost systems through petrophysical joint inversion of seismic refraction and electrical resistivity data. *Geophysical Journal International*, 219(3) :1866–1875, 2019.
- F. M. Wagner and S. Uhlemann. An overview of multimethod imaging approaches in environmental geophysics. *Advances in Geophysics*, 62 :1–72, 2021.
- F. M. Wagner and B. U. Wiese. Fully coupled inversion on a multi-physical reservoir model—part ii : The ketzin co2 storage reservoir. *International Journal of Greenhouse Gas Control*, 75 :273–281, 2018.
- F. M. Wagner, T. Günther, C. Schmidt-Hattenberger, and H. Maurer. Constructive optimization of electrode locations for target-focused resistivity monitoring. *Geophysics*, 80(2) : E29–E40, 2015a.
- F. M. Wagner, T. Günther, C. Schmidt-Hattenberger, and H. Maurer. Constructive optimization of electrode locations for target-focused resistivity monitoring. *Geophysics*, 80(2) : E29–E40, 2015b. ISSN 0016-8033.
- E. L. Wallin, T. C. Johnson, W. J. Greenwood, and J. M. Zachara. Imaging high stage river-water intrusion into a contaminated aquifer along a major river corridor using 2-d time-lapse surface electrical resistivity tomography. *Water Resources Research*, 49(3) :1693–1708, 2013.
- A. Watlet, O. Kaufmann, A. Triantafyllou, A. Poulain, J. E. Chambers, P. I. Meldrum, P. B. Wilkinson, V. Hallet, Y. Quinif, M. V. Ruymbeke, et al. Imaging groundwater infiltration dynamics in the karst vadose zone with long-term ert monitoring. *Hydrology and Earth System Sciences*, 22(2) :1563–1592, 2018.
- M. H. Waxman and L. Smits. Electrical conductivities in oil-bearing shaly sands. *Society of Petroleum Engineers Journal*, 8(02) :107–122, 1968. ISSN 0197-7520.
- M. H. Waxman and E. Thomas. Electrical conductivities in shaly sands-i. the relation between hydrocarbon saturation and resistivity index; ii. the temperature coefficient of electrical conductivity. In *Fall Meeting of the Society of Petroleum Engineers of AIME*. OnePetro, 1972.
- V. Wayal, T. Sitharam, and M. Anjali. Geo-electrical characterization of physical and mechanical properties of zinc tailing. *Journal of Applied Geophysics*, 188 :104315, 2021.
- S. Weber, J. Beutel, R. D. Forno, A. Geiger, S. Gruber, T. Gsell, A. Hasler, M. Keller, R. Lim, P. Limpach, et al. A decade of detailed observations (2008–2018) in steep bedrock

permafrost at the matterhorn hörnligrat (zermatt, ch). *Earth System Science Data*, 11(3) : 1203–1237, 2019.

M. Wehrer, H. Lissner, E. Bloem, H. French, and K. U. Totsche. Electrical resistivity tomography as monitoring tool for unsaturated zone transport : an example of preferential transport of deicing chemicals. *Environmental Science and Pollution Research*, 21(15) : 8964–8980, 2014.

M. Weigand and A. Kemna. Imaging and functional characterization of crop root systems using spectroscopic electrical impedance measurements. *Plant and Soil*, 435(1) :201–224, 2019.

A. Weller, R. Lewis, T. Canh, M. Möller, and B. Scholz. Geotechnical and geophysical long-term monitoring at a levee of red river in vietnam. *Journal of Environmental and Engineering Geophysics*, 19(3) :183–192, 2014.

A. W. Western, R. B. Grayson, G. Blöschl, G. R. Willgoose, and T. A. McMahon. Observed spatial organization of soil moisture and its relation to terrain indices. *Water resources research*, 35(3) :797–810, 1999.

W. R. Whalley, A. Binley, C. Watts, P. Shanahan, I. C. Dodd, E. Ober, R. Ashton, C. Webster, R. White, and M. J. Hawkesford. Methods to estimate changes in soil water for phenotyping root activity in the field. *Plant and Soil*, 415(1) :407–422, 2017.

D. White et al. Geophysical monitoring of the weyburn co2 flood : Results during 10 years of injection. *Energy Procedia*, 4 :3628–3635, 2011.

J. Whiteley, J. Chambers, S. Uhlemann, P. Wilkinson, and J. Kendall. Geophysical monitoring of moisture-induced landslides : a review. *Reviews of Geophysics*, 57(1) :106–145, 2019.

J. Whiteley, A. Watlet, S. Uhlemann, P. Wilkinson, J. Boyd, C. Jordan, J. Kendall, and J. Chambers. Rapid characterisation of landslide heterogeneity using unsupervised classification of electrical resistivity and seismic refraction surveys. *Engineering Geology*, 290 : 106189, 2021.

A. Wicki and C. Hauck. Monitoring critically saturated conditions for shallow landslide occurrence using electrical resistivity tomography. *Vadose Zone Journal*, 21(4) :e20204, 2022.

P. Wilkinson, J. Chambers, S. Uhlemann, P. Meldrum, A. Smith, N. Dixon, and M. H. Loke. Reconstruction of landslide movements by inversion of 4-D electrical resistivity tomography monitoring data. *Geophysical Research Letters*, 43(3) :1166–1174, 2016. ISSN 1944-8007.

- P. B. Wilkinson, P. I. Meldrum, J. E. Chambers, O. Kuras, and R. D. Ogilvy. Improved strategies for the automatic selection of optimized sets of electrical resistivity tomography measurement configurations. *Geophysical Journal International*, 167(3) :1119–1126, 2006.
- P. B. Wilkinson, M. H. Loke, P. I. Meldrum, J. E. Chambers, O. Kuras, D. A. Gunn, and R. D. Ogilvy. Practical aspects of applied optimized survey design for electrical resistivity tomography. *Geophysical Journal International*, 189(1) :428–440, 2012a.
- P. B. Wilkinson, M. H. Loke, P. I. Meldrum, J. E. Chambers, O. Kuras, D. A. Gunn, and R. D. Ogilvy. Practical aspects of applied optimized survey design for electrical resistivity tomography. *Geophysical Journal International*, 189(1) :428–440, 2012b. ISSN 1365-246X.
- P. B. Wilkinson, S. Uhlemann, J. E. Chambers, P. I. Meldrum, and M. H. Loke. Development and testing of displacement inversion to track electrode movements on 3-D electrical resistivity tomography monitoring grids. *Geophysical Journal International*, 200(3) :1566–1581, 2015a. ISSN 1365-246X.
- P. B. Wilkinson, S. Uhlemann, P. I. Meldrum, J. E. Chambers, S. Carrière, L. S. Oxby, and M. Loke. Adaptive time-lapse optimized survey design for electrical resistivity tomography monitoring. *Geophysical Journal International*, 203(1) :755–766, 2015b. ISSN 1365-246X.
- D. J. Williams. Lessons from tailings dam failures—where to go from here? *Minerals*, 11(8) :853, 2021.
- G. W. Wilson. The new expertise required for designing safe tailings storage facilities. *Soils and Rocks*, 44, 2021.
- WMTF. World mine tailings failure - state of world mine tailings portfolio 2020, accès le 17 fév. 2023. 2019. URL <https://worldminetailingsfailures.org/>.
- R. Wu, V. Martin, J. McKenzie, S. Broda, B. Bussière, M. Aubertin, and B. L. Kurylyk. Laboratory-scale assessment of a capillary barrier using fibre optic distributed temperature sensing (fo-dts). *Canadian Geotechnical Journal*, 57(1) :115–126, 2020.
- R. Wu, V. Martin, J. M. McKenzie, S. Broda, B. Bussière, J. Selker, and M. Aubertin. Fiber optic measurements of soil moisture in a waste rock pile. *Groundwater*, 59(4) :549–561, 2021.
- S. Yan, K. Y. Cheng, C. Morris, G. Douglas, M. P. Ginige, G. Zheng, L. Zhou, and A. H. Kaksonen. Sequential hydrotalcite precipitation and biological sulfate reduction for acid mine drainage treatment. *Chemosphere*, 252 :126570, 2020.
- X. Yang, T. A. Buscheck, K. Mansoor, Z. Wang, K. Gao, L. Huang, D. Appriou, and S. A. Carroll. Assessment of geophysical monitoring methods for detection of brine and co2 leakage in drinking water aquifers. *International Journal of Greenhouse Gas Control*, 90 : 102803, 2019.

- N. V. Yurkevich, N. A. Abrosimova, S. B. Bortnikova, Y. G. Karin, and O. P. Saeva. Geophysical investigations for evaluation of environmental pollution in a mine tailings area. *Toxicological & Environmental Chemistry*, 99(9-10) :1328–1345, 2017.
- T. Zhang, S. Liu, and G. Cai. Correlations between electrical resistivity and basic engineering property parameters for marine clays in jiangsu, china. *Journal of Applied Geophysics*, 159 :640–648, 2018.
- P.-F. Zhao, Y.-Q. Wang, S.-X. Yan, L.-F. Fan, Z.-Y. Wang, Q. Zhou, J.-P. Yao, Q. Cheng, Z.-Y. Wang, and L. Huang. Electrical imaging of plant root zone : A review. *Computers and Electronics in Agriculture*, page 105058, 2019.
- X. Zhao, H. Zhang, K. Wei, P. Wang, Q. Ren, and D. Zhang. Flow field fitting method and acoustic doppler velocity measurement : A new approach for detecting leakage pathways in concrete-face rockfill dams. *Earth and Space Science*, 8(11) :e2021EA001875, 2021.
- X. Zhao, H. Zhang, P. Wang, Q. Ren, D. Zhang, L. Yan, and X. Zhu. Flow-field fitting method applied to the detection of leakages in the concrete gravity dam. *Journal of Applied Geophysics*, 208 :104896, 2023.
- Q. Y. Zhou, J. Shimada, and A. Sato. Three-dimensional spatial and temporal monitoring of soil water content using electrical resistivity tomography. *Water Resources Research*, 37 (2) :273–285, 2001.
- T. Zieher, G. Markart, D. Ottowitz, A. Römer, M. Rutzinger, G. Meißl, and C. Geitner. Water content dynamics at plot scale—comparison of time-lapse electrical resistivity tomography monitoring and pore pressure modelling. *Journal of Hydrology*, 544 :195–209, 2017.

ANNEXE A DÉTAILS DES DISPOSITIFS DE LABORATOIRE

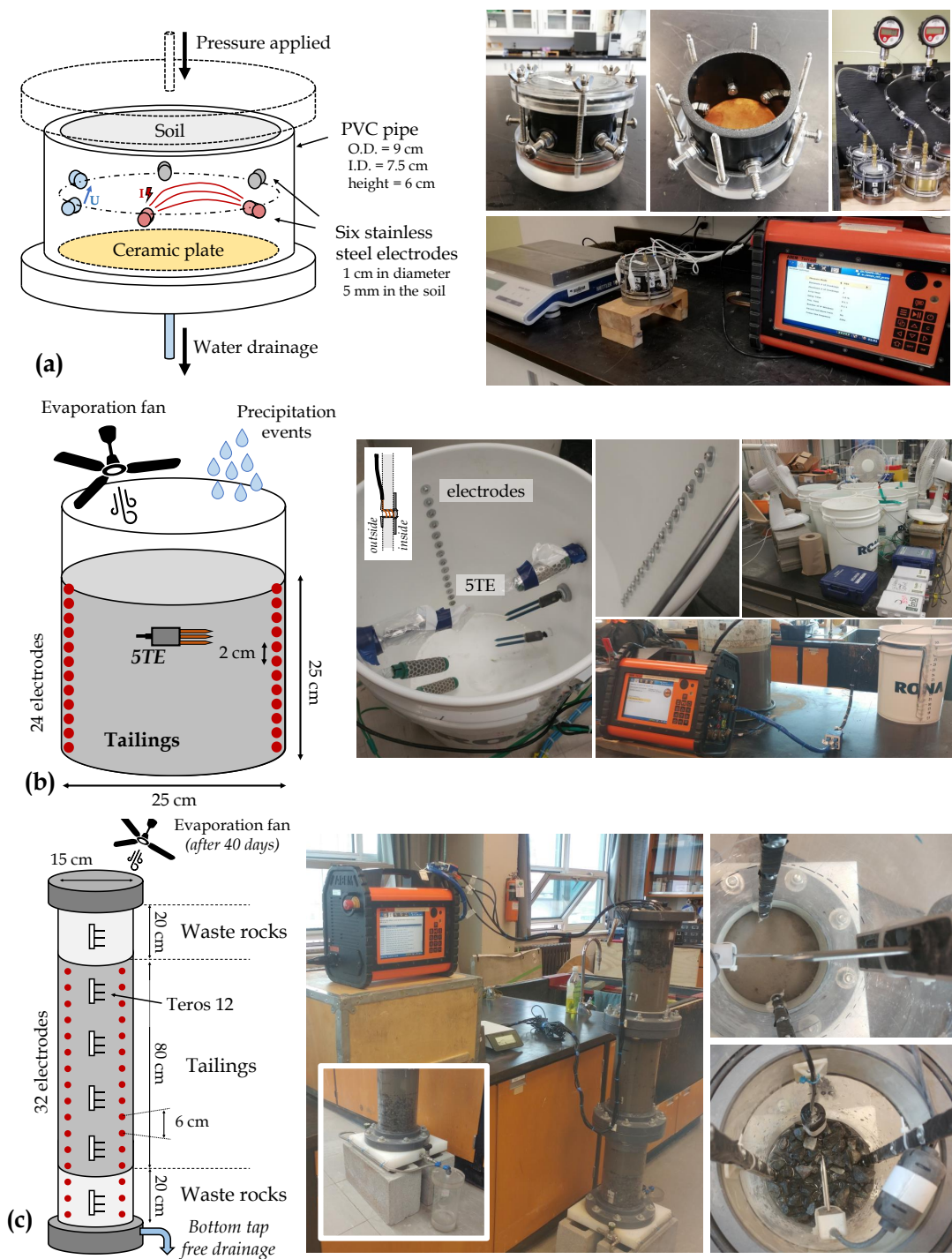


FIGURE A.1 Detailed schematics for the experimental laboratory setups. (a) S1 - electrical resistivity Tempe cell scale (ER-TC), (b) S2 - bucket scale and (c) S3 - column scale.

ANNEXE B DÉTAILS DE L'INSTRUMENTATION DE TERRAIN

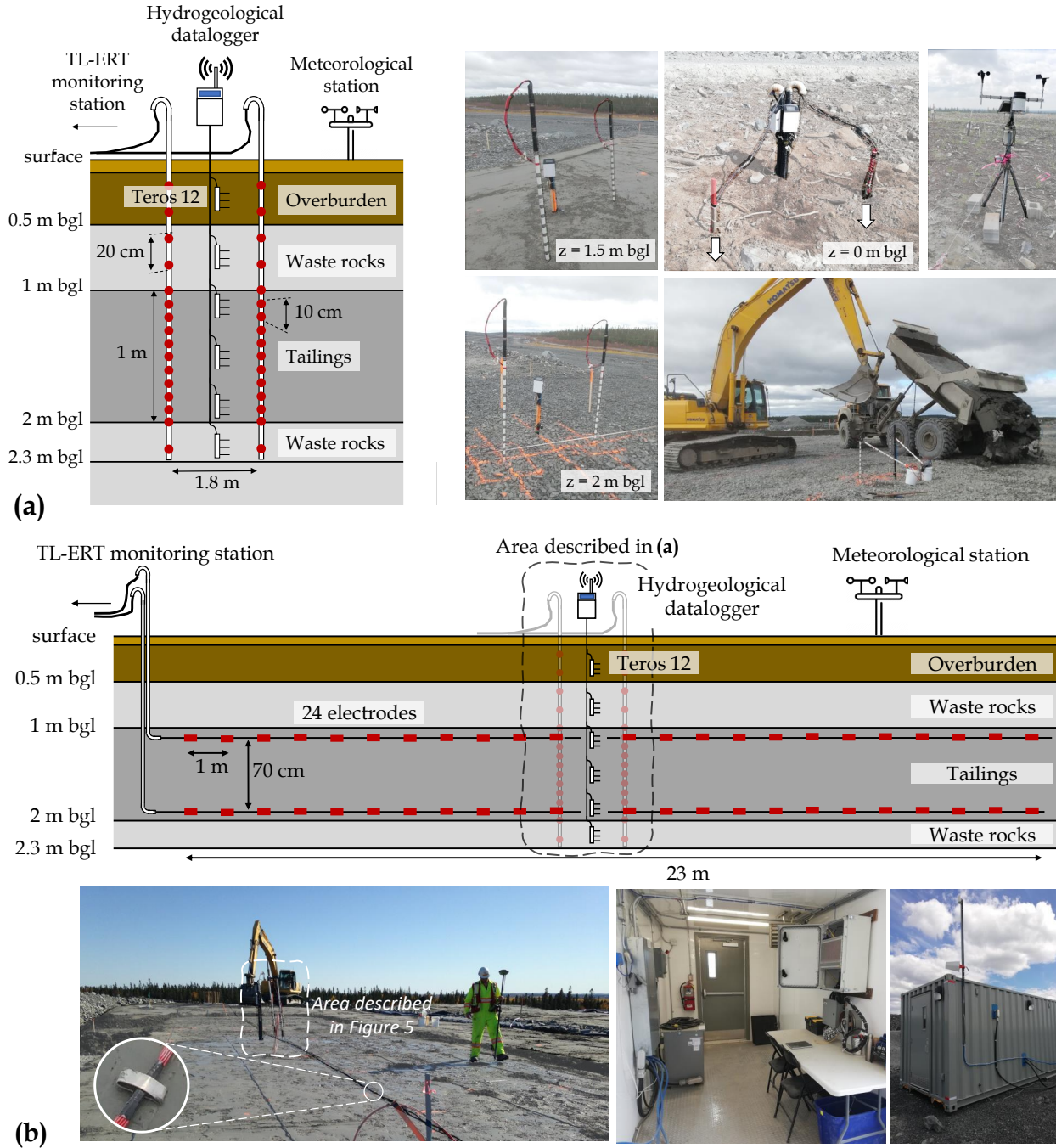


FIGURE B.1 Detailed schematics and photographs for the experimental field cover with capillary barrier effect. (a) S4 - field CCBE at local scale, (b) S5 - field CCBE at pilot scale.

ANNEXE C PROTOCOLE DE MESURES ÉLECTRIQUES

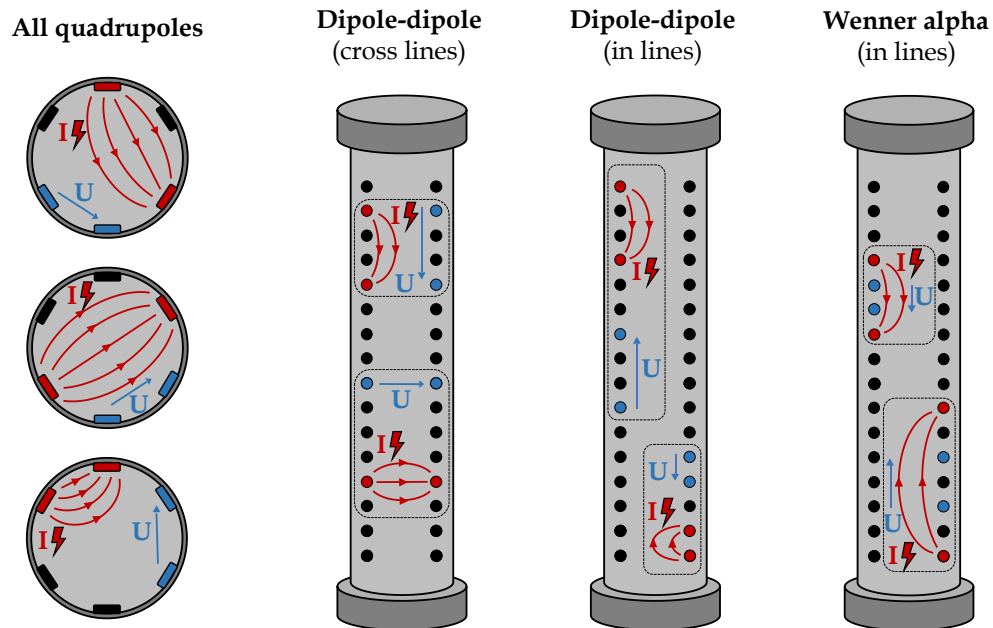


FIGURE C.1 Illustration of the configurations used to carry out TL-ERT monitoring in the tailings at different scales. Red and blue electrodes represent respectively current and potential electrodes.